

DOE/PC/91344--713

SRI International

RECEIVED
DEC 12 1995
OSTI

Topical Report • January 1995

ADVANCED SEPARATION TECHNOLOGY FOR FLUE GAS CLEANUP

Abhoyjit S. Bhowm
Dean Alvarado
Neeraj Pakala
Susanna Ventura

SRI International
333 Ravenswood Avenue
Menlo Park, CA 94025

Kamalesh K. Sirkar
Sudipto Majumdar
Debabrata Bhaumick

New Jersey Institute of Technology
University Heights
Newark, NJ 07102

SRI Project No. PYU-3501

DOE Contract No. DE-AC22-92PC91344

Prepared for:

U.S. Department of Energy
Pittsburgh Energy Technology Center
P.O. Box 10940
MS 921-118
Pittsburgh, PA 15236-0940

Attn: Document Control Center

RECEIVED
USDOE/PETC
95 FEB 17 AM 10:13
ACQUISITION & ASSISTANCE DIV.

CLEARED BY
PATENT COUNSEL

CONTENTS

SUMMARY	S-1
Objectives and Approach	S-1
Summary of Progress	S-3
TASK 1: PROJECT DEFINITION	1-1
TASK 2: CAPACITY, REVERSIBILITY, AND LIFETIME	2-1
SO _x Absorption	2-1
Early Measurements	2-1
Apparatus Modification	2-12
Understanding Discrepancies	2-19
Final Selection	2-21
NO _x Absorption	2-23
Absorption Studies	2-23
Effect of Oxygen	2-31
TASK 3: CHEMICAL SYNTHESIS	3-1
SO _x Absorbents	3-1
Synthesis of the Oligomeric Dimethylaniline (o-DMA)	3-1
Preparation of Propyleneimine and N-Phenylethyleneimine Copolymer	3-6
Synthesis of d-Siloxane and p-Siloxane	3-9
NO _x Absorbents	3-11
Tetrasodium Salt of Cobalt (II) 4,4',4'',4'''-Tetrasulfophthalocyanine 2-Hydrate	3-11
Tetrasodium Salt of Iron (II) 4,4',4'',4'''-Tetrasulfophthalocyanine 2-Hydrate	3-11
EDTA Analogs as NO _x Absorbents	3-12
Synthesis of Poly(allylamine) Functionalized EDTA Analog	3-15
Synthesis of EDTA Analog Copolymer	3-15
Synthesis of Poly(acrylate) Functionalized EDTA Analog	3-16
TASK 4: SO₂ SCRUBBING WITH HOLLOW FIBER CONTACTORS	4-1
Experiments with Prototype HFC	4-5
Liquid Phase Mass Transfer Experiments	4-5
SO ₂ Removal Efficiency Experiments	4-8
Initial Experiments with Hoechst-Celanese HFC	4-8
Mass Transfer Tests with Pure CO ₂ and Water	4-8
Mass Configuration Tests with Pure SO ₂	4-10

Mass Transfer Tests with 10% CO ₂ and Water	4-14
SO ₂ Removal Efficiency Tests	4-14
Mass Transfer Tests on 1000-Fiber Module	4-14
SO ₂ Absorption Tests with Model Flue Gas Mixture and Na ₂ SO ₃ Scrubber	4-18
Mass Transfer Control	4-29
Combined Absorption and Extraction	4-38
TASK 5: MASS TRANSFER RATE STUDIES FOR NO_x SCRUBBING IN HOLLOW FIBER CONTACTORS	5-1
CO ₂ Scrubbing	5-4
SO ₂ Scrubbing	5-11
NO _x Scrubbing	5-11
TASK 6: SO₂ LIQUOR REGENERATION	6-1
Liquid-Liquid Extraction (LLE)	6-1
Distribution Coefficient	6-9
Hollow Fiber Contained Liquid Membrane (HFCLM)	6-19
TASK 7: PARTICLE DEPOSITION	7-1
TASK 14: ECONOMIC EVALUATION	14-1
SO ₂ Absorber	14-1
NO _x Absorber	14-4
Liquid-Liquid Extractor	14-4
REFERENCES	R-1
APPENDICES	
A INITIAL PRESSURE	A-1
B CALCULATION OF H AND H*	B-1
C EQUILIBRIUM CONSTANT FROM BREAKTHROUGH CURVES	C-1
D EQUATIONS USED FOR OVERALL MASS TRANSFER COEFFICIENT CALCULATIONS	D-1
E CALCULATION OF MINIMUM LIQUID FLOW RATE	E-1

DISCLAIMER

This report was prepared as an account of work sponsored by an agency of the United States Government. Neither the United States Government nor any agency thereof, nor any of their employees, makes any warranty, express or implied, or assumes any legal liability or responsibility for the accuracy, completeness, or usefulness of any information, apparatus, product, or process disclosed, or represents that its use would not infringe privately owned rights. Reference herein to any specific commercial product, process, or service by trade name, trademark, manufacturer, or otherwise does not necessarily constitute or imply its endorsement, recommendation, or favoring by the United States Government or any agency thereof. The views and opinions of authors expressed herein do not necessarily state or reflect those of the United States Government or any agency thereof.

ILLUSTRATIONS

2-1	Schematic of sorption apparatus	2-2
2-2	Algorithm for controlling absorption apparatus	2-5
2-3	SO ₂ calibration curve	2-6
2-4	SO ₂ partial pressure in the sample loop as a function of time	2-7
2-5	SO ₂ sorption using DMA	2-10
2-6	Modified absorption apparatus	2-13
2-7	Modified algorithm for controlling absorption apparatus	2-14
2-8	d-Siloxane	2-15
2-9	Equilibrium between d-siloxane and SO ₂ (GC results)	2-17
2-10	Structure of siloxane pentamer	2-18
2-11	Comparison of SO ₂ sorption capacities	2-18
2-12	Calibration curves after 10.1% SO ₂ was left standing in an initially empty absorption apparatus	2-20
2-13	SO ₂ absorption lifetime of d-DMA at 35°C and 50°C	2-24
2-14	Lifetime SO ₂ absorption/desorption run on d-DMA at 50°C	2-25
2-15	NO _x absorption apparatus	2-26
2-16	Exiting NO concentration versus time for the 10-mM Fe(II)-EDTA/990-ppm NO runs	2-28
2-17	NO concentration over time for different scrubbing agents	2-29
2-18	NO _x -absorbing runs using 20 mM Fe(II)-EDTA and 100 ppm NO	2-32
2-19	Experimental flowsheet for NO _x absorption tests with on-line pH measurement	2-33
2-20	NO absorption by Co(II)-phthalocyanine in the presence of oxygen	2-34
2-21	Co(II)-phthalocyanine NO absorption capacity at 50°C	2-36
3-1	First route for synthesis of oligomer of DMA	3-2

3-2	Tetraethylenepentamine pentahydrochloride in the first synthesis route	3-2
3-3	Second route for synthesis of oligomer of DMA	3-3
3-4	Reaction scheme for synthesis of oligomer of DMA	3-4
3-5	Copolymerization scheme of N-phenylaziridine and propyleneimine	3-5
3-6	Silicon-containing DMA analogs	3-10
3-7	Siloxane oligomers functionalized by DMA	3-10
3-8	UV-visible spectrum of tetrasodium salt of iron 4,4',4", 4'''-tetrasulfophthalocyanine	3-13
3-9	Comparison of UV-visible spectra for Fe(II) and Fe(III) phthalocyanine	3-14
4-1	Structure of Celgard fiber netting	4-2
4-2	Wrapping of netting around central tube	4-3
4-3	Flow pattern of gas and liquid in crossflow module	4-4
4-4	Flow patterns in new Hoechst/Celanese crossflow module	4-6
4-5	HFC mass transfer coefficients for pure CO ₂ absorption in water using a crossflow module	4-7
4-6	SO ₂ removal efficiencies with a prototype HFC	4-9
4-7	Schematic of HFC test apparatus	4-10
4-8	Schematic of the crossflow module	4-11
4-9	HFC mass transfer coefficients for pure CO ₂ absorption in water using two crossflow modules	4-11
4-10	Schematic of HFC in the vertical configuration	4-12
4-11	HFC mass transfer coefficients with different module orientations and liquid pressures	4-13
4-12	HFC mass transfer coefficients with pure and dilute CO ₂ feed streams	4-15
4-13	SO ₂ removal efficiencies using water as the absorbent	4-16
4-14	SO ₂ removal efficiencies from simulated flue gas using water as the absorbent	4-17
4-15	HFC mass transfer coefficients for pure CO ₂ absorption in water using a 1000-fiber crossflow module	4-19
4-16	HFC mass transfer coefficients for CO ₂ -N ₂ mixture absorption in water using a 1000-fiber crossflow module	4-20

4-17	Sherwood number versus Reynolds number for CO ₂ absorption in water	4-21
4-18	SO ₂ removal with water at low liquid flow rates	4-22
4-19	SO ₂ removal with 0.01 M Na ₂ SO ₃ solution	4-23
4-20	SO ₂ removal efficiency at various sulfite concentrations	4-24
4-21	Effect of liquid flow rate on overall mass transfer coefficient and SO ₂ removal efficiency at low sulfite concentrations	4-26
4-22	Effect of sulfite on overall mass transfer coefficient	4-27
4-23	SO ₂ removal with water	4-32
4-24	Pure CO ₂ absorption in 1000-fiber module	4-35
4-25	Variation of mass transfer coefficient with gas flow rates at an aqueous sulfite solution flow of 20 mL/min	4-44
5-1	Minimum liquid-to-gas flow rate ratio needed to obtain equilibrium	5-2
5-2	Schematic of HFC apparatus	5-3
5-3	Calibration using a 1.99% CO ₂ cylinder	5-5
5-4	Overall mass transfer coefficient versus water flow rate	5-6
5-5	Fiber openings for 1000- and 200-fiber modules	5-8
5-6	Overall liquid mass transfer coefficient versus liquid flow rate	5-9
5-7	Sherwood number versus Reynolds number for CO ₂ absorption in water	5-10
5-8	GC calibration with 1.46% SO ₂ in N ₂ feed	5-12
5-9	SO ₂ removal water flow rate of 25 mL/min	5-13
5-10	Calibration curve of the NO _x analyzer	5-14
5-11	Percent removal of NO versus Fe(II)-EDTA concentration	5-16
5-12	Calculated solubility of NO in 20 mM Co-phthalocyanine solution at 25°C	5-20
5-13	Effect of gas flow rate on mass transfer coefficient and percent removal	5-23
6-1	Schematic of combined absorption and liquor regeneration setup	6-2
6-2	Schematic of combined absorption and liquor regeneration setup with installation of additional valves for by-pass of the extraction module	6-5
6-3	Schematic of combined absorption and liquor regeneration setup with four-way valve to conduct batch mode recirculation	6-12

6-4	Schematic of batch recirculation mode of operation using a hollow fiber contactor	6-14
6-5	Modified absorption and liquor regeneration setup for distribution coefficient measurement	6-15
6-6	Schematic of combined absorption and liquor regeneration setup modified for HFCLM runs	6-22
7-1	Schematic of Wright nebulizer	7-3
7-2	Size distribution of dispersed silica particles	7-5
7-3	Log-normal distribution of dispersed silica particles	7-6
7-4	Inspiron (400 cm ³) nebulizer performance characteristics	7-8
7-5	Particle size distribution for the sampling time of 1 s	7-9
7-6	Particle size distribution for the sampling time of 40 s	7-10
7-7	Particle capture efficiency in an HFC	7-12
7-8	Variation of gas-side overall mass transfer coefficient with gas flow rate	7-13
7-9	Effect of gas flow on the pressure drop across the HFC	7-15
7-10	Experimental SETUP for particle generation	7-17
7-11	Variation of ΔP_g across HFC	7-18
7-12	Pictures of HFC end caps and gas inlet and outlets ends of fibers	7-19
7-13	Enlarged view of a portion of particle cake formed at gas inlet end of HFC	7-20
14-1	Proposed SO _x /NO _x wet scrubbing with hollow fiber contacting devices	14-2

TABLES

S-1	Project Tasks and Schedule	S-2
S-2	Milestone Log for Contract DE-AC22-92PC91344 at End of Task 7	S-4
2-1	Absorption Measurement Procedure	2-3
2-2	Chromatography Columns Tested for O ₂ /N ₂ /SO ₂ Separation Ability	2-4
2-3	Compounds Synthesized and Tested in SO ₂ Sorption Runs	2-9
2-4	Parameters for SO ₂ Sorption Runs with DMA	2-11
2-5	Results for SO ₂ Sorption Runs	2-11
2-6	SO ₂ Sorption by d-Siloxane	2-12
2-7	SO ₂ Sorption by Siloxane Pentamer	2-16
2-8	Comparison of H* for d-Siloxane and d-DMA	2-19
2-9	SO ₂ Sorption by Dimer DMA	2-21
2-10	Equilibrium Constants (K) Using 100 ppm NO in N ₂ and 0.02 M Aqueous NO _x -Absorbing Solutions at 25°C	2-30
4-1	Results of SO ₂ Absorption in 0.2 M Na ₂ SO ₃	4-28
4-2	Summary of Results on CO ₂ Absorption in 1000-Fiber Unit	4-34
4-3	Summary of Absorption Data in Simultaneous Absorption-Extraction Runs	4-37
4-4	Results of SO ₂ Absorption Runs Using 0.2 M Na ₂ SO ₃ at 20 mL/min	4-39
4-5	Summary of Absorption Data in Simultaneous Absorption-Extraction Runs	4-40
4-6	Results of SO ₂ Absorption Runs Using 0.2 M Na ₂ SO ₃ at 20 mL/min	4-42
4-7	Absorption Data in Absorption-Extraction Runs Using High and Low Flow Rates of DMA	4-46
4-8	Absorption Data to Determine Distribution Constant (m) Using HFCs for Absorption-Extraction	4-48

5-1	Experimental Results on NO _x Absorption Using HFCs	5-18
5-2	Experimental Results on the NO _x Scrubbing with 300-Fiber HFC	5-21
6-1	Summary of Extraction Data in Simultaneous Absorption-Extraction Runs	6-6
6-2	Summary of Extraction Data in Simultaneous Absorption-Extraction Runs	6-7
6-3	Absorption Data in Absorption-Extraction Runs Using High and Low Flow Rates of DMA	6-11
6-4	Determination of Distribution Coefficient	6-18
6-5	Results of Run AE-12 and Other Runs with Higher Recovery of SO ₂ by LLE	6-20
6-6	Geometric Characteristics of the Coated Fiber Module for HFCLM	6-24
7-1	Particle Generation Using Nebulizers	7-4
14-1	Basic for Example Design of 500 MW(e) SO _x /NO _x Plant	14-3
14-2	Cost of Major Equipment and Utility Items in Option A for a 500-MW(e) Power Plant	14-6

SUMMARY

OBJECTIVES AND APPROACH

The objective of this work is to develop a novel system for regenerable SO₂ and NO_x scrubbing of flue gas that focuses on (1) a novel method for regenerating spent SO₂ scrubbing liquor and (2) novel chemistry for reversible absorption of NO_x. In addition, high efficiency hollow fiber contactors (HFC) are proposed as the devices for scrubbing the SO₂ and NO_x from the flue gas. The system will be designed to remove more than 95% of the SO₂ and more than 75% of the NO_x from flue gases typical of pulverized coal-fired power plants at a cost that is at least 20% less than combined wet limestone scrubbing of SO_x and selective catalytic reduction of NO_x. In addition, the process will generate only marketable by-products, if any (no waste streams are anticipated).

The major cost item in existing technology is capital investment. Therefore, our approach is to reduce the capital cost by using high-efficiency hollow fiber devices for absorbing and desorbing the SO₂ and NO_x. We will also introduce new process chemistry to minimize traditionally well-known problems with SO₂ and NO_x absorption and desorption. For example, we will extract the SO₂ from the aqueous scrubbing liquor into an oligomer of dimethylaniline to avoid the problem of organic liquid losses in the regeneration of the organic liquid. Our novel chemistry for scrubbing NO_x will consist of water-soluble phthalocyanine compounds invented by SRI as well as polymeric forms of Fe⁺⁺ complexes similar to traditional NO_x scrubbing media described in the open literature. Our past work with the phthalocyanine compounds, used as sensors for NO and NO₂ in flue gases, shows that these compounds bind NO and NO₂ reversibly and with no interference from O₂, CO₂, SO₂, or other components of flue gas.

The final novelty of our approach is the arrangement of the absorbers in cassette (stackable) form so that the NO_x absorber can be on top of the SO_x absorber. This arrangement is possible only because of the high efficiency of the hollow fiber scrubbing devices, as indicated by our preliminary laboratory data. This cassette (stacked) arrangement makes it possible for the SO₂ and NO_x scrubbing chambers to be separate without incurring the large ducting and gas pressure drop costs necessary if a second conventional absorber vessel were used. Because we have separate scrubbers, we will have separate liquor loops and simplify the chemical complexity of simultaneous SO₂/NO_x scrubbing.

Work is being conducted over a 60-month period (May 1992 through April 1997), encompassing 16 tasks (Table S-1), beginning with studies of the fundamental chemistry and the mass transfer characteristics of small HFC modules in the laboratory. We will then examine the most favorable method of SO₂ liquor regeneration, determine the ability of the HFC devices to withstand particulate matter, and examine the behavior of scalable modules. In the final 15 months of the program, we will determine the fundamental mass transfer behavior of a subscale prototype system. From these data, a computational design model will be devised to guide further scaleup efforts that may follow.

**Table S-1
PROJECT TASKS AND SCHEDULE**

<u>Task Number</u>	<u>Title</u>	<u>Duration</u>
1	Project Definition	5/92 – 8/92
2	Capacity, Reversibility and Lifetime	7/92 – 6/94
3	Chemical Synthesis	7/92 – 6/94
4	SO ₂ Scrubbing with HFCs	7/92 – 9/93
5	NO _x Scrubbing with HFCs	2/93 – 3/94
6	SO ₂ Liquor Regeneration	7/93 – 9/94
7	Particle Deposition	8/93 – 9/94
8	Integrated NO _x Life Tests	8/94 – 4/95
9	Scalable Modules	8/94 – 4/95
10	Computational Model	11/94 – 7/95
11	Construction of Subscale Prototype	8/95 – 1/96
12	Operation of Subscale Prototype	2/96 – 4/97
13	Refinement of Computational Model	9/96 – 4/97
14	Economic Evaluation	Various
15	Reporting	5/92 – 4/97
16	Chemical Synthesis for Process Scaleup	5/94 – 1/96

SUMMARY OF PROGRESS

In Task 1, an overall management plan was submitted to the DOE, and approved. The technical approach has not changed from that plan.

In Task 2, several SO₂ and NO absorbing compounds was tested for reversibility, capacity, and lifetime. For SO₂, d-DMA has been selected as the best choice, while for NO_x, Co(II)-phthalocyanine has been selected as the best choice.

In Task 3, several of the compounds tested in Task 2 have been synthesized.

In Task 4, 99% SO₂ removal efficiency with laboratory modules has been demonstrated and the mass transfer properties of HFCs have been extensively characterized.

In Task 5, 85% NO removal efficiency has been demonstrated with laboratory modules using Co(II)-phthalocyanine solutions.

In Task 6, 99% SO₂ liquor regeneration efficiency with laboratory modules has been achieved.

In Task 7, an 80-hour particle deposition experiment has been completed. Unexpected results stopped further deposition tests.

In Task 14, we completed preliminary economic estimations on the process. The results indicate marked savings in capital investments.

A milestone log is shown in Table S-2.

Table S-2
MILESTONE LOG FOR CONTRACT DE-AC22-92PC91344 AT END OF TASK 7

Element Code	Description	Planned Completion Date	Actual Completion Date	Comments
1	Development of Management Plan	6/92	8/92	
2A	Test First DMA Oligomer	2/93	4/93	Difficult to obtain quality data.
2B	Test First NO _x Scrubbing Compound	6/93	10/93	Two major oil contaminations.
3A	Synthesize 10 g of DMA Oligomer	1/93	1/93	
3B	Synthesize 40 g Phthalocyanine	5/93	6/93	
4	Achieve 99% SO ₂ Removal Efficiency with Laboratory Modules	1/93	1/93	
5	Achieve 85% NO _x Removal Efficiency with Laboratory Modules	5/93	9/93	NO _x analyzer received 8/93 from another DOE contractor. Blocked fibers discovered in one module.
6	Achieve 99% SO ₂ Liquor Regeneration Efficiency with Laboratory Modules	11/93	3/94	Delay in obtaining HFCs from manufacturer.
7	Complete One-Month Particle Deposition Test	2/94		New proposal submitted to examine unexpected results.
8A	Operate Integrated Absorption/Desorption System with Water	10/94		
8B	Complete One-Month Life Test of NO _x Chemistry	3/95		
9	Achieve 97% SO ₂ Absorption and Liquor Regeneration with Scalable Modules	3/95		
11	Operate Subscale Prototype with Water	1/96		
12	Achieve 95% SO ₂ and 75% NO _x Removal Efficiency with Subscale Prototype	1/97		
14	Prepare Detailed Evaluation of Process Economics	3/97		

TASK 1: PROJECT DEFINITION

In this task, we developed a management plan and submitted it to the DOE in August 1992. After its approval, we initiated work on the technical aspects of this project. Our technical approach has not veered from the management plan.

TASK 2: CAPACITY, REVERSIBILITY, AND LIFETIME

The purpose of this task was to establish the reversible absorption capacity of the chemistries we intend to use for SO₂-liquor regeneration and for NO_x scrubbing. Any commercially successful SO₂ and NO_x chemistry must be essentially fully reversible and lose less than 10% of its activity in one year. The real issues are the economics of replacement chemicals and the disposal of spent chemicals. We anticipate that the maximum allowable cost for replacement and renewal of spent chemicals would be about 0.1 mL/kWh in an actual power plant operating environment.

SO_x ABSORPTION

To determine the reversible adsorption capacity, we measured the equilibrium absorption behavior of SO₂ in an automated apparatus designed for this purpose (Figure 2-1). We placed samples of the SO₂ regeneration liquid into the sample cell and repeatedly exposed the liquid to various partial pressures of SO₂ (partial pressures characteristic of flue gas).

Early Measurements

The apparatus used for this study was designed so that dead volume in our system would be minimized. Also a gas cabinet was installed into the system to provide for containment of cylinder leaks, inert purging of gas lines, and automatic shut-off in case of a power failure.

The reversible absorption apparatus measures absorption using a combination of volumetric and chromatographic techniques. The absorption measurement procedure, summarized in Table 2-1, was designed for reducing the time required for each measurement. The time limiting step for a measurement is the diffusion time required to ensure that all the gas is in equilibrium with the liquid.*

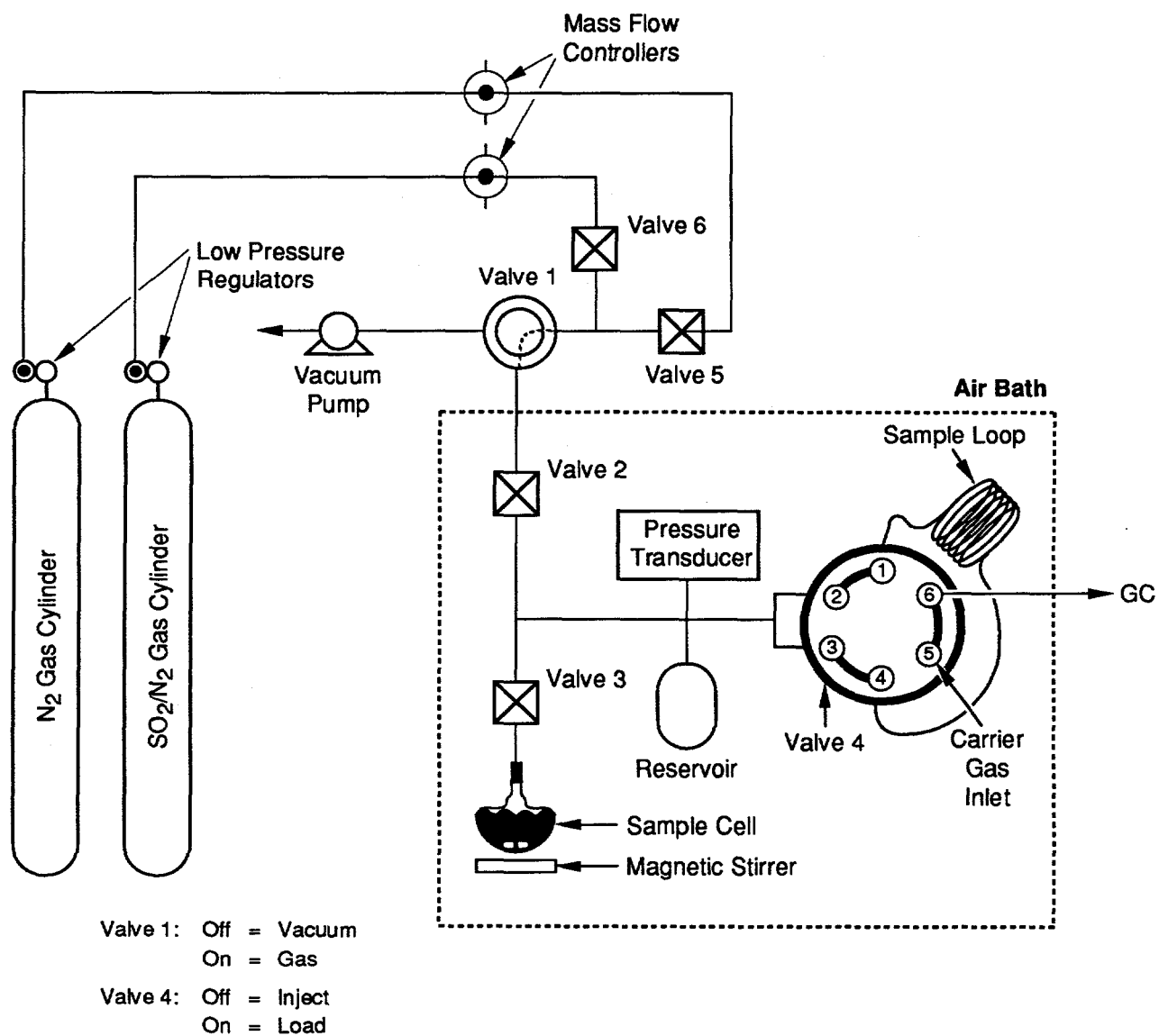
An indication of the time required for diffusion to occur is given by the characteristic diffusion time:

$$\tau = \frac{L^2}{d} \quad (2-1)$$

where

- τ = Characteristic diffusion time
- L = Length of diffusion path
- d = Diffusivity of gas

* It is not practical to force circulation of gas through the GC sample loop because any mechanism forcing circulation would add uncertainties to the internal volume of the apparatus or introduce incompatible materials.



CM-3501-11

Figure 2-1. Schematic of sorption apparatus.

Table 2-1
ABSORPTION MEASUREMENT PROCEDURE

(Refer to Figure 2-1)

1. The region below valve 2 is evacuated.
 2. Valve 3 is closed, the region between valves 2 and 3 is charged with a known quantity of gas (SO_2), and 2 is closed. (Knowing the temperature, pressure, and volume of this region, we can determine the moles of gas charged.)
 3. Valve 3 is opened, allowing the gas to contact the absorbent sample.
 4. The apparatus is given time to allow equilibration between the gas (including that contained in the Reservoir, Sample cell, GC sample loop, and connections) and the liquid.
 5. The total moles remaining in the gas phase after absorption are determined.
 6. The composition of the gas is determined by sending a gas sample to the GC.
 7. The moles of SO_2 absorbed by the liquid are determined by mass balance.
-

The largest contributor to diffusion time in our apparatus is the sample loop. To reduce the diffusion time, we connected both ends of the GC sample loop to the reservoir region and shortened the sample loop by using larger diameter tubing. With these modifications, the characteristic diffusion time is about 10 minutes. We expected the equilibration step in our procedure to be at least ten times the characteristic diffusion time. Before beginning absorption measurements we experimentally determined the actual time required for the entire gas volume to equilibrate with the absorbent.

We began evaluating chromatography columns for SO_2 analysis by GC. Our goal was to identify a column that will separate SO_2 , N_2 , and O_2 . The ability to separate O_2 will allow us to check for leaks on each run. If there is an O_2 peak we will know there is a leak and can correct it (since N_2 is used as the diluent for SO_2 a N_2 peak will not indicate a leak). Many columns can separate SO_2 from O_2/N_2 and O_2 from N_2 , but few can separate all three simultaneously. Table 2-2 lists the columns we have tested and the results.

Table 2-2
CHROMATOGRAPHY COLUMNS TESTED FOR
O₂/N₂/SO₂ SEPARATION ABILITY

<u>Column</u>	<u>Result</u>
Porapak Q	Does not separate O ₂ from N ₂
Molecular sieve 5a	Irreversibly adsorbs SO ₂
Molecular sieve 13x	Irreversibly adsorbs SO ₂
Chromosorb 102	Does not separate O ₂ from N ₂
Carbosphere	Has been ordered but not tested
Haysep DB	Has been ordered but not tested

To help us evaluate the results from absorption experiments, we developed a computer spreadsheet that will calculate the solubility coefficient from a set of experimental results. The spreadsheet can also be used to determine the optimum experimental conditions (the pressure, volume, and composition of the initial gas charge) for the absorption measurements.

To fully automate the absorption procedure, we connected all six valves and the pressure transducer to a Macintosh computer. We programmed the computer according to the algorithm shown in Figure 2-2. The algorithm will check for leaks, desorb gases from the sample liquid, pressurize the apparatus with SO₂, monitor the pressure over time, and determine the equilibrium SO₂ concentration in the apparatus by gas chromatography.

We focused on obtaining three important characteristics of the absorption apparatus: the gas chromatograph calibration curve, sample cell and head space volumes, and the time required for SO₂ to diffuse from the sample cell to the sample loop.

We calibrated the gas chromatograph using a 0.91% SO₂ in N₂ mixture at various pressures. Figure 2-3 shows results for SO₂. We also measured the leak rate of the apparatus as approximately 3 torr/day. This value is lower than the expected operating pressures of 400-800 torr. Thus, the apparatus is essentially leak-free.

In preparation for the experiments, we measured the sample cell and head space volumes by filling the sample cell to a known pressure with N₂ and expanding it into the head space volume. Knowing the initial pressures in the two volumes and the final equilibrium pressure, we can compute the ratio of the two volumes. Next, ball bearings of a known volume were placed in the sample cell and the entire exercise was repeated; this yielded a different ratio of volumes. From the two ratios the actual volumes can be calculated: we calculated the sample cell volume as 17.01 cm³ and the head space volume as 19.81 cm³.

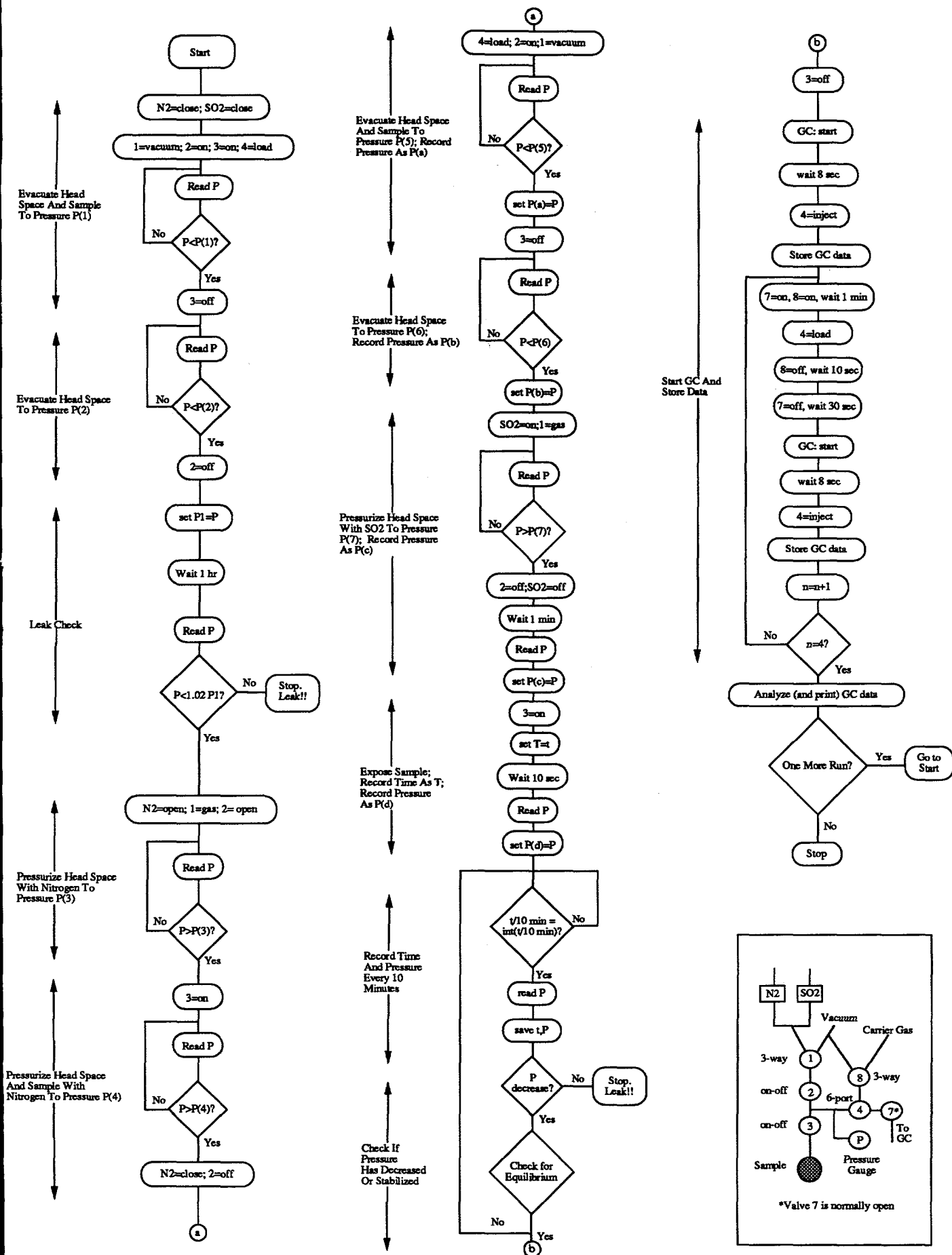
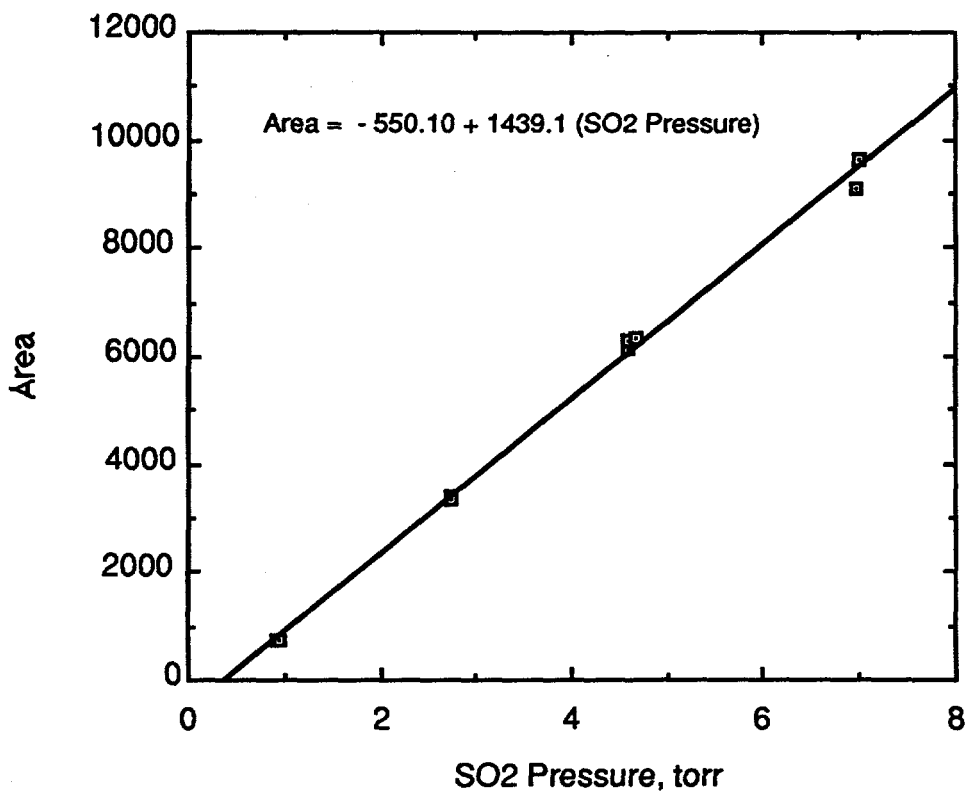


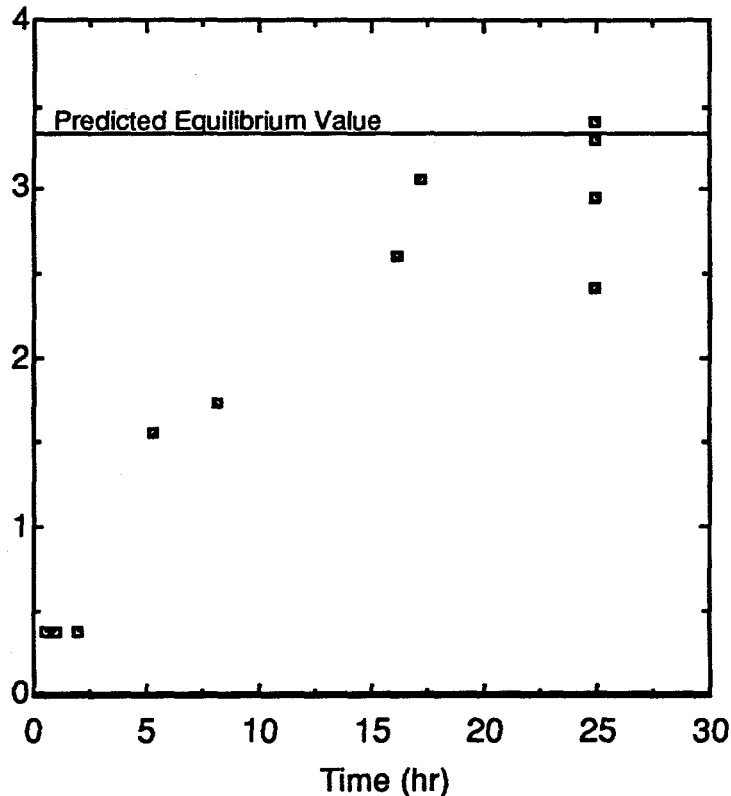
Figure 2-2. Algorithm for controlling absorption apparatus.



CA-3501-86

Figure 2-3. SO₂ calibration curve.

We measured the time required for SO₂ to diffuse from the sample cell to the sample loop by charging the sample cell with 0.91% SO₂ in N₂ and the head space with 100% N₂ to approximately 760 torr. In some cases, the head space was initially evacuated. After a fixed time, the sample loop was checked for SO₂ content. We expect the equilibrium SO₂ partial pressure to be the same as if the head space was initially evacuated. Figure 2-4 shows SO₂ partial pressures in the sample loop from experiments that lasted between 0.5 and 17.2 hours. (The data at 25 hours are for measurements with the head space initially evacuated.) The solid line is the expected value based on the initial SO₂ charge and the above sample cell and head space volumes. Hence, we predict the diffusion time at 760 torr to be between 20-24 hours. At lower pressures, the diffusion time should be proportionately larger.



CAM-3501-85

Figure 2-4. SO₂ partial pressure in the sample loop as a function of time.

The procedure for the sorption runs is as follows: a known amount of liquid is placed in the sample cell and the remaining sample cell and headspace volumes are evacuated. The headspace is then charged with gaseous 10.1% SO₂ in N₂ to a known pressure. At time 0, valve 3 is opened. The total pressure is recorded over time by a pressure transducer, and after equilibrium the headspace partial pressures are measured by a gas chromatograph. The entire apparatus is computer controlled.

To quantify the sorption capacity of liquids, the scientific literature often reports the partition coefficient, H , defined as the equilibrium partial pressure of SO₂ in the vapor divided by the equilibrium mole fraction SO₂ in the liquid. A comparison of the sorption capacity of two liquids based on such a definition, however, is difficult because the two liquids may have different molecular weights. To circumvent this problem, we introduce H^* , a quantity similar to H but a more useful engineering parameter. H^* is defined as the volume of liquid needed to treat a unit volume of SO₂ at STP. H is more common in the scientific literature while H^* is more useful in engineering design calculations. Details of calculations are given in Appendices A and B.

Initially, we conducted SO₂ sorption runs with four compounds: DMA, d-DMA, MAPA, and AMAPA, whose structures and complete names are shown in Table 2-3. Figure 2-5 shows the pressure changes over time for 10.1% SO₂ in N₂ over DMA for four runs. These curves are typical of all other sorption runs. To partially account for slight differences in the initial pressure P(0) between runs, the plots are shown as P/P(0) versus time. By doing so, we do not imply that P/P(0) should collapse the curves into a single line; rather, we simply give the starting point for all curves. Because the headspace, sample cell, and liquid volumes were slightly different, a direct comparison of these numbers is difficult. Table 2-4 details experimental conditions.

If we assume that N₂ does not absorb in the liquid, we can attribute the entire pressure change solely to SO₂ absorption. This gives us the amount of SO₂ absorbed from pressure transducer measurements. From GC measurements, we also obtain the amount of SO₂ absorbed at equilibrium. Thus, we have two independent measurements of the amount of SO₂ absorbed from which we can calculate two independent values for H*, shown in Table 2-5. Note that, for each run, the H* values calculated from the GC data and from the pressure transducer data are not the same. Moreover, the H* values calculated from the GC data increase with run number whereas those calculated from the pressure transducer data fluctuate with run number.

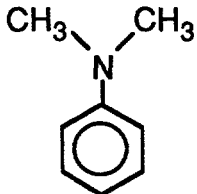
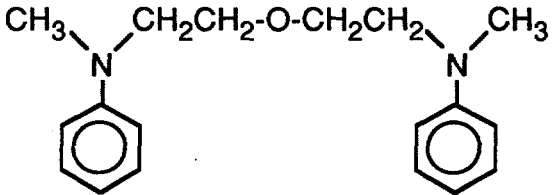
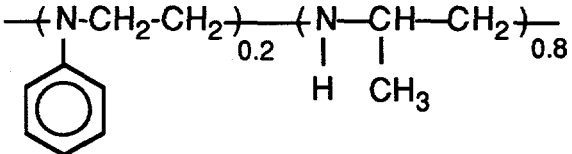
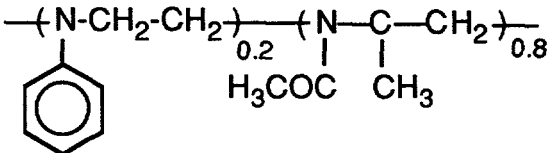
One important reason for the discrepancy and fluctuation is that errors in measuring the final SO₂ partial pressure, P_{SO₂(f)}, are propagated through the calculations. The most important quantity measured in the experiments is the final SO₂ partial pressure. From this quantity, we calculate the amount of SO₂ absorbed by the liquids by subtracting the final SO₂ partial pressure from the initial SO₂ partial pressure. The GC measures the final SO₂ partial pressure, whereas the pressure transducer infers it by assuming that the pressure change over time is due solely to the amount of SO₂ absorbed. Thus, the GC results are more reliable than the pressure transducer results.

The increasing value of H* for DMA and d-DMA indicates that the sorption capacity decreases with each run, assuming the GC data are more reliable. Thus, desorption steps between runs are incomplete or there may be irreversible changes to the liquid with exposure to SO₂. We have modified the apparatus such that it now makes multiple injections of the headspace. This gives us a more reliable analysis of the gas composition. Additionally, we now account for factors such as partial pressure of the liquid and leak rates in our calculations. These modifications have helped close the gap between the GC and transducer results, but not completely. Details of these calculations are given in Appendices A and B.

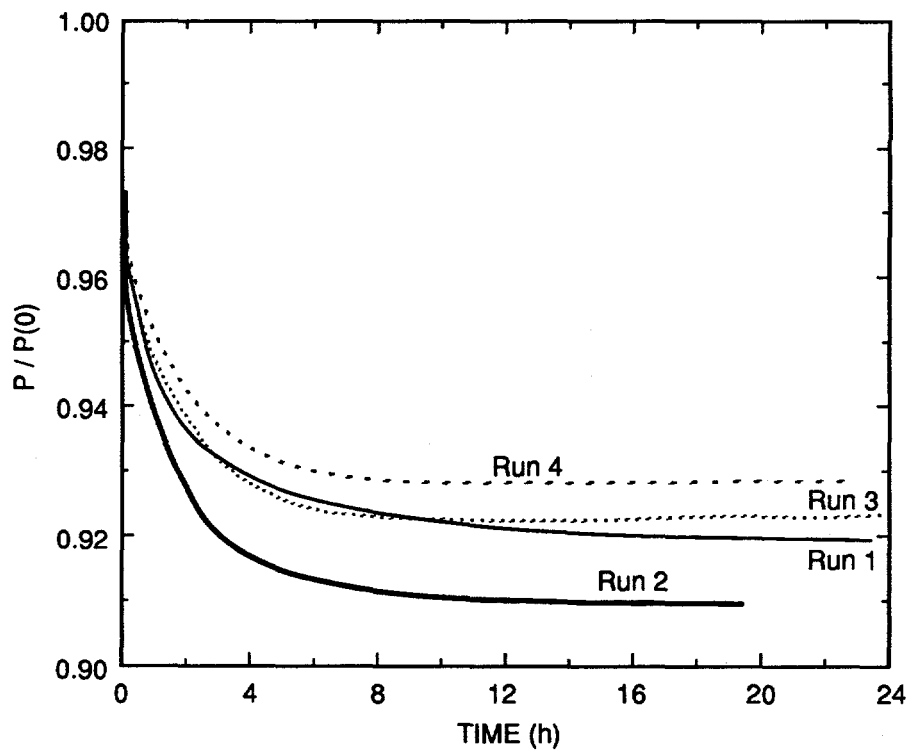
From either the GC or transducer measurements, we reach the favorable conclusion that the sorption capacities of the test liquids were higher than or equal to DMA, but with lower vapor pressure.

$$H_{\text{DMA}}^* \approx H_{\text{d-DMA}}^* > H_{\text{AMAPA}}^*$$

Table 2-3.
COMPOUNDS SYNTHESIZED AND TESTED IN SO₂ SORPTION RUNS

Structure	Name	Abbreviation
	N,N'-Dimethylaniline	DMA
	2,2'-Bis(N-methyl-N-phenylamino)ethyl ether	d-DMA
	Poly(2-methylaziridine-co-N-phenylaziridine)	MAPA
	Poly(N-acetyl-2-methylaziridine-co-N-phenylaziridine)	AMAPA

CM-3501-12D



CAM-3501-13B

Figure 2-5. SO_2 sorption using DMA.

**Table 2-4
PARAMETERS FOR SO₂ SORPTION RUNS WITH DMA**

<u>Parameter</u>	<u>Symbol</u>	<u>Units</u>	<u>Value</u>
SO ₂ mole fraction in charge gas	y ⁰	—	0.101
Temperature	T	K	308.15
Headspace volume	VHS	cm ³	19.81
Sample cell volume	VSC	cm ³	17.01
Liquid volume	V _L	cm ³	0.67
Liquid vapor pressure	VP	torr	1.5224
Liquid molar concentration	CL	mol/cm ³	0.00789

**Table 2-5
RESULTS FOR SO₂ SORPTION RUNS**

<u>Liquid</u>	<u>Run</u>	<u>H*, cm³ liq/cm³ SO₂ (STP)</u>		
		<u>Predict^a</u>	<u>GC</u>	<u>Transducer</u>
DMA, 35°C	1	0.3611	0.3518	0.4203
DMA	2	0.3623	0.3544	0.3792
DMA	3	0.3625	0.3649	0.4504
DMA	4	0.3623	0.3671	0.4751
Average		0.3620	0.3596	0.4312
d-DMA, 35°C	1		0.3471	0.4677
d-DMA	2		0.3560	0.4200
d-DMA	3		0.3639	0.4207
Average			0.3557	0.4361
MAPA, 80°C	1,2	Complete, Irreversible Absorption		
AMAPA, 80°C	1		0.2434	0.3569
AMAPA	2		0.2202	0.2973
Average			0.2318	0.3271

^a From R. J. Demyanovich and S. Lynn, Ind. Eng. Chem. Res. 26, 548-555 (1987).

The value for H_{MAPA}^* is not compared since SO_2 showed complete, irreversible absorption into MAPA. The boiling points of these compounds are

$$T_{DMA} \approx 194^\circ C, \quad T_{d-DMA} \gg 300^\circ C, \quad T_{AMAPA} \gg T_{d-DMA}$$

Hence, the vapor pressures of d-DMA and AMAPA are much lower than that for DMA.

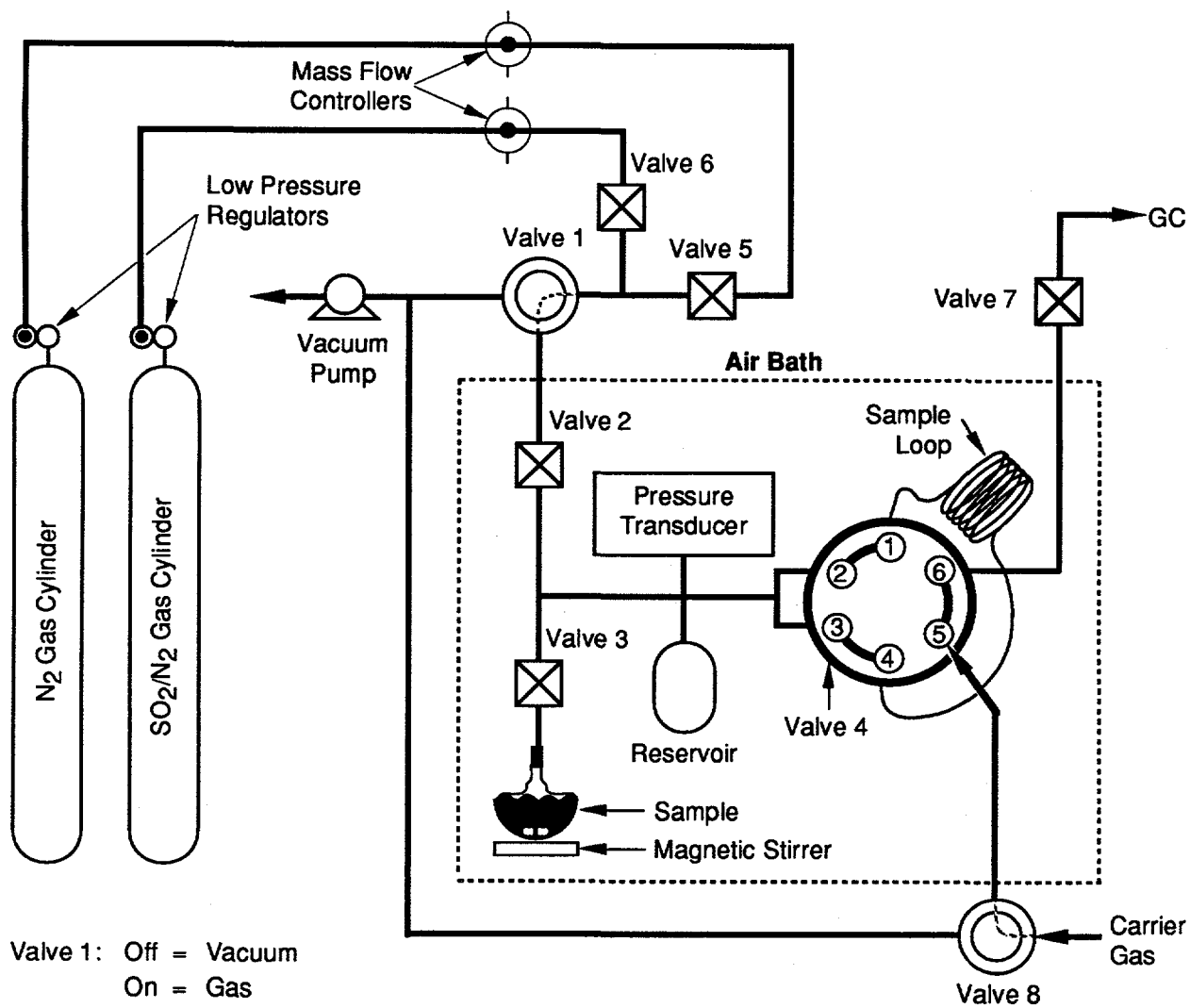
Apparatus Modification

Before performing more sorption runs, we modified control of the absorption apparatus such that it now injects multiple samples of the headspace when the system reaches equilibrium. With this modification, we can calculate an average SO_2 concentration from several injections rather than a single injection. This modification essentially added valves 7 and 8 (see Figure 2-6). These valves, along with the remaining six valves, are connected to a computer to control the apparatus. The new algorithm for the computer program is shown in Figure 2-7.

With the modifications complete, we measured the sorption capacity of a siloxane dimer, d-siloxane, whose structure is shown in Figure 2-8. Its synthesis is described in Task 3. We tested the compound to various atmospheres of 10.1% SO_2 in N_2 at $35^\circ C$. Four runs were made: two with an initial total pressure of 520 torr, one with 416 torr, and another with 274 torr. The final pressures for each run, along with the value of H^* calculated from the pressure transducer and GC measurements, are shown in Table 2-6. Recall that H^* is defined as the volume of liquid needed to absorb 1 cm^3 of SO_2 at STP and has the units of cm^3 liq/ cm^3 (STP) SO_2 . The key observation here is that H^* for the d-siloxane is inversely related to the final pressure. That is, the lower the final pressure, the more liquid is needed to absorb 1 cm^3 SO_2 at STP.

Table 2-6
 SO_2 SORPTION BY d-SILOXANE

Run No.	P _{tot} , Init. (torr)	P(F), SO_2 (torr)	H^* , Transducer	H^* , GC
1	520.14	8.95	0.406	0.294
2	520.16	8.80	0.457	0.293
3	416.14	6.17	0.470	0.358
4	274.14	2.68	1.056	0.513



Valve 1: Off = Vacuum
On = Gas

Valve 4: Off = Inject
On = Load

Valve 8: Off = Connect to Valve 4
On = Connect to Vacuum

Sample Cell = Volume below valve 3, including liquid

Head Space = Volume between valve 2, valve 3, pressure transducer, reservoir, and valve 4 in the load position (includes sample loop).

CM-3501-11E

Figure 2-6. Modified absorption apparatus.

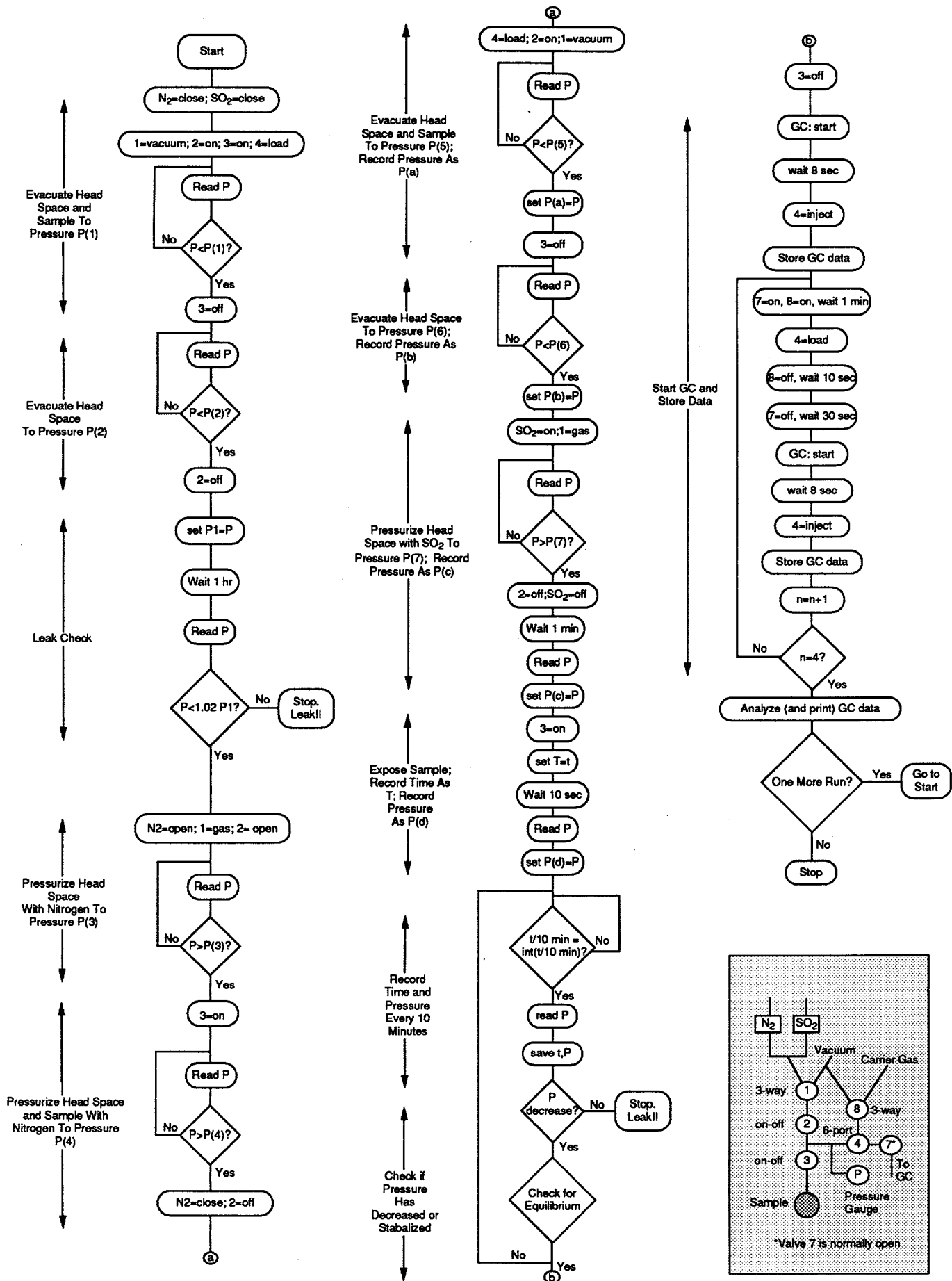
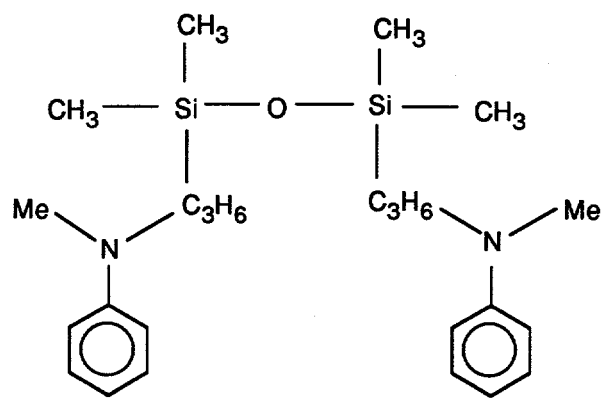


Figure 2-7. Modified algorithm for controlling absorption apparatus.

CAM-3501-53



CAM-3501-36A

Figure 2-8. d-Siloxane.

We also computed the partition coefficient H for the four siloxane runs. Recall that H is defined as the final partial pressure of SO_2 divided by the mole fraction of SO_2 in the liquid at equilibrium. Thus, H has the units of torr/mole-fraction. A plot of the final SO_2 partial pressure versus the mole fraction SO_2 in the liquid should be linear. Figure 2-9 shows such a plot for the four d-siloxane runs. The curve through the four points is linear, but it fails to go through the origin. We suspect that, at such high mole-fractions, the SO_2 -siloxane system may be nonideal and thus Henry's law would fail. Indeed, other researchers have reported nonideal behavior with SO_2 -DMA systems at comparable concentrations (Demyanovich and Lynn, 1987).

The d-siloxane compound we tested seems more reversible than the d-DMA (the SO_2 sorption capacity of d-DMA decreased with each run). However, as shown in Table 2-6 for the d-siloxane results, the first and second runs gave identical sorption capacity. We further tested the d-siloxane to reversibility and capacity tests.

Next, we studied the sorption capacity of a siloxane pentamer similar to the dimer siloxane described above. The capacity of the siloxane pentamer, whose structure is shown in Figure 2-10, was found to be comparable to that of the siloxane dimer. However, since the pentamer was more viscous than the dimer, it might be less adaptable to industrial applications. Table 2-7 summarizes the H^* values calculated for the siloxane pentamer.

We next compared the sorption capabilities for some of the compounds tested so far in this study. Figure 2-11 shows several trends in this comparison. In all cases, the H^* values calculated from transducer-measured pressures are higher than those calculated from GC values. This issue has been previously addressed. Also, for some of the compounds even though the initial total pressure was the same for each run, the final SO_2 pressure was not always the same. In the case of d-DMA, the final SO_2 pressure increased slightly each run, indicating that d-DMA is slowly losing its sorption capacity. Finally, all the GC H^* values for the compounds listed fell between 0.3 and 0.5.

Table 2-7
 SO_2 SORPTION BY SILOXANE PENTAMER

<u>Run No.</u>	<u>Initial Total Pressure</u>	<u>Final SO_2 Pressure (torr)</u>	<u>H^*, Transducer</u>	<u>H^*, GC</u>
1	596.62	6.75	0.370	0.288
2	596.90	5.30	0.555	0.280

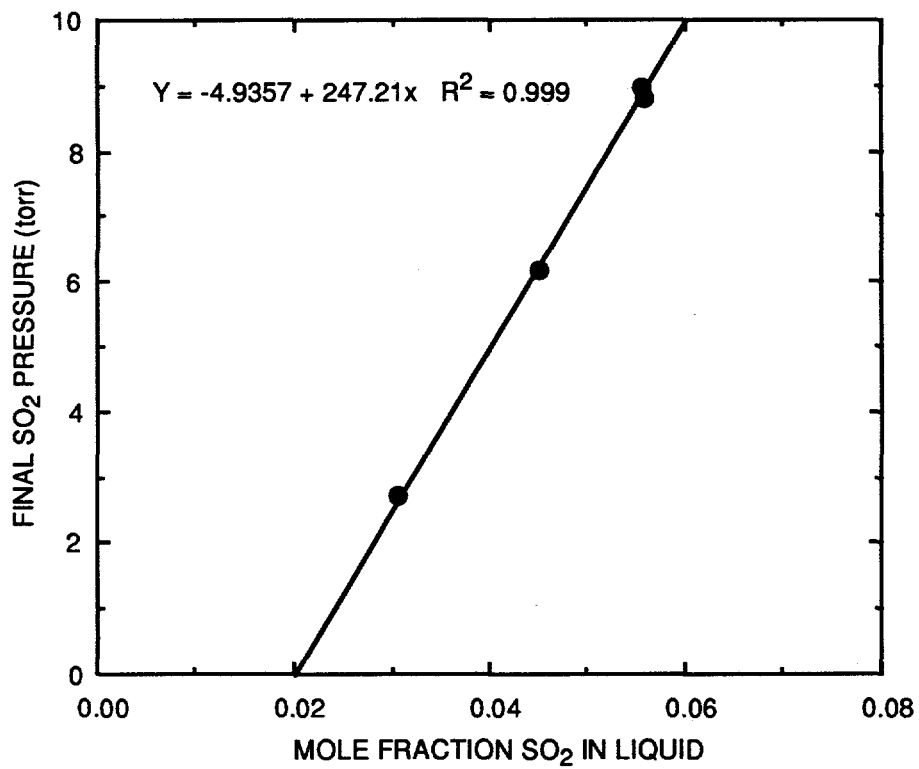
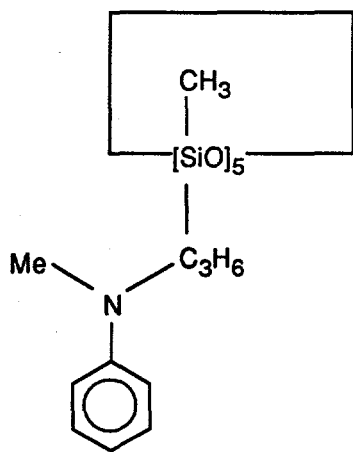
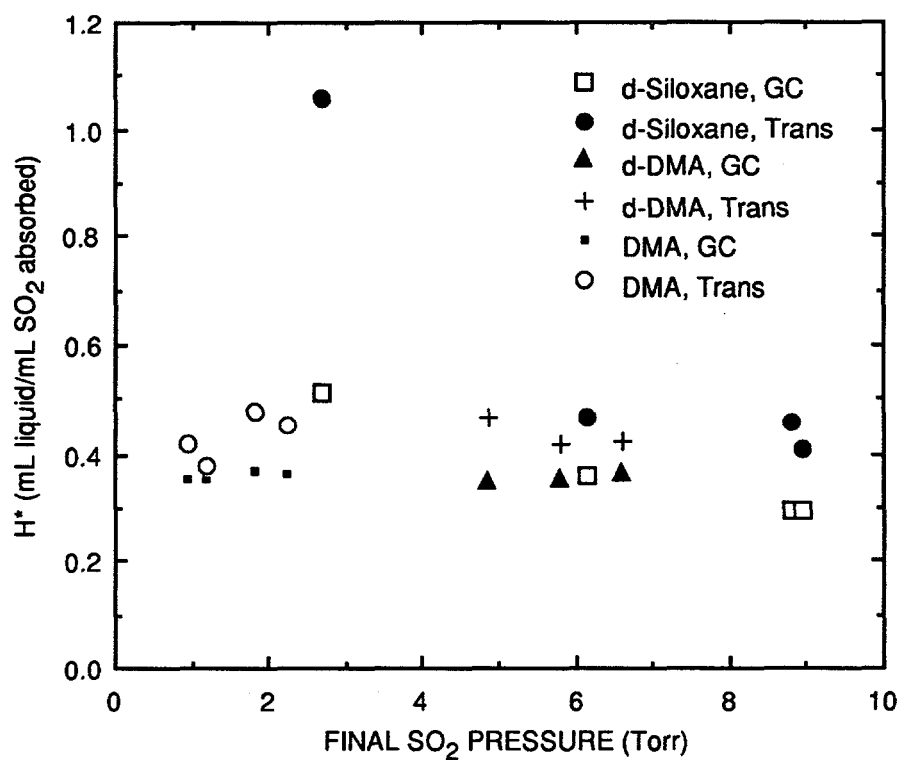


Figure 2-9. Equilibrium between d-siloxane and SO₂ (GC results).



CAM-3501-36B

Figure 2-10. Structure of siloxane pentamer.



CAM-3501-44

Figure 2-11. Comparison of SO₂ sorption capacities.

The DMA monomer was determined to be too volatile for further study while the DMA oligomers (except d-DMA) were found to be too viscous for industrial application. The only two remaining choices were the d-DMA and d-siloxane. The characteristics of these two compounds are very similar, as shown in Table 2-8.

Table 2-8
COMPARISON OF H* FOR d-SILOXANE AND d-DMA

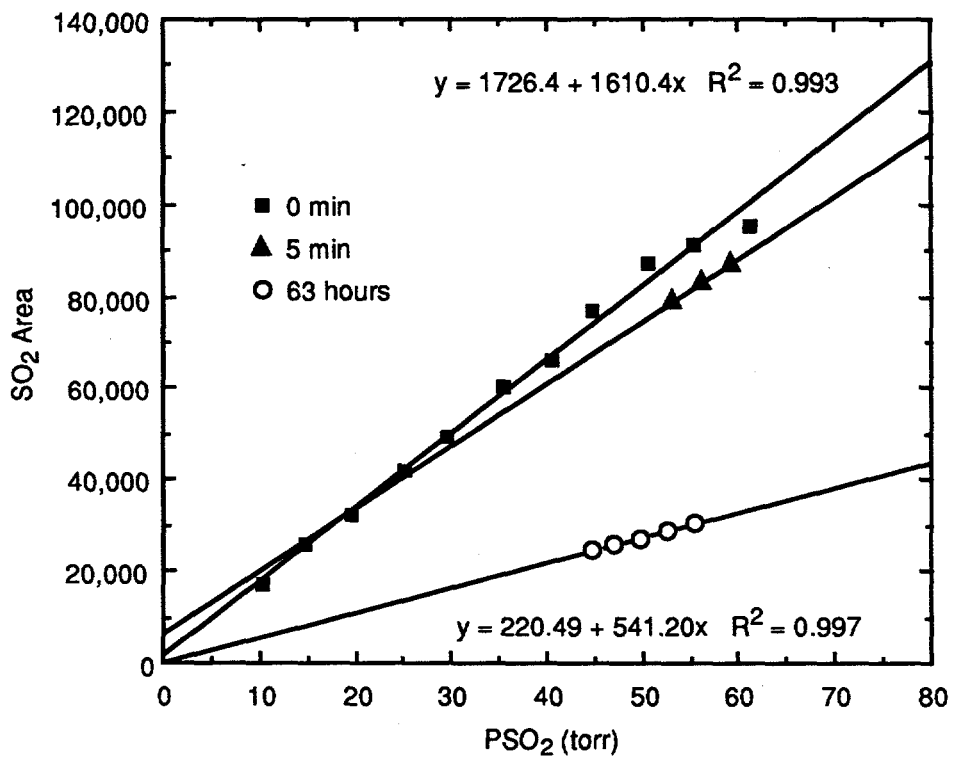
<u>Liquid</u>	<u>Run No.</u>	<u>Initial Total Pressure</u>	<u>Final SO₂ Pressure (torr)</u>	<u>H*, Transducer</u>	<u>H*, GC</u>
d-Siloxane	1	520.14	8.95	0.406	0.294
	2	520.16	8.80	0.457	0.293
	3	416.14	6.17	0.470	0.358
	4	274.14	2.68	1.056	0.513
d-DMA	1	418.95	4.86	0.468	0.347
	2	416.78	5.79	0.420	0.356
	3	417.13	6.62	0.421	0.364

For the same initial charge pressure, the siloxane and the d-DMA have similar H* values. However, since the d-DMA seemed to slightly lose some capacity with each run (increasing H*), the d-siloxane compound was initially thought to be more efficient. However, as discussed later, this loss in d-DMA's capacity is an artifact.

Understanding Discrepancies

Several tests were performed to examine the difference between GC and transducer-measured H* values.

In the first test, a blank run was made using an empty vial as the sample cell. The empty sample cell and head space were charged with 10.1% SO₂ gas and the system was left to stand for 63 hours. During this time, the pressure transducer measured no significant change in overall pressure. After this length of time, part of the gas was injected into the GC and the area of the SO₂ peak was measured. Next, a calibration of the GC was immediately performed using the same gas as that with which the system had been charged. Finally, another 10.1% SO₂ sample was charged into the system and allowed to stand just 5 minutes. This sample was then injected into the GC. Figure 2-12 plots the results from these three sets of injections. Since no liquid absorbent was present, the three lines should collapse onto each other. Because this is not the case, it appears that SO₂ is being lost over time.



CAM-3501-54

Figure 2-12. Calibration curves after 10.1% SO₂ was left standing in an initially empty absorption apparatus.

Since it was evident that this loss of SO₂ may be interfering with test results, tests similar to the one detailed above were performed to isolate sections of the apparatus that were responsible for the loss of SO₂. Also, a similar test was run using CO₂ instead of SO₂ to ensure that the problem was SO₂-specific; and it was. The SO₂ loss was found to be occurring in the valve just above the sample cell in the apparatus (valve 3). When the valve was taken apart, some residual matter was found, presumably the remnants of one or more previous experiments. Perhaps the residue had been splattered into and collected by the valve during a run. Since the valve was contaminated, a new valve was ordered and put in place.

To prevent splattering from occurring in the future, the sample vial design was modified by partially blocking off the neck of the vial. This modification allowed gases to flow through easily, and minimized liquids from being splashed directly onto the valve. We decided to retest some of our previous samples with the new valve.

The first few retests were made to ensure that the contamination problem had been corrected. These tests consisted of charging the head space and sample cell (with no absorbent present) with 10.1% SO₂ gas and allowing the system to stand for approximately 42 hours. After this period of time, the gas in the apparatus was analyzed with the gas chromatograph and compared with a calibration curve that had been made using the 10.1% SO₂ gas. These tests showed that the contamination problem had been solved, within the error limits of our experiments.

Final Selection

Since the tests performed previously on the dimer DMA (d-DMA) were not necessarily valid (it was not known whether the contamination occurred before or after the tests), four d-DMA tests were repeated. The results of these tests are shown in Table 2-9. In reading this table, recall that H* is defined as the volume of liquid needed to absorb an unit volume of SO₂ at STP and has the units of cm³ liq/cm³ (STP) SO₂.

Table 2-9
SO₂ SORPTION BY DIMER DMA

Run No.	Initial Total Pressure (torr)	Final SO ₂ Pressure (torr)	H*, Transducer	H*, GC
1	764.51	4.96	0.538	0.442
2	762.81	4.853	0.552	0.442
3	953.23	3.60	0.794	0.339
4*	502.85	2.98	0.663	0.995

* A large leak occurred during run 4, making the data for run 4 questionable.

Runs 1 and 2 were with one batch of d-DMA while runs 3 and 4 were with another batch. Runs 1 and 2 gave the same H^* , a result we did not observe in our previous set of runs. In the earlier runs, we observed a decrease in sorption capacity with each run. Runs 3 and 4 are using a second batch of d-DMA and may involve leaks. These data are more suspect.

Moreover, the values of H^* for these tests are slightly higher than the values found in earlier tests on d-DMA. The earlier H^* values were closer to 0.35 in the GC calculations (see Table 2-5). This difference is most likely the result of contamination, which made the initial capacity seem better. We now believe d-DMA may be a good candidate for SO_2 absorption and plan to continue reversibility tests with it.

After the last dimer DMA run was made, some oil from the vacuum pump leaked into the system, contaminating the lines and valves. Contaminated parts were either cleaned or replaced.

After the repairs to the apparatus were completed, we decided to use pure SO_2 for the remaining SO_x absorption experiments. This enabled us to run the experiments with a smaller head space in the apparatus, which resulted in quicker run times and less gas leaks. We installed the pure SO_2 gas cylinder into the gas cabinet.

The concentration of this cylinder is 99.98% SO_2 (Liquid Carbonic; San Carlos, CA). We ran two new sets of experiments on the d-DMA to determine its reversibility for SO_2 absorption. The first set had a temperature of 35°C, and the second set had a temperature of 50°C. In each experiment, we placed approximately 0.5 mL of d-DMA into the sample cell of the SO_2 absorption apparatus. During the 35°C run, we pressurized the apparatus to 900 torr with 99.98% SO_2 . Then we exposed the sample to the gas and recorded the final equilibrium pressure above the sample cell. After the SO_2 pressure reached a steady state, we evacuated the space above the sample cell with a vacuum pump to remove the SO_2 absorbed into the d-DMA. After the d-DMA was free of SO_2 , we repeated the run with the same sample at the same temperature. This absorption run was performed five more times. For the 50°C experiments, we used a fresh 0.5-mL sample of d-DMA in the absorption apparatus. Then, we repeated the absorption and desorption runs as done before with the 35°C sample.

The data from both the 35°C and the 50°C experiments were used to calculate d-DMA's capacity for SO_2 absorption in each run. As stated earlier, the absorption capacity is defined as H^* , having units of cm^3 d-DMA/ cm^3 (STP) SO_2 . These values are shown as a function of their experimental run number in Figure 2-13. For the first few experiments, the H^* values of d-DMA at 35°C and 50°C are similar, indicating that, initially, d-DMA's SO_2 absorption capacity is independent of flue gas temperature. During the later runs of the experiments, d-DMA at 50°C

shows an increase in H^* , leading to lower absorption capacity. Also in Figure 2-13, the H^* for the 50°C d-DMA still appears to be increasing. Therefore, additional experiments were conducted with the same sample and temperature to determine its final value for H^* .

The absorption capacity for SO_2 is characterized by H^* , which has units of cm^3 d-DMA/ cm^3 (STP) SO_2 . For a constant volume of d-DMA, a large H^* would denote a small SO_2 absorption capacity, and a small H^* would signify a large absorption capacity. As stated above, we observed that H^* at 50°C for the fifth run increases significantly (Figure 2-13), and again decreased on the sixth run. Therefore, not much SO_2 was absorbed on the fifth run, but more of it was absorbed on the sixth one.

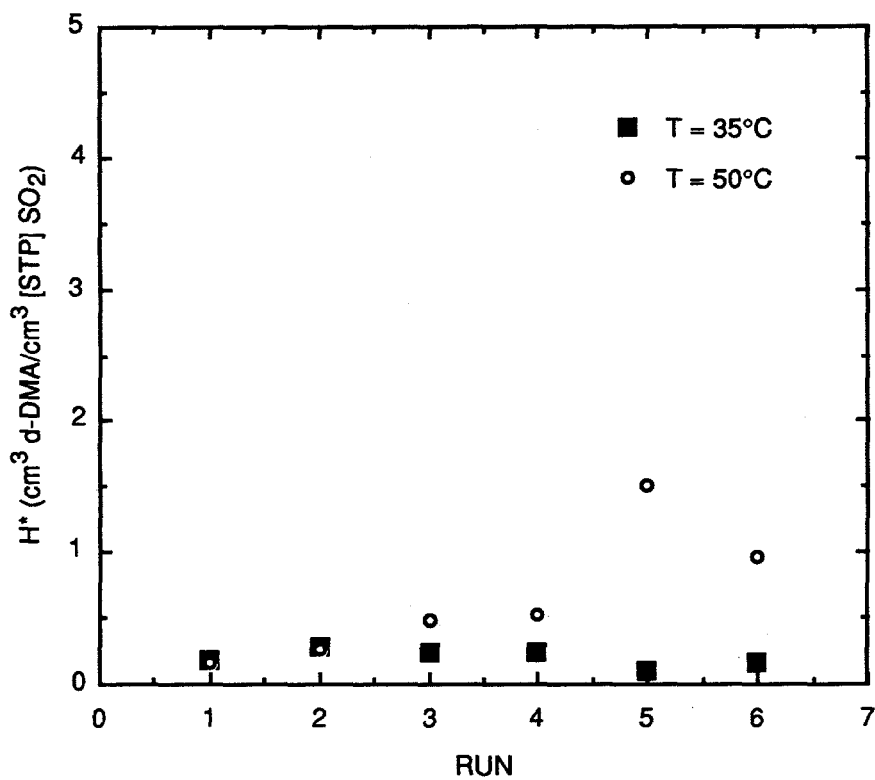
We followed the same procedure as before for measuring d-DMA's SO_2 absorption capacity. Six more runs were performed with the same 0.5 mL sample of d-DMA at 50°C. The H^* values for these runs were then calculated and plotted in Figure 2-14. In this figure, the first six runs are the ones reported in Figure 2-13. Runs 7 through 12 show a higher absorption for SO_2 than runs 5 and 6. Also, the H^* values of runs 9 through 12 are similar to the ones observed in the earliest runs of this d-DMA sample. A probable reason for the higher values of H^* in runs 5 and 6 could be that the d-DMA was not sufficiently desorbed of its SO_2 from the previous run. This would be the cause for its lower absorption capacity during these two runs. Therefore, d-DMA's ability for absorbing SO_2 does not degrade upon repeated exposure to SO_2 at the temperature of 50°C. Our next step will be to increase the temperature to 100°C and perform another run.

NO_x ABSORPTION

Absorption Studies

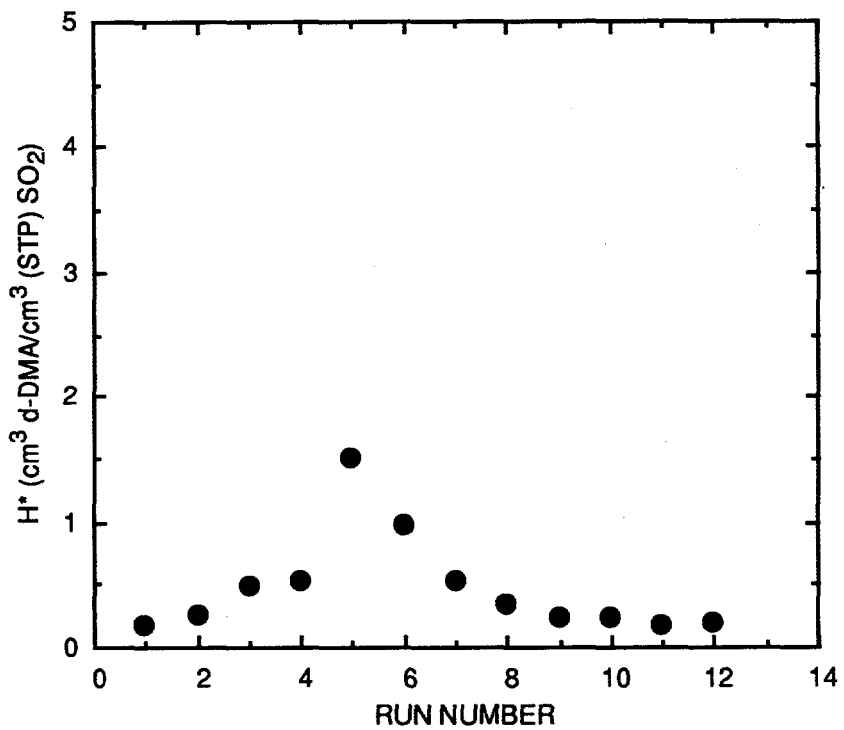
The completed assembly of the NO_x -absorption apparatus is shown in Figure 2-15. A mixture of NO_x/N_2 is blended with N_2 and humidified by passing it through a bubbler containing deionized water (Millipore Milli-Q Water Purification System) and then scrubbed by passing it through another bubbler containing a NO_x -absorbing solution. The NO_x depleted gas emerging from the second bubbler is sent to the NO_x analyzer. By monitoring the flow rates and the inlet and outlet NO_x concentrations at the bubblers over time, we can calculate the amount of NO_x absorbed by the solution. Initially, we tested our apparatus by duplicating experiments reported in the literature (Sada et al., 1984). Sada et al. report the equilibrium constant K at 35°C for the reaction





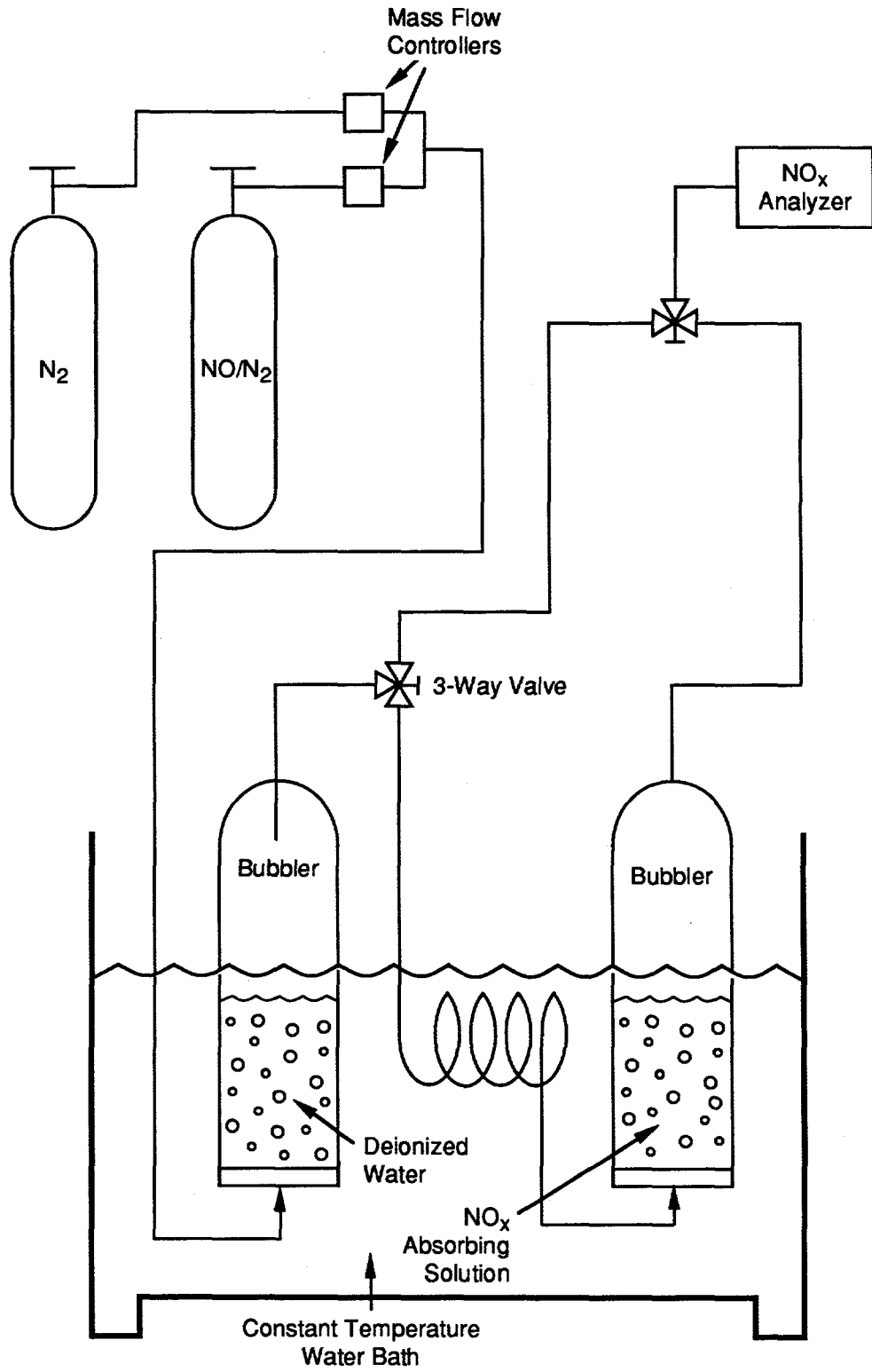
CAM-3501-76

Figure 2-13. SO₂ absorption lifetime of d-DMA at 35°C and 50°C



CM-3501-79

Figure 2-14. Lifetime SO₂ absorption/desorption run on d-DMA at 50°C.



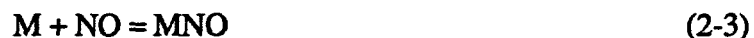
CM-4334-21A

Figure 2-15. NO_x absorption apparatus.

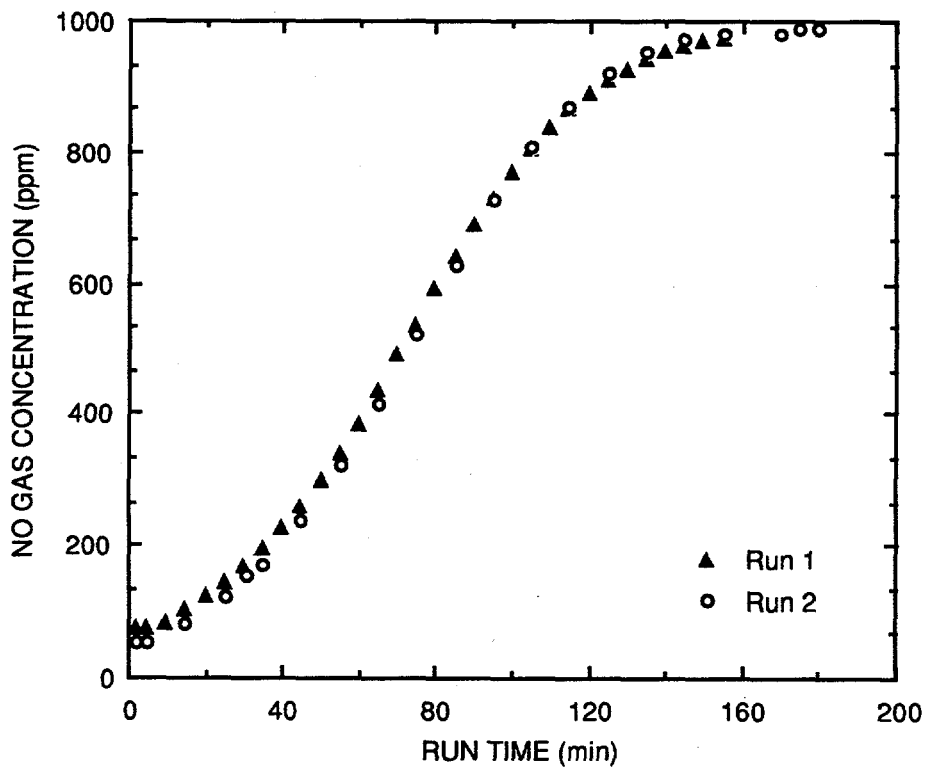
to be 9.9×10^5 L/mol. Our first goal was to duplicate this result using the NO_x absorption apparatus. A 900 sccm, 990 ppm NO/balance N_2 gas stream was used as the simulated flue gas. The NO_x -absorbing solution for this experiment was a 450-mL, 0.01-M solution of $\text{Fe}^{\text{II}}(\text{EDTA})^{2-}$ prepared by adding equimolar amounts of ethylenediaminetetraacetic acid disodium salt-dihydrate and ferrous sulfate-heptahydrate (both from Sigma Chemical Co., St. Louis, MO). The scrubbing solution was kept at 35°C , and the gas was humidified and preheated to 35°C before entering the bubbler. The exiting gas stream was sent to the NO_x analyzer where its NO concentration was recorded over time. The experimental run was stopped once the exiting gas stream's NO concentration reached the inlet concentration. This experiment was performed twice to test the reproducibility of the apparatus. The results of the two experiments are shown in Figure 2-16. These data were then used to calculate the equilibrium constant (K) for the reaction shown in Eq. (2-2). Details of this calculation are given in Appendix C. The values of K from both experiments were calculated to be 9.41×10^5 L/mol and 1.03×10^6 L/mol, respectively. They are close to one another, indicating reproducibility, and are within 5% of that reported by Sada et al.

In our next series of experiments, we performed additional NO_x -absorption runs with solutions of Fe(II)-EDTA, Fe(III)-phthalocyanine, Fe(II)-phthalocyanine, Co(II)-phthalocyanine, Ni-phthalocyanine, and Cu-phthalocyanine-3,4',4'',4'''-tetrasulfonic acid, tetrasodium salt, 85% pure (Aldrich Chemical Company, Inc., Milwaukee, Wisconsin) (Refer to Task 3 of this report for synthesis procedures). These experiments were conducted with a 0.02 M NO_x -absorbing solution, a flue gas concentration of 100 ppm NO, and a gas/liquid temperature of 25°C , similar to the NO_x scrubbing experiments with the hollow fiber contactor (Task 5). In all the absorption runs, a 50-mL volume of a NO_x -absorbing solution was used; other conditions were similar to the two previous NO_x -absorption runs.

The results from these experiments are shown in Figure 2-17. Note that we have plotted the axes in dimensionless quantities: C/C_0 versus Qt/V , where C is the measured exiting NO concentration, C_0 is the inlet NO concentration, Q is the gas flow rate, t is the run time, and V is the liquid volume. As outlined in Appendix C, these results may be used to calculate the reaction equilibrium constant K of the reaction

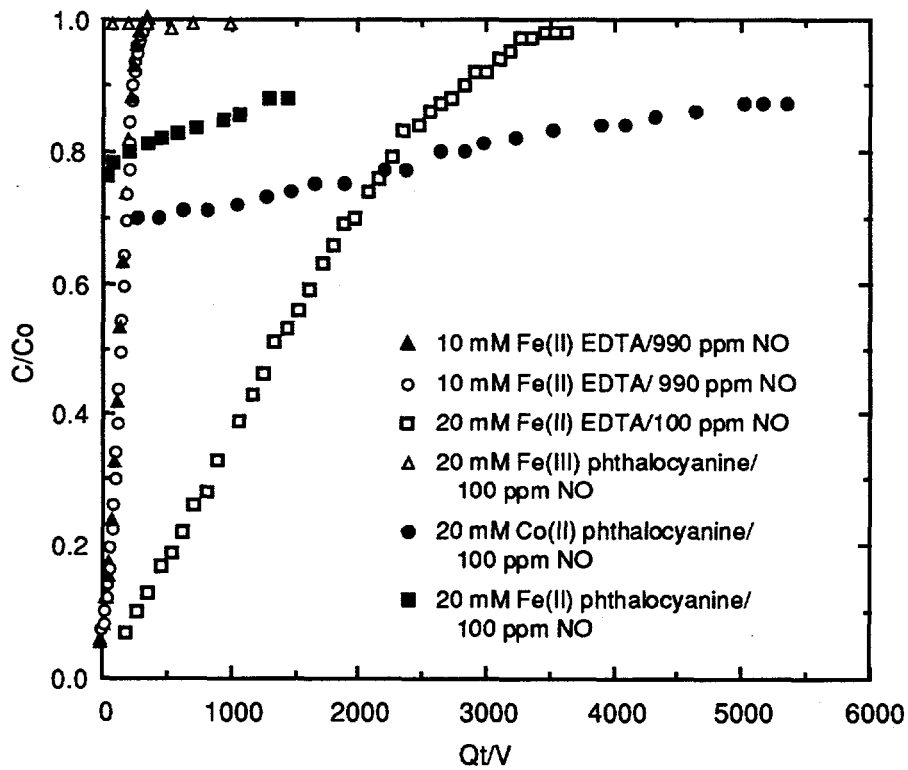


where M represents the NO-binding compound. The results of this exercise are given in Table 2-10. As shown in the table, the K value for the 0.02 M Fe(II)-EDTA solution is higher than the one for the 0.01 M solution (reported above). We believe that is due to the lower temperature.



CAM-3501-56

Figure 2-16. Exiting NO concentration versus time for the 10-mM Fe(II)-EDTA/990-ppm NO runs.



CAM-3501-57A

Figure 2-17. NO concentration over time for different scrubbing agents.

Table 2-10
EQUILIBRIUM CONSTANTS (K) USING 100 ppm NO IN N₂ AND
0.02 M AQUEOUS NO_x-ABSORBING SOLUTIONS AT 25°C

<u>Compound</u>	<u>Equilibrium Constant, K (L/mol)</u>
Fe(II)-EDTA	2.89 x 10 ⁶
Fe(III)-phthalocyanine	0
Fe(II)-phthalocyanine	3.41 x 10 ⁵
Co(II)-phthalocyanine	2.03 x 10 ⁶
Ni-phthalocyanine	0
Cu-phthalocyanine	0

Also in Table 2-10 are the K values found for the phthalocyanine solutions. K could not be calculated for Fe(III) phthalocyanine, Ni-phthalocyanine, or Cu-phthalocyanine solutions because NO_x removal was not observed. Overall, the Fe(II)-EDTA solution is the best NO_x-absorbing compound followed by Co(II)-phthalocyanine and by Fe(II)-phthalocyanine. The Co(II)-phthalocyanine did absorb almost as much NO_x as the Fe(II)-EDTA, but it appears the kinetics to do so are much slower. However, this may not be an issue since kinetics do not usually dominate absorption in a hollow fiber contactor; mass transfer does.

We also repeated the experiment of determining the NO absorption capacity of Fe(II)-EDTA (described above) to see if our results would be reproducible at 100 ppm NO. A 50-mL, 0.02-M Fe(II)-EDTA solution was made by mixing equimolar amounts of FeSO₄ • 7 H₂O and Na₂-EDTA. As before, gas from a 1.04% NO/balance N₂ cylinder was diluted by adding N₂ to form a 900-sccm, 100-ppm NO feed stream. The feed was sent through the NO_x-absorbing apparatus where it was heated, humidified, and contacted with the Fe(II)-EDTA solution. The temperature of the gas and of the Fe(II)-EDTA was set at 25°C. The exiting NO concentration was monitored over time by the NO_x analyzer until it reached the feed's concentration of 100 ppm NO.

The results of this experiment are very close to those of the original Fe(II)-EDTA experiment. As shown in Figure 2-18, the breakthrough curves from both experiments are similar. Also, the calculated equilibrium constants, K , for the reaction listed in Eq. (2-2) from both experiments agree closely. In the first experiments reported in Table 2-10, K was found to be 2.89×10^6 L/mol. In this experiment, K was calculated to be 2.7×10^6 L/mol. These values differ only by 6.5%. Therefore, we have confirmed the NO absorption capacity for Fe(II)-EDTA for 990 ppm and 100 ppm NO feeds.

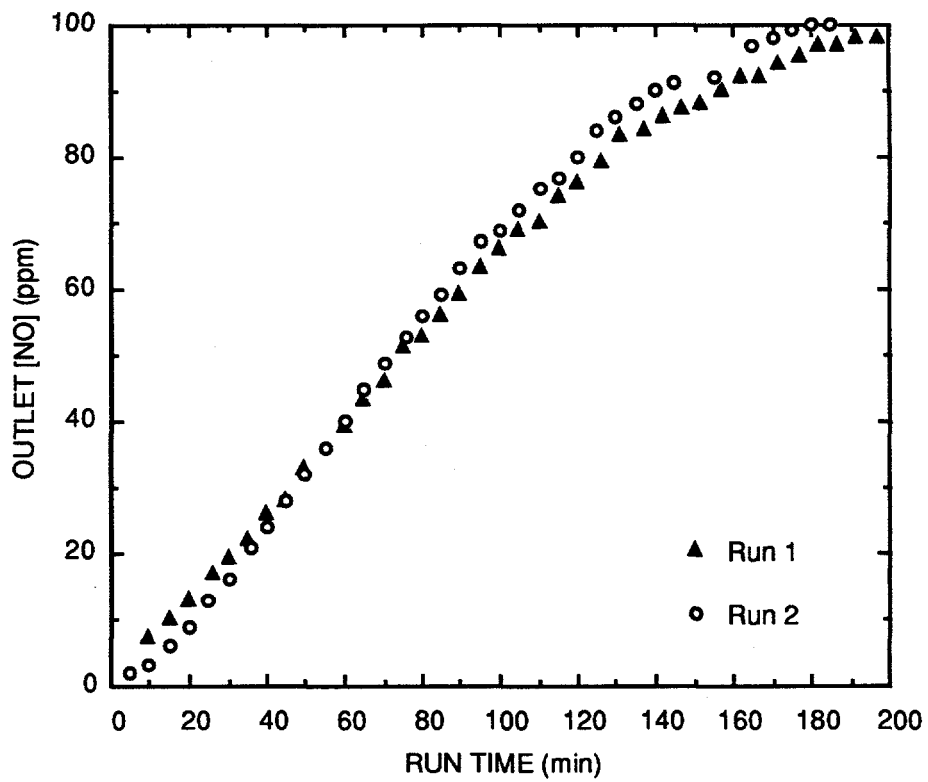
We also tested a series of new NO_x-absorbing compounds, and we modified the NO_x-absorbing apparatus to fit the characteristics of these new scrubbing compounds.

We continued the research work in two directions. To better understand the NO_x absorption chemistry, we modified our original NO_x absorption apparatus to continuously monitor the pH of the absorbing solution, as shown in Figure 2-19. The pH variation of the solution with NO loading would provide us with more insight into the chemical interactions of the species present in the solution. Also, several experiments were conducted using the modified apparatus after its testing with the base case of Fe(II)EDTA solution. The objective of these experiments was to test new chemicals as well as to reexamine already tested chemicals with feed gas streams containing representative compositions of coal-burning power plant flue gases.

Effect of Oxygen

Flue gases from coal-burning utility stations often consist of several hundred ppm of NO and 3% to 4.5% of O₂. We incorporated these compositions into our experimental runs to simulate realistic conditions. Approximately 50 mL of the polymeric analogue to Fe(II) EDTA (synthesis described in Task 3 at two pH, 6 and 4.2) was tested for NO absorption capacity. The feed gas flow rate for these experimental runs was 900 sccm (500 ppm NO with balance N₂). The newly synthesized chemicals did not exhibit any NO absorption and hence are not considered in further work.

It has long been established in the literature that iron chelates oxidize in the presence of O₂, which deactivates their activity toward absorption of NO. From our past experimental data on nonferrous chelates (Table 2-10), it is evident that Co-phthalocyanine is another promising candidate agent. Therefore, we conducted an experimental run using 50 mL of 0.02 M Co-phthalocyanine solution with 4.5% O₂ in the feed gas stream. The variation of outlet NO concentration and pH of the solution with time are shown in Figure 2-20. The equilibrium constant (K) is calculated to be 5.2×10^6 L/mol. This encouraging high K value in the presence of oxygen prompted us to take this absorption chemistry further in Task 5 where we studied the NO-absorption behavior in an HFC.



CAM-3501-58

Figure 2-18. NO_x-absorbing runs using 20 mM Fe(II)-EDTA and 100 ppm NO.

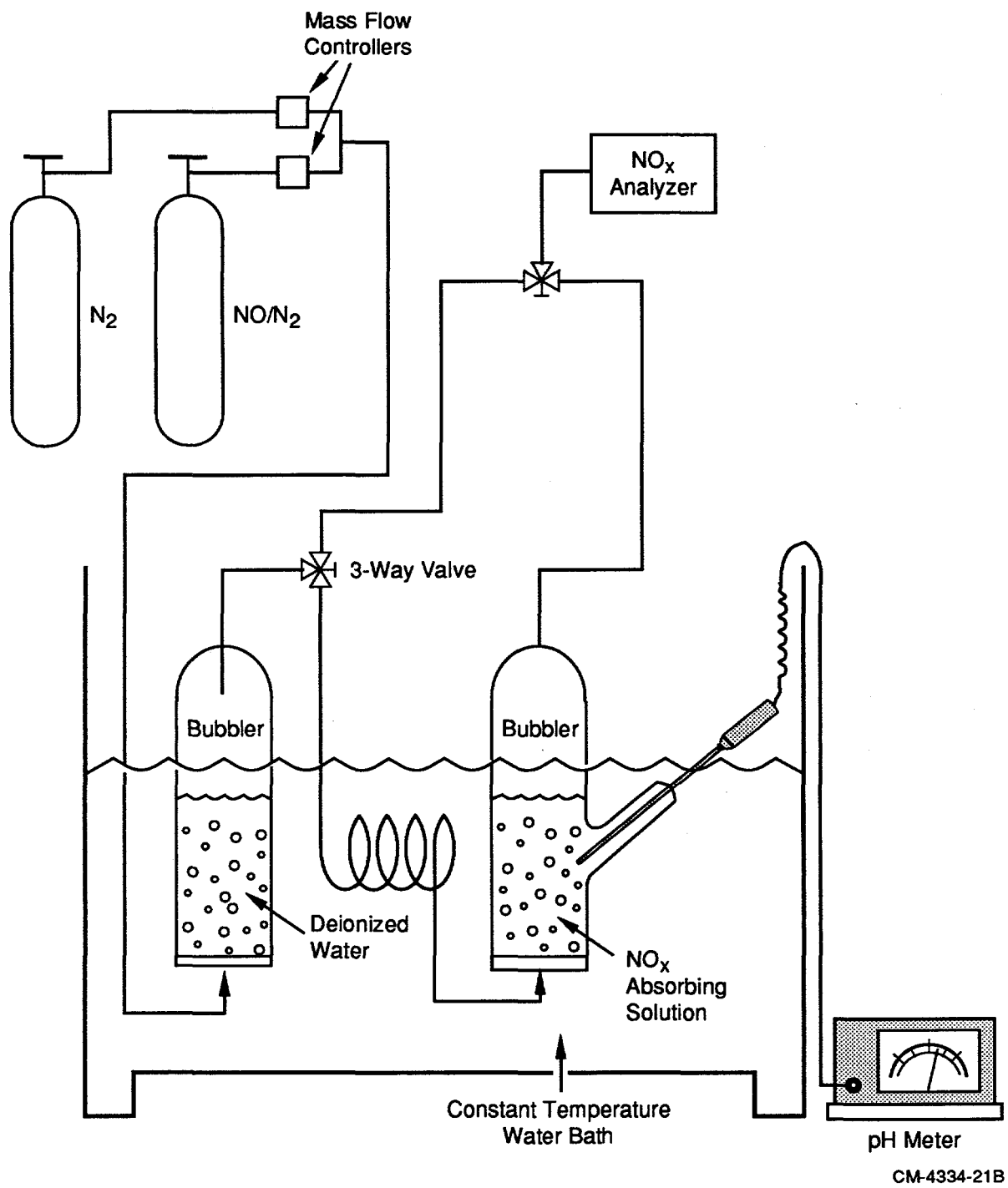
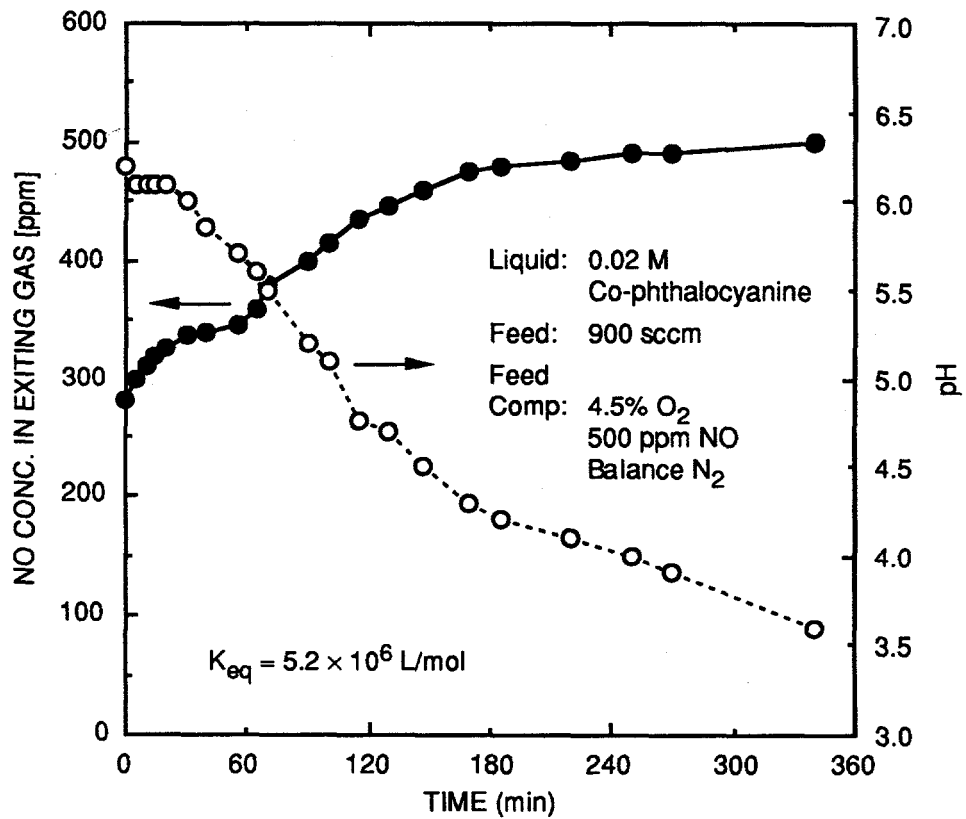


Figure 2-19. Experimental flowsheet for NO_x absorption tests with on-line pH measurement.



CM-3501-62

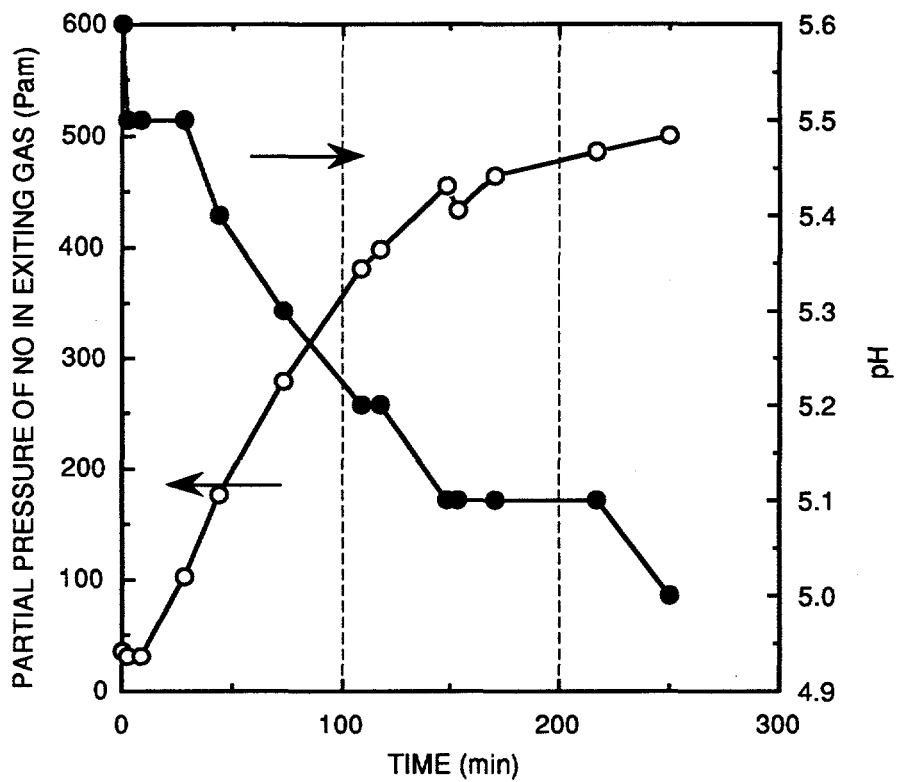
Figure 2-20. NO absorption by Co(II)-phthalocyanine in the presence of oxygen.

Next, we performed two new NO_x absorption experiments with two absorbing solutions: Co(II)-phthalocyanine and Co(II)-EDTA. The gas composition for both the experiments were 500 ppm NO, 4.5% O₂, and balance N₂. From our previous NO_x absorption experiments with Co(II)-phthalocyanine, we noticed that this solution had a NO_x capacity comparable to Fe(II)-EDTA. However, the kinetics of the NO complexation reaction in the cobalt solution were slower than that of the Fe(II)-EDTA. This behavior is shown in Figure 2-20 where the slope of NO concentration of the gas leaving the absorption bubbler is tending to be flat (slope ~ 0) with time. In all the earlier Fe(II)-EDTA runs, the slopes of NO concentrations were steeper than the one shown in the figure. To overcome the slow kinetics of this solution, we conducted another 500 ppm NO absorption run using a 50-mL, 100-mM Co(II)-phthalocyanine solution at elevated temperatures.

The temperature of the aqueous liquid was heated to 50°C using a water bath. The results of this experiment are shown in Figure 2-21. As expected, increasing the concentration and the temperature of the cobalt solution increased the rate of the NO complexing reaction as pictured in Figure 2-21. The initial concentration of NO in the gas coming out of the bubbler reached nearly 30 ppm as opposed to 300 ppm in Figure 2-20. This shows that increasing the Co solution concentration and temperature has increased the rate at which NO was bound. The equilibrium constant, K, for this experiment was calculated to be 7.04×10^5 L/mol. As a result, we used this 100-mM Co(II)-phthalocyanine solution heated to 50°C in the NO_x scrubbing experiments for Task 5. These results are presented under Task 5.

From chemical synthesis work (Task 3), we received a 20-mM solution of Co(II)-EDTA, prepared by mixing equimolar amounts of Co(II) sulfate hydrate (Aldrich Chemical Co; Milwaukee, WI) and EDTA (Sigma Chemical Co., St. Louis, MO). We performed a NO_x absorbing experiment with 50-mL of the 20-mM Co(II)-EDTA solution. The temperature of the gas and the solution were maintained at 50°C. We ran this experiment to determine Co(II)-EDTA's ability to bind NO. However, at the beginning of the run, we observed only 4% removal of NO using this compound. This implies that Co(II)-EDTA would not be a good candidate scrubbing solution for NO.

We are considering further tests with Co(II)-phthalocyanine as our prime candidate for replacing Fe(II)-EDTA as a NO_x absorbing compound.



CM-3501-71

Figure 2-21. Co(II)-phthalocyanine NO absorption capacity at 50°C.

TASK 3: CHEMICAL SYNTHESIS

The objectives of this task were to synthesize an oligomer of dimethylaniline (DMA) for our study of SO₂ liquor regeneration and to synthesize compounds suitable for reversible absorption of NO_x in aqueous solutions. We chose to make an oligomer of DMA for SO₂ liquor regeneration to reduce the vapor pressure of the SO₂ regeneration media, thereby minimizing any losses of the SO₂ regeneration chemical.

SO_x ABSORBENTS

We have identified two routes for synthesizing oligomers of DMA. In the first, as described in the original management plan, we convert low molecular weight poly(ethyleneimine) to the corresponding chloroamine polymer, followed by benzylation as shown in Figure 3-1. To standardize the chemistry of this approach, we use tetraethylenepentamine pentahydrochloride, shown in Figure 3-2. Chlorination and benzylation reactions are optimized on this model reagent before proceeding with the reaction on the polyethyleneimine oligomer.

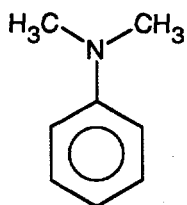
In the second route, we synthesize 1-phenylaziridine from the commercially available 2-anilinoethanol as shown in Figure 3-3. 2-Anilinoethanol is treated with sulfuric acid to afford the desired 2-anilinoethyl sulfate. Cyclization to yield 1-phenylaziridine is then accomplished by treatment with aqueous sodium hydroxide. Conventional ring-opening polymerization is then carried out.

To date, we have synthesized several polymers of DMA, all via the second synthesis route. The first, an oligomer of DMA, resulted in an insoluble (to most solvents) solid that is unsuitable for use as an absorbent. Second, to produce a liquid material, we synthesized DMA copolymers. A 50:50 (mole ratio) copolymer of N-phenylaziridine and propyleneimine also resulted in a solid. Third, reducing the ratio of N-phenylaziridine to propyleneimine ratio to 30:70, however, produced a viscous liquid at room temperature. Fourteen grams of the 30:70 copolymer were prepared to study its absorption properties. The reaction scheme for the DMA oligomer is shown in Figure 3-4, and for the copolymer in Figure 3-5. Details of the synthesis procedure follow.

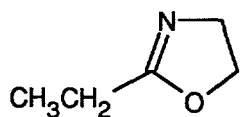
Synthesis of the Oligomeric Dimethylaniline (o-DMA)

We prepared o-DMA by polymerization of N-phenylaziridine according to the four-step scheme shown in Figure 3-4.

Dimethylaniline (DMA):

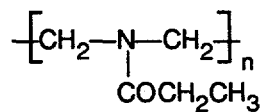


Synthesis of Oligomer of DMA:

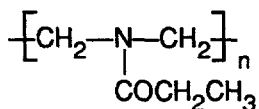


2-ethyl-oxazoline

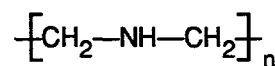
Methylsilylate
(Catalyst)



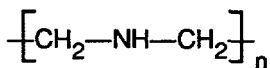
Poly[N-(carboxyethyl)-ethyleneimine]



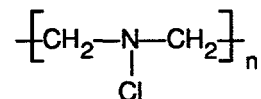
8 N HCl



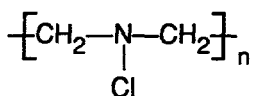
Poly(ethyleneimine)



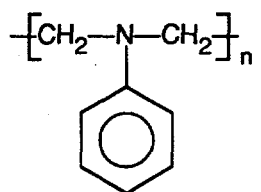
NaOCl



Poly(N-chloroethyleneimine)



Benzene
96% H₂SO₄/Fe(II)



Oligomer of DMA

CAM-360583-47A

Figure 3-1. First route for synthesis of oligomer of DMA.



CM-3501-1

Figure 3-2. Tetraethylenepentamine pentahydrochloride in the first synthesis route.

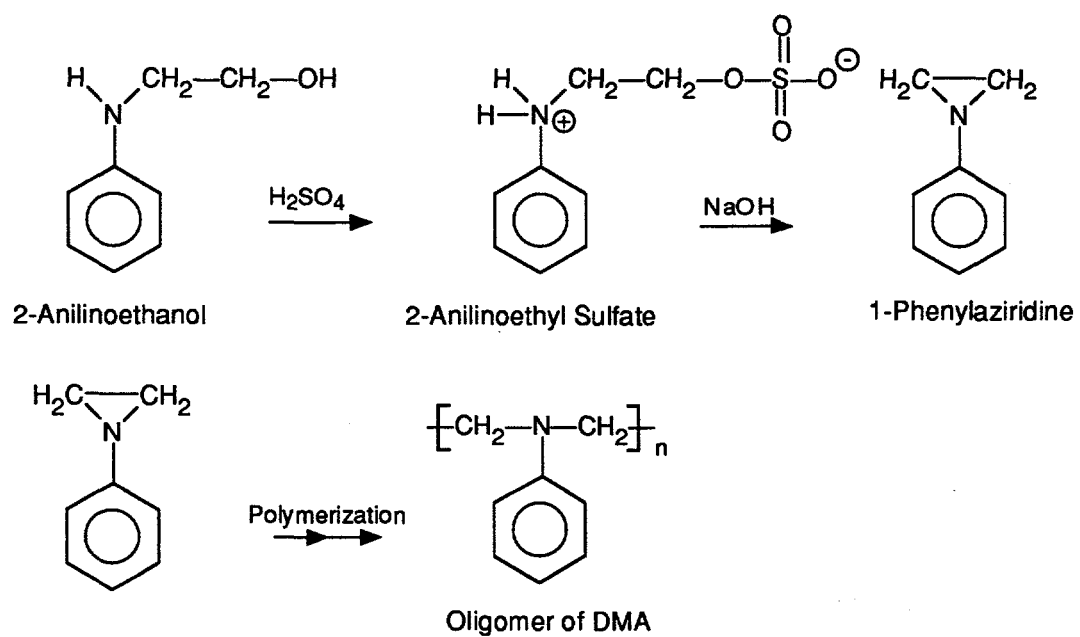


Figure 3-3. Second route for synthesis of oligomer of DMA.

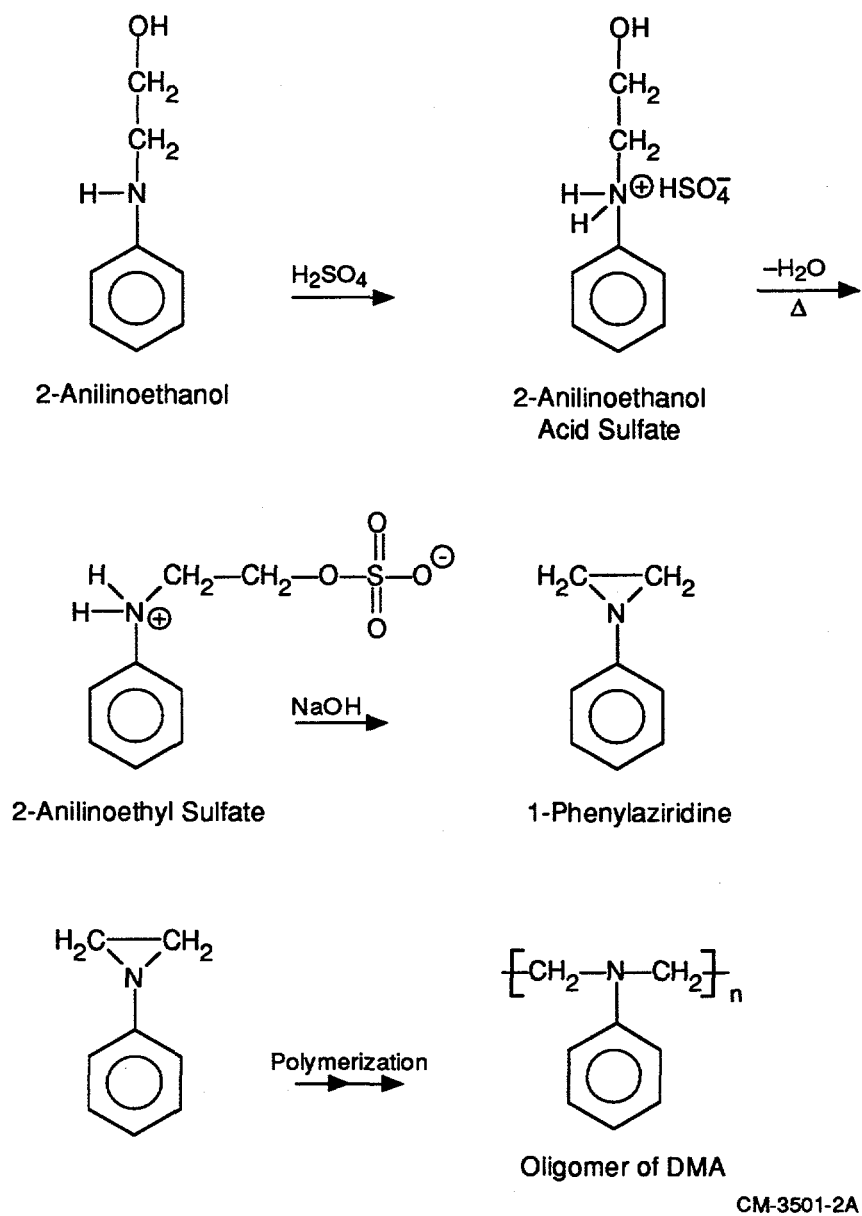
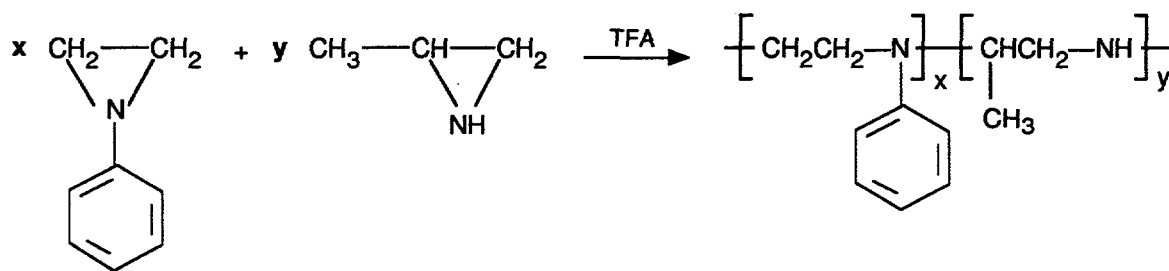


Figure 3-4. Reaction scheme for synthesis of oligomer of DMA.



CM-3501-5

Figure 3-5. Copolymerization scheme of N-phenylaziridine and propyleneimine.

Step 1: Synthesis of 2-Anilinoethanol Acid Sulfate. 2-Anilinoethanol (13.7 g, 0.1 mol) was diluted with water (13.7 g) and cooled to 0°C. This solution was added to 96.4% H₂SO₄ (10.1 g, 0.1 mol) diluted with 10.1 g of water. After mixing, the water was removed by rotary evaporation, and the product was precipitated out by addition of acetone. The mixture was thoroughly stirred, and the solid product was filtered and dried to give a white solid (yield: 22 g, 93%). The product was characterized by ¹H NMR: (δ, D₂O): 3.3 - 3.8 (m, 4 H), 7.5 (s, 5H).

The thermal gravimetric analysis of the product showed three steps of decomposition on heating from 40°C to 550°C. The first step begins at 125°C and ends at 150°C due to the loss of water, the reaction desired for Step 2 of the synthesis.

Step 2: Synthesis of 2-Anilinoethyl Sulfate. 2-Anilinoethanol acid sulfate (4.7 g, 0.02 mol) was heated at 130°C under a vacuum of 5 mmHg for one hour to yield quantitatively the desired product (2-anilinoethanol sulfate). Upon heating, the starting material melted and water condensed out to yield a pale brown viscous liquid that turned into a glassy solid after cooling to room temperature. The solid was stirred with methanol, filtered, and dried to yield the product (4.2 g, 96.7% yield).

Step 3: Synthesis of 1-Phenylaziridine. A solution of 2-anilinoethylsulfate (136 g, 0.63 mol) and sodium hydroxide (100 g, 2.5 mol) in water (800 mL) was stirred at 110°C for 90 minutes, during which the color changed from clear gray to dark brown and finally to yellow. This solution was then steam-distilled at 160°C; we separated the product from the condensate by extraction with ether, forming a turbid aqueous layer and a pale yellow organic layer. More product was extracted into the organic layer (the aqueous layer turned clear) by addition of potassium hydroxide (20 g) to the aqueous phase. The ether solution was dried over anhydrous sodium sulfate, the ether was evaporated off, and the remaining yellow liquid was distilled at 64.4°C and 10.1 mmHg, resulting in a 65% yield of 1-phenylaziridine. The product was characterized by FT-NMR: ¹H-NMR (δ/CDCl₃): 2.15 (s, 4 H, CH₂), 7.2 (m, 5H, aromatic H).

Step 4: Polymerization of 1-Phenylaziridine. The polymerization procedure is the same as that described below for the propyleneimine/N-phenylethyleneimine copolymer except that only freshly distilled N-phenylaziridine was used.

Preparation of Propyleneimine and N-Phenylethyleneimine Copolymer (70:30)

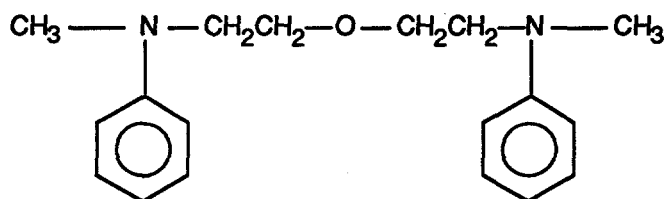
Because the homopolymer of N-phenylaziridine was found to be a solid that was insoluble in most organic solvents, we decided to copolymerize N-phenylaziridine with commercially available propyleneimine to optimize solubility and produce an amorphous or liquid polymer at room temperature.

The copolymerization was conducted in acetonitrile in the presence of trifluoroacetic acid (TFA) as catalyst. A strong acid catalyst was selected to favor the formation of an oligomer with low molecular weight. We found that the polymerization should be quenched after about 30 minutes to preferably yield an oligomer. Initially, we copolymerized N-phenylaziridine and propyleneimine in the relative molar ratio of 1:1. The resulting polymer was a waxy solid at room temperature. In an attempt to synthesize a liquid polymer, we reduced the relative ratio of N-phenylaziridine and propyleneimine to 30:70. In this case the resulting copolymer was a viscous liquid at room temperature. This polymer was found to be insoluble in water, while soluble in chloroform and only partially soluble in tetrahydrofuran. The polymerization scheme is shown in Figure 3-5 and the experimental procedure is described below.

Procedure for Preparing Propyleneimine and N-Phenylethyleneimine Copolymer.

Freshly distilled propyleneimine (6.4 g, 70 mole%, b.p. = 66°C) and N-phenylaziridine (5.73 g, 30 mole%, b.p. = 64°C/10.1 mm) were dissolved in acetonitrile (20 mL) in a 50-mL round-bottomed flask fitted with a stirring bar and a septum cap. The solution was stirred and cooled to -78°C in acetone/dry ice bath. Trifluoroacetic acid (3.66 g or 2.47 mL, 20 mole%) was then added through a syringe under stirring, and the acetone/dry ice bath was removed. The whole reaction mixture was brought to room temperature and stirred for 30 minutes. Benzylamine (3.37 g or 3.43 mL, 20 mole%) was added to quench the reaction, and the solution was stirred for 30 minutes. Acetonitrile was distilled off, and the residue was repeatedly washed with hexane (3 x 30 mL). After drying, a pale yellow viscous liquid was obtained (yield = 14 g). The product was characterized by FT-NMR: ¹H NMR (δ/CDCl₃): 1.1 (broad singlet), 2.0-3.0, (broad singlet), 4.0 (broad singlet), 6.4-7.4 (multiplet).

Synthesis of d-DMA. The structure of 2,2'-bis(N-methyl-N-phenyl)ethylether is shown below.



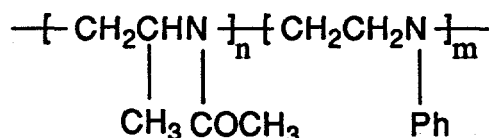
2,2'-bis(N-methyl-N-phenyl)ethylether

This compound consists of two DMA-analog functional groups linked by oxyethylene. Although we previously observed that even low molecular weight DMA oligomers are highly insoluble, this compound has good solubility in organic solvents because of the oxyethylene group. 2,2'-Bis(N-methyl-N-phenyl)ethylether represents a functionalized dimer of DMA (referred to as d-DMA) and

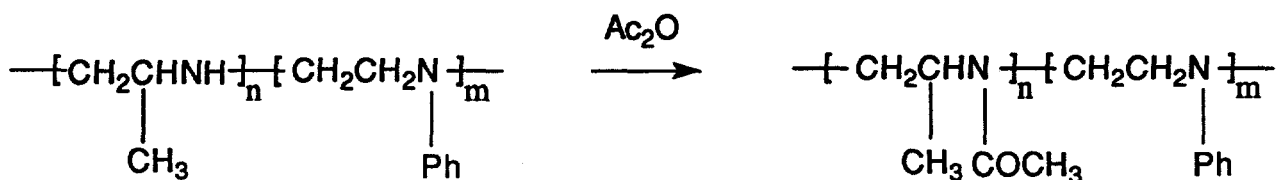
has been studied for its SO₂ liquor regeneration properties: its performance has been compared with that of DMA. Because of its higher molecular weight, d-DMA has a lower vapor pressure than DMA. The synthesis of 2,2'-bis(N-methyl-N-phenyl)ethylether is described next.

We added n-butyl lithium (1.28 g, 10 mL of 2 M n-butyl lithium in cyclohexane) dropwise to a stirred solution of N-methylaniline (2.14 g, 0.02 mol) in dry THF (20 mL) at -10°C under argon atmosphere. The reaction mixture was allowed to attain room temperature and stirred for 1/2 hour. Bischloroethyl ether (1.43 g, 0.01 mol) was added and the reaction mixture was refluxed overnight. The mixture was cooled and filtered to remove precipitated LiCl. Cyclohexane and THF were removed from the filtrate by rotary evaporation. The residue was dissolved in chloroform, washed with water and saturated NaCl solution, and dried over anhydrous Na₂SO₄. A brownish yellow liquid remained after rotary evaporation to remove chloroform. This liquid was distilled under vacuum to remove any unreacted starting materials. Thin layer chromatography indicated the product to be pure. The procedure yielded 2.5 g of 2,2'-bis(N-methyl-N-phenyl)ethylether (88% yield). The product was characterized by NMR: ¹H-NMR (S/CDCl₃): 2.98 (s, 6H, N-Me), 3.51 (t, 4H, CH₂O), 3.58 (t, 4H, CH₂-N); 6.7-7.3 (m, 10H, aromatic CH). ¹³C-NMR (ppm/CDCl₃): 38.98 (N-Me); 52.60 (CH₂O); 68.86 (CH₂N); 112.14, 116.27, 129.21 (o, m, p-phenyl CH); and 221.0 (aromatic >C<).

Synthesis of MAPA and AMAPA. Another compound synthesized for SO₂ liquor regeneration, acetylated poly(1-methylaziridine-N-phenylaziridine) is shown as follows.



This oligomer, abbreviated MAPA, was prepared by acetylation of the correspondent copolymer of 1-methylaziridine and N-phenylaziridine (described earlier). By acetylation of poly(1-methylaziridine-N-phenylaziridine), abbreviated AMAPA, we have converted the basic secondary amine to the correspondent amide with markedly lower basicity. This is expected to minimize possible irreversible adsorption of SO₂ at basic sites other than the DMA analog -CH₂(NPh)CH₂ functional group. The reaction scheme is illustrated as follows.



The starting copolymer (whose synthesis was described earlier) was dissolved in benzene and treated with anhydrous acetic anhydride at reflux for a few hours. The solvent was then evaporated off, and the functionalized polymer was isolated. The acetylation reaction was confirmed by FT-IR.

Synthesis of d-siloxane and p-siloxane

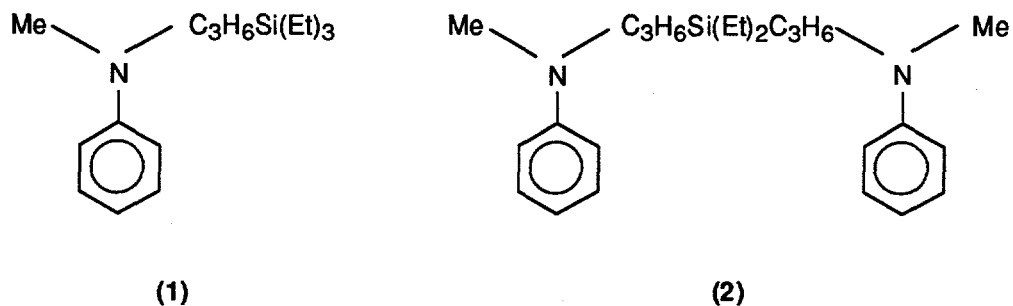
We also synthesized silicon-containing DMA analogs, structures for which are shown in Figure 3-6, and siloxane oligomers functionalized by DMA moieties, structures for which are shown in Figure 3-7. The low vapor pressure and viscosity of low molecular weight siloxane oligomers are very desirable properties of the newly developed SO₂ absorbent material.

The synthesis of (1) and (2) in Figure 3-6 is a two-step reaction: first N-methyl N-allylaniline is formed, followed by hydrosilylation reaction of trimethylsilane and dimethylsilane, respectively. The synthesis of (3) and (4) in Figure 3-7 is by hydrosilylation of tetramethyldisiloxane and pentamethylcyclopenta-siloxane with N-methyl N-allylaniline. The synthesis of (1) and (2) is presented next. The synthesis of (3) and (4) is similar.

Preparation of N-methyl N-allylaniline. To a solution of N-methylaniline (924.9 g, 0.23 mol) in dry THF (75 mL) at 0°C under argon atmosphere, n-BuLi in cyclohexane (116 mL, 2 M solution) was added dropwise under stirring. The reaction was stirred for 30 minutes at 0°C, and allylbromide (28 g, 0.23 mol) in dry THF (50 mL) was added dropwise to this yellow reaction mixture. Upon addition of allylbromide, the reaction mixture turned clear pale yellow. The reaction was stirred at room temperature for 30 min and then refluxed overnight. The reaction was cooled, and all the volatile materials were allowed to evaporate completely. The residue was taken in ethylether, washed with water (3 x 50 mL), and dried over anhydrous MgSO₄. The solvent was evaporated using a rotary evaporator. The residual pale yellow liquid was vacuum distilled, and the product was obtained in 88% yield (b.p. 66° - 68°C at 5 mmHg). The product was characterized by ¹H and ¹³C NMR.

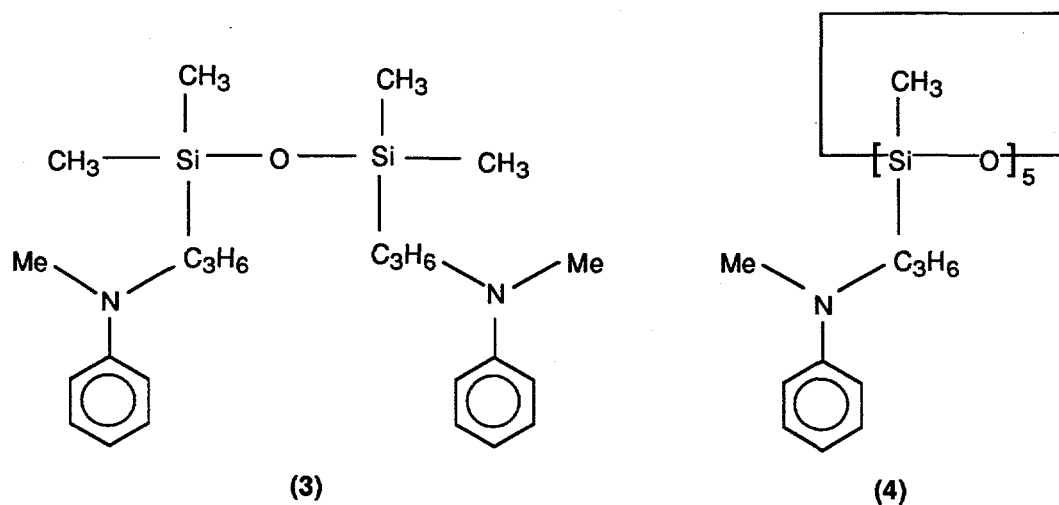
Hydrosilylation of N-methyl N-allylaniline. Hydrosilylation reactions were conducted in toluene at 80°C in the presence of chloroplatinic acid as a catalyst. The typical reaction time was 18 hours.

Compound (1) (Figure 3-6) was found to distill at 115°C at 0.38 mmHg, and compound (2) did not distill even at 130°C at 0.5 mmHg. The vapor pressure of these compounds is therefore significantly lower than that of DMA, which has a boiling point of 194°C at atmospheric pressure.



CAM-3501-35

Figure 3-6. Silicon-containing DMA analogs.



CAM-3501-36

Figure 3-7. Siloxane oligomers functionalized by DMA.

We also synthesized about 20 g of the dimer siloxane by hydrosilylation of tetramethyldisiloxane with N-methyl N-allylaniline, as described earlier. Low viscosity, high boiling point, low vapor pressure, and good reversibility make these promising materials for SO_x absorption.

NO_x ABSORBENTS

Our major focus in synthesizing an NO_x absorbent with high capacity lifetime and reversibility has been water-soluble phthalocyanine. Tetrasodium salts of cobalt (II) and iron (II) 4, 4', 4'', 4'''-tetrasulfophthalocyanine were synthesized as follows.

Tetrasodium Salt of Cobalt(II) 4, 4', 4'', 4'''-Tetrasulfophthalocyanine 2-Hydrate

The monosodium salt of 4-sulfophthalic acid (30 g, 111.9 mmol), ammonium chloride (3.3 g, 61.6 mmol), urea (40.8 g, 673.3 mmol), ammonium molybdate (0.5 g, 0.4 mmol), and cobalt(II) sulfate hydrate (5.1 g, 32.9 mmol) were ground together until homogeneous. (The monosodium salt of 4-sulfophthalic acid was obtained by neutralization of a 50% aqueous solution of 4-sulfophthalic acid with 15 N NaOH and purified by washing with 95% ethanol). The solid mixture was transferred to a 500-mL three-necked flask fitted with a condenser and a mechanical stirrer. After nitrobenzene (40 mL) was added to the flask, the reaction mixture was heated to 180°C for 10 hr and then allowed to cool to room temperature. The crude product was filtered, ground, and washed with methanol several times. Then, the dark black powder was stirred with 400 mL methanol for 24 hours, filtered, stirred with 400 mL methanol for another 24 hours and filtered. The resulting blue solid was dissolved in water (350 mL) and filtered. The filtrate was concentrated with a rotary evaporator and dried under vacuum at 60°C for 16 hours to get 26.0 g dark blue solid. (95%, λ_{max} , 656 nm, $\epsilon = 37000 \text{ M}^{-1} \text{ cm}^{-1}$).

Tetrasodium Salt of Iron (II) 4, 4', 4'', 4'''-Tetrasulfophthalocyanine 2-Hydrate

The monosodium salt of 4-sulfophthalic acid (30 g, 111.9 mmol), ammonium chloride (3.3 g, 61.6 mmol), urea (40.8 g, 673.3 mmol), ammonium molybdate (0.5 g, 0.4 mmol) and iron(II) sulfate heptahydrate (9.0 g, 32.4 mmol) were ground together until homogeneous. The solid mixture was transferred to a 500-mL three-necked flask fitted with a condenser and a mechanical stirrer. After nitrobenzene (40 mL) was added to the flask, the reaction mixture was heated to 180°C for 20 hours and then allowed to cool to room temperature. The crude product was filtered, ground, and washed with methanol several times. Then the dark black powder was stirred with 400 mL methanol for 24 hours, filtered, stirred with 400 mL methanol for another 24 hours, and filtered. The resulting blue solid was dissolved in water (400 mL) and filtered.

The filtrate was concentrated with a rotary evaporator and dried under vacuum at 60°C for 16 hours to get 22.5 g dark blue solid. (82%, λ_{\max} , 630 nm, $\epsilon = 30900 \text{ M}^{-1} \text{ cm}^{-1}$, $\lambda_{\max}(\text{sh})$, 664 nm, $\epsilon = 18000 \text{ M}^{-1} \text{ cm}^{-1}$).

One more metal phthalocyanine, the tetrasodium salt of copper 4,4',4'',4'''-tetrasulfophthalocyanine, was purchased from Aldrich. Because the purity of this compound is 85%, we attempted to purify it by precipitation.

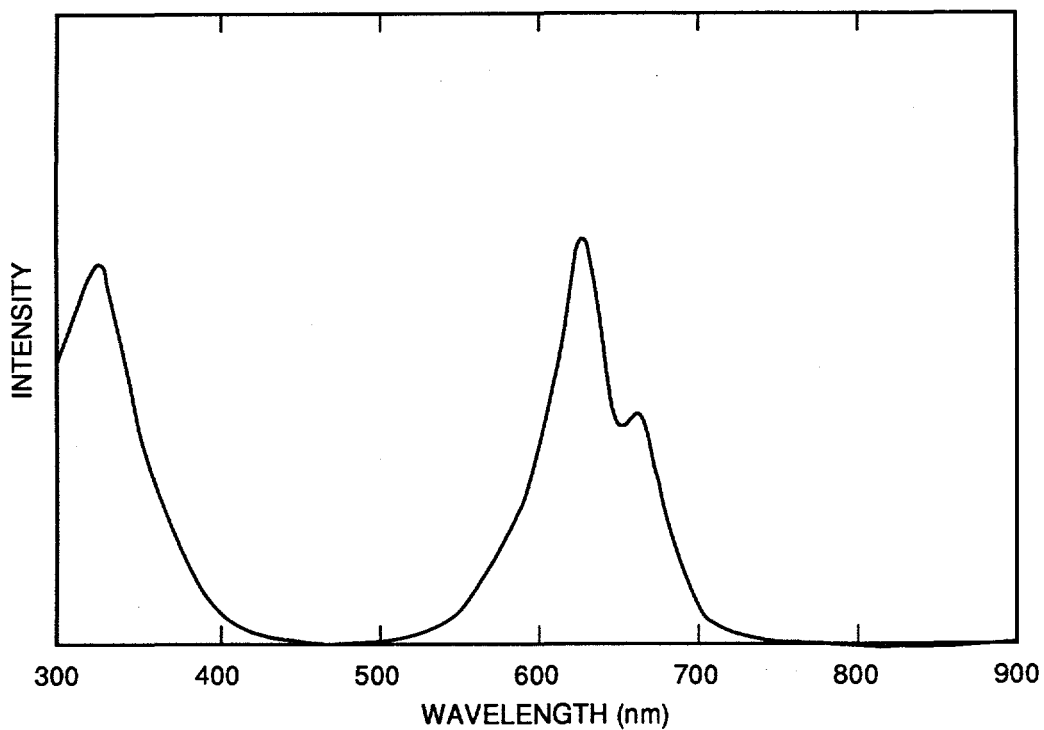
Also, an additional tetrasodium salt of iron 4,4',4'',4'''-tetrasulfophthalocyanine (about 160 g) was synthesized as previously described. A detailed analysis of the UV-visible spectrum of this phthalocyanine compound in water has shown that the phthalocyanine compound is constituted by a mixture of Fe(II) and Fe(III) phthalocyanines. As shown in Figure 3-8, the absorption maximum at 630 nm corresponds to the Fe(III) compound, while the shoulder at 664 nm is attributed to the Fe(II) compound. We intend to convert the Fe(III) phthalocyanine compound to the corresponding Fe(II) compound by either electrochemical or chemical reduction. We will initially attempt to use the electrochemical method because of the high reversibility of Fe(II)/Fe(III) transformation.

We electrochemically converted the Fe(III) phthalocyanine to the corresponding Fe(II) compound as follows. Electrolysis was performed on an aqueous solution of Fe(III) phthalocyanine (8 g in 100 mL) using a lead cathode and a platinum wire anode. The electrolysis was conducted under nitrogen using a current of 50 mA. It was not necessary to add any supporting electrolyte because of the ionic nature of the phthalocyanine compound. Therefore, after reduction, no further purification was necessary and the solution was directly used for NO_x absorbing tests. The reduction of Fe(III) phthalocyanine to Fe(II) phthalocyanine was monitored by VIS spectroscopy. Figure 3-9 compares the VIS spectra of Fe(II) and Fe(III) phthalocyanine. We also prepared the tetrasodium salt of Ni(II) 4,4',4'',4'''-tetrasulfophthalocyanine.

EDTA ANALOGS AS NO_x ABSORBENTS

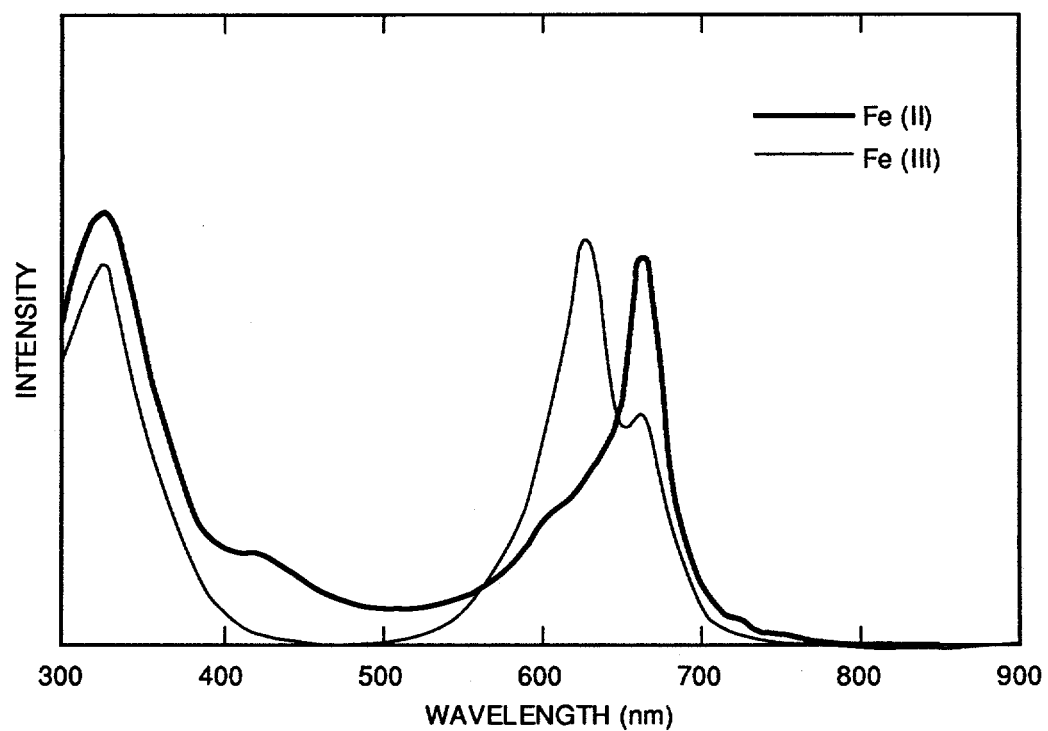
Nitric oxide is known to form a coordination complex with Fe^{2+} -EDTA whose reaction rates are very fast. The drawback of this chemistry is that the regeneration process has proved to be expensive because the Fe^{2+} species is oxidized readily to the ineffective Fe^{3+} species.

To overcome the limitations of the Fe^{2+} -EDTA NO_x removal process, we also developed polymeric analogs to EDTA. This approach was conducted in parallel to the development of phthalocyanine based sorbents. To date no information has been reported on the lifetime of polymeric analogs to EDTA, but we expect that their lifetime will vary with the nature of the polymer backbone and that the reversible absorption capacity for NO will vary with structural changes.



CM-3501-51

Figure 3-8. UV-visible spectrum of tetrasodium salt of iron 4,4',4'',4''' — tetrasulfophthalocyanine.

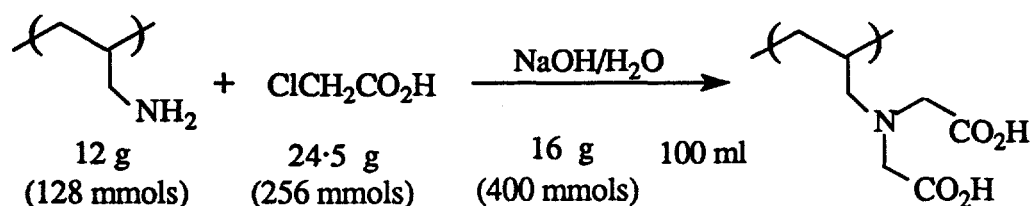


CM-3501-51A

Figure 3-9. Comparison of UV-visible spectra for Fe(II) and Fe(III) phthalocyanine.

As a result, we studied the synthesis of polymeric analogs to EDTA. To be of practical use, these polymers should be soluble in water. Accordingly, we initially focused on the functionalization of polyethyleneimine, a water-soluble polymer. In one approach, we functionalized poly(ethyleneimine) by alkylation with chloroacetic acid. The resulting polymer was found to be soluble in water. However, upon addition of Fe^{2+} , a crosslinked gel was formed. We believe that gelation is taking place because of the intermolecular formation of the Fe^{2+} complex. To minimize intermolecular complexation and instead favor the intramolecular process, it is desirable to functionalize the polymer with iminodiacetic acid. Accordingly, we attempted to functionalize polyethyleneimine with ethylenediaminetetracetic dianhydride. However, the resulting polymer was partially crosslinked.

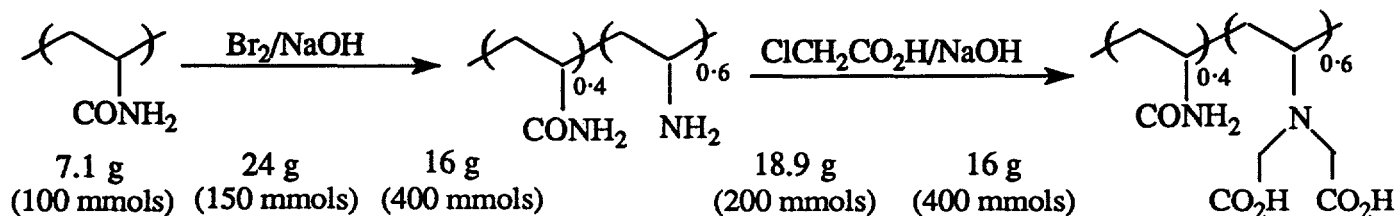
Synthesis of Poly(allylamine) Functionalized EDTA Analog



The reaction mixture was heated at 90°C for 4 hours. NMR indicated that there were small amounts of unreacted $\text{ClCH}_2\text{CO}_2\text{H}$. Additional 8 g of $\text{ClCH}_2\text{CO}_2\text{H}$ and 8 g NaOH were added, and the reaction was heated for an additional 4 hours.

After cooling to room temperature, the reaction mixture was acidified to pH 1.5 by concentrated HCl and a white precipitate was thus obtained. The product was filtered, washed with acetone, and dried. A solution of 20 mM of this polymer with FeSO_4 was prepared at pH 4.2 and pH 6 for further testing on NO_x absorption.

Synthesis of EDTA Analog Copolymer



A solution of hydroxyethyl ethylenediaminetriacetic acid (EDTA) and acryloyl chloride was stirred at 0°C for 2 hours and at room temperature for 1 hour. The excess of acryloylchloride and DMF was evaporated, yielding a syrupy product. The NMR spectrum of the material was consistent with the desired product.

Polymerization of the product was sluggish. Three portions of 100 mg of AIBN were necessarily added. The mixture was heated at 70°C for three days to bring the polymerization to completion. We plan to prepare Fe(II) and Co(II) complexes of the synthesized polyacrylate EDTA analog.

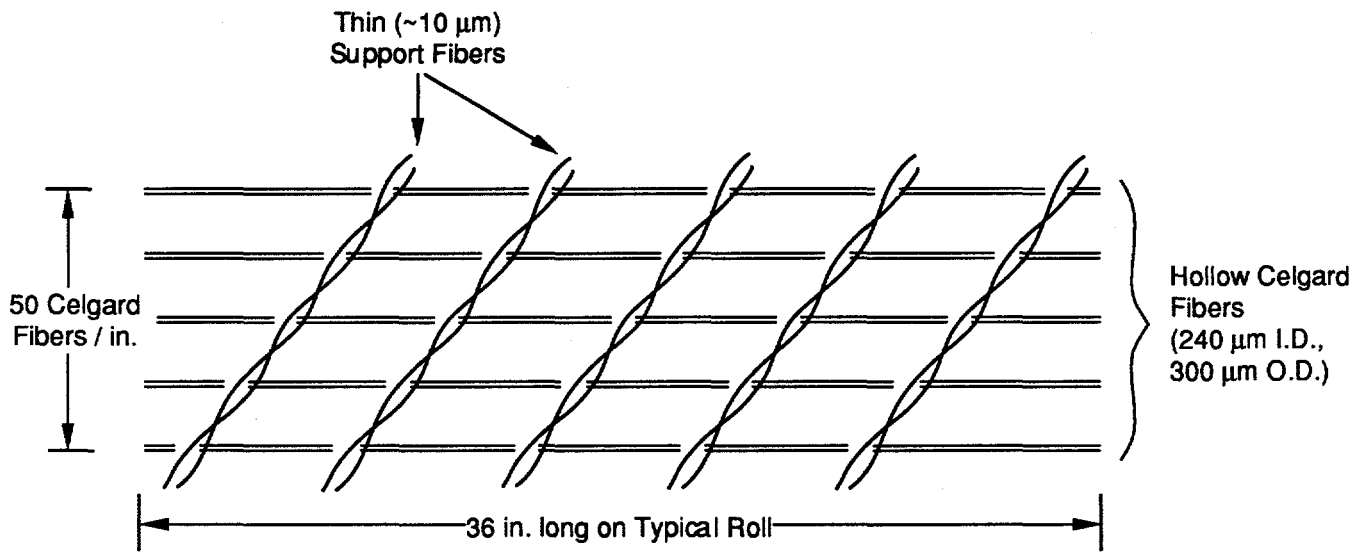
TASK 4: SO₂ SCRUBBING WITH HOLLOW FIBER CONTACTORS

The objective of this task was to determine the fundamental mass transfer characteristics of hollow fiber contactors (HFCs) for scrubbing SO₂ from a simulated flue gas. These devices have been shown to be capable of removing more than 99% of the SO₂ from a simulated flue gas. However, the principles of mass transfer in HFCs are not established on a sound basis, especially for a system with a liquid-phase chemical reaction.

Under subcontract to SRI, Dr. K. Sirkar at the New Jersey Institute of Technology (NJIT) was responsible for Task 4. The goal was to gather a series of steady mass transport data under various conditions by systematically varying the gas flow rate, the liquid flow rate, the liquid composition, and the HFC module properties such as the length and diameter of the hollow fibers and the fiber packing fraction of the module. Experiments were performed both at room temperature and 70°C. This work was done with small modules in cylindrical form so as to achieve a well defined flow distribution in the module. Along with the mass transport rate data, we compiled gas-side and liquid-side pressure drop data.

During the early stages of the project, SRI established the NJIT subcontract and reached an agreement with Hoechst/Celanese (HC) on exactly what modules would be tested in the first two years of the project. HC agreed to supply modules that have a "crossflow" geometry and contain enough fibers so that feed gas flows could be kept below 10 liters/min (a practical laboratory upper limit) and so we could achieve a wide range of SO₂ and NO_x scrubbing efficiencies. The term "crossflow" refers to the fact that the feed gas will flow at 90° to the scrubbing liquor in the module. Since this geometry will be the geometry of the large-scale modules, our lab results should be scalable.

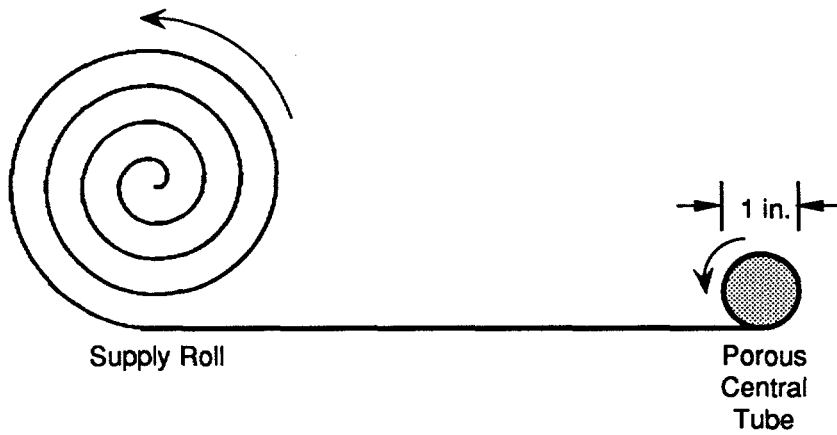
To understand the flow geometry of the HC module, it is helpful to envision how the module is made. First, the hollow fibers (300- μ m-O.D. Celgard fibers) are woven with a netting made of very narrow polyester fibers (about 10 μ m diameter; Figure 4-1). This netting comes on a roll like a roll of carpet. The roll is typically 36 inches long (along axis of roll; this is the length of the hollow Celgard fibers). Transverse to the axis are 50 Celgard fibers per inch. To make a module, HC starts with a porous central tube. Netting is wrapped around this central tube continually, adding layer upon layer until the netting reaches a suitable thickness (e.g., 4 inches, Figure 4-2). This module roll is glued and cut to a desired length (currently HC prefers 11- and 27-inch lengths). The ends of the module are potted with epoxy and cut, and end caps are attached. In a finished module, a liquid passes into the central tube and then flows radially outward over the hollow fibers. The gas is passed down the lumen of each fiber (Figure 4-3).



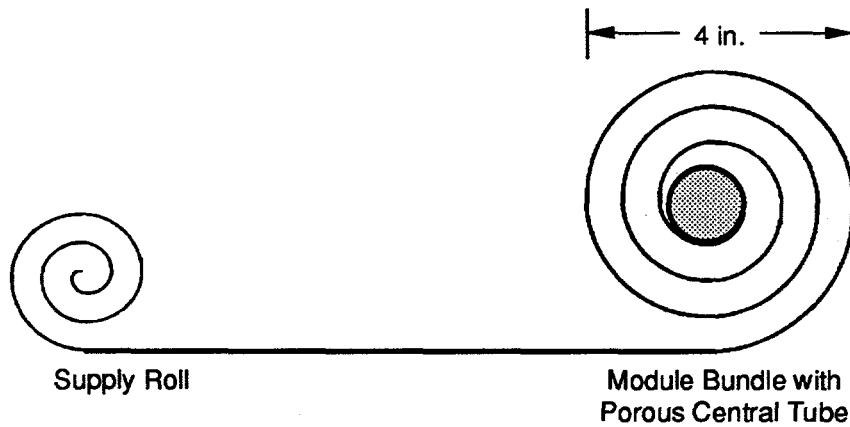
CM-340525-40

Figure 4-1. Structure of Celgard fiber netting.

The support fibers are interwoven transverse to the Celgard hollow fibers.



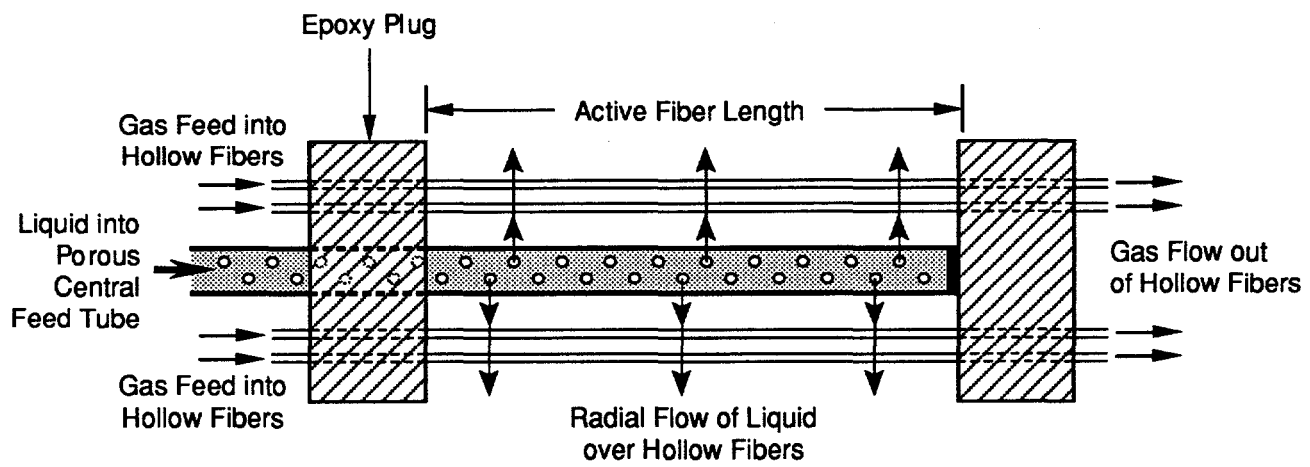
(a) Beginning of wrapping process



(b) End of wrapping process

CM-340525-41

Figure 4-2. Wrapping of netting around central tube.



CM-340525-42

Figure 4-3. Flow pattern of gas and liquid in crossflow module.

The fluid passed into the central tube flows radially across the hollow fibers.

The HFC modules were not received from HC until late December 1992, limiting us to prototype modules for the initial efforts.

EXPERIMENTS WITH PROTOTYPE HFC

Liquid Phase Mass Transfer Experiments

Two sets of liquid phase mass transfer experiments were performed using pure CO₂ as the gas and water as the scrubbing liquid. In the first set of experiments pure gas was used to eliminate the gas phase mass transfer resistance. The second set of experiments differed from the first in that the HFC module was dried under vacuum between experiments to prevent water from condensing in the fiber pores between experiments. When water fills the pores, a dissolved gas molecule must travel the pore length through the liquid. Since diffusion rates are lower in liquids than in gases, this results in a higher mass transfer resistance. The second set of experiments (where the module was dried under vacuum) resulted in mass transfer coefficients three times greater than those in the first set (where the module was not dried).

These experiments were performed using a prototype Hoechst/Celanese HFC with the flow geometry (crossflow) similar to the new HC product (Figure 4-4). The prototype module had an outside diameter of 2 inches and contained 6084 fibers, each with an inside diameter of 240 μm and an outside diameter of 300 μm . The active length of each fiber was 24.1 cm (13,800 cm² of active contact area based on the outside diameter of the fiber).

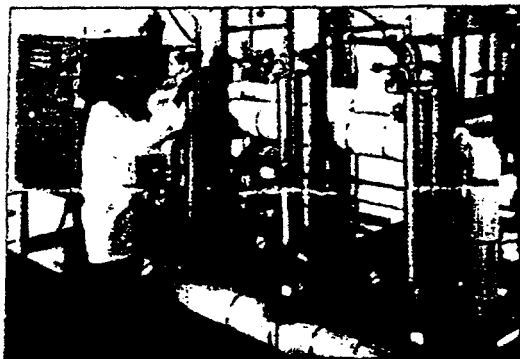
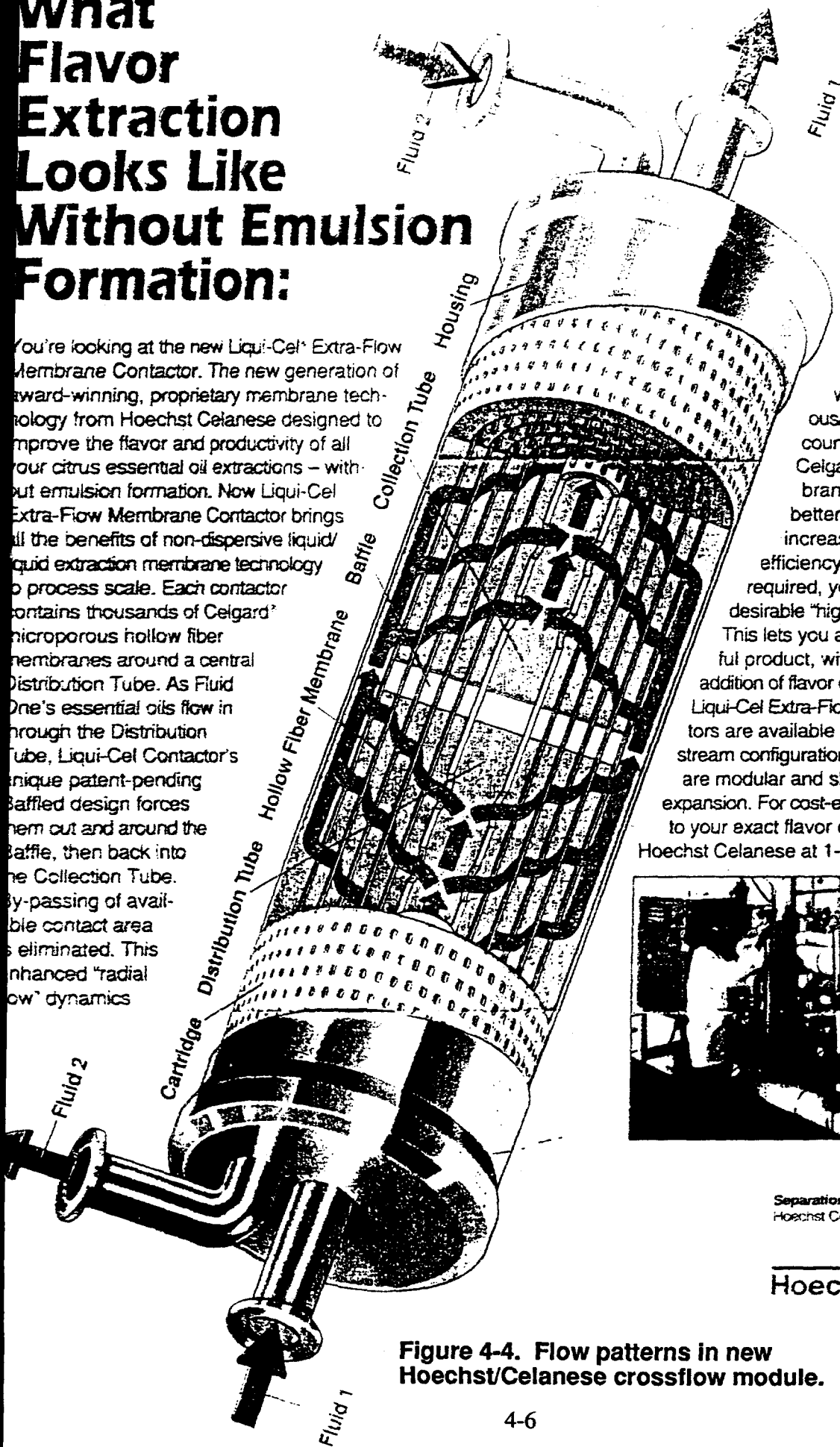
The results from the first set of experiments (not dried) are shown in Figure 4-5. We found that the overall mass transfer coefficient had very little dependence on the liquid flow rate in contrast to the earlier HC countercurrent module design (Karoor, 1992). This result indicates a greater efficiency of mass transfer in the liquid phase. The quantitative significance of the result must await further data, but it was a favorable and unexpected result. The mass transfer coefficient shown in Figure 4-5 is defined in Appendix D.

The results from the second set of experiments (vacuum dried) are also shown in Figure 4-5. The overall mass transfer coefficient was three times higher than obtained during the first set of experiments. Again, the overall mass transfer coefficient had very little dependence on the liquid flow rate, indicating that the liquid phase resistance is negligible under these operating conditions.

What Flavor Extraction Looks Like Without Emulsion Formation:

You're looking at the new Liqui-Cel® Extra-Flow Membrane Contactor. The new generation of award-winning, proprietary membrane technology from Hoechst Celanese designed to improve the flavor and productivity of all your citrus essential oil extractions – without emulsion formation. Now Liqui-Cel Extra-Flow Membrane Contactor brings all the benefits of non-dispersive liquid/liquid extraction membrane technology to process scale. Each contactor contains thousands of Celgard® microporous hollow fiber membranes around a central Distribution Tube. As Fluid One's essential oils flow in through the Distribution Tube, Liqui-Cel Contactor's unique patent-pending Baffled design forces them out and around the Baffle, then back into the Collection Tube. By-passing of available contact area is eliminated. This enhanced "radial flow" dynamics

brings the essential oils into direct contact with Fluid Two's aqueous/organic stream flowing countercurrent through the Celgard® hollow fiber membranes, thereby achieving better fluid distribution – for increased flow capacity and efficiency. Because heat is not required, you never vaporize the desirable "high notes" of the flavors. This lets you achieve a more flavorful product, without the subsequent addition of flavor enhancers. Right now, Liqui-Cel Extra-Flow Membrane Contactors are available in a range of process stream configurations. Liqui-Cel Systems are modular and skid-mounted for easy expansion. For cost-effective customization to your exact flavor extraction needs, call Hoechst Celanese at 1-800 235-4273 today!



Separations Products Division
Hoechst Celanese Corporation

Hoechst Celanese


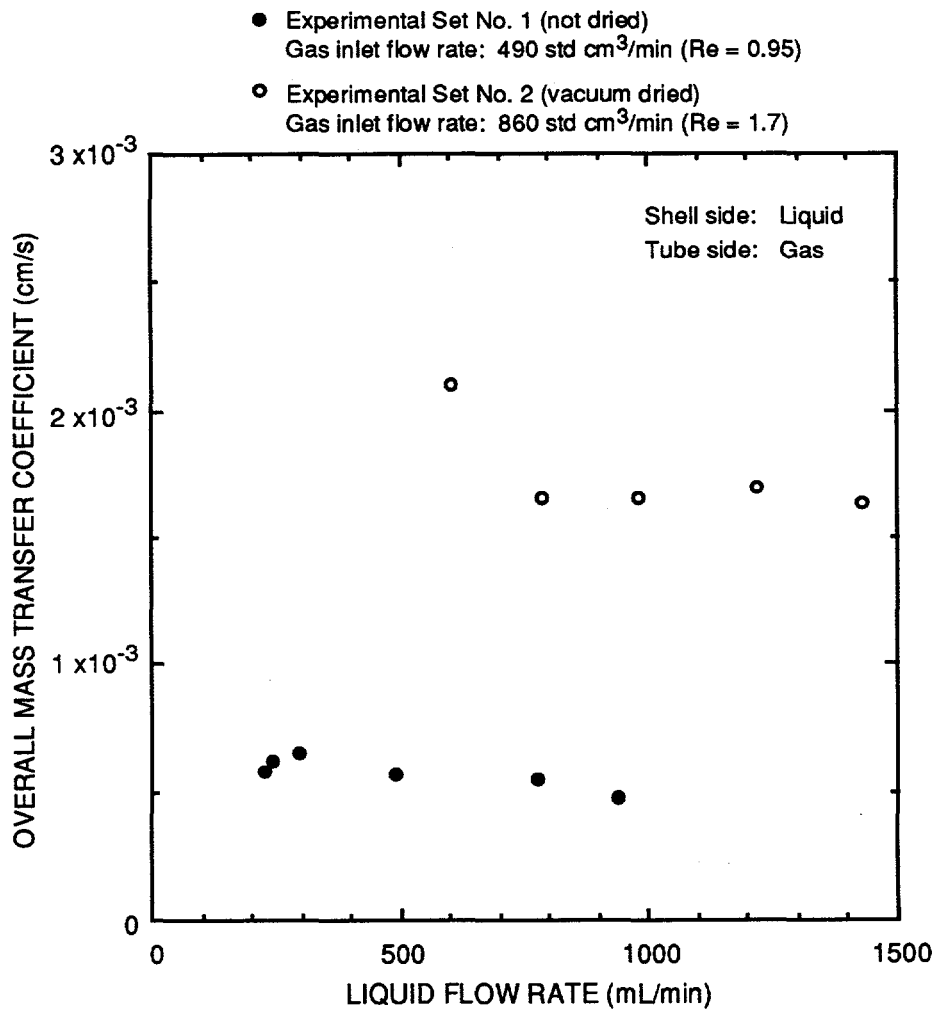
Hoechst 

Figure 4-4. Flow patterns in new Hoechst/Celanese crossflow module.



CM-3501-4A

Figure 4-5. HFC mass transfer coefficients for pure CO₂ absorption in water using a crossflow module.

The mass transfer coefficient is relatively insensitive to liquid flow rate.

SO₂ Removal Efficiency Experiments

For the very first few experiments, we used a small module available from earlier projects (the modules described above were too large for these tests). The module has an outside diameter of 0.25 inch and contains 75 fibers, each with an inside diameter of 240 μm and an outside diameter of 300 μm . The active length of each fiber was 18 cm (127 cm^2 of active contact area based on the outside diameter of the fiber). A gas mixture containing 1.61% SO₂ in N₂ was fed to the fiber lumen at 92.9 std cm^3/min at a pressure slightly above atmospheric. Pure water was pumped through the shell side at 2 to 3 psi higher than the gas stream pressure.

During the experiments, water was found to be leaking into the fiber lumen (because this module had been used extensively for an earlier project). However, these experiments served the purpose of generating preliminary results before we used the new HC modules. The results for experiments with liquid flow rates between 50 and 200 mL/min are shown in Figure 4-6. We found the SO₂ removal rate to be about 70% at low water flow rates and over 96% at increased water flow rates.

INITIAL EXPERIMENTS WITH HOECHST-CELANESE HFC

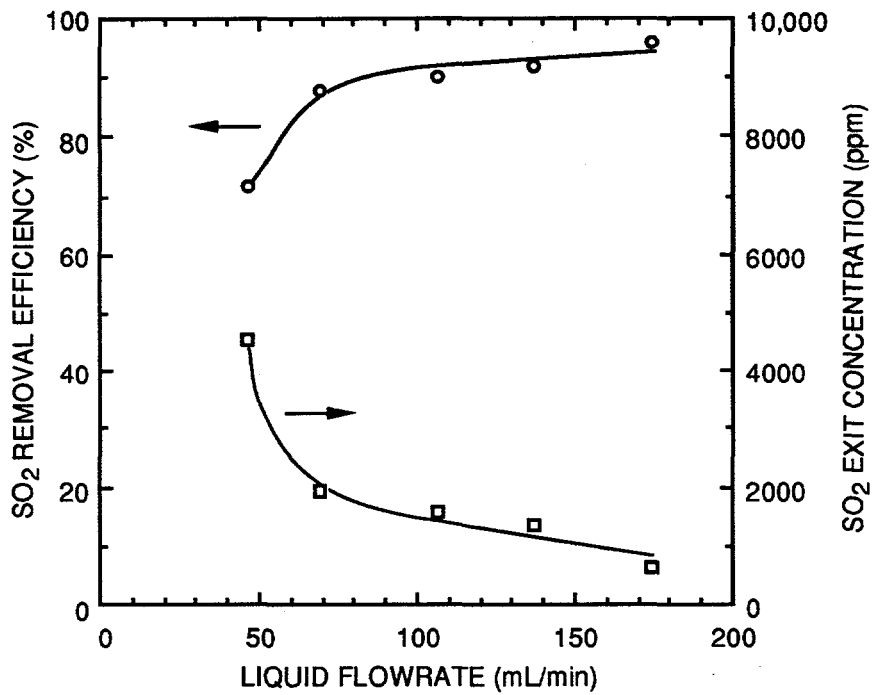
During the first quarter of 1993, we began experiments with the new crossflow modules received from Hoechst Celanese. We conducted four sets of experiments:

- Mass transfer tests with pure CO₂ and water to determine the liquid phase resistance.
- Module configuration tests with pure SO₂.
- Mass transfer tests with 10% CO₂ and water to determine the significance of the gas phase (including membrane pore) resistance.
- SO₂ removal efficiency tests to demonstrate the effectiveness of the proposed technology.

Later in the year, we performed mass transfer tests on a larger HFC module containing 1000 fibers, using a CO₂/water system, and SO₂ absorption tests that used a model flue gas mixture and aqueous solutions of Na₂SO₃ as the scrubbing medium. All these tests were performed on the apparatus illustrated in Figure 4-7.

Mass Transfer Tests with Pure CO₂ and Water

The rate of mass transfer is a function of liquid-side film resistance, gas-side film resistance, and pore resistance (a stagnant gas phase in the flue gas application). To determine the liquid-side film resistance, we performed mass transfer tests with pure CO₂ and water. When a



CAM-3501-6

Figure 4-6. SO₂ removal efficiencies with a prototype HFC.
Water was used as the scrubbing medium.

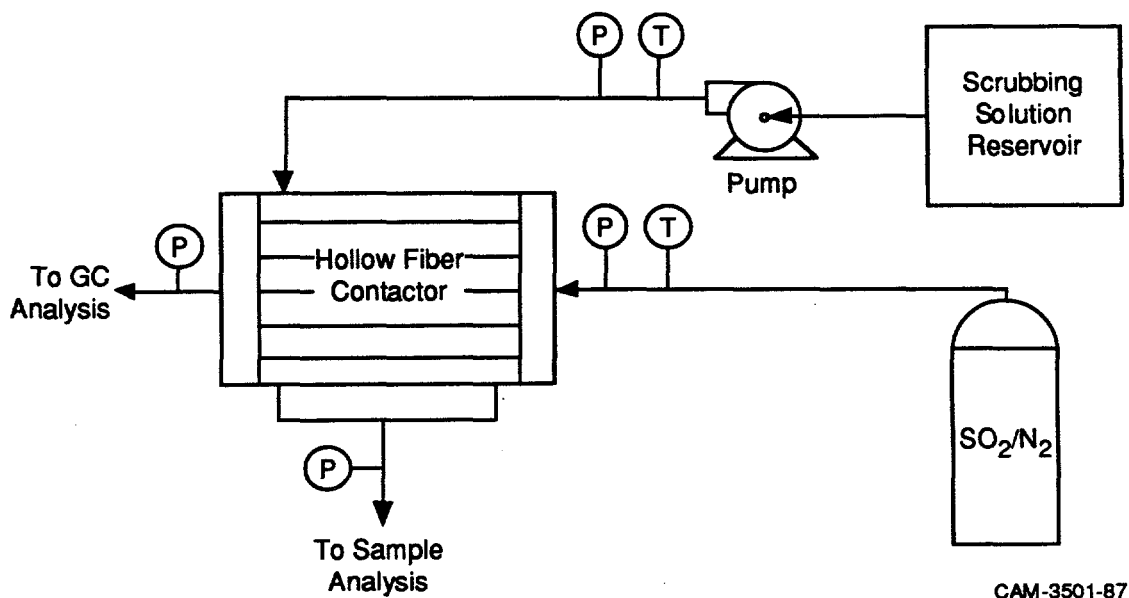


Figure 4-7. Schematic of HFC test apparatus.

pure gas is absorbed into a liquid, there is no resistance in the gas phase; thus a measured resistance is due only to the liquid-side film resistance. The new HC crossflow module used in these experiments contained 200 fibers, each with an inside diameter of 240 μm and an outside diameter of 300 μm . The active length was 23 cm and the contact area (based on outer diameter) was 433 cm^2 . A schematic of the module is shown in Figure 4-8. The results of these tests are shown in Figure 4-9 for two versions of HC's HFC module. The new module has an overall mass transfer coefficient as high as the prototype module, but at much lower liquid flow rates. At higher flow rates, the new module has the potential for even greater mass transfer rates.

Module Configuration Tests with Pure SO_2

Our second set of experiments was aimed at determining the effect of module orientation and liquid pressure on the rate of mass transfer. In Figure 4-10 the module is mounted vertically with water exiting from only one port. The flow in this case is a combination of counter current and crossflow. Mass transfer coefficients resulting from this configuration were lower than those from the horizontally mounted module (Figure 4-11).

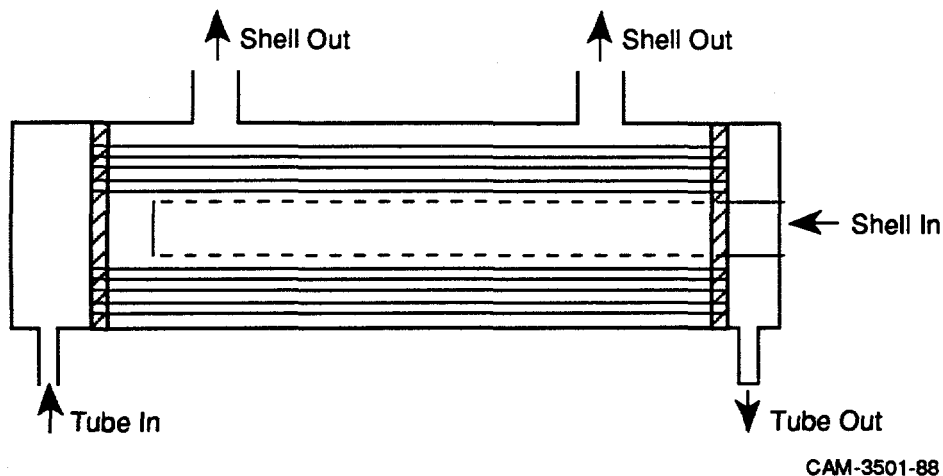


Figure 4-8. Schematic of the crossflow module.
Liquid flow through the shell-side and gas through to tube side.

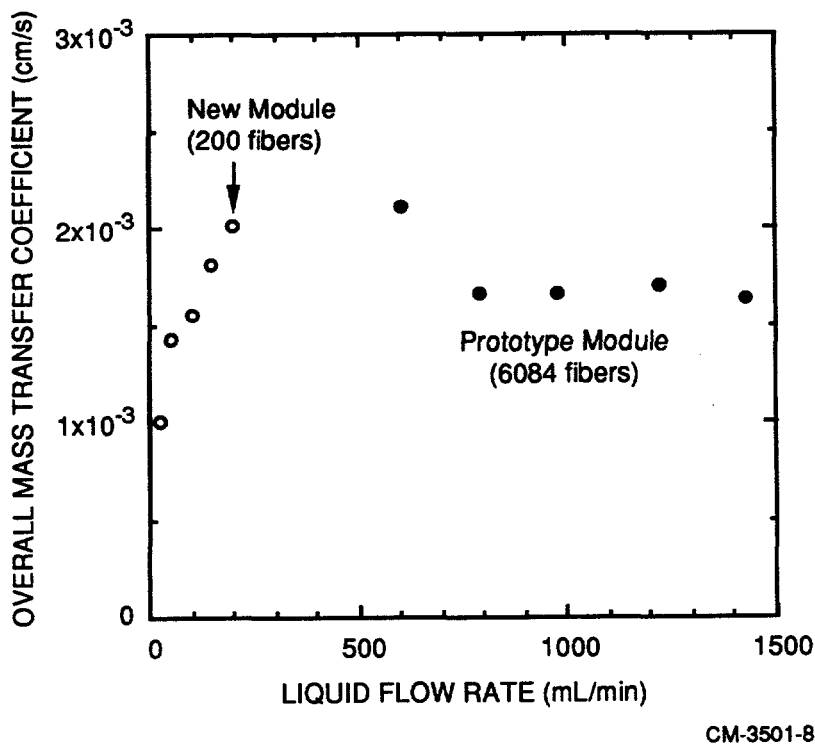
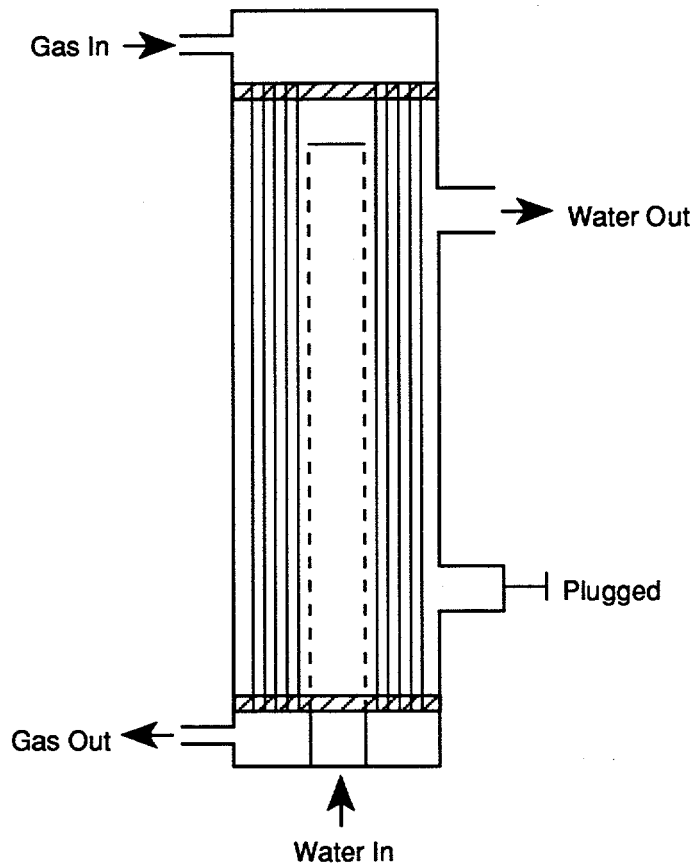


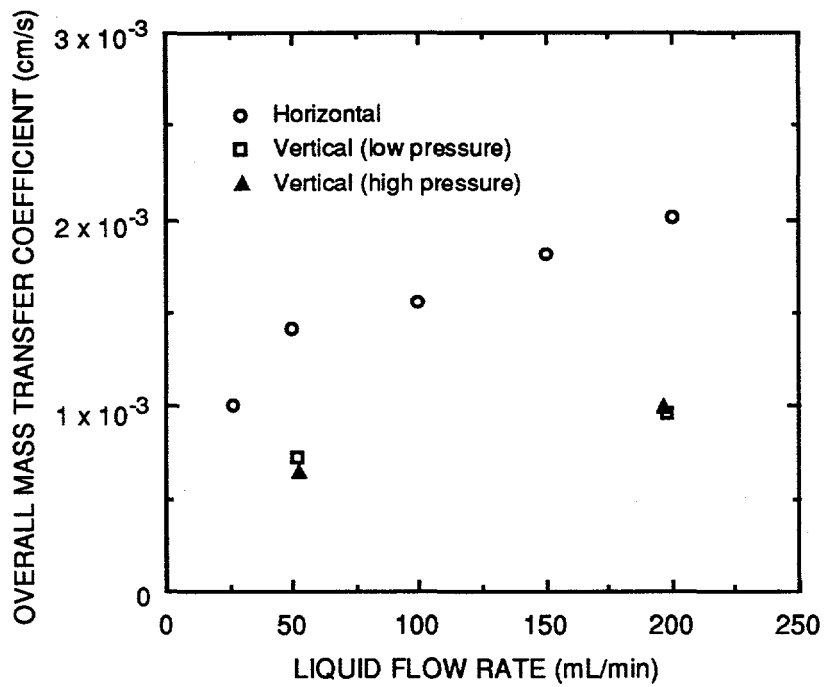
Figure 4-9. HFC mass transfer coefficients for pure CO₂ absorption in water using two cross flow modules.

The new module has an overall mass transfer coefficient as high as the prototype module, but at much lower liquid flow rates. Higher mass transfer coefficients are probably achievable with higher liquid flow rates.



CM-3501-9

Figure 4-10. Schematic of HFC in the vertical configuration.
Liquid exits the module only through the top port.



CM-3501-10

Figure 4-11. HFC mass transfer coefficients with different module orientations and liquid pressures (pure CO₂ absorption in water).

Mounting the module horizontally resulted in higher mass transfer coefficients; liquid pressure had no effect on mass transfer coefficient.

In the experiments described so far, the liquid was maintained at a pressure of 1-3 psig. In two additional experiments (using the vertical configuration) we increased the pressure to 10 psig, maintaining the same gas flow rate. The results in Figure 4-11 show that the liquid pressure does not affect the overall mass transfer coefficient.

Mass Transfer Tests with 10% CO₂ and Water

The third set of tests, with 10% CO₂, was performed to determine if the gas phase resistance is significant in the HFC module. The overall mass transfer coefficient was determined using 10% CO₂ under the same conditions as with pure CO₂. The results of these tests are shown in Figure 4-12 and compared with the pure CO₂. The mass transfer coefficients with 10% CO₂ are indistinguishable from those with pure CO₂, which indicates that the gas-phase resistances (gas-side film and pore resistances) are negligible compared to the liquid resistances.*

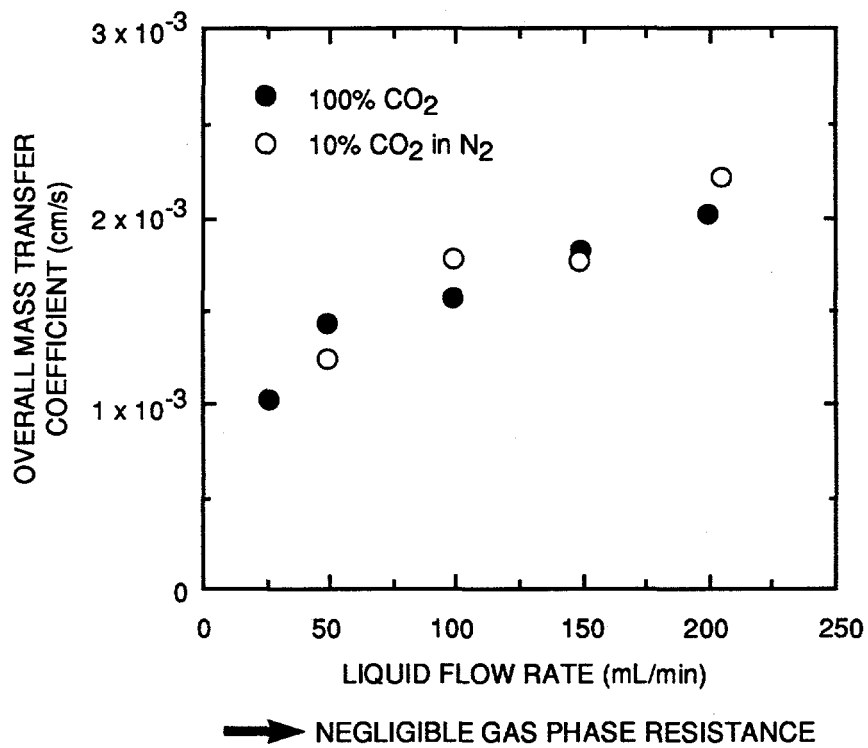
SO₂ Removal Efficiency Tests

The fourth set of experiments was performed to demonstrate the effectiveness of the HFC scrubbing technology for removing SO₂ from flue gas. We scrubbed SO₂ (1.6% SO₂ in nitrogen) with water at various liquid flow rates. Figure 4-13 shows that, for all but the lowest flow rate, there was no detectable SO₂ remaining in the gas after scrubbing. Further, we used a simulated flue gas mixture with water at different gas flow rates in the same module. Even at high gas flow rates (~500 std cm³/min), no SO₂ was detected in the purified gas stream (Figure 4-14). These high SO₂ removal efficiencies demonstrate the high mass transfer rates that can be achieved with HFCs.

Mass Transfer Tests on 1000-Fiber Module

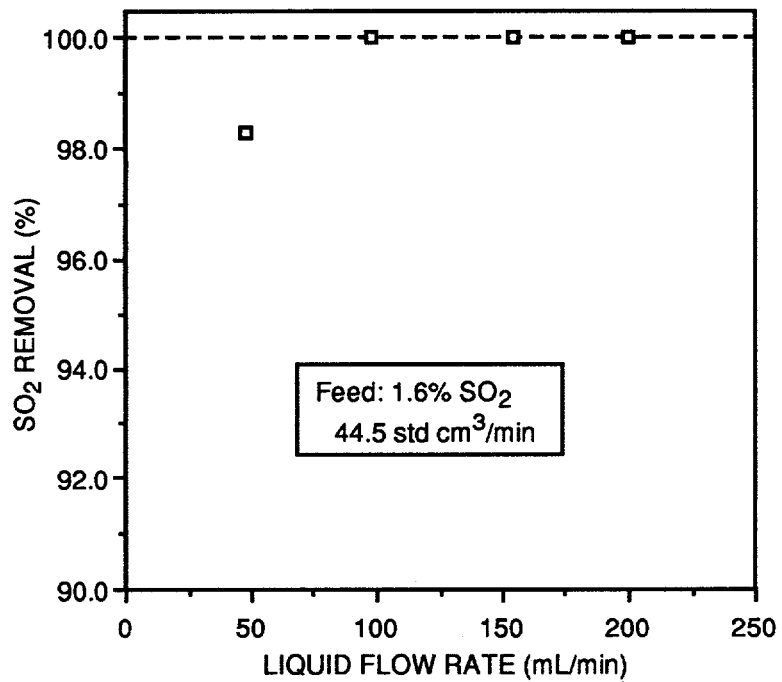
Next, we evaluated the mass transfer characteristics of a larger module containing 1000 fibers, using the CO₂/water system. We also conducted SO₂ removal efficiency experiments at low water flow rates and SO₂ removal efficiency experiments with aqueous Na₂SO₃ as the scrubbing medium.

* These experiments show that the gas-phase resistance is negligible for the case of CO₂ absorption from a 10% mixture into pure water only, however, it is reasonable to infer that the gas-phase resistance for SO₂ would also be small.



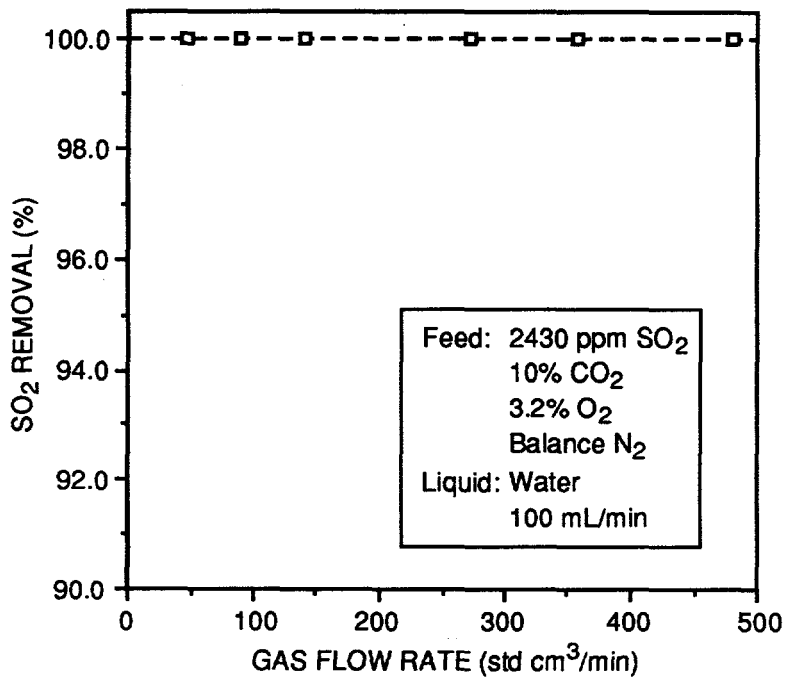
CAM-3501-22

Figure 4-12. HFC mass transfer coefficients with pure and dilute CO₂ feed streams (liquid absorbent is water).



CAM-3501-89

Figure 4-13. SO₂ removal efficiencies using water as the absorbent.
For liquid flow rates above 100 mL/min, no SO₂ could be detected in the gas outlet.



CAM-3501-90

Figure 4-14. SO₂ removal efficiencies from simulated flue gas using water as the absorbent.

No SO₂ could be detected in the outlet over the range of gas flow rates studied.

Mass transfer experiments were performed with a 1000 fiber Hoechst Celanese crossflow module* using both pure and dilute (10%) CO₂ as the feed gas. The overall mass transfer coefficients, shown in Figures 4-15 and 4-16, are similar to those obtained with the smaller (200-fiber) module. These and previous mass transfer coefficient data were reduced to correlation between the Sherwood number, Reynolds number, and Schmidt number (Figure 4-17). The mass transfer coefficients resulting from our experiments with Hoechst Celanese crossflow module were significantly higher than those obtained by other researchers.

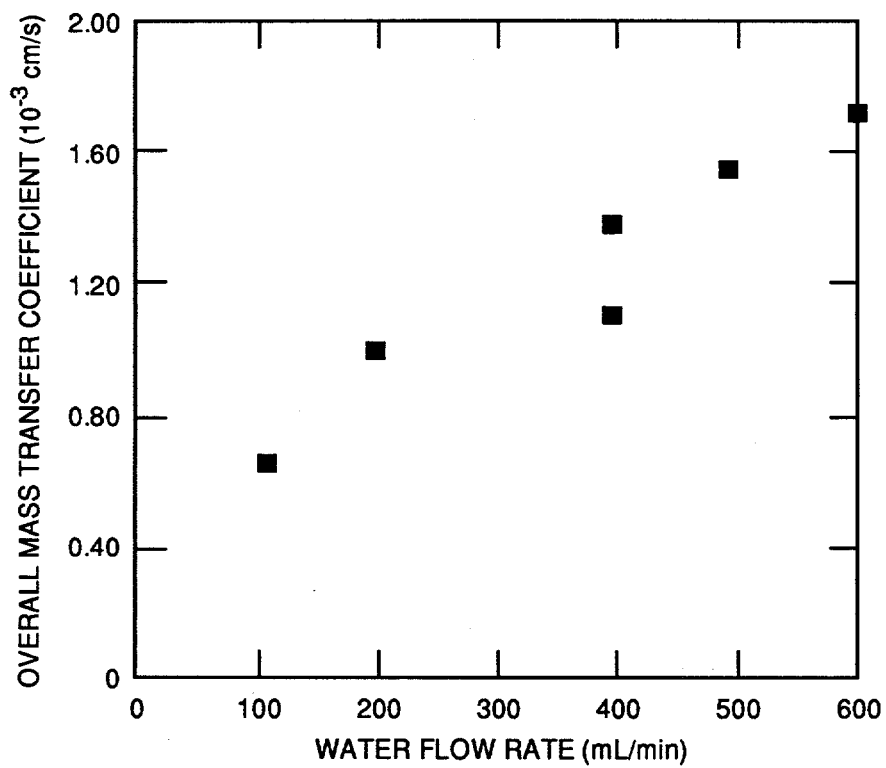
SO₂ Absorption Tests with Model Flue Gas Mixture and Na₂SO₃ Scrubber

We focus next on SO₂ absorption experiments that used a model flue gas mixture and aqueous solutions of Na₂SO₃ as scrubbing medium. The tests were conducted in a Hoechst Celanese crossflow module (unbaffled) containing 200 fibers, each with an active length of 23 cm. The inside and outside diameters of the hollow fibers were 240 μm and 300 μm, respectively. The active contact area was 433.5 cm² based on the outside diameter. The module achieved very high removal of SO₂, often 100% from the same model flue gas using deionized water. These experiments with deionized water used gas flow rates of 0-500 sccm and water flow rates of 50-100 mL/min. The model flue gas contained 2430 ppm SO₂, 3.17% O₂, 10% CO₂, and the balance N₂. The gas was supplied to the tube side of the module from a certified standard gas mixture cylinder (Matheson, East Rutherford, NJ). For aqueous Na₂SO₃ solutions, the gas flow rate was varied between 0-1000 sccm whereas the flow rate of aqueous Na₂SO₃ solution through the shell side was maintained between 5 to 30 mL/min. The sulfite concentrations studied were 0.01 and 0.05 M.

Earlier, we reported virtually 100% SO₂ removal efficiencies at a water flow rate of 100 mL/min. To obtain the operational characteristics of the HFC module when the SO₂ removal efficiency is less than 100%, we used a lower water flow rate, 50 mL/min. These results are shown in Figure 4-18. We also conducted SO₂ removal efficiency experiments using Na₂SO₃ as the scrubbing medium. We achieved high removal efficiencies (>90%) with liquid flow rates about 100 times lower than were used when water was the scrubbing medium, as shown in Figure 4-19.

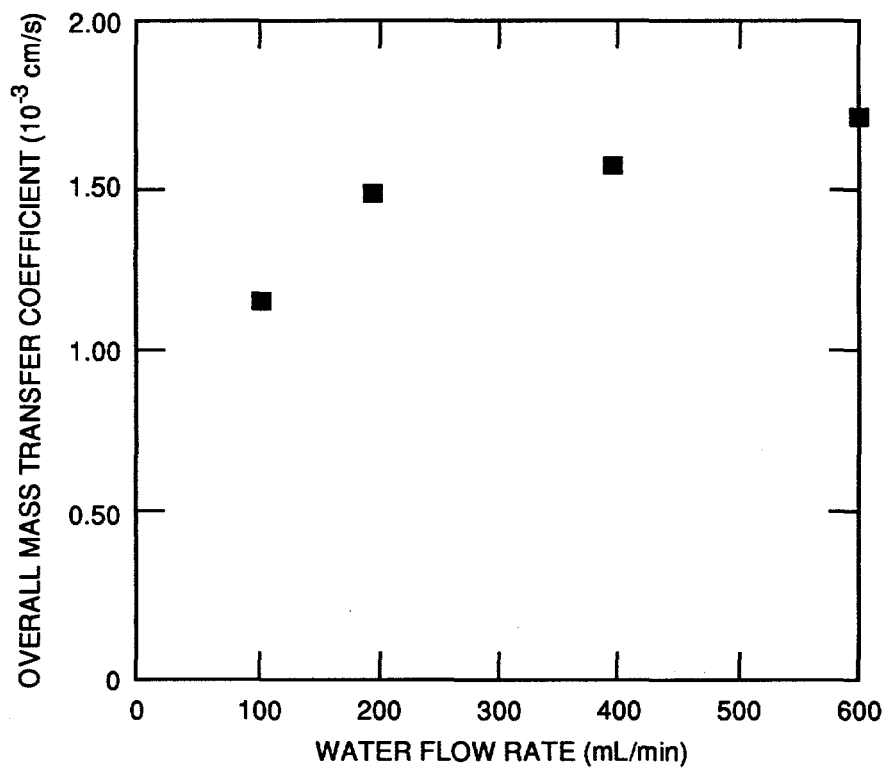
The percentage removal of SO₂ at different sulfite concentrations and flow rates are also plotted in Figure 4-20. For a given liquid flow rate and sulfite concentration, the percentage removal decreases with increasing gas flow rate. When the concentration of the sulfite solution is raised from 0.01 to 0.05 M, considerably higher SO₂ removal rate is obtained because of the

* The module contains 1000 hollow fibers, each with an active length of 23 cm. The inside and outside diameters of the hollow fibers are 240 mm and 300 mm respectively. The active contact area is 2170 cm² based on the outside diameter. The module is unbaffled.



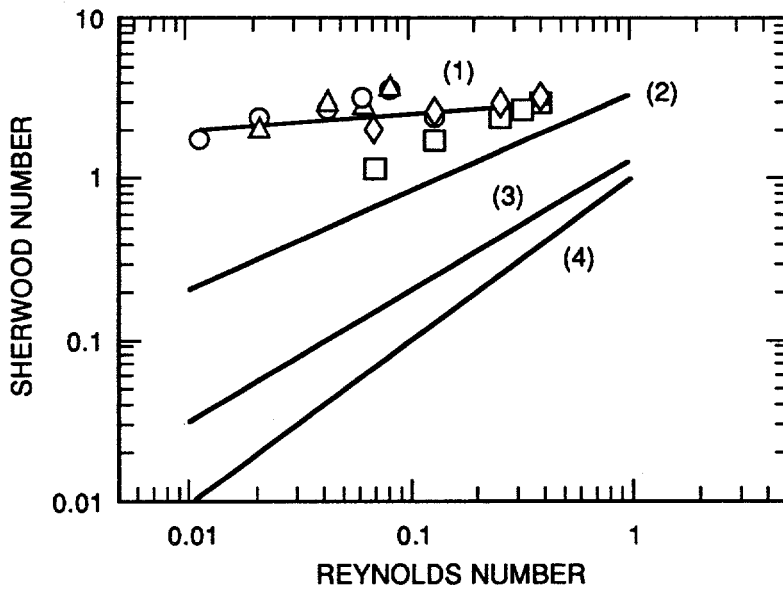
CM-3501-15

Figure 4-15. HFC mass transfer coefficients for pure CO₂ absorption in water using a 1000-fiber crossflow module.



CM-3501-16

Figure 4-16. HFC mass transfer coefficients for $\text{CO}_2\text{-N}_2$ mixture absorption in water using a 1000-fiber crossflow module.

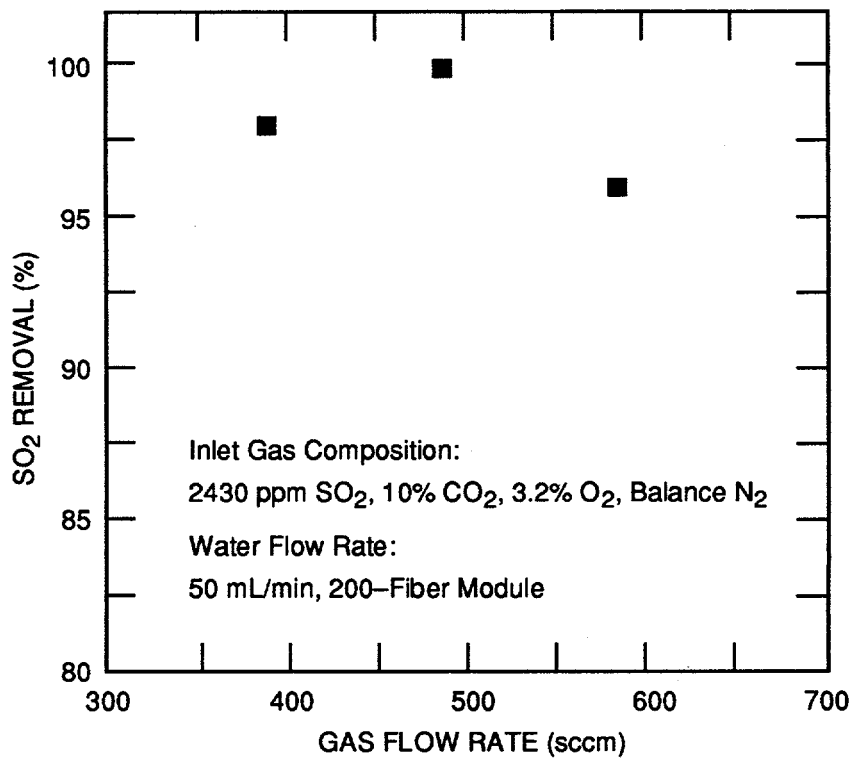


Module	Pure CO ₂	CO ₂ -N ₂
200 Fibers	○	△
1000 Fibers	□	◇

- (1) This work
 $Sh = 0.38 Re^{0.08} Sc^{0.33}$
- (2) Kreith and Black, 1986
 $Sh = 0.39 Re^{0.59} Sc^{0.33}$
- (3) Wickramasinghe et al., 1992
 $Sh = 0.15 Re^{0.8} Sc^{0.33}$ for $Re > 2.5$
- (4) Literature correlation (Yang and Cussler, 1986)
 $Sh = 0.39 Re^{1.0} Sc^{0.33}$ for $Re > 2.5$

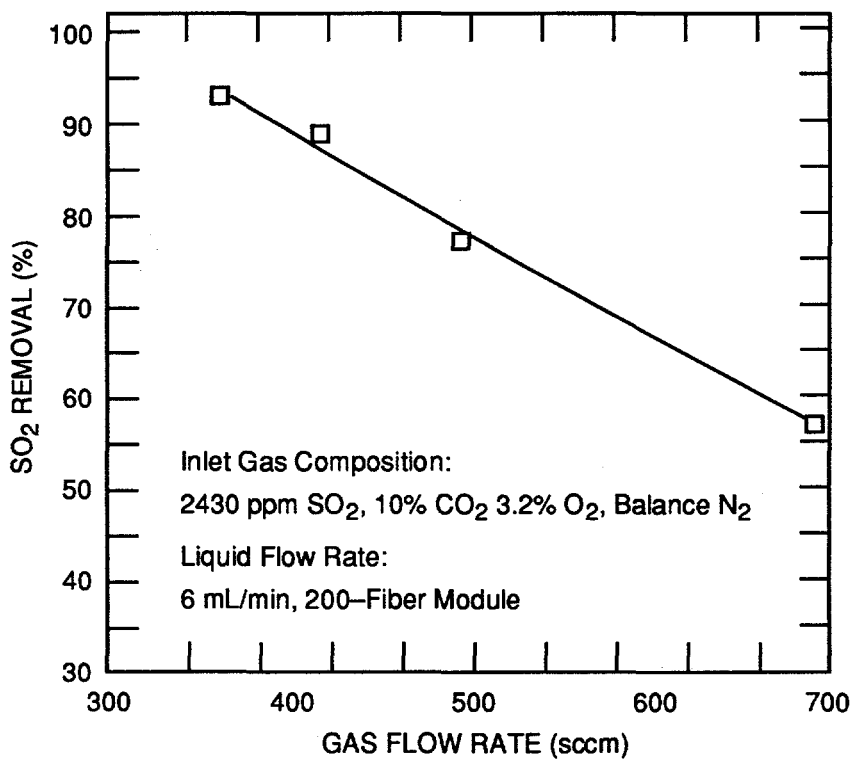
CM-3501-17

Figure 4-17. Sherwood number versus Reynolds number for CO₂ absorption in water.



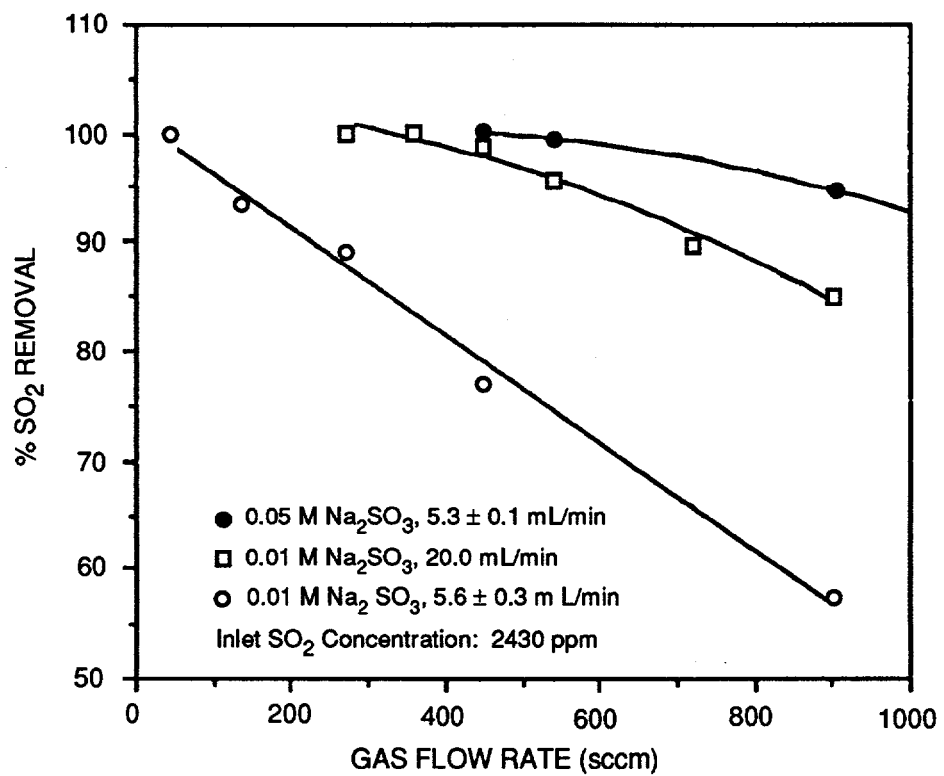
CM-3501-18

Figure 4-18. SO₂ removal with water at low liquid flow rates.



CM-3501-19

Figure 4-19. SO₂ removal with 0.01 M Na₂SO₃ solution.



CAM-3501-32

Figure 4-20. SO₂ removal efficiency at various sulfite concentrations.

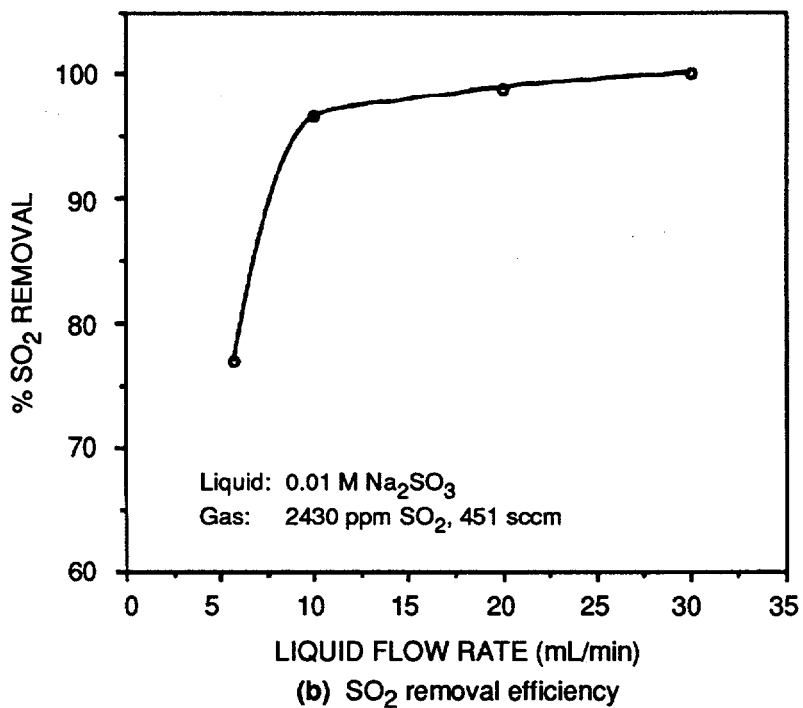
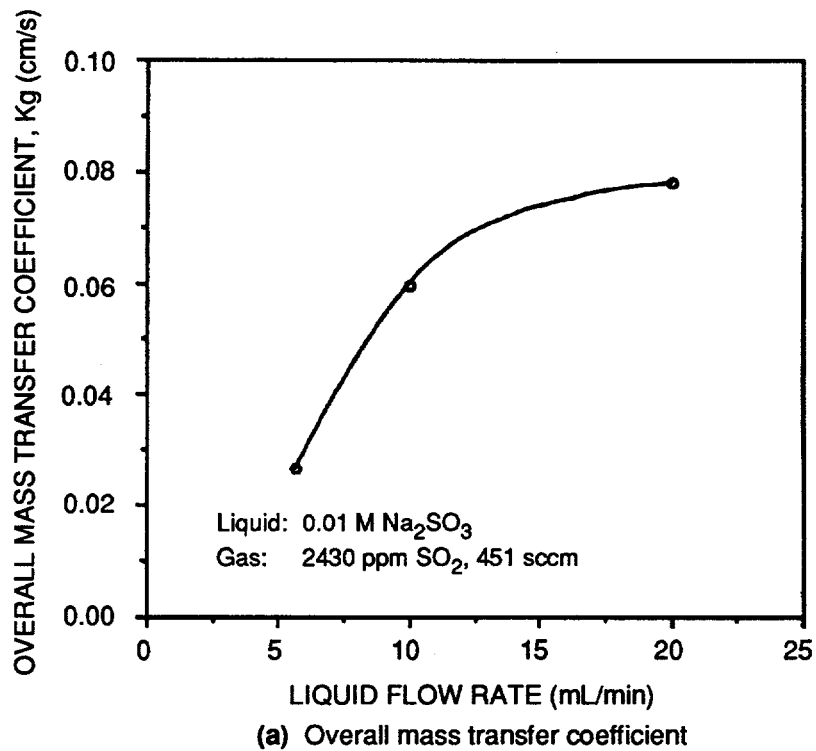
increase in the absorption capacity of the liquid. For 0.01 M Na_2SO_3 solution, more SO_2 is absorbed as the liquid rate is increased from 5 to 20 mL/min. Such a behavior suggests that the liquid phase might offer considerable resistance to mass transfer at low sulfite concentrations.

Figure 4-21(a) shows the effect of liquid flow rate on the overall gas phase based mass transfer coefficient for SO_2 . The data were taken at a constant gas flow rate of 451 sccm. The overall mass transfer coefficient (K_g) increases with higher liquid flow rates. The SO_2 removal efficiency as a function of liquid flow rate is plotted in Figure 4-21(b). SO_2 is completely removed when the liquid flow rate is 30 mL/min. Note that it is not possible to calculate the overall mass transfer coefficient when the outlet gas stream does not contain SO_2 since a logarithmic-mean driving force is used in its calculation.

The effect of gas flow rate variations between 0 to 1000 sccm on the overall mass transfer coefficients is shown in Figure 4-22 at two sulfite concentrations. The liquid flow rate was maintained around 5.6 mL/min in this set of experiments. (Only two data points are shown for 0.05 M Na_2SO_3 solution because the SO_2 removal was 100% for lower gas flow rates.) In both cases, the overall mass transfer coefficient is nearly independent of the gas flow rate, indicating that the liquid film resistance is controlling at low sulfite concentrations. At higher sulfite concentrations, the controlling resistance is expected to shift from liquid to gas phase.

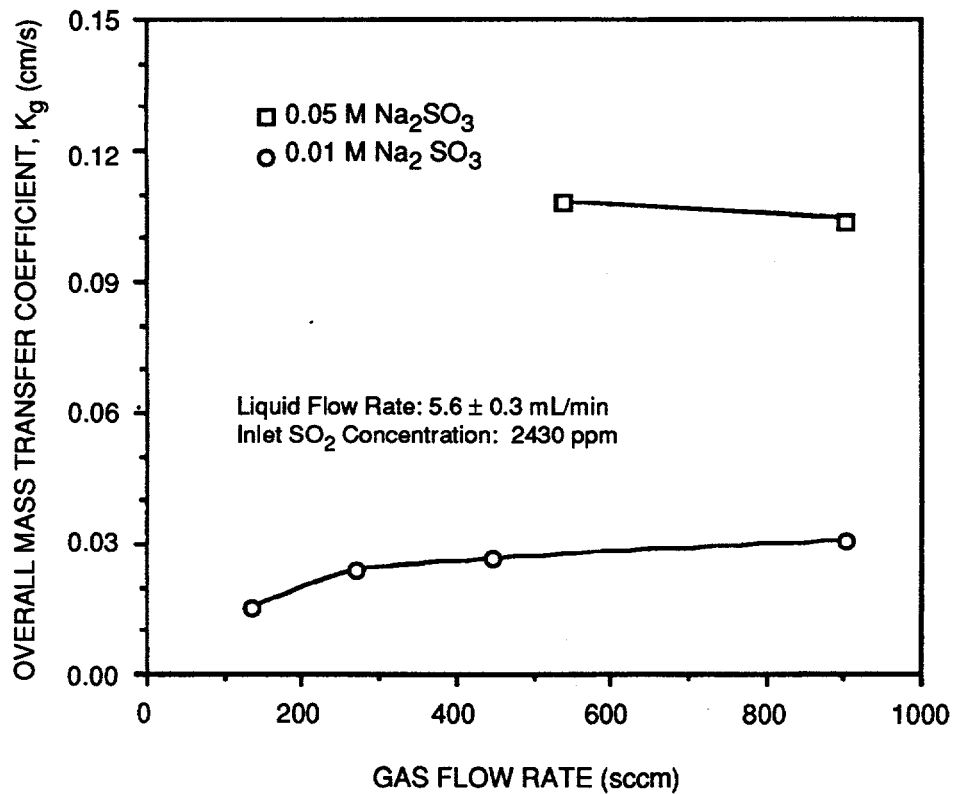
Next, we present results of raising the concentration of Na_2SO_3 in the liquid to determine the critical concentration where the gas phase resistance controls the absorption. To obtain gas-phase-controlled transfer, a series of runs were conducted using 0.2 M aqueous Na_2SO_3 . The SO_2 absorption capacity of 0.2 M Na_2SO_3 solution is high; so we opted for a lower liquid flow rate of 5 mL/min and a relatively high gas flow rate range of 1800-2750 sccm in the first set of runs. Such a combination was expected to bring out gas-phase-controlled absorption and still have some SO_2 in the outlet gas stream. An experiment yielding complete removal of SO_2 is not useful since the mass transfer coefficient cannot be determined. Obtaining a steady residual concentration of SO_2 at the outlet gas stream was the experimental goal; gas and liquid flow rates were varied at a specified sulfite level in the liquid. Certified mixtures of model flue gases from different cylinders were used. The average composition was 2250 ± 350 ppm SO_2 , 3% O_2 , 10% CO_2 , and the balance N_2 .

The results are presented in Table 4-1. Two out of five runs having a liquid flow rate of 5 mL/min reached steady state; i.e., the effluent gas stream attained a constant SO_2 composition with time. Three other runs yielded continually increasing SO_2 level at the outlet. Initially, we concluded that the pores remained wet from the previous run and became more so in the course of a given run, resulting in poor performance. After each run, therefore, the module was cleaned



CAM-3501-33

Figure 4-21. Effect of liquid flow rate on overall mass transfer coefficient and SO₂ removal efficiency at low sulfite concentrations.



CAM-3501-34

Figure 4-22. Effect of sulfite on overall mass transfer coefficient.

Table 4-1
RESULTS OF SO₂ ABSORPTION IN 0.2 M Na₂SO₃

Run No.	Temp. (°C)	Liquid Flow (mL/min)	Gas Flow (sccm)	Inlet SO ₂ Composition (ppm)		Steady State	Outlet SO ₂ (ppm)	SO ₂ Removal (%)	K _g (cm/s)
				Dry	Humid				
1	21.5	5.3	1809	2430	---	Yes	115	95	0.207
2	21.0	5.0	2713	2430	---	Yes	205	91	0.249
3	22.0	5.1	2261	2610	---	No	---	---	---
4	23.0	4.9	1809	2610	---	No	---	---	---
5	22.0	5.0	1809	2610	---	No	---	---	---
6	22.0	9.9	1809	2610	---	Yes	55	98	0.267
7	21.5	10.0	2261	2610	---	Yes	90	97	0.288
8	22.0	10.0	2713	2610	---	No	---	---	---
9	25.5	9.9	2713	2020	---	No	---	---	---
10	29.0	10.0	2713	---	1927	Yes	53	97	0.367
11	27.0	10.1	2713	---	2082	Yes	290	86	0.201
12	28	20	2713	2210	2050	Y	65	97	0.349
13	23	20	2713	2210	2082	Y	71	96	0.337

and dried thoroughly. Both the shell and tube sides were simultaneously washed with running deionized (DI) water, first with water warmed to 45°C and then with water at room temperature. Then the module was vacuum dried overnight. This was followed by runs having 5 mL/min of liquid flow rate and gas flow rate of 1800-2260 sccm; however, we could not reproduce the steady state results.

The liquid flow rate was increased to 10 mL/min in later runs. Steady state conditions were observed for 1809 and 2261 sccm gas flow rates. Again, runs with a gas flow rate of 2713 sccm did not attain steady state. The HFC module was carefully dried, but repeated runs failed to yield constant level of SO₂ at the exit gas. We concluded that salt deposition was taking place from 0.2 M sulfite solution within or near the pores since the high gas flow rate must have been drying up the liquid layer at the gas membrane interface.

We realized that proper humidification of the feed gas entering the HFC was necessary to prevent the sulfite solution from drying near the pores inside the module. The model flue gas was humidified by using two separate hollow fiber contactors connected in series at the inlet gas line. The shell sides of these modules had stagnant water maintained at 5 psi. Trials with N₂ gas flowing at about 2700 sccm showed that the stream attained 96% humidity within 2 hours. In such humidifying modules, a part of the flue gas SO₂ will be absorbed into the water in the shell side, and there will be an equilibrium between the water and the inflowing gas. We decided to measure the SO₂ content of such incoming flue gas by GC only after the experimental run reaches steady state. The first run with humidified flue gas attained a steady state within 5 hours. The effluent SO₂ concentration was about 50 ppm, indicating SO₂ removal to be 97%. In the next run, the inlet SO₂ concentration was higher. This run achieved steady state after 7 hours. The effluent had 86% of SO₂ removed. Some salt deposition and pore wetting probably occurred, giving rise to poor performance in the contactor. To minimize the possible drying of liquid inside the module at these high gas flow rates, we later increased the liquid flow rate to 20 mL/min.

MASS TRANSFER CONTROL

Thus, we reported results of SO₂ absorption experiments using 0.2 M aqueous Na₂SO₃ solution in a crossflow module containing 200 hollow fibers. At higher sulfite concentrations the controlling resistance to mass transfer should shift to the gas phase since there is little or no resistance in the liquid phase. The process becomes efficient since higher absorption can be achieved by increasing the gas flow rate. Experiments to obtain such gas-phase-controlled transfer are useful for determining the optimum concentration of aqueous Na₂SO₃ to be used in the flue gas desulfurization. We considered 0.2 M sulfite concentration as high and fashioned our experiments in the following manner. At a certain gas flow rate, if there is no increase in mass transfer due to

variation in the liquid flow rate, the transfer is not controlled by the liquid-phase-resistance. In that liquid flow rate range where the mass transfer increases with increased gas flow rates, it can be claimed that gas-phase-control is achieved.

We started with low liquid flow rates and high gas flow rates. Several of our runs did not attain steady state at liquid flow rates of 5 and 10 mL/min and a gas flow rate of 2713 sccm. We concluded that drying of liquid solution was occurring and salt deposition was taking place from 0.2 M sulfite solution within or near the pores since the high gas flow rate must have been drying up the liquid layer at the gas-membrane interface. The model flue gas was humidified to prevent the sulfite solution from drying near the pores inside the module. Two runs with humidified incoming flue gas attained steady state after 5 and 7 hours. The second run yielded a lower mass transfer coefficient. Some salt deposition and pore wetting probably occurred, giving rise to poorer performance in the contactor.

We ran experiments with an increased liquid flow rate of 20 mL/min to minimize the possible drying of liquid inside the module at these high gas flow rates. Two runs were conducted using a model flue gas with an initial composition of 2210 ppm SO₂, 3% O₂, 9.9% CO₂ and balance N₂. The results are presented in the last two rows of Table 4-1. Both runs had incoming gas humidified. The first run (No. 12) reached steady state after 5 hours. The effluent SO₂ concentration was 65 ppm. The SO₂ removal was 97%. The following run (No. 13) was conducted to reproduce the preceding run. After about 5 hours, run 13 achieved steady state and yielded reproducible results. The effluent had 96% SO₂ removed. The operating temperatures of these two runs differed by 5°C, which probably caused the variation in the final values in K_g.

As mentioned before, we had difficulty in obtaining steady state runs using 5-10 mL/min of liquid flow rate. Runs 1, 2, 6, and 7 achieved steady state using dry gas. The K_g values increased when the liquid flow rate was changed from 5 to 10 mL/min while the gas flow rates were between 1810-2260 sccm. The increase is probably related more to the increased absorption capacity of a higher liquid flow rate. Run 11 was an attempt to reproduce run 10. A pseudo-steady-state condition was obtained at 5-7 hours where the SO₂ level at the exit gas oscillated near 290 ± 20 ppm. Although the incoming gas was humidified, the process performed poorly as indicated by the low value of K_g. We concluded that it was not a reproducible run.

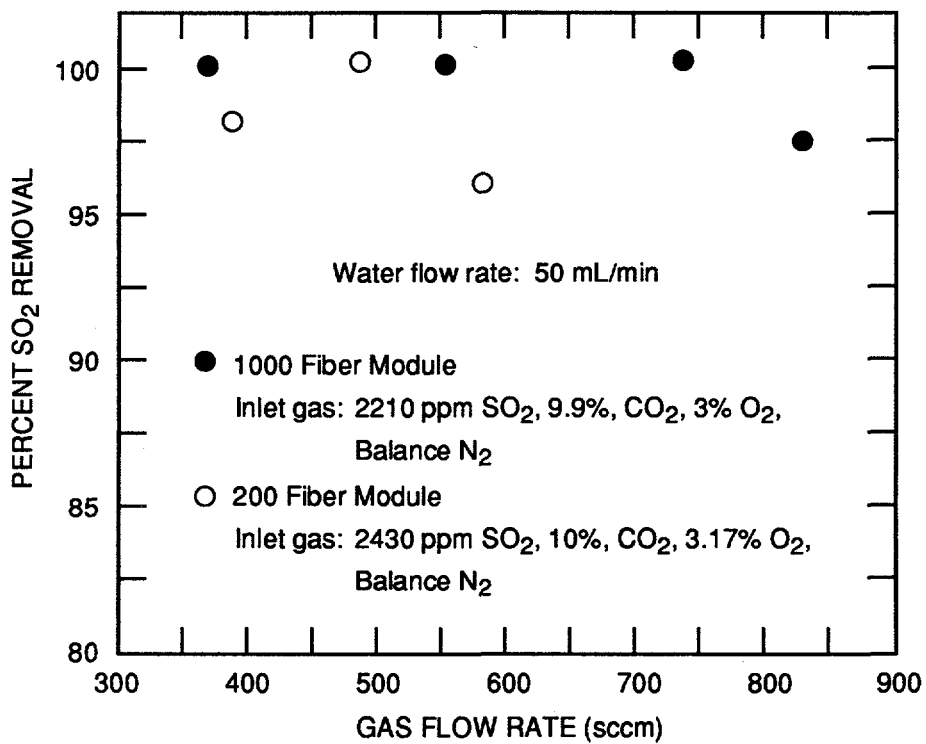
Three runs (10, 12, and 13) achieved steady state conditions using humidified incoming gas at a flow rate of 2713 sccm. The operating temperature of run 10 was high at 29°C and probably caused an increased reaction. A comparison of the K_g values of these runs shows that the changes in the liquid flow rate from 10 to 20 mL/min did not contribute significantly to the

overall SO₂ absorption. This suggests that the mass transfer may not be controlled by the liquid-phase-resistance at 0.2 M sulfite concentration. It is likely that the gas-phase-controlled transfer can be achieved by using this or higher levels of Na₂SO₃ in the scrubbing liquor.

Hence, we performed additional experiments. The liquid flow rate was at 20 mL/min and the gas flow rate was increased from 2713 to about 4500 sccm. The K_g values should increase; if that increment is significant, then gas-phase-control is indicated. Similar gas flow rates were used in a separate set of experiments where the liquid flow rate was 30 mL/min. Due to increased absorptive capacity at that liquid flow rate, all SO₂ can get absorbed. However, we expect to obtain steady state condition at much higher gas flow rates and some SO₂ in the exit gas stream. Such results at two different liquid flow rates and at several high gas flow rates, can highlight the role of gas-phase-control in SO₂ transfer.

In continuation of characterizing the operational characteristics of the 1000 fiber module, we also performed several SO₂ absorption experiments using DI water as the scrubbing medium. A model flue gas was supplied to the tube side and water was pumped through the shell side. The flue gas contained 2210 ppm SO₂, 3% O₂, 9.9% CO₂, and balance N₂. Gas flow rates of 370-840 sccm and a water flow rate of 50 mL/min were used. Very high removal for SO₂ was observed, mostly 100%. The results are plotted in Figure 4-23, describing the percent SO₂ removal efficiency. The plot also includes the results obtained previously, for the 200-fiber module in similar experiments using the same water flow rate. Another experiment, not shown in the plot, was conducted with 25 mL/min of water flow rate and 370 sccm of gas flow rate. It achieved 98% SO₂ removal efficiency.

NJIT's main objective was to conduct experiments for regenerating SO₂ scrubbing liquor, namely, the spent aqueous Na₂SO₃ solution obtained from a simultaneously run absorption experiment. We used the 1000-fiber HFC module for the liquid-liquid extraction run and the 200-fiber HFC module for SO₂ absorption. The major reasons for using this arrangement are as follows: Since the walls of the fibers are hydrophobic, water does not wet the fiber walls, and the pores within the fiber walls are filled with gas, ensuring rapid diffusion. A small contactor, therefore, suffices in this operation. However, during liquid-liquid extraction, the organic liquid will penetrate the hydrophobic fiber walls and fill their pores. Diffusion through these liquid-filled pores will be several orders of magnitude smaller than diffusion through the gas-filled pores. Hence, liquid-liquid extraction needs a larger module. Details of the liquid-liquid extraction runs are provided later. The extracting organic solvent dimethylaniline (DMA) wets the fiber material. Its removal from the module could be difficult and time consuming, and so the 1000-fiber module is being used for extraction runs only. Prior to starting the extraction runs, this 1000-fiber unit was used for a series of CO₂ absorption experiments. In previous runs,



CM-3501-42

Figure 4-23. SO₂ removal with water.

the values of the overall mass transfer coefficient (K_{Olm}) in pure CO_2 absorption were found to be smaller than those obtained for a gas mixture of 10% CO_2 and balance N_2 . The effort described below was directed toward examining that issue.

Pure CO_2 was fed into the tube-side of the 1000-fiber unit. The scrubbing liquid was DI water obtained from a Barnstead E-pure water purification system. The water was pumped through the shell side of the module. The shell side contains a large volume of water, which absorbs CO_2 coming through the fiber pores. The experimental system is allowed to reach a steady state, defined by a constant gas flow rate at the exit. Previous runs took 2-3 hours to reach steady state. We duplicated those runs first.

In the first run (No. 1, Table 4-2), the water flow rate was 100 mL/min. A pseudo-steady-state condition was observed at the end of 5 hours. In the second run, we monitored the gas-side pressure drop within the module using a manometer between the entrance and exit of the module. The manometric liquid was water, colored with microgram quantities of KMnO_4 . The run reached a steady state between 2 and 3 hours and was ended after 4 hours. The manometer showed an increase of pressure drop by 30%-40%. Several experiments were then run for about 4 to 5 hours. Often, the manometer showed increased pressure drops at the tube side as the run progressed. These may be attributed to blockage of pores by water vapor. Typically, a run was ended when such pressure drops became twice the initial pressure drop. A summary of these results is presented in Table 4-2. The overall mass transfer coefficients (K_{Olm}) are calculated from readings obtained at steady state condition. Occasionally, we noticed a minor drift as time went on.

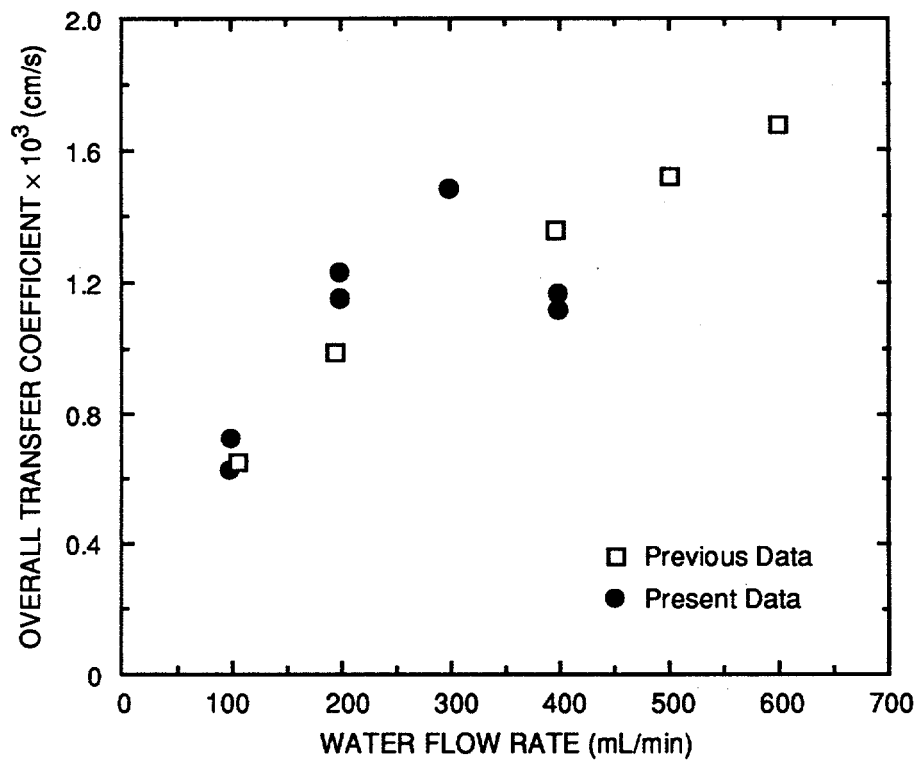
The above results are plotted in Figure 4-24. Earlier data on CO_2 absorption using the 1000-fiber module are also plotted. The values are similar to previous results. There is some scatter, yet the experimental results are reproducible. The values of the overall mass transfer coefficient (K_{Olm}) in absorption of pure CO_2 turned out to be smaller than those obtained with a mixture of 10% CO_2 and balance N_2 . We observed some increase in the pressure drop on the gas side. Such increased pressure drop indicated possible pore blockage, which might have affected the experimental results with pure CO_2 by reducing the mass transfer rate. We know that there is no gas-phase resistance in absorption of pure CO_2 in water. So the liquid-side resistance prevails. If pore blockage becomes significant, then the resistance to liquid side mass transfer will increase during a run.

Table 4-2
SUMMARY OF RESULTS ON CO₂ ABSORPTION IN 1000-FIBER UNIT

Run No.	Water Flow Rate (mL/min)	Percent Increase from Initial Pressure Drop by Manometer Reading	Mass Transfer Coefficient $K_{olm} \times 10^3$ (cm/s)	
			Present Result	Earlier Result
1	101	No manometer	0.73	---
2	100	30	0.63	---
	108	---	---	0.65
3	200	20	1.23	---
4	200	60	1.15	---
	200	---	---	0.99
5	300	20	1.48	---
6	400	60	1.16	---
7	400	50	1.12	---
	400	---	---	1.36
	500	---	---	1.52
	600	---	---	1.68

We also conducted work on simultaneous absorption of SO₂ by aqueous solution of Na₂SO₃ and regeneration of the spent liquor by extraction with dimethylaniline (DMA). A few runs were not useful because of the problems in pumping liquid at a low flow rate and difficulties in handling DMA. Three runs were completed. Results of the liquid-liquid extraction part are presented in a later section. In this section, we provide details on the absorption part of each of these three runs.

The first trial run used aqueous 0.2 M Na₂SO₃ solution as the absorbent. It was pumped through the shell side of the 200-fiber module at 20 mL/min. The residual composition of SO₂ at the outlet of this module was measured by sampling the treated flue gas in a GC. When a steady state condition for absorption was reached, the composition of SO₂ in the effluent attained a constant level. Such steady state conditions were reached after 6 hours. The effluent sulfite solution was then fed into the tube side of the 1000-fiber module and liquid DMA was pumped through the shell side of this extractor unit. We monitored the pH of both the aqueous effluent from the absorption unit and that from the liquid-liquid extraction unit. We anticipated that the



CAM-3501-45A

Figure 4-24. Pure CO₂ absorption in 1000-fiber module.

pH of the stream after the extraction step would increase since SO_2 was removed from it by DMA. We did not notice any such change (see results of run 1 in Table 4-2. The SO_2 concentration in DMA at the exit was determined by wet chemistry, which indicated SO_2 flux across the organic phase to be 4.6×10^{-10} mole/cm² s. The corresponding SO_2 flux from the flue gas to the aqueous phase in the absorption step was 1.02×10^{-8} mole/cm² s. The low fraction of SO_2 recovered by liquid-liquid extraction suggested that there was less free SO_2 available for removal at this step. Probably, a significant part of the SO_2 in the aqueous phase reacted with Na_2SO_3 to form NaHSO_3 .

In the following runs, the procedure for sampling the organic phase was improved. Also, in these runs, sulfite solution was not used to absorb SO_2 . Instead, DI water was used. We expected that more free SO_2 should be available for removal by the liquid extraction step. Also, it might be easier to monitor the pH changes of such an acidic aqueous solution as SO_2 is removed from it by DMA. A summary of results relating the absorption part of these experiments are presented in Table 4-3. Water was used as absorbent in runs 2 and 3. Run 2 did not show much changes of pH in the aqueous effluent caused by extraction with DMA. The next run with a higher water flow rate showed noticeable change.

Our purpose in conducting absorption-only experiments was to obtain a situation where the resistance to mass transfer shifts to the gas phase. We assume that a sulfite concentration of 0.2 M aqueous Na_2SO_3 was suitable to bring out that condition. In this type of experiment, the liquid flow rate was 20 mL/min and the gas flow rate was increased from about 2700 to 4500 sccm. There could be drying of sulfite solution near the pores inside the module at high gas flow rates, giving rise to an unsteady process and poorer performance in the contactor. Humidification of the incoming model flue gas has prevented such drying of liquid inside the module.

Two absorption-only experiments were conducted using 0.2 M Na_2SO_3 solution under identical conditions using a model flue gas with an initial composition of 2400 ppm SO_2 , 3% O_2 , 10% CO_2 , and the balance N_2 . One run was conducted with humidified incoming flue gas, and the other used dry gas from the cylinder. The purpose was to examine if steady state and good performance from the contactor could be achieved without humidifying the flue gas. Such experiments were not conducted earlier using the sulfite-liquid flow rate at 20 mL/min. The results are presented in Table 4-3, which also includes results of previously obtained steady state runs using a liquid flow of 20 mL/min. The runs are numbered accordingly. The inlet gas was not humidified in run 16. Run 14 describes the absorption part of the above absorption-extraction

Table 4-3
SUMMARY OF ABSORPTION DATA IN SIMULTANEOUS ABSORPTION-EXTRACTION RUNS

Run No.	Aqueous Absorbent		Flow Rate (sccm)	Flue Gas		Absorptive Flux of SO ₂ (mole/cm ² s)	Steady State pH of Aqueous Stream	
	Type	Flow Rate (mL/min)		SO ₂ Composition (ppm)			After Absorption	After Extraction
				Inlet	Outlet			
1	0.2 M Na ₂ SO ₃	20	2722 (Humidified)	2260	105	1.02 x 10 ⁻⁸	7.4	7.4
2	Water	22	901	2400	617	2.78 x 10 ⁻⁹	5.0	5.05
3	Water	50	908	2400	207	3.41 x 10 ⁻⁹	2.8	5.4

run with sulfite solution in Table 4-4. The performance of the HFC in the absorbing the model flue gas with Na_2SO_3 appears reproducible at this liquid flow rate, as evidenced by the reproducible values of K_g .

To evaluate the performance of the HFC in absorbing a model flue gas, we studied the extent of several reactions that occur simultaneously between the component gases and the sulfite liquor. The results of some experiments with 0.2 M Na_2SO_3 , were analyzed. Specifically, the conversions of SO_2 and CO_2 were compared. The reaction between SO_2 and aqueous Na_2SO_3 was rapid; it could be considered instantaneous. Preliminary analysis of steady state data showed that a ratio of about 4:1 was maintained between the amount reacted for SO_2 and CO_2 . Typically in a run, the composition of SO_2 dropped from an initial value of 2200 ppm to a value less than 100 ppm. The amount of CO_2 consumed in a parallel reaction was approximately 500 ppm. The initial concentration of CO_2 was close to 10% by volume. Thus, its depletion can be considered less significant with respect to that of SO_2 .

COMBINED ABSORPTION AND EXTRACTION

Initially, we conducted one absorption-only run and six simultaneous absorption runs of SO_2 by an aqueous solution of Na_2SO_3 and regeneration of the spent liquor by extraction with dimethylaniline (DMA). Details on the absorption part of these runs are presented in this section.

The sulfite liquor was pumped through the shell side of the 200-fiber module. The first three runs, AE-4 to AE-6, used a model flue gas with an initial composition of 2300 ppm of SO_2 , 2.9% O_2 , 10.5% CO_2 , and the balance N_2 . The second three runs, AE-7 to AE-9, used a model flue gas with an initial composition of 2170 ppm of SO_2 , 3.13% O_2 , 10.8% CO_2 , and the balance N_2 . The residual composition of SO_2 at the outlet of this module was measured by sampling the treated flue gas in a GC. A steady state condition for the absorption process was reached after about 5-6 hours. The effluent sulfite solution was then fed into the tube side of the 1000-fiber module and liquid DMA was pumped through the shell side of this extractor unit. The SO_2 concentration in DMA at the exit was determined by wet chemistry, from which its flux at the extraction stage was calculated. The corresponding SO_2 flux from the flue gas to the aqueous phase in the absorption step was obtained from material balance. The run-parameters and the absorptive fluxes are presented in Table 4-5.

In run AE-4, the flue gas was humidified before being fed into the module. Dry gas from the cylinder was used in runs AE-5 and -6. The flow rate of the sulfite liquor was changed to 10 mL/min in run AE-6 to examine its effect on the extraction process. We monitored the pH of both the aqueous effluent from the absorption unit and that from the extraction unit. An increase

Table 4-4
RESULTS OF SO₂ ABSORPTION RUNS USING 0.2 M Na₂SO₃ AT 20 mL/min

Run No.	Temp. (°C)	Liquid Flow Rate (mL/min)	Gas Flow Rate (sccm)	SO ₂ Composition (ppm)			SO ₂ Removal (%)	Kg (cm/s)
				Dry	Humid	Outlet		
12	28	20	2713	2210	2050	65	97	0.349
13	23	20	2713	2210	2082	71	96	0.337
14	20	20	2723	2400	2260	105	96	0.324
15	22	20	2705	2400	2243	67	97	0.345
16	20	20	2723	2400	---	58	98	0.367

Table 4-5

SUMMARY OF ABSORPTION DATA IN SIMULTANEOUS ABSORPTION-EXTRACTION RUNS

Run No.	Aqueous Absorbent		Flow Rate (sccm)	Flow Rate (mL/min)	Flue Gas SO ₂ Composition (ppm)		Absorptive Flux of SO ₂ (mole/cm ² s)	Steady State pH of Aqueous Stream	
	Type	Flow Rate (mL/min)			Inlet	Outlet		After Absorption	After Extraction
AE-4*	0.2 M Na ₂ SO ₃	20	2722 (Humidified)	20	2250	69	1.02 x 10 ⁻⁸	7.35	7.4
AE-5*	0.2 M Na ₂ SO ₃	20	2704 (Dry)	20	2300	43	1.05 x 10 ⁻⁸	7.7	7.8
AE-6**	0.2 M Na ₂ SO ₃	10	2732 (Dry)	10	2300	100	1.038 x 10 ⁻⁸	7.3	7.3
AE-7*	0.2 M Na ₂ SO ₃	20	2732	20	2170	44	0.996 x 10 ⁻⁸	7.55	7.75
AE-8*	0.2 M Na ₂ SO ₃	20	2732	20	2170	60	0.990 x 10 ⁻⁸	7.4	7.5
AE-9***	0.2 M Na ₂ SO ₃	30	5000	30	2170	142	1.721 x 10 ⁻⁸	7.3	7.65

* DMA flow rates were different at the extraction stage.

** The liquid flow rate at the absorption part was decreased.

*** Both the gas and liquid flow rates at the absorption part were increased.

in the pH of the stream after extraction was anticipated since SO₂ was removed at this step. We did not observe any significant change (see Table 4-5). Dry gas from the cylinder was used in runs AE-7, -8, and -9. The flow rate of the DMA was varied at the extraction stage; otherwise the absorption segment of runs AE-7 and -8 were similar to that of Runs AE 5 and 6. In run AE-9, the flow rate of the sulfite liquor was increased to 30 mL/min to examine its effect in reducing the boundary layer resistance at the downstream extraction process. The gas flow rate was increased to 5 slpm to adapt to the increased liquid flow rate and help attain low residual concentration of SO₂ at the outlet of the absorption unit. After about 3 hours, the SO₂ level in the treated flue gas reached a value of 144 ± 5 ppm. It remained there for the rest of the runtime of 4 hours, which included the extraction process. It was the highest gas flow rate we ever used. A steady absorption process was in effect with an increased flow of aqueous sulfite liquor. The high flow rate of the liquid allowed the operation without any pore drying although the incoming flue gas was not humidified. We monitored the pH of both the aqueous effluents from the absorption unit and that from the extraction unit. A minor increase in the pH of the stream after extraction was observed in these three runs. See Table 4-5.

In continuing our efforts to obtain a situation where the resistance to mass transfer shifts to the gas phase, two absorption-only experiments were conducted. The first, A-17, was run with the flow rate of the humidified incoming flue gas set at approximately 3630 sccm and other conditions were identical to those absorption-only runs reported previously. The model flue gas had an initial composition of 2300 ppm SO₂, 2.9% O₂, 10.5% CO₂, and the balance N₂. The results are presented in Table 4-6, which also includes results of absorption part of the above extraction-absorption runs with the sulfite solution.

In the second absorption-only experiment, run A-18, the model flue gas had an initial composition of 2170 ppm SO₂, 3.13% O₂, 10.8% CO₂, and the balance N₂. It was humidified before being fed into the module. The flow rate of this incoming flue gas was 4500 sccm. Increase of the gas flow rate was in line with the experimental pattern we adopted in recently completed absorption-only runs when other conditions were identical. The incoming flue gas was humidified by passing it through the tube side of two HFC modules whose shell sides were filled with water maintained at 10 psig. The high gas flow rate of 4500 sccm introduced a larger amount of moisture in the stream. It was difficult to remove this moisture completely from the sample effluent going into the GC by the Nafion membrane drier. After 3 hours, the effluent compositions of SO₂, other components and water vapor attained a constant level. The SO₂ composition was 148 ± 8 ppm with repetitive fluctuations showing a steady state run condition. The results are presented in Table 4-6, which includes results of absorption part of the above extraction-absorption runs.

Table 4-6
RESULTS OF SO₂ ABSORPTION RUNS USING 0.2 M Na₂SO₃ AT 20 mL/min

Run No.*	Temp. (°C)	Liquid Flow Rate (mL/min)	Gas Flow Rate (sccm)	SO ₂ Composition (ppm)			SO ₂ Removal (%)	Kg (cm/s)
				Dry	Humid	Outlet		
AE-4	19	20	2732	2300	2250	69	97	0.345
AE-5	22	20	2704	2300	---	43	98	0.395
AE-6	19	10	2723	2300	---	80	97	0.332
A-17	20	20	3630	2300	2243	100	96	0.397
AE-7	19	20	2732	2170	---	44	98	0.384
AE-8	19	20	2732	2170	---	60	97	0.354
AE-9	19	30	5000	2170	---	142	93	0.465
A-18	18.5	20	4500	2170	2150	148	93	0.416
A-15	22	20	2704	2400	2243	67	97	0.345
A-12	28	20	2713	2210	2050	65	97	0.349

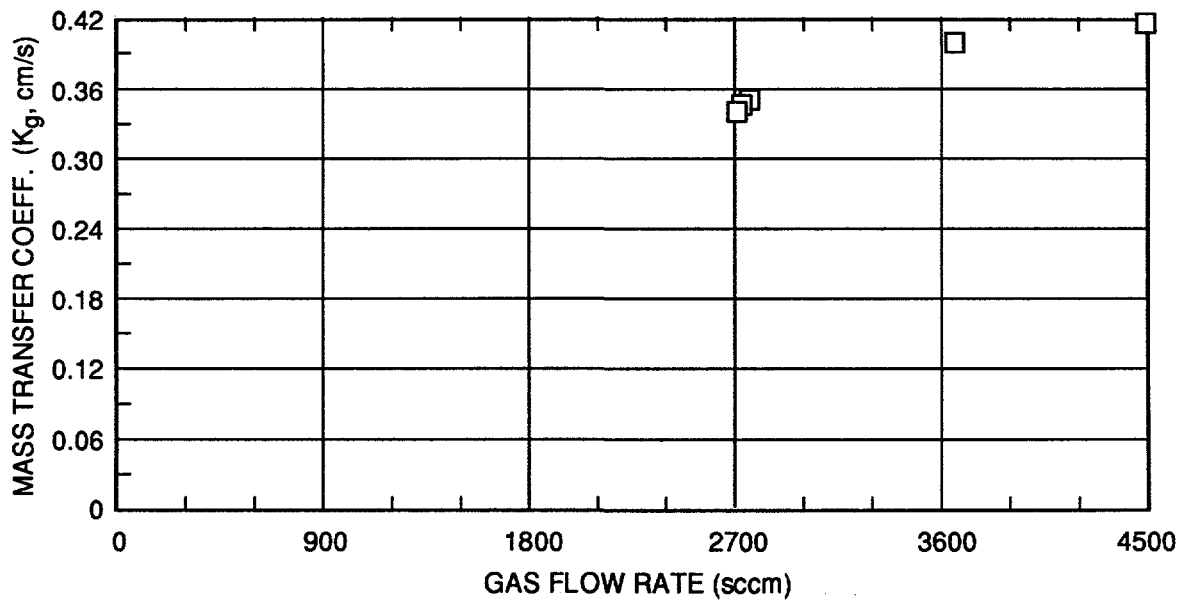
*AE - indicates absorption-extraction run.
A - for absorption-only run.

The steady state condition for the absorption process was achieved in many runs, using a flow rate of 20 mL/min for the aqueous-sulfite-solution and gas flow rates varying between 1800-4500 sccm. Most runs used liquid and gas flow rates as 20 mL/min and about 2700 sccm, respectively, a combination often used in absorption-extraction runs. Typical values of the mass transfer coefficient obtained from some of these runs are plotted in Figure 4-25 against the corresponding gas flow rates. Sample values are from Table 4-6. The plot shows a pattern in which K_g increases with the gas flow rate, and that dependency becomes smaller at higher gas flow rates. The data trend is toward gas-phase controlled mass transfer.

Previously, an analysis of results of some flue-gas-absorption experiments with 0.2 M Na_2SO_3 was reported. We compared the conversions of SO_2 and CO_2 that occurred simultaneously. The analysis suggested that the reaction between SO_2 and aqueous Na_2SO_3 can be considered instantaneous. Typically, a ratio of about 4:1 was maintained between the amount reacted for SO_2 and CO_2 . The depletion of CO_2 was less significant with respect to that of SO_2 .

A separate run was also conducted using 0.2 M Na_2SO_3 to absorb a gas mixture of CO_2 - N_2 containing 9.89 % CO_2 . A model flue gas usually consists of about 2500 ppm SO_2 , 10% CO_2 , 3% O_2 , and the balance N_2 . The purpose in this experiment was to gather data on the extent of reaction that could occur between CO_2 and the sulfite liquor in the 200-fiber contactor in the absence of SO_2 and O_2 . The gas flow rate was about 2700 sccm and the liquid flow rate was 20 mL/min, similar to those of a typical run in absorbing flue gas. A steady state condition was obtained after about two hours, and the run continued for an additional hour. An estimation of GC results indicated that 4.34% of the incoming CO_2 reacted with the sulfite solution. It amounted to a removal of 4290 ppm from 98,900 ppm of inlet CO_2 . In the case of flue gas absorption, the SO_2 composition dropped typically from about 2300 to 50-80 ppm. The amount of CO_2 consumed in a parallel reaction was estimated to be approximately 500 ppm. The selectivity of reactions with sulfite is favored for SO_2 . We plan to continue to examine the speed of the reactions of SO_2 with the sulfite solution.

Earlier, an experiment was conducted on absorption of SO_2 by DI water and its simultaneous recovery by extraction with dimethylaniline(DMA). The absorption part of run AE-11 is similar to that part of run AE-3 using water as the absorbent. These two runs differed in their LLE segments. The flow rate of the organic phase was 40 mL/min in run AE-11 and 6 mL/min in AE-3. The extraction part of the run AE-11 resembles the extraction part of the run AE-10. The purpose in using a high flow-rate of DMA was to examine its effect in removing SO_2 from the aqueous phase. We also developed an experimental setup to find the values of



CM-3501-59

Figure 4-25. Variation of mass transfer coefficient with gas flow rates at an aqueous sulfite solution flow of 20 mL/min.

distribution coefficient (m_1) for SO₂ in organic-aqueous phases. We present results of these LLE runs and such flow assembly in later sections in Task 6 after describing the absorption part of these runs.

The aqueous phase (DI water/sulfite liquor) was pumped through the shell side of the 200-fiber module. The runs used a model flue gas with an initial composition of 2230 ppm of SO₂, 3.13% O₂, 11.0% CO₂, and the balance N₂. Both runs AE-10 and -11 used dry gas from the cylinder. When the absorption process reached steady state, the aqueous effluent was fed into the tube side of the 1000-fiber module used for LLE. In this extractor unit, liquid DMA was pumped through the shell side. The flow rate of the DMA (~40 mL/min) was the highest value used so far. The run-parameters and the absorptive fluxes are presented in Table 4-7.

The absorption part of run AE-11, similar to that part of run AE-3 using water as the absorbent, had a flow rate of incoming flue gas of 908 sccm. The flow rate of water on the shell side of the HFC unit was 50 mL/min. A steady state for the absorption was achieved in about 3 hours with a SO₂ concentration in the treated gas of 150 ± 5 ppm. The pH value of the aqueous effluent from the absorption unit was 2.7. When LLE operation was initiated at 5 hours, the pH of this stream beyond the extraction unit increased to 5.6. Evidently, a high removal of SO₂ from the aqueous stream was occurring. The run continued for about 8 hours. The results are summarized in Table 4-7. The absorption performance of the current run AE-11 matches that of run AE-3. The two runs differed in LLE segments only.

In the absorption part of run AE-10, the gas flow rate was 2459 sccm. The absorption segment of this run was partly similar to a previously completed run AE-6. The flow rate of the sulfite liquor was 10 mL/min instead of the usual 20 mL/min to raise the level of SO₂ in the aqueous phase. After about 3 hours, the SO₂ level in the treated flue gas reached a value of 40+5 ppm. Such a steady state condition remained for the rest of the runtime of 7 hours, which included the extraction process. We monitored the pH of both aqueous effluent from the absorption unit and that from the extraction unit. We did not observe any significant change. The higher concentrations of SO₂ in the aqueous phase and an increased residence time for the aqueous phase in the LLE module were expected to cause high recovery by extraction. (See Table 4-7).

Additional experiments were conducted to measure distribution coefficient (m_1) of SO₂ between the aqueous and organic phases. The procedure involved contacting and thus establishing equilibrium between constant volumes of SO₂-rich aqueous phase and fresh DMA. This was attained by operating two HFCs. In the first unit, a steady state condition for absorption of SO₂ into an aqueous phase was obtained. The tube side of the second module was fed with a constant volume of this SO₂-laden effluent. A constant volume of fresh DMA was then introduced at the

Table 4-7
ABSORPTION DATA IN RECENT ABSORPTION-EXTRACTION RUNS USING HIGH AND LOW FLOW RATES OF DMA

Run No.	Aqueous Absorbent		Flow Rate (sccm)	Flue Gas		Absorptive Flux of SO ₂ (mole/cm ² s)	Steady State pH of Aqueous Stream	
	Type	Flow Rate (mL/min)		Inlet	Outlet		After Absorption	After Extraction
AE-10*	0.2 M Na ₂ SO ₃	10	2459	2230	40	0.9250 x 10 ⁻⁸	7.1	7.1
AE-6**	0.2 M Na ₂ SO ₃	10	2732	2300	100	1.038 x 10 ⁻⁸	7.3	7.3
AE-11*	Water	50	908	2230	147	3.25 x 10 ⁻⁹	2.7	5.4
AE-3**	Water	50	908	240	207	3.41 x 10 ⁻⁹	2.8	5.4

* DMA flow rate during extraction ~40 mL/min.

** DMA flow rate during extraction ~6 mL/min.

shell side of that unit. Continuous contacting between both these phases was maintained by keeping them in two separate closed-loop circulation. A LLE process operated, transferring SO₂ from the aqueous to the organic phase in batch mode. The experiment was continued for a long time, ensuring that equilibrium had been reached between the phases. The composition of SO₂ in each phase changed gradually and reached a constant value. The final concentration of SO₂ in DMA was measured. Its initial composition in the aqueous phase was known beforehand from mass-balance of the absorption process.

We present results of these new runs and their procedures in the section on Task 6 after describing the absorption part of these runs. The runs are numbered as AEM-1 and AEM-2. The aqueous phase (DI water/sulfite liquor) was pumped through the shell side of the 200-fiber module. The runs used a model flue gas with an initial composition of 2230 ppm of SO₂, 3.13% O₂, 11.0% CO₂, and the balance N₂. Both runs AEM-1 and AEM-2 used dry gas from the cylinder. When the absorption process reached a steady state, a known volume of the aqueous effluent was fed into the tube side of the 1000-fiber module. A four-way valve was used to disengage the first module. The shell side of the extractor unit was filled with fresh DMA. After introducing a constant volume of DMA, another four-way valve was used to disengage inflow of new DMA. Two pumps were run simultaneously to circulate the aqueous phase and the organic phase in two separate loops. The fibers were wetted by DMA. The contacting of the phases took place in the tube-side of the extractor. Table 4-8 presents the run-parameters and the absorptive fluxes.

Three experiments were conducted, two of which involved measurement of the distribution coefficient (m_i) of SO₂ between the aqueous and organic phases. The objective was to measure accurately such m_i values and obtain reproducibility of the results with those reported earlier. The runs are numbered AEM-3 and AEM-4. Details of the procedure are similar to the runs performed earlier. The third run, AE-12, involved absorption of SO₂ in 0.2 M Na₂SO₃ solution and its simultaneous recovery by extraction with DMA. The flow rate of the organic phase was 102 mL/min. The purpose of using such a high flow rate of DMA was to achieve complete recovery of SO₂. This is in line with one of the milestones of the project, i.e., achieving 99% SO₂ recovery at the LLE stage. As stated before, the results and procedures of the LLE stage will be discussed in Task 6 of this report.

The m_i -runs AEM-3 and -4 used a model flue gas having the following composition: 2230 ppm SO₂, 3.13% O₂, 11.0% CO₂, and the balance N₂. Run AE-12 used a gas containing 2300 ppm of SO₂, 3.22% O₂, 11.0% CO₂, and the balance N₂. All three runs used dry gas from a cylinder. We present the run-parameters and the absorptive fluxes in Table 4-7.

Table 4-8
ABSORPTION DATA TO DETERMINE DISTRIBUTION CONSTANT (m) USING HFCs FOR ABSORPTION-EXTRACTION

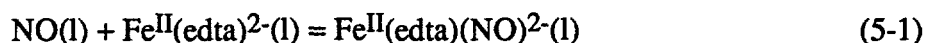
Run No.	Aqueous Absorbent		Flow Rate (sccm)	Flue Gas		pH of Aqueous Stream		SO ₂ Transfer (mole/s)	Concentration of SO ₂ in Aqueous Phase (mole/cm ³)	
	Type	Flow Rate (mL/min)		Composition (ppm)	SO ₂ Composition (ppm)	Initial	Final			
AEM-1	0.2 M Na ₂ SO ₃	20	2732	Inlet	2230	43	9.4	7.3	4.43 x 10 ⁻⁶	13.3 x 10 ⁻⁶
AEM-2	Water	45	908	Inlet	2230	85	5.6	3.0	1.45 x 10 ⁻⁶	1.9 x 10 ⁻⁶
AEM-3	Water	45	908	Inlet	2230	116	5.6	3.2	1.43 x 10 ⁻⁶	1.9 x 10 ⁻⁶
AEM-4	0.2 M Na ₂ SO ₃	20	2718	Inlet	2230	44	9.4	7.3	4.42 x 10 ⁻⁶	13.3 x 10 ⁻⁶
AE-12	0.2 M Na ₂ SO ₃	20	2718	Inlet	2300	42	9.3	7.3	4.57 x 10 ⁻⁶	13.7 x 10 ⁻⁶

We fabricated a module to undertake process studies on contained liquid membrane technique to regenerate the aqueous absorbent. Details of construction are presented in Task 6 of this report.

TASK 5: MASS TRANSFER RATE STUDIES FOR NO_x SCRUBBING IN HOLLOW FIBER CONTACTORS

The objective of this task was to determine the mass transfer characteristics of hollow fiber contactors (HFCs) for scrubbing NO_x from a simulated flue gas. NO and N₂ are blended at controlled rates, passed through a humidifier, checked for composition, heated, and fed into the lumens of the hollow fibers. The scrubbing liquid is pumped at a controlled flow rate, filtered, heated, and fed into the shell-side of the hollow fiber module. Pressure and temperature probes at various locations allow us to monitor and control the experimental conditions.

Initially we used aqueous solutions of [Fe^{II}(edta)]²⁻ as the scrubbing solution. The chelate is known to complex with NO according to the liquid-phase reaction:



Based on this expression and assuming counter-current flow, Appendix E shows that the minimum liquid flow rate necessary to treat a given gas flow rate is given as

$$\frac{\text{Liquid Flow rate; L/min}}{\text{Gas Flow rate; L(STP)/min}} = \frac{10^{-6}}{22.4} \frac{1 + K\alpha[\text{NO(g)}][\text{Fe}^{\text{II}}(\text{edta})^{2-}(\text{l})]_{\text{initial}}}{\alpha\{1 + K\alpha[\text{NO(g)}] + K[\text{Fe}^{\text{II}}(\text{edta})^{2-}(\text{l})]_{\text{initial}}\}} \quad (5-2)$$

where K is the equilibrium constant of the reaction shown in Eq. (5-1) and α is the partition coefficient between gas and liquid phase NO.

From literature, we obtained the value of K as 9.90×10^5 L/mol and the value of α as 1.788×10^{-9} mol/L-ppm. Figure 5-1 shows results of calculations using Eq. (5-2). Note that a higher initial Fe^{II}(edta)²⁻ concentration in the liquid phase allows a higher gas to liquid ratio to be used. These data were used to help design the HFC apparatus.

From these data, we completed construction of the HFC test apparatus shown in Figure 5-2 and moved it to a hood to alleviate safety concerns. While waiting for a NO_x analyzer from DOE, we duplicated early experiments reported by NJIT under Task 3 of this project. Successful duplication would ensure that our test apparatus was performing similar to other researchers.

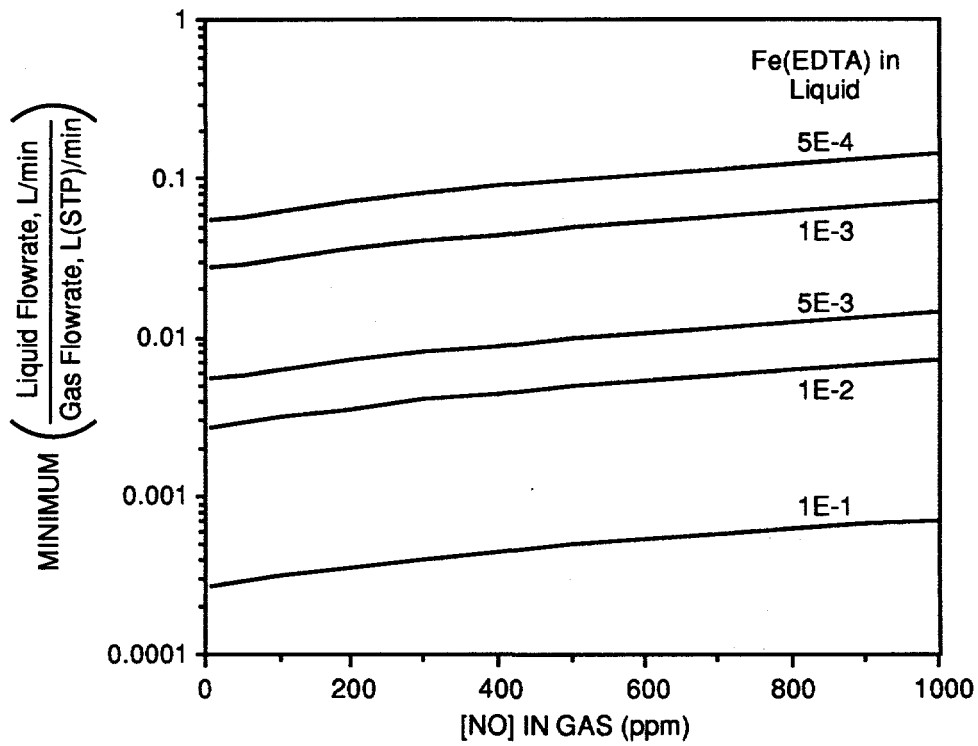
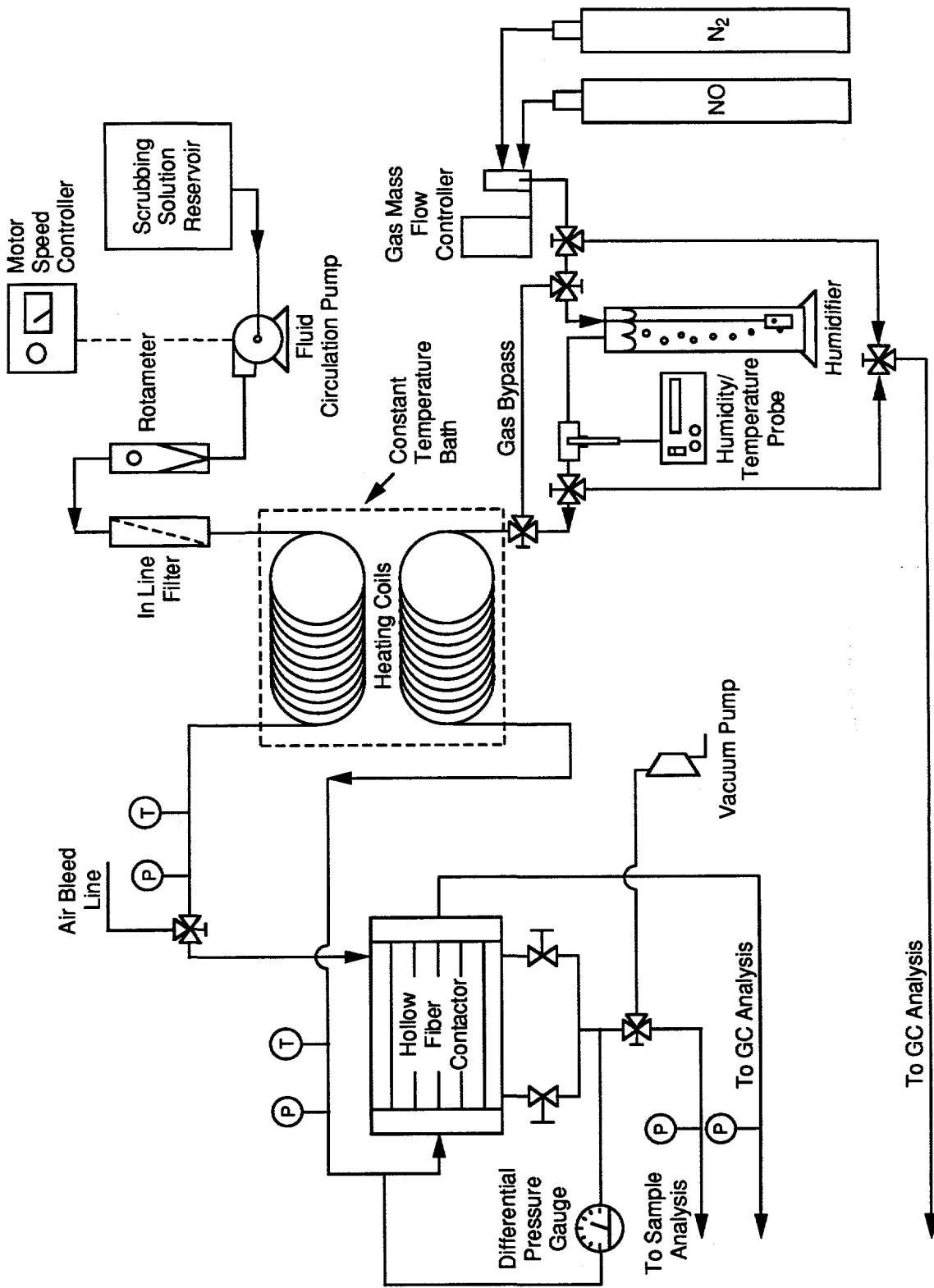


Figure 5-1. Minimum liquid-to-gas flow rate ratio needed to obtain equilibrium.



CAM-3501-39

Figure 5-2. Schematic of HFC apparatus.

CO₂ SCRUBBING

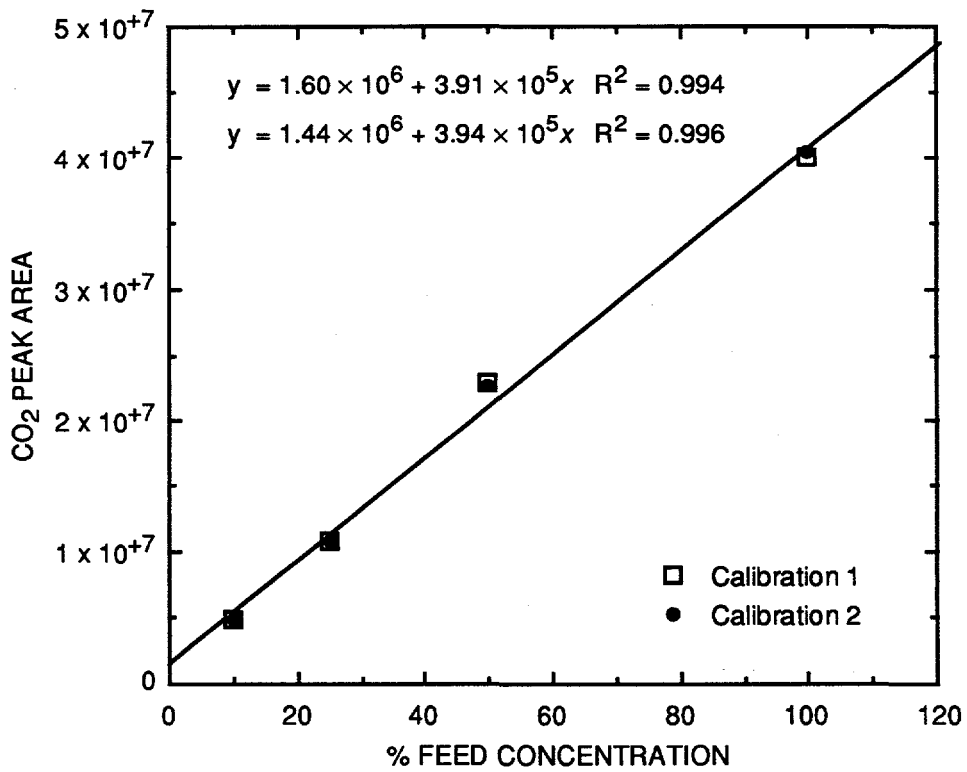
The first experiments we repeated were those using a 1000-fiber HFC with 300- μ m-OD and 240- μ m-ID fibers and an active length of 23 cm. Our experiments, like those at NJIT, focused on CO₂ scrubbing with water. Two sets of experiments were conducted at room temperature. The first was with a 1.99% CO₂, 2.01% N₂, and the balance He gas mixture from a cylinder (Liquid Carbonic, Chicago, IL) flowing through the fiber lumens and deionized water (Milli-Q, Millipore Corporation, Medford, MA) flowing in the shell side. The gas flow rate was set at 80 sccm and the water flow rate varied between 25 and 100 mL/min. The second set of experiments was conducted identically to the first, except that the gas feed was 50% CO₂ in N₂, obtained by blending pure CO₂ and pure N₂ from cylinders. Overall mass transfer coefficients (MTC) were calculated for both sets of experiments.

The gas chromatograph was first calibrated by blending known flow rates of the feed cylinder gas with known flow rates of N₂ from a cylinder. The blended gas of known composition was then sampled with a gas chromatograph (Hewlett Packard Model 5890), resulting in a calibration curve like the one shown in Figure 5-3. These calibrations were made frequently, especially at the end of a run.

Our results, along with those of NJIT (see Task 4) are plotted in Figure 5-4. Two observations are immediate. First in our modules, the MTCs with 1.99% CO₂ were lower than the ones with 50% CO₂. This indicates existence of a gas-phase resistance. Conversely, the MTC reported by NJIT was the same for 100% CO₂ and 10% CO₂, which indicates no gas phase resistance in their module. Hence, our results and NJIT results differ in gas-phase resistances. The second immediate observation is that the magnitude of MTC we measured was about 3-8 times lower than that reported by NJIT. Hence, our results and NJIT results differ in magnitude of MTCs.

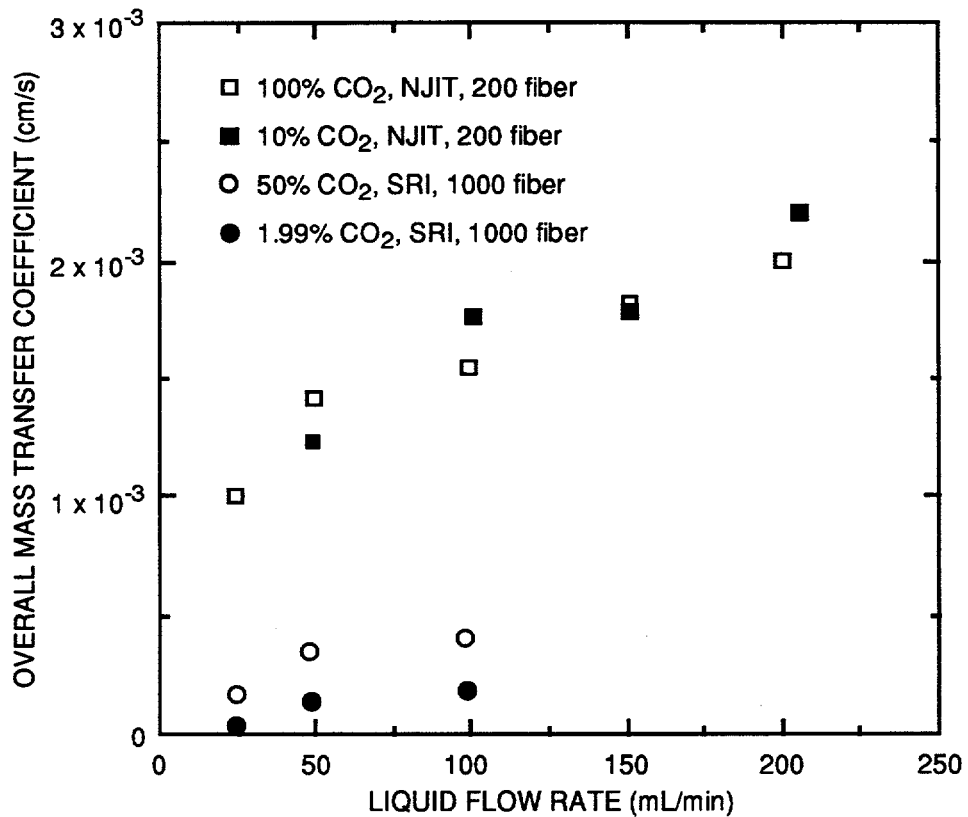
Clearly, these two differences indicate that our modules and NJIT modules are different. We visually inspected our module under a microscope and noted that up to 10%-15% of the fiber ends were blocked. The blockage appeared to be epoxy or fiber material sheared during manufacturing. Although the percent blockage was low, it may have changed the hydrodynamics within the module to yield different results.

Since then, we contacted Hoechst Celanese to learn how to open the fiber ends and have removed the 1000-fiber module from our process line. In the meantime, we conducted the same experiments with the 200-fiber HFC.



CAM-3501-37

Figure 5-3. Calibration using a 1.99% CO₂ cylinder.



CAM-3501-38

Figure 5-4. Overall mass transfer coefficient versus water flow rate.

Before continuing the experiments, we photographed the ends of both the 200-fiber and the 1000-fiber HFCs. These are shown in Figure 5-5. We counted 301 fibers in the "200"-fiber HFC and 1155 fibers in the "1000"-fiber HFC. Moreover, as shown in Figures 5-5.1 and 5-5.2, the 301-fiber module has all of its fibers' ends completely open. However, as shown in Figures 5-5.3 and 5-5.4, the 1155-fiber module has about 10%-15% of its fibers' ends blocked. As will be shown shortly, we believe the blockage leads to unsatisfactory performance of the 1155-fiber HFC. We sent this module back to Hoechst-Celanese with copies of our photographs, and they have agreed to replace the 1155-fiber HFC at no additional cost.

We also completed a series of experiments: scrubbing gases of various concentrations of CO₂ with water using the 301-fiber Hoechst Celanese HFC. These experiments were essentially duplicates of those performed earlier at the NJIT in Task 4 of this project. Deionized water in our experiments was obtained from a Millipore Milli-Q water purification system (Millipore Corp., Bedford, MA). Three gas compositions were used: 1.91% CO₂/2.01% N₂/balance He, 50% CO₂/balance He, and 99.99% CO₂. Scrubbing experiments were conducted at room temperature with water flow rates between 25 and 160 mL/min and a gas flow rate of 80 sccm.

For the three gas compositions, the overall liquid mass transfer coefficient (K_{Olm}) versus water flow rate is plotted in Figure 5-6; earlier data reported by NJIT are also plotted. Note that K_{Olm} of the 1.91% CO₂ and the 50% CO₂ experiments at SRI are fairly similar, but K_{Olm} of the pure CO₂ experiment is slightly higher. This indicates a slight gas-side resistance, unlike NJIT data. Still, the gas phase resistance is small.

The overall mass transfer coefficients and liquid flow rates were reduced to Sherwood numbers and Reynolds numbers (based on outer fiber diameter) and are plotted in Figure 5-7 along with NJIT results (see Task 4). From this figure, our results for the 301-fiber HFC appear to be similar to NJIT results, especially at higher Reynolds numbers. The relatively flat slope of these data points indicates that the overall resistance does not depend much on the liquid flow rate.

As reported earlier, we conducted an additional set of experiments with CO₂ with the "1000"-fiber HFC, but many fibers in this module were found to be blocked. The effect of these blocked fibers can be seen in the low Sherwood numbers found in Figure 5-7. As a result, we believe that the 1000-fiber HFC was not performing adequately.

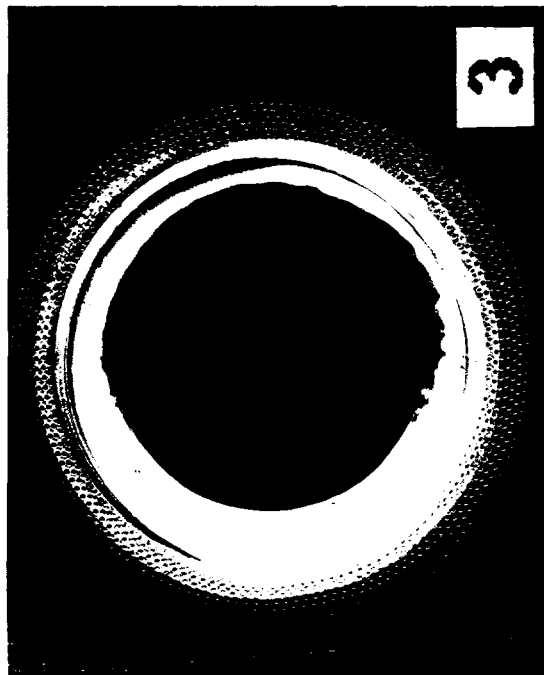
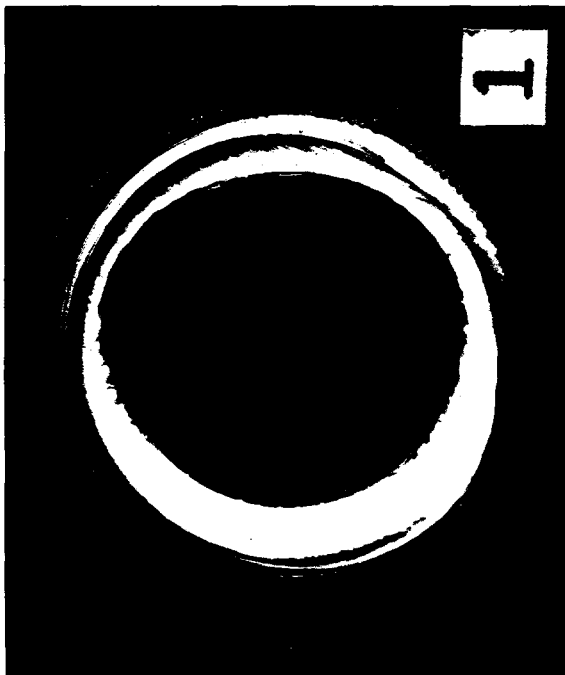
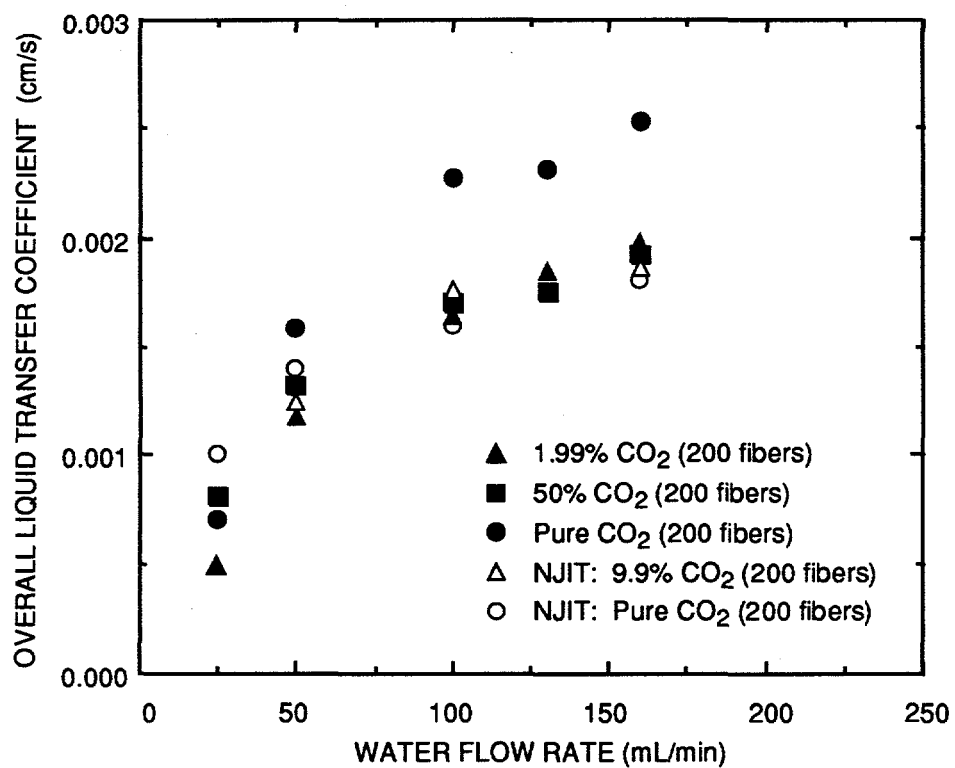
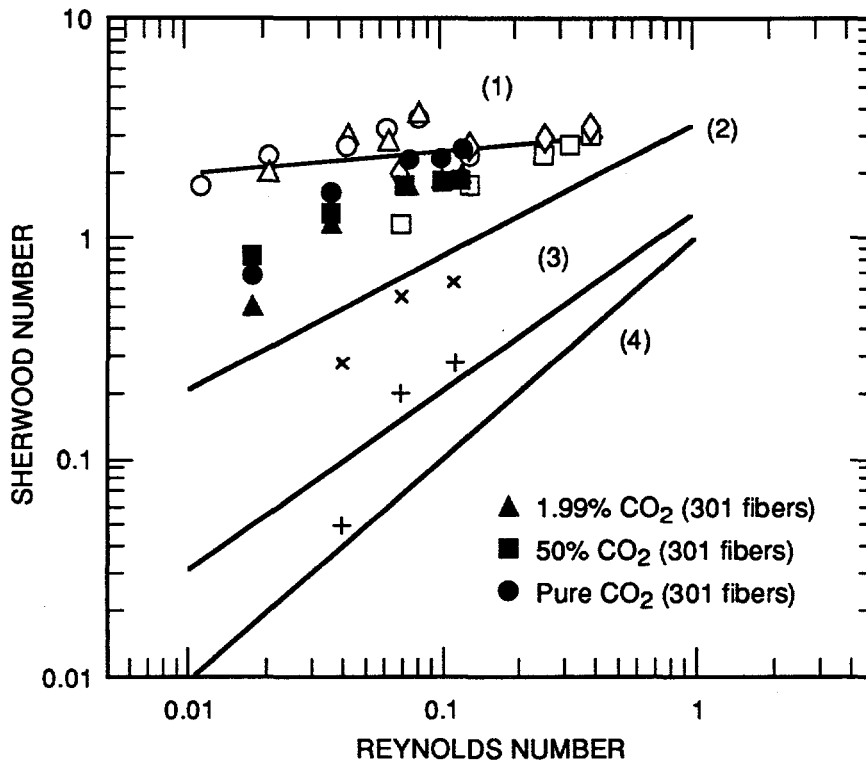


Figure 5-5. Fiber openings for 1000 and 200 fiber modules.



CAM-3501-43

Figure 5-6. Overall liquid mass transfer coefficient versus liquid flow rate.



Module	Pure CO ₂		CO ₂ -N ₂		
	NJIT	SRI	NJIT, 9.9%	SRI, 1.99%	SRI, 50%
200 Fibers	○		△		■
301 Fibers		●		▲	■
1000 Fibers	□		◇		
1155 Fibers				+	x

(1) NJIT Combined Data
 $Sh = 0.38 \quad Re^{0.08} \quad Sc^{0.33}$

(2) Kreith and Black, 1986
 $Sh = 0.39 \quad Re^{0.59} \quad Sc^{0.33}$

(3) Wickramasinghe et al., 1992
 $Sh = 0.15 \quad Re^{0.8} \quad Sc^{0.33} \quad \text{for } Re > 2.5$

(4) Literature correlation (Yang and Cussler, 1986)
 $Sh = 0.39 \quad Re^{1.0} \quad Sc^{0.33} \quad \text{for } Re > 2.5$

CM-3501-49A

Figure 5-7. Sherwood number versus Reynolds number for CO₂ absorption in water.

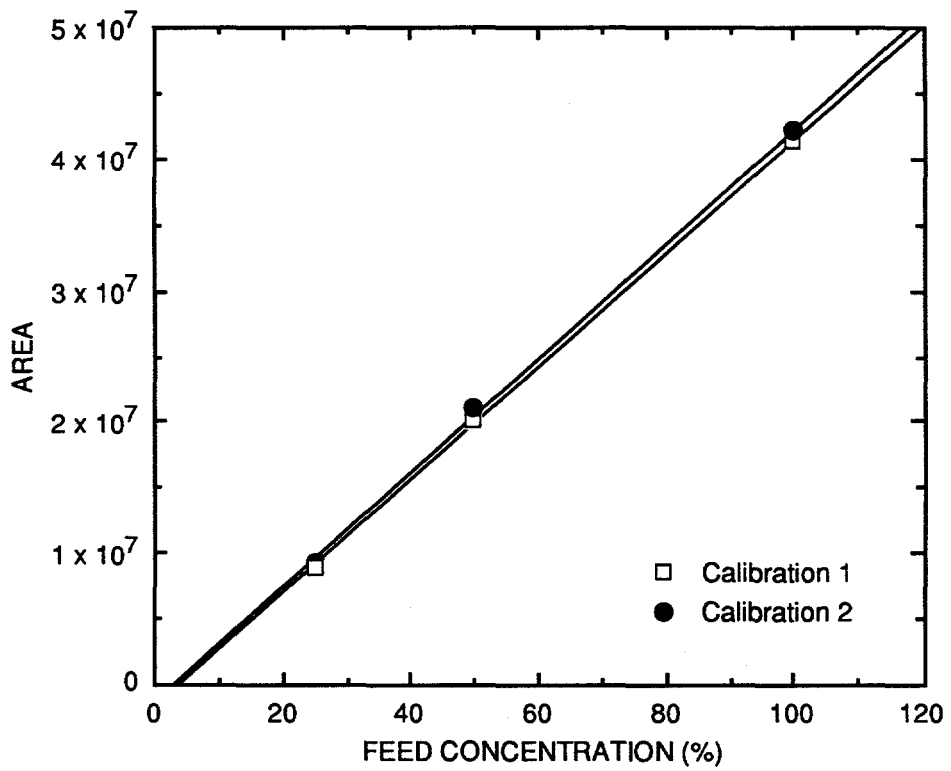
SO₂ SCRUBBING

Next, we tested the performance of our 301-fiber HFC with a simulated flue gas containing 1.46% SO₂ and a balance of N₂. This was done to compare our HFC's performance with the one used by New Jersey Institute of Technology (NJIT). Before doing any experimental runs, we calibrated our GC (Hewlett-Packard Model No. 5890) with this gas mixture blended with N₂. The results of the calibration can be seen in Figure 5-8, which shows that the calibration is linear and nearly goes through the origin. Next, we planned to duplicate the procedures from the SO₂ experiments completed at NJIT. Therefore, the flue gas flow rate was set at 44.5 sccm, and the chosen range of the water flow rate was 25-125 mL/min. According to NJIT's findings, 98% removal of SO₂ from a 1.6% SO₂ flue gas was obtained at a liquid flow rate of 50 ml/min. At higher liquid flow rates, 100% removal of SO₂ was observed. When we performed the same experiment with our HFC, we found that 100% of the SO₂ was scrubbed from the simulated flue gas at a liquid flow rate of only 25 mL/min. As a result, we decided to keep the water flow rate at 25 mL/min and to increase the gas flow rate until SO₂ could be detected in the exiting gas stream. Assuming that the mass transfer coefficient obtained from the CO₂/H₂O experiments would be the same for an SO₂/H₂O system, we calculated that to get 10%, 25%, and 50% of the SO₂ feed concentration in the exiting gas stream, gas flow rates of 148 sccm, 240 sccm, and 460 sccm, respectively, would be needed at a water flow rate of 25 mL/min. Three experiments with SO₂ were completed based on the previous calculations.

With a gas flow rate of 148 sccm and a water flow rate of 25 mL/min, no SO₂ was detected at the gas outlet. At a gas flow rate of 240 sccm, 92.9% removal of SO₂ was observed. Also, with the gas flow rate increased to 427.4 sccm, 73.8% of the SO₂ was removed from the flue gas. These results are shown graphically in Figure 5-9. Since the actual amount of SO₂ removal is higher than predicted by the previous calculations, the overall mass transfer coefficient at 25 mL/min of H₂O for SO₂ scrubbing differs from the one for CO₂ scrubbing.

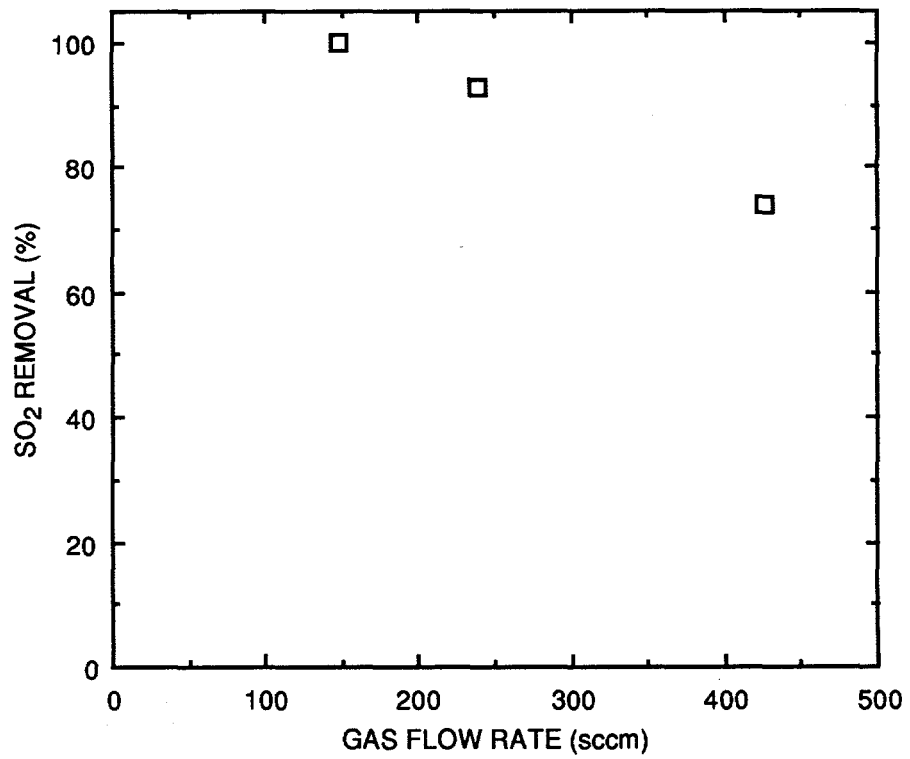
NO_x SCRUBBING

Later, we received the NO_x analyzer from another DOE contractor. It was calibrated with a 1.04% NO/balance N₂ gas cylinder blended with N₂. The calibration curve, shown in Figure 5-10, is linear.



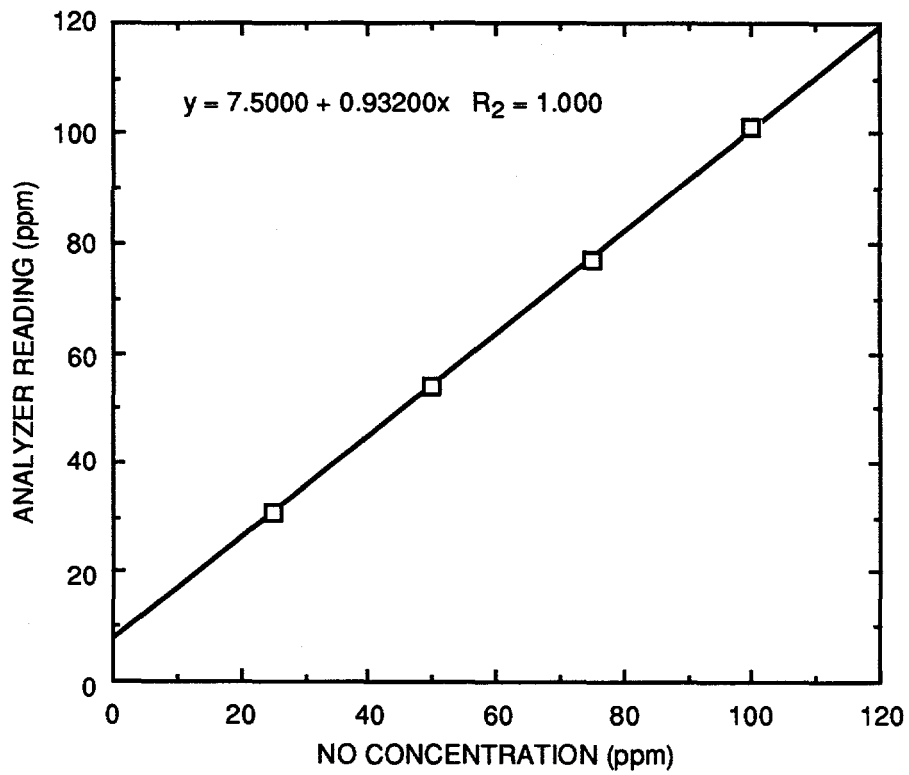
CAM-3501-46

Figure 5-8. GC calibration with 1.46% SO₂ in N₂ feed.



CAM-3501-47

Figure 5-9. SO₂ removal water flow rate of 25 mL/min.



CAM-3501-50

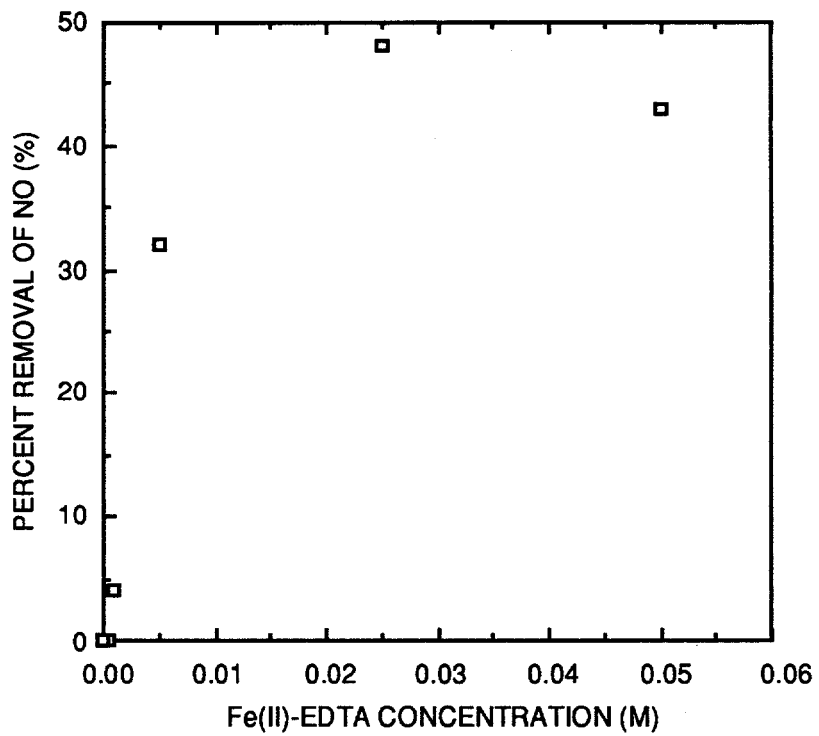
Figure 5-10. Calibration curve of the NO_x analyzer.

We began studying NO_x removal from a simulated flue gas stream using our 301-fiber hollow fiber contactor. For these experiments, we blended 1.04% NO with N_2 to arrive at a 100-ppm gas mixture; 900 sccm of this mixture was sent through the HFC and then to the NO_x analyzer. For our first experiment, we used DI water set at either 25 or 50 mL/min as the scrubbing liquid. At both flow rates, none of the NO was removed from the flue gas. This was expected since NO is known to be insoluble in water.

In the next series of experiments, we used aqueous solutions of Fe(II)-EDTA as the scrubbing liquid. The range of Fe(II)-EDTA concentrations we used was 0.0005 to 0.05 M, and liquid flow rates between 25 and 300 mL/min. The results of these experiments are shown in Figure 5-11, where the percent removal of NO increases with increasing concentrations of Fe(II)-EDTA. For instance, with a 0.0005-M solution, 0% of the NO is removed. Subsequently, with a 0.05-M solution, nearly 50% NO removal is achieved. Also, according to Figure 5-11, the absorption capacities of the 0.025-M and 0.05-M solutions are similar. This is because the Fe(II)-EDTA solution appeared to be saturated at these higher concentrations, meaning that the solubility limit was probably reached around 0.02-0.025 M. Therefore, increasing the Fe(II)-EDTA concentration any further would not necessarily improve the NO scrubbing performance of the HFC. We also found that increasing the liquid flow rates during all the experimental runs did not affect NO removal, indicating that the gas-side resistance dominates mass transfer.

Next we decreased the gas flow rate of 100-ppm NO through the HFC from 900 sccm to 300 sccm. To meet the gas flow requirement for the NO_x analyzer, 600 sccm of N_2 was blended with the flue gas stream after it left the HFC. The scrubbing liquid was 0.02 M Fe(II)-EDTA at flow rates between 25 and 200 mL/min. The result of this experiment is that 79.9% of the NO was scrubbed from the simulated flue gas— independent of the liquid flow rate. Next, we decreased the flue gas flow rate through the HFC to about 200 sccm. Consequently, 700 sccm of N_2 had to be blended with the flue gas after the HFC to keep the 900-sccm flow rate requirement for the analyzer. The same concentration of Fe(II)-EDTA and liquid flow rates were used in this experiment. In this case, 85% of NO was removed from the flue gas— independent of the liquid flow rate. Because increasing the liquid flow rates does not significantly affect the percentage of NO removal, the gas-side resistance seems to dominate mass transfer in these experiments. Achieving 85% NO_x removal was milestone 5 for this project; we have met that milestone.

After completing these runs, we calculated the overall liquid-side mass transfer coefficients (K_{o1m}) for the 301-fiber HFC by using the experimental results from the NO_x -absorption runs (Task 2). After determining the equilibrium constant (K) for the 100-ppm NO/20-mM Fe(II)-EDTA run, we calculated and plotted the total concentration of NO absorbed in the liquid solution



CAM-3501-55

Figure 5-11. Percent removal of NO versus Fe(II)-EDTA concentration.

as a function of the NO concentration in the gas. At the lower gas phase concentrations of NO, the curve is fairly linear. As a result, the partition coefficient (H) for a 20-mM Fe(II)-EDTA solution was estimated to be the slope of the curve at the lower NO gas phase concentrations. The slope would equal H, and this was calculated to be 6.961×10^{-5} mol/L-atm. With H, we determined the K_{olm} for the 301-fiber HFC. This calculation was performed using the data from the HFC experiments where 80%-85% NO removal was observed. In the experiment with 20-mM Fe(II)-EDTA and a gas flow rate of 290 sccm, about 80% of the NO was scrubbed from the flue gas. K_{olm} calculated for this experiment is 7.15×10^{-6} cm/s. Also, for the experiment with a 200-sccm gas flow rate, more than 85% NO removal was achieved. The K_{olm} for this experiment was calculated to be 7.51×10^{-6} cm/s. Since these values of K_{olm} are much lower than that obtained using CO₂, we decided to continue characterizing the 301-fiber HFC with Fe(II)-EDTA as the scrubbing solution. One possibility is that there may be pore condensation between runs or perhaps deposition of Fe(II)-EDTA crystals onto pores during a run.

Also, we received a new 1000-fiber HFC from Hoechst-Celanese. The fiber openings on both ends of this HFC looked better than our original one. However, we found that Hoechst-Celanese sent us a module with a baffle at its center. Our previous 1000-fiber HFC did not have this baffle. Therefore, Hoechst-Celanese volunteered to make us a new HFC without a baffle. We received the new module, photographed the module ends, and counted 1169 fibers. We then proceeded to do similar experiments with this HFC.

After meeting Milestone 5, we concentrated our efforts on achieving 85% NO_x removal with an alternate scrubbing agent. From the reversible NO_x absorption experimental results (Task 2), we demonstrated that SRI synthesized Co(II)-phthalocyanine compound functions as a suitable binding agent for NO. In addition, the enhanced activity of this chemical reagent in the presence of O₂ for reversible absorption of NO has given us an added incentive to further exploit the chemistry in hollow fiber contactors. Accordingly, we conducted two process runs using the aqueous Co-phthalocyanine solution in the 301-fiber HFC.

Simulated flue gas to the process was prepared by mixing appropriate amounts of NO, N₂, and O₂. The composition of the feed gas was 500 ppm NO, 4.5% O₂, and the balance N₂ to the HFC. The exiting NO concentration was constantly monitored. Key results from the experiments, summarized in Table 5-1 show that a NO removal rate as high as 51% was obtained with a nominal aqueous solution flow rate of 4.6 ml/min. This high performance of the module gave us the confidence that we could achieve 85% NO removal rates rather easily by changing key process parameters.

Table 5-1
EXPERIMENTAL RESULTS ON NO_x ABSORPTION USING HFCs

Run No.	Feed Gas		Flowrate (sccm)	Aqueous Solution		pH		Outlet NO Concentration	Steady State	Flux (mole/cm ² /s)	NO Transfer Rate (mole/s)	% Removal
	NO (ppm)	O ₂ (%)		Type	Concentration (mM)	Initial	Final					
CP-1*	500	4.50	900	Co-phth	20	6.10	3.60	407	Y	1.12×10^{-10}	7.33×10^{-9}	22
CP-2	500	4.50	100	Co-phth	20	6.10	5.90	251	Y	2.83×10^{-11}	1.83×10^{-8}	51

* The concentration of Co-phthalocyanine solution is likely to be low because water was present in the HFC before the solution was introduced.

One observation made during the second experiment was that the module performance was unaffected by the variation of liquid flow-rate. However, decreasing the feed gas flow rate by a factor of 9 (Table 5-1) increased the removal rate by a factor of 2.5 for about the same liquid flow rate. This behavior explains that the gas phase resistance is dominating the liquid phase resistance for the mass transfer. This observation agrees well with the earlier data on Fe(II)EDTA runs. In any event, additional experimental runs were necessary to identify the key process parameters that affect the overall system performance and to achieve NO removal of 85% (target value). To do so, we calculated overall liquid side mass transfer coefficients (K_{Olm}) in the following manner.

The calculation of K_{Olm} becomes somewhat involved when the solubility of NO in Co-phthalocyanine solution does not follow a linear relationship. Indeed, as can be seen in Figure 5-12 the equilibrium relationship is highly nonlinear. This relationship has been calculated from $K = 5.2 \times 10^6$ L/mol reported in Task 2 of this report. Thus, we cannot use the conventional log-mean driving force to calculate K_{Olm} . Rather, the overall mass transfer coefficient is given as [Cussler (1984)]

$$K_{Olm} = \frac{L}{Aaz} \int_0^{C_L} \frac{dC_L}{C^* - C_L} \quad (5-3)$$

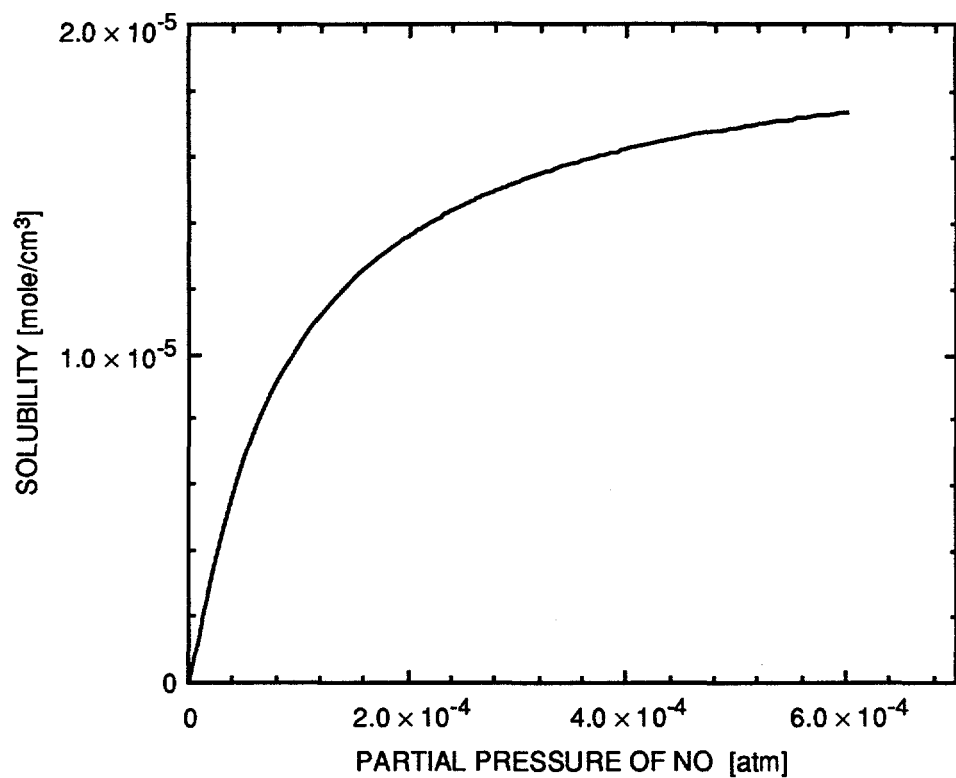
Here, L denotes the volumetric liquid flow rate, A is the cross-sectional area of the module, a is the specific surface area of the contactor, z is the length of the module, C_L is the concentration of NO (physical and chemical) in liquid, and C^* is the liquid phase NO concentration that is in equilibrium with the gas phase NO partial pressure.

The integral in the above equation must be numerically evaluated after expressing C^* in terms of C_L . This can be accomplished by writing solute mass balance on the section of the module encompassing one end to any other point over the length. It can be written as

$$P_g = P_{ga} + \frac{RTL}{G} C_L \quad (5-4)$$

where P_g indicates the partial pressure of NO in gas phase, P_{ga} is NO partial pressure in outlet gas stream, and G denotes the volumetric gas flow rate.

Now the integral in Equation (5-3) can be numerically calculated by using Equation (5-4) and Figure 5-12 to determine K_{Olm} . Using this method, the mass transfer coefficients were obtained to be 6.74×10^{-6} and 1.78×10^{-6} cm/s, respectively, for the two experimental runs presented in Table 5-1. Again, these results compare well with the previous NO_x absorption runs using EDTA solutions.



CM-3501-63

Figure 5-12. Calculated solubility of NO in 20 mM Co-phthalocyanine solution at 25°C.

Next, we focused our efforts on identifying and studying critical process parameters when using Co(II)-phthalocyanine solution. The overall mass transfer resistance for the absorption of NO into liquid can be characterized by three resistances, contributed by the gas phase, the liquid phase, and the membrane pore stagnant gas phase. From the results of past studies, we believe that the membrane resistance is negligible compared to the other resistances. Therefore, we performed several experiments to study the mass transfer effects of the other (gas and liquid) phases.

Table 5-2 presents the experimental results along with calculated overall mass transfer coefficients (K_{Og}) based on the gas phase. From the table, it is evident that K_{Og} increases with increasing gas flow rate, which demonstrates the existence of a gas phase resistance to mass transfer. However, the percent removal of NO remains approximately the same. This behavior implies a need for a larger HFC to improve the percent NO removal.

Table 5-2
EXPERIMENTAL RESULTS ON THE NO_x SCRUBBING WITH 300-FIBER HFC

NO (ppm)	Feed Gas		Scrubbing Liquid 20 mM		% Removal	$K_{Og} \times 10^3$ (cm/s)
	O ₂ (%)	Flow rate (sccm)	Type	Flow rate (mL/min)		
500	4.5	100	3-Ph	4.6	51	1.9
2300	4.5	100	3-Ph	4.1	62	2.5
500	4.5	40	3-Ph	4.1	50	0.7
500	4.5	40	3-Ph	0.5	50	0.7

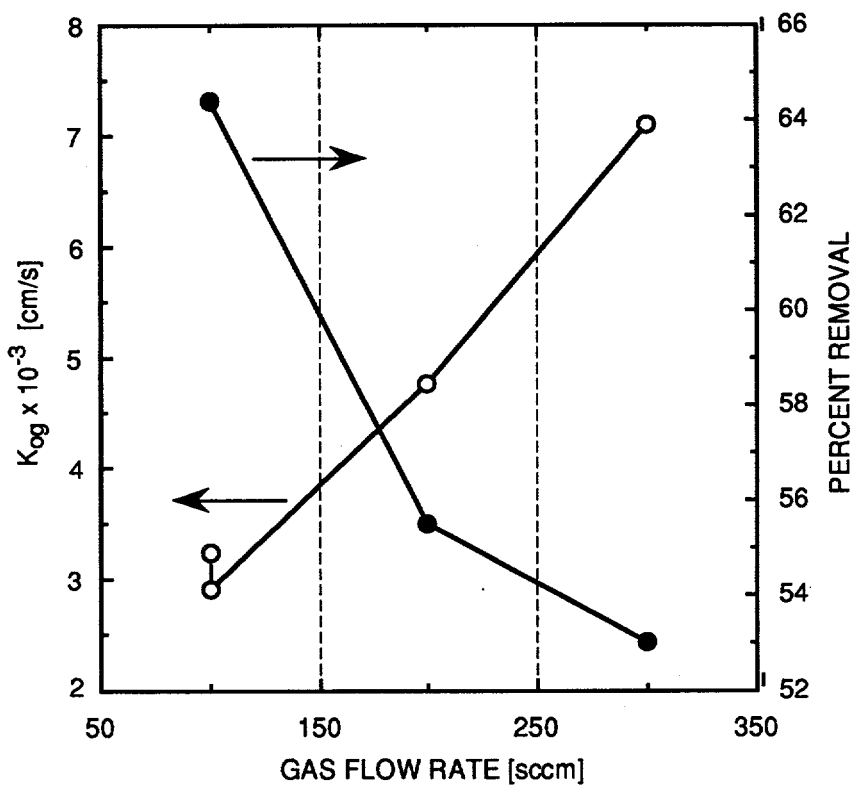
As shown in the table, liquid flow rate does not affect the mass transfer. This could be due to the solution having either a very high absorption capacity or a very low affinity toward binding NO. However, Task 2 results show that the former reasoning is incorrect because the absorption rate (dC_I/dt) of NO with Co-phthalocyanine solution is slower than that using Fe(II)-EDTA solution.

To increase the absorption rate, we conducted the experiments at 50°C. Also, we attempted to increase the NO absorption rates by increasing the Co(II)-phthalocyanine concentration. The results of these experiments are presented below.

The feed flue gas composition to the HFC was 500 ppm NO, 4.5% O₂, and the balance N₂. The liquid flow rate was approximately maintained at 1 mL/min. In the first set of experiments, the liquid entering the HFC was heated to 50°C by an electrical tape wound around to the liquid-carrying 1/4-inch stainless steel tube. The temperature of the heating tape was controlled by a thermostat. An operation similar to the gas carrying tubing did not increase the temperature of the gas stream even at the maximum power output levels of the thermostat because of the low gas flow rates (~100 sccm) used for the experiments. Therefore, for all the runs, the entering gas stream was essentially at 25°C and the entering liquid stream temperature was 50°C.

Figure 5-13 shows the variation of the mass transfer coefficient (K_{Og}) and the percent removal of NO with the gas flow rate. As mentioned earlier, the percent removal decreases with the increase in gas flow rate while K_{Og} increases. This phenomenon is desirable for obtaining high NO flux rates into the liquid stream at even low driving forces. Thus, to obtain high percent removals, the operation requires a higher number of fibers in the module. The maximum NO removal obtained was 64.4%. For all these runs, the Co(II) phthalocyanine concentration was 0.02 M.

Another approach we can adapt to increase the NO absorption capabilities is to increase the Co(II) phthalocyanine concentration in the liquid. We conducted a run at 0.1 M concentration of Co(II)-phthalocyanine. The gas flow rate was 100 sccm, the liquid inlet temperature was 50°C, and the remaining parameters were the same as in earlier runs. The observed percent removal of NO was 84.3%. This high removal capabilities of aqueous Co(II) phthalocyanine system at actual flue gas temperatures gave us confidence in proceeding further with the study to set up a regeneration process for the Co(II) phthalocyanine scrubbing solution.



CM-3501-72

Figure 5-13. Effect of gas flow rate on mass transfer coefficient and percent removal.

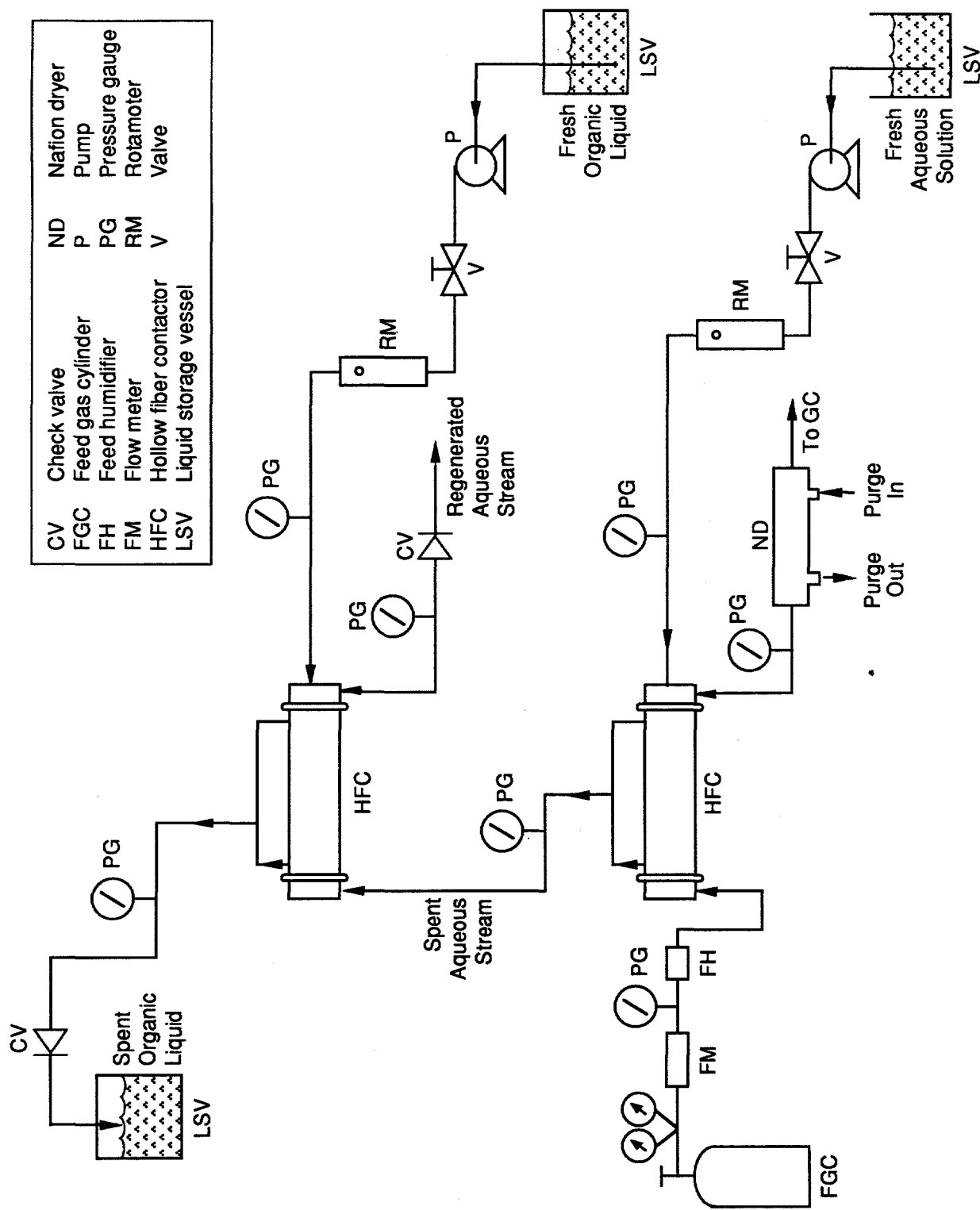
TASK 6: SO₂ LIQUOR REGENERATION

The objective of this task was to determine the fundamental mass transfer characteristics of hollow fiber contactors for regenerating SO₂ scrubbing liquor with organic solvents having a high affinity for SO₂. Two alternative processes were suggested in the research proposal: liquid-liquid extraction (LLE) and extraction via hollow fiber contained liquid membrane (HFCLM) technique. It was proposed to use dimethylaniline (DMA) and/or an oligomer of dimethylaniline as an organic extractant. In the first process, SO₂ was extracted from the aqueous solution into the organic liquid in a module having a single set of fibers, whereas in the second process the organic was used as a SO₂ selective membrane in a contained liquid membrane device containing two sets of fibers.

LIQUID-LIQUID EXTRACTION (LLE)

Initially, we explored the LLE technique in a hollow fiber module. We conducted absorption of SO₂ with an aqueous solution in one hollow fiber module and regeneration of the spent aqueous solution in a second module. The experimental setup was designed for simultaneous operations of absorption and extraction. The modified combined setup is shown in Figure 6-1. First, a model flue gas mixture (2400 ppm SO₂, 9.76% CO₂, 3.03% O₂, and the balance N₂) was humidified and sent through the tube side of a crossflow module containing 200 hollow fibers (fiber ID and OD, 240 and 300 μm, respectively). The feed gas flow rate was 2713 sccm and the gas composition after humidification was 2260 ppm SO₂, 9.76% CO₂, 3.03% O₂, and the balance N₂. An aqueous solution of 0.2 M Na₂SO₃ solution was pumped through the shell side at the rate of 20 cm³/min. The exit aqueous stream from the first module was sent through the tube side of the second hollow fiber module containing 1000 fibers (fiber ID and OD, 240 and 300 μm, respectively). The exit pressure of the aqueous stream was maintained higher than 5 psig by a check valve provided at the outlet of the second module. However, the organic flow through the second module was not initiated at this time.

The pH of the fresh aqueous solution was measured at the beginning of the experiment, and the pH of the spent absorbent solution was measured at regular intervals during the experiment. The steady state of the absorption experiment was monitored by sampling the treated flue gas in a gas chromatograph. Normally, it took 5 to 7 hours to achieve a steady state under these operating conditions. The flow of the organic (DMA) through the second HFC was started when a reasonable steady residual SO₂ composition was achieved at the first module outlet. The flow rate of DMA was set at about 6 cm³/min. The organic liquid spontaneously wets the pores of the hollow fibers. By keeping the organic phase pressure at 1/3 psig, we were able to maintain a



CV	Check valve	ND	Nafion dryer
FGC	Feed gas cylinder	P	Pump
FH	Feed humidifier	PG	Pressure gauge
FM	Flow meter	RM	Rotameter
HFC	Hollow fiber contactor	V	Valve
LSV	Liquid storage vessel		

CAM-3501-40A

Figure 6-1. Schematic of combined absorption and liquor regeneration setup.

stable aqueous-organic interface at each pore mouth on the fiber inside diameter. It was anticipated that we could monitor the steady state of the liquid-liquid extraction experiment by monitoring the change in pH of the exit aqueous solution stream at the second module outlet, but we did not notice any appreciable change in the solution pH.

The extraction experiment was continued for at least 2 hours, and organic samples were collected and analyzed in the following manner. For a given period of time, the spent organic liquid line was directly introduced in a flask containing excess NaOH solution of known concentration. The SO₂ from the organic solution reacted with NaOH in the aqueous phase. The total mixture was then titrated with HCl solution using phenolphthalein as an indicator. The SO₂ concentration in DMA was calculated from the titration values to be 8.0×10^{-6} mol/cm³ and the flux of SO₂ was found to be 4.6×10^{-10} mol/cm² s. We are exploring other analytical techniques to determine the SO₂ concentration in the organic liquid. Analysis of the aqueous phase is preferred. Ion chromatography is a possibility for this purpose. SO₂ concentration in the organic liquid can then be determined from the difference in the aqueous phase concentrations at the module inlet and outlet.

We conducted further test runs on simultaneous absorption and extraction using DI water (instead of an aqueous solution of 0.2 M Na₂SO₃ solution) as an absorbing liquid and DMA as an organic extractant. The module having 200 hollow fibers (fiber ID and OD, 240 and 300 μm, respectively) was used for gas absorption. A certified gas mixture consisting of 2400 ppm SO₂, 9.76% CO₂, 3.03% O₂, and the balance N₂ was sent directly through the tube-side without humidification, whereas deionized water was allowed to flow through the shell-side. The exit water stream was introduced to the tube-side of the second crossflow hollow fiber module having 1000 fibers (fiber ID and OD, 240 and 300 μm, respectively). We waited 3 to 4 hours to achieve a steady state in the absorption apparatus.

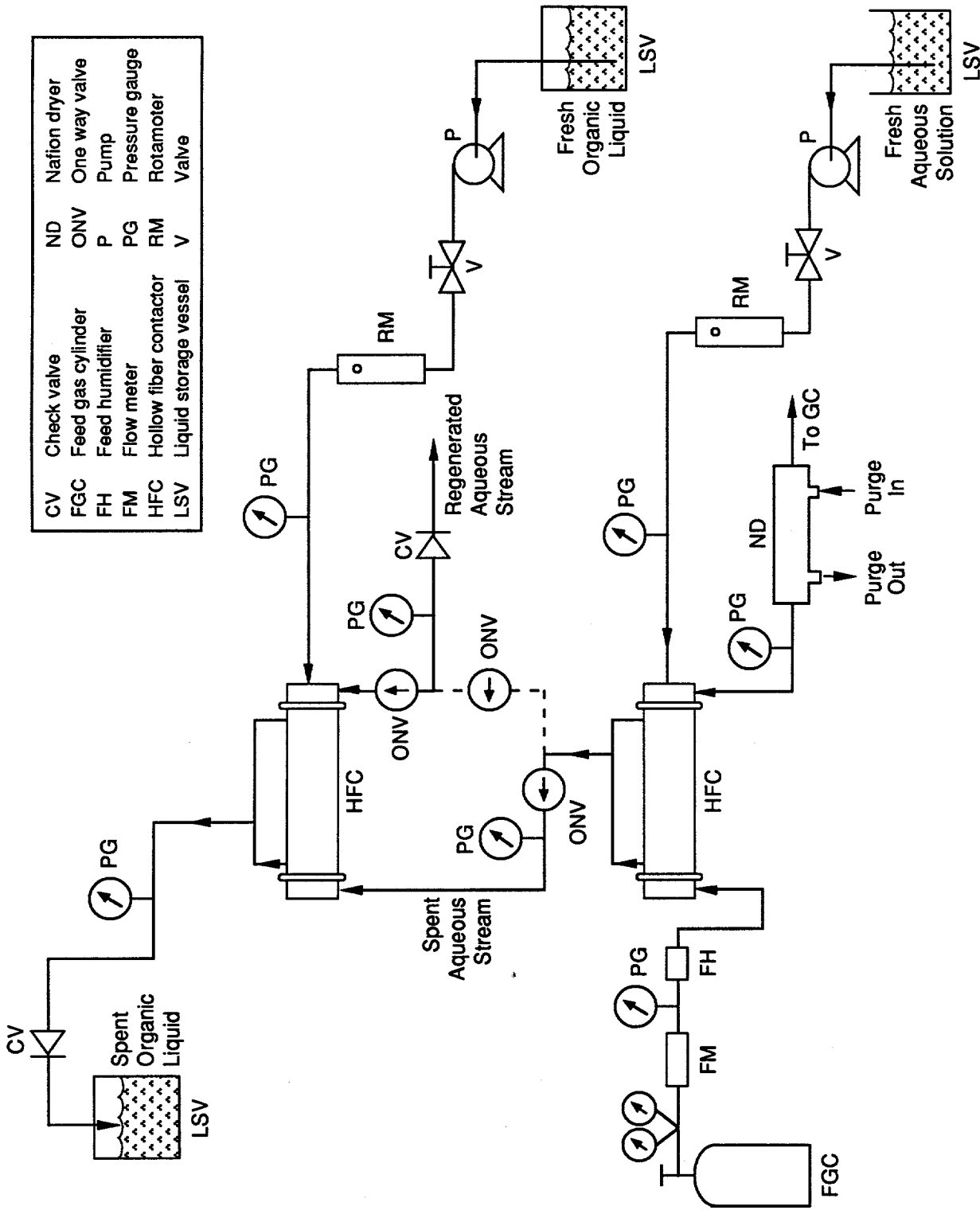
The extraction part of the experiment was initiated with organic flow in the shell-side when a steady outlet gas composition was achieved. The gas composition was monitored at a regular interval by a gas chromatograph. In the first module (absorption section), water pressure was higher than the gas pressure to immobilize the gas-liquid phase interface on the OD of the fibers. In the other module, the aqueous-organic interface was immobilized on the ID of the fibers with higher water pressure in the tube-side. The pH of the deionized feed water and the outlet water streams of the first and second modules were measured. During the runs, we noticed a faint yellow color in the regenerated water stream, but the phase interface in the extraction section was stable and no emulsion was observed. At the end of each experiment, we disconnected the absorption module from the setup. The module was thoroughly washed with water and dried under vacuum conditions. No such cleaning procedure was adopted for the extraction

module. However, during an earlier absorption part of a run, water from the tube-side of the second module penetrated through the fibers and appeared in the shell side outlet along with DMA. Apparently, some DMA from the fiber pores (leftover from a previous run) dissolved in the aqueous phase.

To prevent this kind of failure, we modified the setup by installing three additional valves in the aqueous line. These valves allow the aqueous stream to bypass the second module (extraction) altogether when we run our experiment only in absorption mode (i.e., when we wait for a steady state to be achieved in the absorption apparatus). The liquid flow to the second module is initiated in the following order. First, the organic phase is allowed to flow through the shell-side so that the fiber pores are wetted thoroughly and the organic appears in the lumen side. Then the aqueous flow at higher pressure is channeled through the tube-side of the module to drive the organic liquid out. This method of operation appears to overcome the problem we have faced.

Earlier, we mentioned that we modified the setup by installing three additional valves in the aqueous line to allow the aqueous stream to bypass the second module (extraction) altogether when we run our experiment only in absorption mode. The modified combined absorption/extraction setup is shown in Figure 6-2. A certified gas mixture consisting of 2300 ppm SO₂, 10.5% CO₂, 2.9% O₂, and the balance N₂ was sent through the tube-side of module containing 200 hollow fibers (fiber ID and OD, 240 and 300 μm, respectively). An aqueous solution of 0.2 M Na₂SO₃ was passed through the shell-side. The exit aqueous stream was introduced to the tube-side of the second crossflow hollow fiber module containing 1000 fibers (fiber ID and OD, 240 and 300 μm, respectively) only when a steady state in the absorption apparatus was achieved. In all runs a constant model feed flue gas flow rate of ~2700 sccm was maintained. In the first run (AE-4, Table 6-2), the feed gas was humidified but in the other two cases, the model flue gas was introduced without humidification.

We also improved the procedure for measuring the SO₂ concentration in the organic phase. The spent organic liquid is discharged into the bottom section of a burette filled with excess NaOH solution. The procedure increases the contact time and enables the free SO₂ to react completely as the organic liquid travels upward through the aqueous solution. The SO₂ concentration in DMA is determined by titrating the total mixture with HCl solution. We made two successful experiments in which a constant feed gas flow rate of about 900 sccm was used. The water flow rates were varied from ~20 to 50 mL/min. In both cases the flow rate of DMA was maintained at 6 mL/min. Table 6-1 summarizes the extraction data, including the SO₂ concentration in DMA and the flux of SO₂ during regeneration.



CV	Check valve	ND	Nation dryer
FGC	Feed gas cylinder	ONV	One way valve
FH	Feed humidifier	P	Pump
FM	Flow meter	PG	Pressure gauge
HFC	Hollow fiber contactor	RM	Rotameter
LSV	Liquid storage vessel	V	Valve

CAM-3501-40B

Figure 6-2. Schematic of combined absorption and liquor regeneration setup with installation of additional valves for by-pass of the extraction module.

Table 6-1
SUMMARY OF EXTRACTION DATA IN SIMULTANEOUS ABSORPTION-EXTRACTION RUNS

Run No.	Aqueous Absorbent		Flue Gas Flow Rate (sccm)	SO ₂ Concentration in DMA (mole/cm ³)	Extractive Flux of SO ₂ (mole/cm ² s)	SO ₂ Transfer (mole/s)		Percent Recovery by Extraction
	Type	Flow Rate (mL/min)				Absorption	At Extraction	
1	0.2 M Na ₂ SO ₃	20	2722 (Humidified)	8.0×10^{-10}	4.6×10^{-10}	4.42×10^{-6}	7.98×10^{-7}	18
2	Water	22	901	1.45×10^{-5}	1.19×10^{-9}	1.2×10^{-6}	1.45×10^{-6}	~100
3	Water	50	908	8.85×10^{-6}	5.1×10^{-10}	1.48×10^{-6}	8.84×10^{-7}	59

Table 6-2
SUMMARY OF EXTRACTION DATA IN SIMULTANEOUS ABSORPTION-EXTRACTION RUNS

Run No.	Aqueous Absorbent		Flue Gas Flow Rate (scfm)	Flow Rate of DMA (mL/min)	SO ₂ Concentration In DMA (mole/cm ³)	Extractive Flux of SO ₂ (mole/cm ² s)	SO ₂ Transfer (mole/s)		Percent Recovery by Extraction
	Type	Flow Rate (mL/min)					At Absorption	At Extraction	
AE-6	0.2 M Na ₂ SO ₃	10	2723 (Dry)	6.1	2.93 x 10 ⁻⁶	1.72 x 10 ⁻¹⁰	4.50 x 10 ⁻⁶	2.98 x 10 ⁻⁷	6.6
AE-4	0.2 M Na ₂ SO ₃	20	2732 (Humidified)	6.9	4.97 x 10 ⁻⁶	3.30 x 10 ⁻¹⁰	4.43 x 10 ⁻⁶	5.72 x 10 ⁻⁷	13.0
AE-9	0.2 M Na ₂ SO ₃	30	5000 (Dry)	6.4	6.21 x 10 ⁻⁶	3.82 x 10 ⁻¹⁰	7.46 x 10 ⁻⁶	6.62 x 10 ⁻⁷	8.9
AE-5	0.2 M Na ₂ SO ₃	20	2704 (Dry)	4.05	6.68 x 10 ⁻⁶	2.60 x 10 ⁻¹⁰	4.54 x 10 ⁻⁶	4.51 x 10 ⁻⁷	9.9
AE-4	0.2 M Na ₂ SO ₃	20	2732 (Humidified)	6.9	4.97 x 10 ⁻⁶	3.30 x 10 ⁻¹⁰	4.43 x 10 ⁻⁶	5.72 x 10 ⁻⁷	13.0
AE-7	0.2 M Na ₂ SO ₃	20	2723 (Dry)	16	2.67 x 10 ⁻⁶	4.11 x 10 ⁻¹⁰	4.32 x 10 ⁻⁶	7.12 x 10 ⁻⁷	16.5
AE-8	0.2 M Na ₂ SO ₃	20	2732 (Dry)	31	3.31 x 10 ⁻⁶	9.75 x 10 ⁻¹⁰	4.29 x 10 ⁻⁶	1.69 x 10 ⁻⁶	39.4
AE-10	0.2 M Na ₂ SO ₃	10	2459 (Dry)	38	3.33 x 10 ⁻¹⁰	12.17 x 10 ⁻¹⁰	4.01 x 10 ⁻⁶	2.11 x 10 ⁻⁶	52.6

Three runs were done: AE-4, -5, and -6. In runs AE-4 and AE-5 (Table 6-2), the flow rate of the aqueous solution was kept at 20 mL/min, but the organic flow rate was changed from 6.9 to 4 mL/min. At the higher organic flow rate, the SO₂ concentration in DMA was lower but the total SO₂ transfer was higher. Comparing runs AE-4 and -6, we see that the SO₂ transfer rate decreased by about 50% when the aqueous flow rate was changed from 20 ml/min to 10 mL/min. A summary of extraction data and the flux of SO₂ during regeneration is shown in Table 6-2. In these runs only a maximum of 13% of the absorbed SO₂ was recovered by the organic liquid. In our earlier runs with water, we obtained much higher recoveries. Therefore, further experiments were performed at higher flow rates.

Next, to study the effect of organic and aqueous flow rates on the SO₂ transfer in the extraction process, we conducted additional test runs on simultaneous absorption and extraction with an aqueous solution of 0.2 M Na₂SO₃ solution as an absorbing liquid and DMA as an organic extractant. In membrane solvent extraction, the overall resistance to solute transfer comes from three resistances in series: the aqueous and organic film resistances and the membrane resistance. Increasing the fluid flow rates could reduce the aqueous and organic resistances and improve mass transfer.

In the next set of experiments the gas mixture used as a feed to the absorption module had a composition of 2170 ppm SO₂, 3.13% O₂, 10.8% CO₂, and the balance N₂. These runs are numbered AE-7, -8, and -9 in Table 6-2. The aqueous and organic flow rates were varied systematically in the combined setup, and the SO₂ concentration in the DMA was determined. The effect of aqueous absorbent flow rate variation is presented in the first part of the table, whereas that of organic flow rate variation is presented in the second part. In all runs except run AE-9, a constant feed flue gas flow rate of ~2700 sccm was maintained. We see an increase in SO₂ transfer in the extraction process (by a factor of 2.2) as the absorbent flow rate was increased from 10 to 30 mL/min, keeping the organic flow rate constant at ~6 mL/min. Note that in run AE-9 the gas flow rate to the absorption module was 5000 sccm. This very high gas flow rate was used to obtain a reasonable amount of SO₂ at the exit gas stream. It was anticipated that all the SO₂ present would be absorbed at the lower gas flow rate of ~2700 sccm and aqueous Na₂SO₃ solution flow rate of 30 mL/min. A higher organic flow rate under these conditions would result in a higher percent recovery in the extraction process.

The second part of Table 6-2 presents the data obtained by varying the organic flow rate. In all these runs the feed gas and the aqueous solution flow rates were maintained at constant values. The SO₂ transfer in the extraction process increased substantially as the organic flow rate was increased from 4 to 31 mL/min. We were able to recover about 40% of the absorbed

SO₂ from the aqueous solution when the organic liquid flow rate was 31 mL/min. It is possible to recover even more of the absorbed SO₂ by manipulating the aqueous and organic flow rates and by providing a larger contact area.

Finally, we conducted an additional run, AE-10. A certified gas mixture consisting of 2230 ppm SO₂, 11% CO₂, 3.20% O₂, and the balance N₂ was passed through the tube-side of module containing 200 hollow fibers, without humidification. The flue gas flow rate was about 2450 sccm. An aqueous solution of 0.2 M Na₂SO₃ was passed through the shell-side. The exit aqueous stream was allowed to bypass the extraction module during the time period needed to achieve a steady state in the absorption apparatus. Once a steady outlet gas composition was achieved, the extraction part of the experiment was initiated with DMA flow in the shell side and by introducing the exit aqueous stream to the tube-side of the second crossflow hollow fiber module containing 1000 fibers. Normally, it took 3 to 5 hours to achieve a steady state in the absorption part of the experiment. However, out of three trial runs, we were able to achieve a steady state in only one. Two runs were abandoned when we did not get a constant outlet SO₂ composition in more than a 6-hour period.

In our earlier experimental results, we saw that the SO₂ transfer in the extraction increased substantially with increase in organic flow rate. Therefore, in run AE-10, the organic flow rate was kept at a high value of 38 mL/min whereas the aqueous flow rate was maintained at 10 mL/min as shown in Table 6-2. Under these conditions, it was possible to recover more than 50% of the absorbed SO₂ from the loaded aqueous 0.2 M Na₂SO₃ solution. As the organic flow rate is increased from ~4 mL/min to 38 mL/min (9.4 times), the extractive flux of SO₂ increased from 2.60×10^{-10} to 12.17×10^{-10} mole/cm²/s (4.7 times). The total SO₂ transfer also increased from a value of 4.51×10^{-7} to 2.11×10^{-6} mole/s. Further increase in SO₂ recovery is possible with even higher organic flow rate. However, we do not plan to use higher organic flow rate at this time.

DISTRIBUTION COEFFICIENT

We systematically studied the absorption of SO₂ by an aqueous 0.2 M Na₂SO₃ solution and subsequent regeneration of the spent liquor by extraction with DMA. The results indicated that the SO₂ transfer in the extraction stage increases substantially with increase in organic flow rate. We were able to recover as much as 50% of the absorbed SO₂ from the loaded aqueous 0.2 M Na₂SO₃ solution into DMA (run AE-10) using a 1000-fiber module. Further increase in SO₂ recovery is possible with even higher organic flow rates. However, to demonstrate that higher SO₂ recovery is achievable in the extraction unit, we used an alternative strategy. We switched back to water absorbent instead of aqueous 0.2 M Na₂SO₃ solution. To achieve a high

removal efficiency (90+%) using 0.2 M Na₂SO₃, we would need to make the DMA circulation rate very high (see runs AE-10 and AE-6 in Table 6-3), which is impractical in the laboratory. As a result, one alternative was that we absorb SO₂ with water (for the same SO₂ flux, a higher water flow rate is needed than for 0.2 M Na₂SO₃ since SO₂ is much more soluble in 0.2 M Na₂SO₃). The extraction of SO₂ from spent water is much easier than from spent 0.2 M Na₂SO₃ (SO₂ solubility is higher in 0.2 M Na₂SO₃), and this allows up to 93% of the SO₂ being extracted—while maintaining practical water and DMA flow rates.

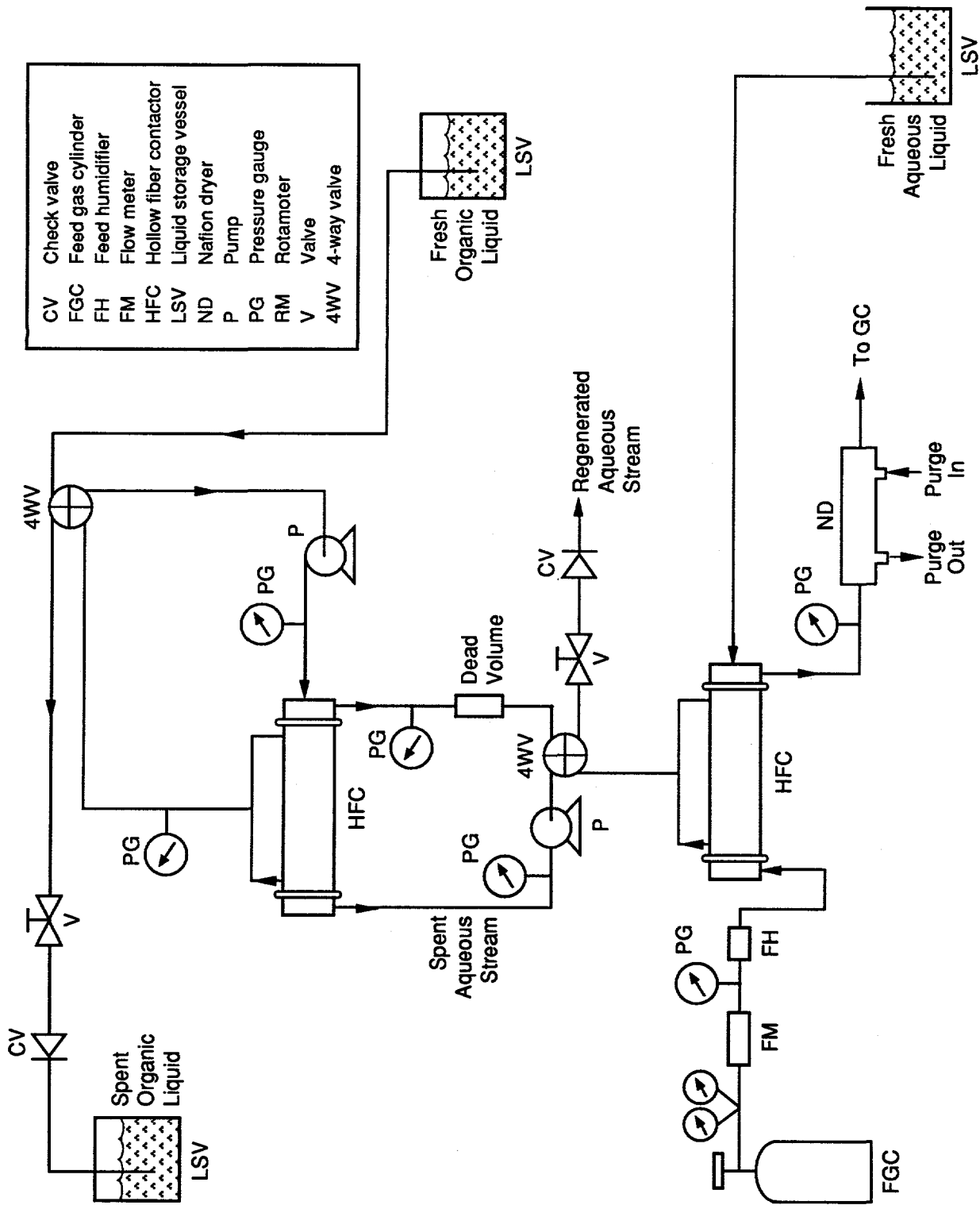
Water was introduced to the shell-side of the 200-fiber crossflow module at a flow rate of 50 ml/min. A model flue gas mixture having 2230 ppm SO₂, 3.2% O₂, 11% CO₂, and the balance N₂ was passed through the tube-side of the module without any humidification. The exit water stream loaded with SO₂ was then diverted to the tube-side of the second crossflow hollow fiber module containing 1000 fibers. DMA was passed through the shell-side at a high flow rate of 42 mL/min. The SO₂ concentration in the DMA at steady state was determined in a manner described earlier.

The results of this water run are also shown in Table 6-3 (Run AE-11). Water has a lower absorption capacity of SO₂ than aqueous 0.2 M Na₂SO₃ solution. The SO₂ transfer in this particular absorption run is about 1.4×10^{-6} mole/s, which is much less than $\sim 4 \times 10^{-6}$ mole/s obtained in general with aqueous 0.2 M Na₂SO₃ solution. But with a high DMA flow rate of ~ 40 mL/min, more than 90% of the SO₂ was extracted from the water stream into the DMA. For comparison, we also show a run (AE-3) taken with a lower DMA flow rate.

To analyze the extraction results in a meaningful manner and to predict the system behavior, we need to know the distribution coefficient of SO₂ between the aqueous and organic phases. Due to the volatility of the solute in this case, these measurements cannot be performed in the traditional manner such as using a separatory funnel. Therefore, we conducted this measurement in a batch recirculation mode. Earlier, we modified the experimental setup for this particular measurement. The arrangement is shown in Figure 6-3. The exit aqueous stream from the first module passes through a four-way valve before entering the tube-side of the second module. Similarly, the organic stream in the shell-side of the second module passes through a four-way valve. Note that flow meters from both lines have been removed and the position of the pumps has been changed. An additional dead volume is provided in the aqueous liquid line. The absorption part of the experiment was conducted in the usual fashion. Once a steady state was achieved (as confirmed by the GC) in the absorption apparatus, the four-way valve in the aqueous solution exit line was switched to a batch recirculation mode for the second module. Fresh DMA was also pumped in a batch circulation mode in the shell-side of the second module. The composition of SO₂ in each phase changed slowly but asymptotically to a final equilibrium value.

Table 6-3
ABSORPTION DATA IN ABSORPTION-EXTRACTION RUNS USING HIGH AND LOW FLOW RATES OF DMA

Run No.	Aqueous Absorbent		Flue Gas Flow Rate (sccm) (dry)	Flow Rate of DMA (mL/min)	SO ₂ Concentration in DMA (mole/cm ³)	Extractive Flux of SO ₂ (mole/cm ² s)	SO ₂ Transfer (mole/s)		Percent Recovery by Extraction
	Type	Flow Rate, (mL/min)					At Absorption	At Extraction	
AE-10	0.2 M Na ₂ SO ₃	10	2459	38.0	3.33×10^{-6}	12.17×10^{-10}	4.01×10^{-6}	2.11×10^{-6}	52.6
AE-6	0.2 M Na ₂ SO ₃	10	2723	6.1	2.93×10^{-6}	1.72×10^{-10}	4.50×10^{-6}	2.98×10^{-7}	6.6
AE-11	Water	50	908	42.0	1.85×10^{-6}	7.55×10^{-10}	1.41×10^{-6}	1.31×10^{-6}	92.9
AE-3	Water	50	908	6.0	8.85×10^{-6}	5.1×10^{-10}	1.48×10^{-6}	8.84×10^{-7}	59



CM-3501-61

Figure 6-3. Schematic of combined absorption and liquor regeneration setup with four-way valve to conduct batch mode recirculation.

The final concentration of SO₂ in DMA was determined by a titrimetric method described earlier. From the gas absorption measurement, the composition of SO₂ in the aqueous stream at the start of the recirculation experiment was known. The equilibrium SO₂ concentration in the aqueous phase may be determined from material balance equations and thus the distribution coefficient can be calculated.

Later, experiments were conducted to determine the distribution coefficient of SO₂ between the aqueous and organic phases. As stated earlier, the distribution coefficient measurement experiments cannot be carried out in a traditional separatory funnel method because the solute SO₂ is volatile. These measurements were conducted in a batch recirculation mode, as shown in Figure 6-4.

In this arrangement, a known volume of aqueous solution (V_w) loaded with a known initial composition of SO₂ (C) comes into contact with a known volume of fresh organic solvent (V_o) in a hollow fiber extraction module in crossflow. The known fluid volumes of both phases are circulated through the module such that a part of the aqueous solution is in continuous contact with the organic solvent. The composition of SO₂ in two reservoirs (Figure 6-4) changes slowly and asymptotically to final equilibrium values. If the final compositions of the solute in aqueous and organic phases are C_w and C_o, respectively, then by material balance

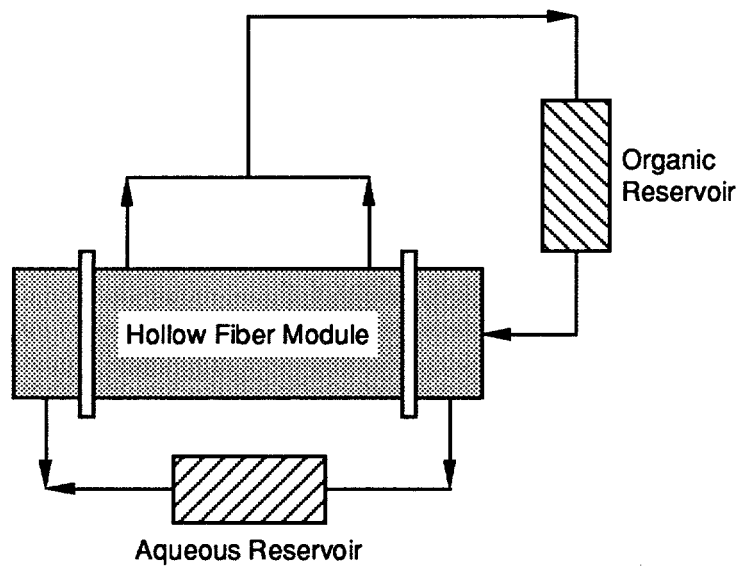
$$V_2 C_2^f = V_o C_o^f + V_w C_w^f \quad (6-1)$$

$$C_w^f = C_w^i - \frac{V_o}{V_w} C_o^f \quad (6-2)$$

If the final organic phase concentration, C_o^f, is measured from the experiment, the final aqueous phase concentration may be calculated from Eq. (6-2). Then the distribution coefficient (m_i) is determined from the following relation.

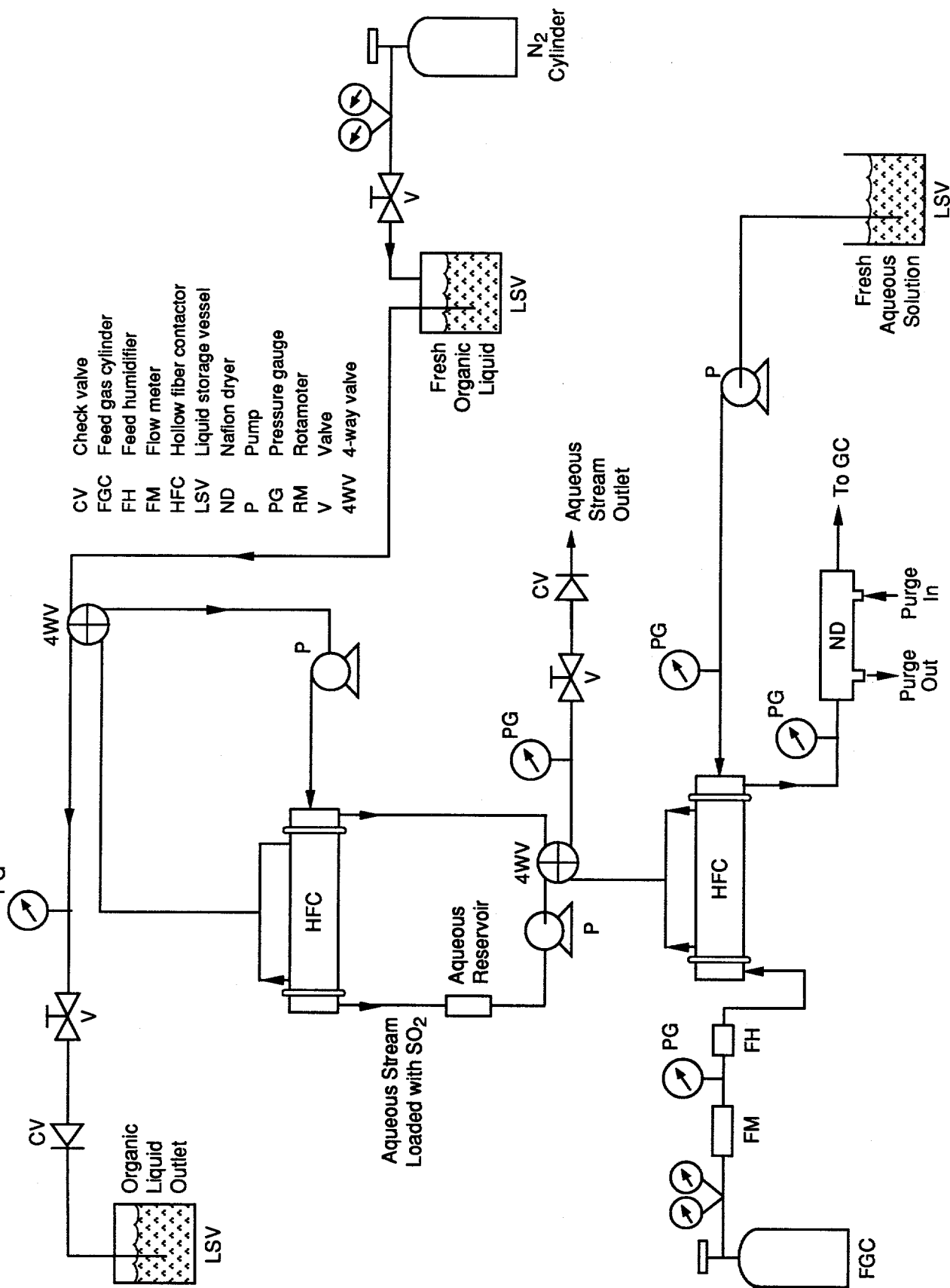
$$m_i = \frac{C_o^f}{C_w^f} \quad (6-3)$$

A modified diagram of the experimental setup used for distribution coefficient measurement is shown in Figure 6-5. The arrangement shown in Figure 6-5 supersedes the one shown in Figure 6-3. The setup and the procedure for the experiments were further modified since we encountered problems with the earlier arrangement, which was found to be inadequate. The following experimental procedure was established after a few iterations.



CM-3501-64

Figure 6-4. Schematic of batch recirculation mode of operation using a hollow fiber contactor.



CM-3501-65

Figure 6-5. Modified absorption and liquor regeneration setup for distribution coefficient measurement.

A model flue gas mixture gas consisting of 2230 ppm SO₂, 11% CO₂, 3.13% O₂, and the balance N₂ was sent through the tube-side while an aqueous phase was pumped through the shell side of the 200-fiber absorption module. The exit aqueous stream from this first module was passed through a four-way valve, then a second aqueous solution pump and an aqueous reservoir (volume of 75 mL) before entering the tube-side of the 1000-fiber extraction module. During the absorption part of the experiment, the aqueous line was not connected to the second hollow fiber module. Further, the second pump in the aqueous line was also not in operation. Once a steady gas composition was achieved at the flue gas outlet line (thus the steady state SO₂ composition in the aqueous phase, C, was also known), the aqueous lines were connected to the second hollow fiber module. The system was allowed to run for another 30 minutes after which the four-way valve was switched to the batch recirculation mode of operation in the second module. The absorption part of the experiment was discontinued at this time. The second pump in the aqueous line was not yet turned on. The recirculation loop was filled with the aqueous solution, but there was no flow.

At this point the organic flow through the shell-side of the second module was initiated. The pump (placed after the four-way valve in the organic line) required priming by pressurizing the organic storage vessel with a N₂ cylinder. As soon as the hollow fiber module and the recirculation loop were filled with the organic solvent, the organic pump was shut off and immediately the four-way valve was switched to the recirculation mode of operation. Contacting of the two phases were then initiated by starting the aqueous phase flow and then the organic flow in the corresponding recirculation loop. The second module was operated under these conditions for about 2 hours. After this, a known amount of DMA sample from the hollow fiber module was withdrawn from the module inlet line, directly into a burette containing excess NaOH solution of known concentration. The SO₂ from the organic solution reacted with NaOH in the aqueous phase. The total mixture was then back-titrated with standard HCl solution using phenolphthalein as an indicator. The SO₂ concentration in DMA (C₀) was calculated from the titration values. The volume of both aqueous loops (including module and dead volume) were measured accurately after the completion of the experiment to determine the final aqueous phase concentration via Eq. (6-2). The distribution coefficient was then calculated using Eq. (6-3).

Distribution coefficient measurement experiments were conducted both for aqueous 0.2 M Na₂SO₃ solution-SO₂-DMA and water-SO₂-DMA systems. For aqueous Na₂SO₃ solution-SO₂-DMA system, the SO₂ concentration at the outlet of the absorption module was found to be 13.3×10^{-6} mole/cm³ of solution. The SO₂ concentration in DMA after equilibration was determined to be 1.8×10^{-6} mole/cm³. A distribution coefficient value of about 0.2 was obtained.

From our earlier experience with water absorbent, we anticipated that a higher m_i value would result. However, we faced difficulty in determining m_i of the water-SO₂-DMA system. At the end of the experiment, the two phases were transferred into two separate vessels and water-oil emulsion was found in both phases. Even though the extent of water contamination in DMA was not known, the SO₂ concentration in DMA was determined to develop a rough estimate of distribution coefficient. The change in SO₂ concentration in the water phase was found to be large, whereas that in the organic phase was small. This led to an additional uncertainty in the concentration measurement. A very rough estimate of distribution coefficient would be ~10. Due to the large shell volume in the HFC itself, the volume of the organic in the recirculation loop is much larger than the aqueous volume. For water-SO₂-DMA system, it is probably a better idea to have a much larger aqueous reservoir than the organic reservoir. The reverse may be true for Na₂SO₃ solution-SO₂-DMA since the SO₂ concentration in 0.2 M Na₂SO₃ solution is much larger to start with.

Earlier, we studied the absorption of SO₂ by water or an aqueous 0.2 M Na₂SO₃ solution in a hollow fiber contactor and subsequent regeneration of the spent liquor in a second hollow fiber contactor via liquid-liquid extraction with DMA. We have reported preliminary results on the measurement of the distribution coefficient (m_i) of SO₂ in an experiment involving batch recirculation mode. Also, we have conducted additional measurements of distribution coefficients for both aqueous 0.2 M Na₂SO₃ solution-SO₂-DMA and water-SO₂-DMA systems. Further, to demonstrate 99% SO₂ liquor regeneration efficiency in laboratory modules, we have conducted an extraction run for a very high DMA flow rate.

The experimental setup for m_i determination, shown in Figure 6-5 has gone through some minor changes in its operational procedure to prevent the formation of an aqueous-oil emulsion. In addition, the size of the aqueous reservoir was larger than the organic reservoir for water-SO₂-DMA system (run AEM-3). For aqueous 0.2 M Na₂SO₃ solution-SO₂-DMA system, a larger organic reservoir was used. We have confidence in these measurements because we did not see any breakthrough of phases at the end of the runs. The results and the distribution coefficients are reported in Table 6-4.

For simultaneous absorption and extraction runs, a feed gas containing 2300 ppm SO₂, 3.22% O₂, 11% CO₂, and the balance N₂ was passed through the tube-side of the 200-fiber module without any humidification. A constant feed gas flow rate of ~2700 sccm was maintained. An aqueous 0.2 M Na₂SO₃ solution was introduced into the shell-side at a flow rate of 20 mL/min. Once a steady state was achieved in the absorption module, the exit aqueous flow was directed through the tube-side of the second hollow fiber module containing 1000 fibers. The extraction part of the experiment was initiated with DMA flow in the shell-side of the

Table 6-4
DETERMINATION OF DISTRIBUTION COEFFICIENT (m)

Run No.	Aqueous Absorbent	Volumes In Circulation (mL)		Initial Concentration of SO ₂ in Aqueous Phase (C _w ⁱ) (mole/cc)	Equilibrium Concentration of SO ₂		Distribution Coefficient m = C _o ^f /C _w ^f
		Aqueous (V _w)	Organic (V _o)		Organic Phase (C _o ^f) (mole/cm ³)	Aqueous Phase (C _w ^f) (mole/cm ³)	
AEM-3	Water	562	375	1.90 x 10 ⁻⁶	2.35 x 10 ⁻⁶	0.33 x 10 ⁻⁶	7.1
AEM-4	0.2 M Na ₂ SO ₃	145	368	13.3 x 10 ⁻⁶	2.86 x 10 ⁻⁶	6.04 x 10 ⁻⁶	0.47

second module. The DMA flow rate was maintained at a high value of 102 mL/min (run AE-12). Under these conditions, we were able to recover almost all of the absorbed SO₂ from the loaded aqueous 0.2 M Na₂SO₃ solution. The extractive flux of SO₂ was 26.87 x 10⁻⁶ mole cm²/s. The results are presented in Table 6-5 (along with other data representing higher SO₂ recovery by extraction). With this high flux, we have achieved ~100% extraction efficiency, meeting a milestone in this task.

HOLLOW FIBER CONTAINED LIQUID MEMBRANE (HFCLM)

In addition to liquid-liquid extraction (LLE), the hollow fiber contained liquid membrane (HFCLM) technique may also be used to regenerate aqueous SO₂ scrubbing liquor. An HFCLM permeator containing two sets of fibers has been fabricated. The first set of fibers are made of microporous hydrophobic polypropylene (Hoechst-Celanese, Charlotte, NC; Celgard X-10, ID: 240 μm, OD: 290 μm). The second set of fibers are made of silicone rubber (Baxter Healthcare Corp., Edison, NJ; silicone tubing, ID: 0.012 inch, OD: 0.025 inch). Following the method described in the literature (S. Majumdars et al., 1988), we prepared two separate fiber mats, one containing 200 Celgard fibers and another containing 100 silicone tubings. An integrated mat was then created by placing one mat on top of the other. Distilled water was spread over the integrated mat, and the fibers were gathered gently and slowly to form a bundle. The bundle was inserted directly into a specially constructed permeator shell where a Teflon pipe was used to keep the fibers in a defined volume. The two sets of fibers were separated at each end of the permeator through the openings of a Y-connection. The Celgard fibers were potted with two layers of resin mixtures, first with a silicone rubber (RTV 118, GE, Waterford, NY) and then with an epoxy resin (C4-D, Beacon Chemical Co., Mt. Vernon, NY). The silicone tubings were potted with an additional layer of silicone rubber (RTV 615A and 615B, GE, Waterford, NY). The effective length of the module is 18 inches.

We initiated process studies to determine the mass transfer characteristics of the newly built contained liquid membrane (CLM) module for regenerating aqueous SO₂ scrubbing liquor with organic solvent having a high affinity for SO₂. The module, often described as HFCLM permeator contains two sets of fibers: microporous hydrophobic polypropylene (Celgard X-10, ID: 240 μm, OD: 290 μm) and silicone rubber tubules (ID: 0.012 inch, OD: 0.025 inch). Details on making the device were provided earlier. We tested the module with water at a pressure differential of 15 psi. The silicone tubule side showed leaks. We repotted the exterior end of that side with epoxy. The following trial with water at 15 psi did not show any leaks. We

Table 6-5
RESULTS OF RUN AE-12 AND OTHER RUNS WITH HIGHER RECOVERY OF SO₂ BY LLE

Run No.	Aqueous Absorbent		Flue Gas Flow Rate (sccm) (dry)	Flow Rate of DMA (mL/min)	SO ₂ Concentration In DMA (mole/cm ³)	Extractive Flux of SO ₂ (mole/cm ² s)	SO ₂ Transfer (mole/s)		Percent Recovery by Extraction
	Type	Flow Rate, (mL/min)					At Absorption	At Extraction	
AE-12	0.2 M Na ₂ SO ₃	20	2718	102	2.74 x 10 ⁻⁶	26.87 x 10 ⁻¹⁰	4.57 x 10 ⁻⁶	4.66 x 10 ⁻⁶	~100
AE-10	0.2 M Na ₂ SO ₃	10	2459	38	3.33 x 10 ⁻⁶	12.17 x 10 ⁻¹⁰	4.01 x 10 ⁻⁶	2.11 x 10 ⁻⁶	52.6
AE-11	Water	50	908	42.0	1.85 x 10 ⁻⁶	7.55 x 10 ⁻¹⁰	1.41 x 10 ⁻⁶	1.31 x 10 ⁻⁶	92.9
AE-3	Water	50	908	6.0	8.85 x 10 ⁻⁶	5.1 x 10 ⁻¹⁰	1.48 x 10 ⁻⁶	8.84 x 10 ⁻⁷	59.0

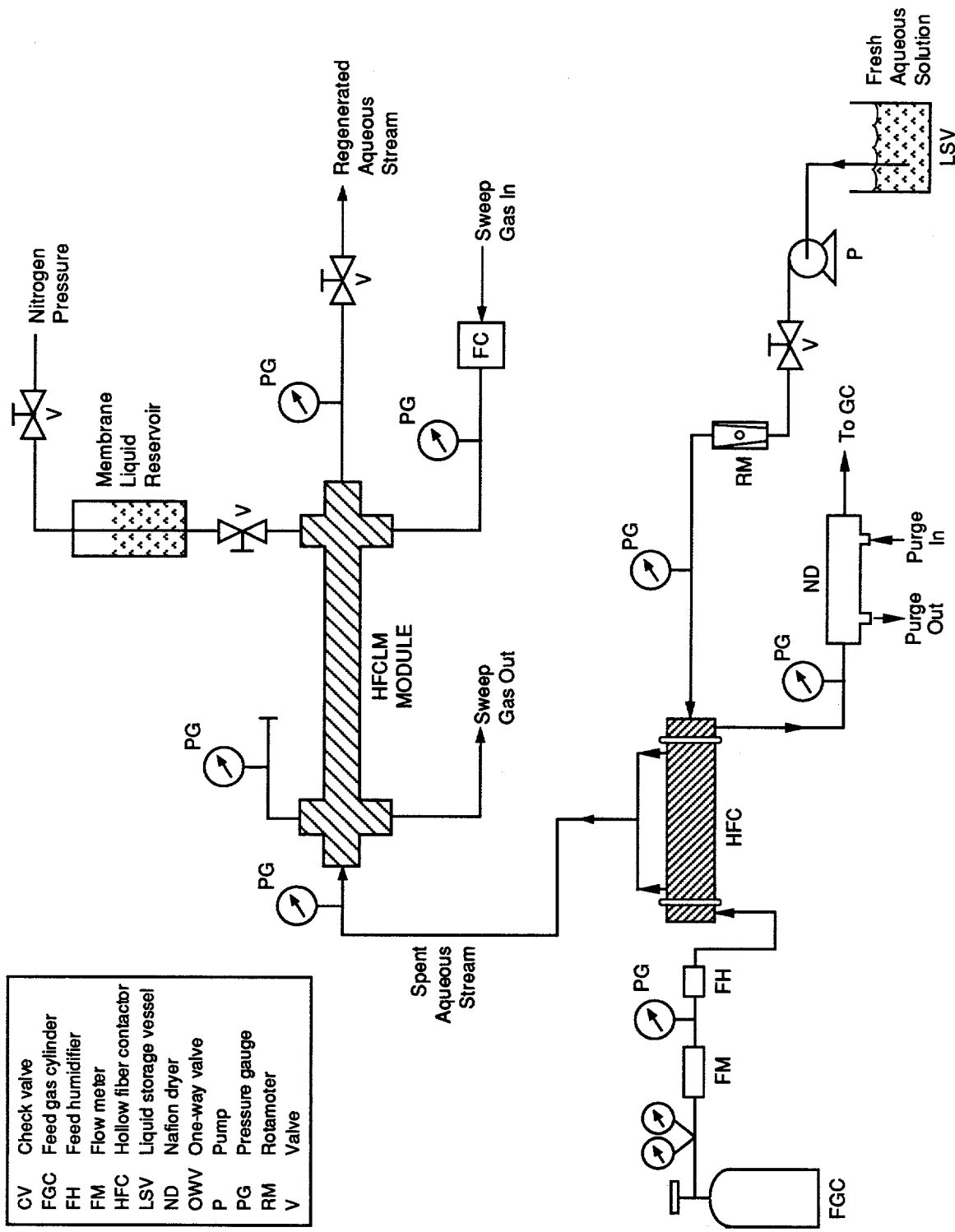
monitored the permeation of CO₂ through the module, in polymeric mode and using water as the CLM. The data yielded an effective membrane thickness of the CLM as 1050 μm. Experiments were then conducted using aqueous sulfite solution-SO₂-DMA and water-SO₂-DMA systems.

A typical absorption-HFCLM run comprises three simultaneous steps for transfer of SO₂: absorption into aqueous solution, extraction with organic, and recovery by vacuum or sweep-gas. The experimental assembly is shown in Figure 6-6. It is similar to one used in absorption-extraction runs. We added line connections to allow application of vacuum and/or passage of sweep gas through the permeator and a reservoir for the organic liquid to maintain a constant volume for the liquid membrane. A feed gas containing 0.23% SO₂, 3.22% O₂, 11% CO₂, and the balance N₂ was passed through the tube-side of the 200-fiber module without any humidification. The aqueous absorbent was introduced into the shell-side. Once a steady state was achieved in the absorption module, the exit aqueous flow was directed through the tube-side of the Celgard fibers in the HFCLM permeator. The extraction was in effect by the DMA at the shell-side of the module, acting as the contained liquid membrane. The pervaporation process is caused by application of a vacuum through the bore of the PDMS rubber tubules; it draws out the SO₂ from the DMA-CLM.

In exploratory runs, a constant volume of He was passed through the silicone tubules, acting as sweep gas. Such trials were done before adopting the vacuum mode of operation. Higher flow of He can establish a sizable gradient for the partial pressure of SO₂ so that the DMA phase strips off SO₂. It is possible that such a gradient attains the level available by using vacuum. The effluent sweep gas can be fed to a GC to determine its SO₂ content and to evaluate the performance of the pervaporation.

The first trial run used 0.2 M Na₂SO₃ solution as the absorbent at 20 mL/min and the model flue gas at 2730 sccm. Such combination is commonly used in our absorption experiments using the sulfite liquor. The run continued for 9 hours. The volume of DMA inside the module as CLM was about 75 mL. The flow rate for He was initially at 150 mL/min and was then lowered to 50 and 10 mL/min, respectively. Under these conditions, the GC results did not show any trace amount of SO₂ at the effluent sweep-gas. The possible causes were: SO₂ was not extracted from the SO₂-laden aqueous 0.2 M Na₂SO₃ solution, or the pervaporation did not recover SO₂ from the organic phase.

Previous LLE runs with DMA showed that it was easier to recover SO₂ from water than that from the reactive sulfite solution. So in the next run, water was the absorbent instead of 0.2 M Na₂SO₃. The run used the most common parameters for absorption of SO₂ with water: 907 sccm of model flue-gas flow rate and 50 mL/min of water flow rate. The run continued for



CM-3501-65A

Figure 6-6. Schematic of combined absorption and liquor regeneration setup modified for HFCLM runs.

CV	Check valve
FGC	Feed gas cylinder
FH	Feed humidifier
FM	Flow meter
HFC	Hollow fiber contactor
LSV	Liquid storage vessel
ND	Nation dryer
OWV	One-way valve
P	Pump
PG	Pressure gauge
RM	Rotameter
V	Valve

7 hours. The GC measurements did not show SO₂ at the effluent sweep-gas stream of He at 150, 50 and 10 cm³/min. A pH value of 5.8 was measured at 4 hours onward for the aqueous stream collected at the exit of the HFCLM unit. Often we measured a pH of 3 for the outlet stream of the absorption unit after about 3 hours. This occurs after the absorption process reaches a steady state condition under such experimental conditions. The neutral effluent of the HFCLM unit suggested that the DMA-liquid-membrane stripped SO₂ from the aqueous stream, but our measurement did not show the presence of SO₂ in the sweep-gas.

For the next run, 100 mL of DMA was first contacted with SO₂ by purging with a gas mixture containing 1.65% SO₂ and balance N₂ for about 1/2 hour under a pressure of 4 psig. Then the shell-side of the HFCLM permeator was filled with this DMA solution. Otherwise, the run duplicated the preceding run. Again, the effluent sweep gas stream did not show traces of SO₂. A preliminary estimate suggested that more time was required to make the DMA solution saturated with SO₂ in the above procedure.

We attempted to regenerate the aqueous SO₂ scrubbing liquor using the DMA again. A sample of fresh DMA was equilibrated with SO₂ in a flask by bubbling a model flue gas mixture containing 0.23% SO₂, 3.22% O₂, 11% CO₂, and the balance N₂. A sweep helium gas at a constant flow rate of 15 mL/min was then bubbled through the flask. The GC analysis of the helium stream showed SO₂. Then we conducted a similar experiment using the HFCLM permeator to strip off SO₂ from SO₂ enriched DMA. About 100 mL of DMA was first equilibrated with SO₂ by purging it with the model flue gas mixture. The shell-side of the HFCLM permeator was then filled with the DMA solution. A constant flow rate of He was passed through the silicone tubules to strip the SO₂ from the CLM. A GC analysis of the effluent did not show traces of SO₂. It was concluded that the resistance of the thick silicone tubule wall was too high.

The module was then dried using vacuum followed by a flow of N₂ through the shell-side (a regular procedure after each trial). After the above run, we found that the silicone rubber was so swollen that N₂ could not be passed through the lumen of the tubules even at a pressure of 15 psig. The module was washed with 50% acetone in water and then dried by applying vacuum to the shell side for one day. Still the silicone tubes did not allow any passage of N₂. The rubber tubules were probably heavily swollen by long exposure to DMA and were then blocked inside at its potted sections. The module was inoperable.

Continuing our study, we used a separate HFCLM module available in our laboratory. It contains two sets of fibers: microporous Celgard and coated Celgard. An ultrathin nonporous skin of silicone rubber on the outside surface of the microporous hollow fibers provided the coating. Such a skin has a typical thickness of 1 μm, and so it will have a very high permeation

rate for SO₂ in the above application. The permeator was thoroughly washed with a solution of acetone in water and then vacuum dried. Leak tests were performed, and none were found. Details of the module are given in Table 6-6.

Table 6-6
GEOMETRIC CHARACTERISTICS OF THE COATED FIBER MODULE FOR HFCLM

Effective length, cm	18	
ID of the shell, cm	0.238	
Fiber type	Coated Celgard	Celgard
	X-10	X-10
ID/OD, μm	100/142	100/142
Number	26	26
Transfer area, cm ²	17.7	32.5
Fiber details		
Tortuosity	3.5	
Porosity	0.2	
Packing Factor	0.18	

The new module was used to repeat the run with the HFCLM permeator containing silicone tubules, as described above. The GC analysis showed SO₂ in the effluent sweep of He. Obviously, the resistance of the thin skinned fiber was much lower than that of the silicone tubules. The results of this experiment established the feasibility of the CLM technique for extracting SO₂ from SO₂-laden DMA solution.

A few runs were then conducted using water-SO₂-DMA and aqueous sulfite solution-SO₂-DMA systems. A model flue gas containing 0.23% ppm SO₂, 3.22% O₂, 11.0% CO₂, and the balance N₂ was passed through the tube-side of the 200-fiber absorption module without any humidification. The aqueous absorbent was introduced into the shell-side of this unit. Once a steady state was achieved, a small fraction of the exiting aqueous stream of about 0.3-0.6 mL/min was directed through the tube-side of the Celgard fibers in the HFCLM permeator. The HFCLM module had about 10-15 mL of SO₂-laden DMA as the CLM. He gas was passed at a flow rate of 15 mL/min through the lumen of the coated fiber.

The first run used water as the absorbent at 45 mL/min and the model flue gas at 908 mL (STP)/min. Such a combination is commonly used in our absorption experiments using water. The run continued for 9 hours. The GC results showed SO₂ at the effluent sweep-gas from the HFCLM unit. However, a steady concentration of SO₂ in the sweep stream was not seen. The possible cause was the unstable interface between water and liquid DMA membrane inside the HFCLM permeator. Water droplets were seen in the sample liquid membrane collected at the end of the experiment. We have experienced the limited miscibility of DMA in water before, and that caused difficulty in maintaining a stable interface.

In the next run, 0.2 M Na₂SO₃ served as the absorbent. The run employed the most commonly used parameters for absorption of SO₂ with sulfite liquor: a flow rate of 2686 mL (STP)/min of model flue-gas and an aqueous flow rate of 17 mL/min. The model flue gas contained 0.225% SO₂, 3.29% O₂, 11% CO₂, and the balance N₂. The run continued for 7 hours. The measured pH of the outlet stream from the absorption unit was 7.2 after about three hours. This stream was then introduced to the HFCLM unit. After one hour, a pH value of 7.3 was obtained in the aqueous stream collected at the exit of the HFCLM unit, after the absorption process reached a steady state condition. This was indicated by a constant value for the trace SO₂ concentration in the exit gas stream from the absorption module. Also, the GC measurement of the effluent sweep-gas stream from the HFCLM permeator showed a steady value for the concentration of SO₂. The flow rate of the SO₂-carrying sulfite solution through the HFCLM unit was 0.3 mL/min. A high pressure of about 18 psig was needed to pass the aqueous phase through the HFCLM permeator due to the very small number of fibers.

Our calculations showed that this experiment recovered about 1% of the SO₂ that was absorbed by the aqueous sulfite solution. Two days later, the experiment was repeated. Only the flow rate of the sulfite solution was different, which was at 0.6 mL/min. The rest of the parameters were similar to those of the preceding run. The run recovered about 0.7% of the SO₂ that was absorbed by the sulfite liquor. The use of coated fibers in these two runs demonstrated that it is possible to regenerate the aqueous SO₂ scrubbing liquor with organic DMA as the CLM in a larger unit.

TASK 7: PARTICLE DEPOSITION

The objective of this task was to determine whether deposition of particulate matter on the inside of the hollow fibers significantly affects the mass transfer efficiency and whether the effect, if any, is reversible. This study of particulate matter is essential since, in a coal-fired power plant application, even downstream of a high efficiency bag filter, there will be nearly 30 mg of particulate matter per cubic meter of flue gas (30 mg/m^3). Therefore, any SO_2/NO_x technology that purports to be practical must deal with this issue and must be robust in the presence of these low level particle concentrations. The size range of the particulate matter that needed to be considered here was 0.2 to 0.3 μm , since this size corresponds to the minimum in the efficiency curve of a bag filter in an actual power plant.

The methodology required to conduct this task in a systematic fashion consisted of six steps: (1) selection of suitable particle generation method to simulate a particle-laden flue gas stream, (2) procurement of typical fly ash material in the desired size range, (3) design of an experimental setup to aerosolize the particles into the flue gas feed stream to the HFC, (4) particle characterization and analysis equipment downstream of the HFC, (5) trial operation of the whole particle generation-analyzing system using inert gases, and (6) mass transfer studies in HFC using simulated flue gas. The most widely used techniques for generating solid particles into gas stream are dry-dispersion and wet-particle dispersion. Dry powders are dispensed by dust feeding equipment (e.g., fluidized bed dust generator). Dust feeding systems are appropriate for generating particles of 0.5 to 100 μm with air flow rates ranging from 10 to 50 L/min. High operating air flows are required to minimize particle agglomeration especially at submicron particle ranges. However, the wet-particle generation method appears to be appropriate because of its flexibility involved with operating parameters, leading to increased control on designing the generating system.

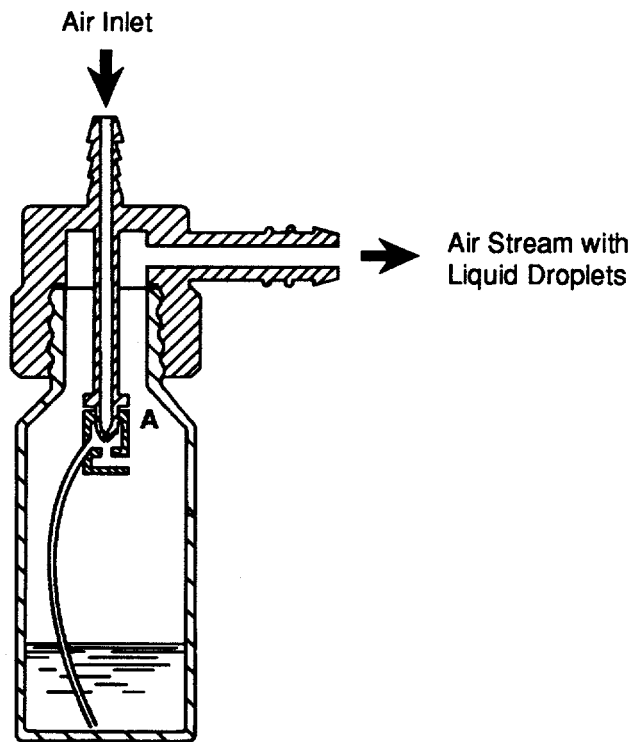
Liquid aerosol generation is one of the common methods for generating particles for inhalation and air pollution studies. Similar to these studies, when quantifying the effect of these particles on mass transfer in an HFC, two important parameters are concentration and size distribution of the particulate matter. These parameters dictate the selection of the type of liquid aerosol generator. Several techniques are available to mechanically disperse liquids to form aerosols. Some of the common methods are air nebulizers, spinning-disc atomizers, ultrasonic nebulizers, and vibrating orifice generators. We chose to work with the pneumatic nebulizers because of their ability to generate very fine droplets at suitable gas flow rates and cost-effectiveness.

In these pneumatic nebulizers, compressed air is used to atomize the liquid into droplets. In the Wright nebulizer, shown in Figure 7-1, air passes through a narrow tube to position A. The high velocity air emerging from this tube creates a low-pressure region at the tube exit, drawing liquid from the reservoir upward through a liquid feed tube. The emitted liquid is atomized by high-velocity air into small droplets. Large droplets impinge onto the upper wall of the curved exit duct, and the smaller droplets remain aerosolized. Clearly, the critical parameters in selecting a nebulizer are the liquid droplet size distribution, the liquid delivery rate, and the gas flow rate. Since numerous models and designs of medical nebulizers are available, choosing the appropriate type of nebulizer was difficult.

For the selection process, we completed some initial calculations to estimate key parameters. All the calculations are presented in Table 7-1. Each nebulizer, based on its design, will have a certain gas-to-liquid flow rate and a corresponding mass median aerodynamic diameter (MMAD). For the desired particle concentration and MMAD in the gas stream, the calculations shown in Table 7-1 are used to generate the required parameters for the nebulizer. The second half of the table gives lumped particle cluster size based on assuming that the coalesced particles form a perfect sphere. The last row in the table indicates the particle size and particle concentration in gas stream suitable for the present study. Knowing the feasibility of particle generation, the next step was to acquire liquid-borne fly ash particles.

The fly ash material must be typical of that found in flue gas streams to produce realistic effects from our laboratory studies. The composition of coal ash typically contains about 58% silica, 27% alumina, and trace amounts of other metal oxides (EPRI Report #CS-2894). Since the majority of ash contains silica material, we decided to procure liquid samples of colloidal silica dispersion. A silica dispersion sample containing 30 wt% of solid particles was kindly supplied by CABOT Corporation, IL.

Other important factors that concerned us were the size range and the nature of the size distribution of these silica particles present in the liquid phase. We have used a Horiba particle analyzer to study the size range, and the results are given in Figure 7-2. About 50% of particles are in the range of 0.1 to 0.3 μm , which is the required size range. Results from Figure 7-2 are also plotted on log-normal probability axes to test the type of distribution (Figure 7-3). While the plot exhibits the bimodal behavior, the dashed line covers about 90% of particles, and for all practical purposes, the trace amounts of particles above 90% can be neglected. Therefore, we assumed that the particles would follow the log-normal distribution. The distribution can be characterized by knowing two parameters: the geometric mean and the geometric standard deviation. The concentration of solids in the supplied colloidal silica dispersion was 30 wt% in deionized water. This liquid dispersion was diluted appropriately while using the nebulizers.



CM-3501-60A

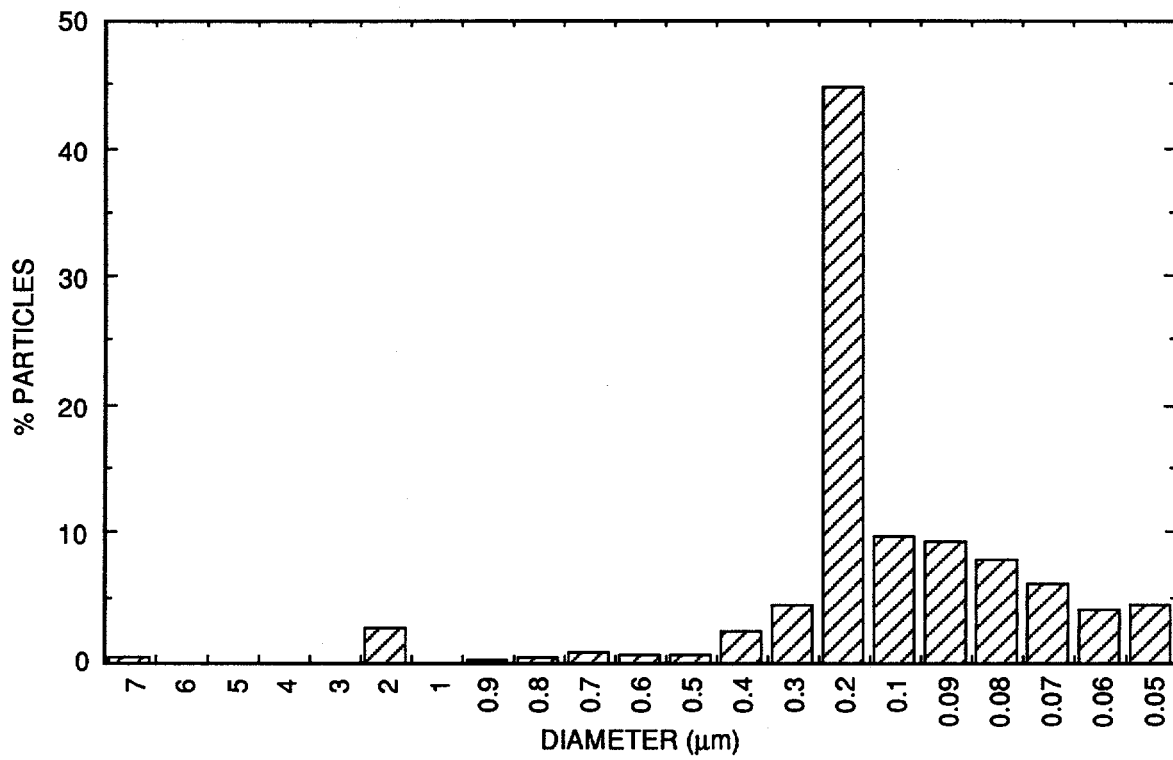
Figure 7-1. Schematic of Wright nebulizer.

**Table 7-1
PARTICLE GENERATION USING NEBULIZERS**

Gas Flow (s/m)	12	Solid particle size (μ)	0.2
Liquid Deliv. (mL/min)	0.3	Particle density (g/cm ³)	2.5
Liquid Drop (μ m)	3	Mass of solid particle	1.048×10^{-11}
Rate of formation of droplets (#/min)	2.12×10^{10}		

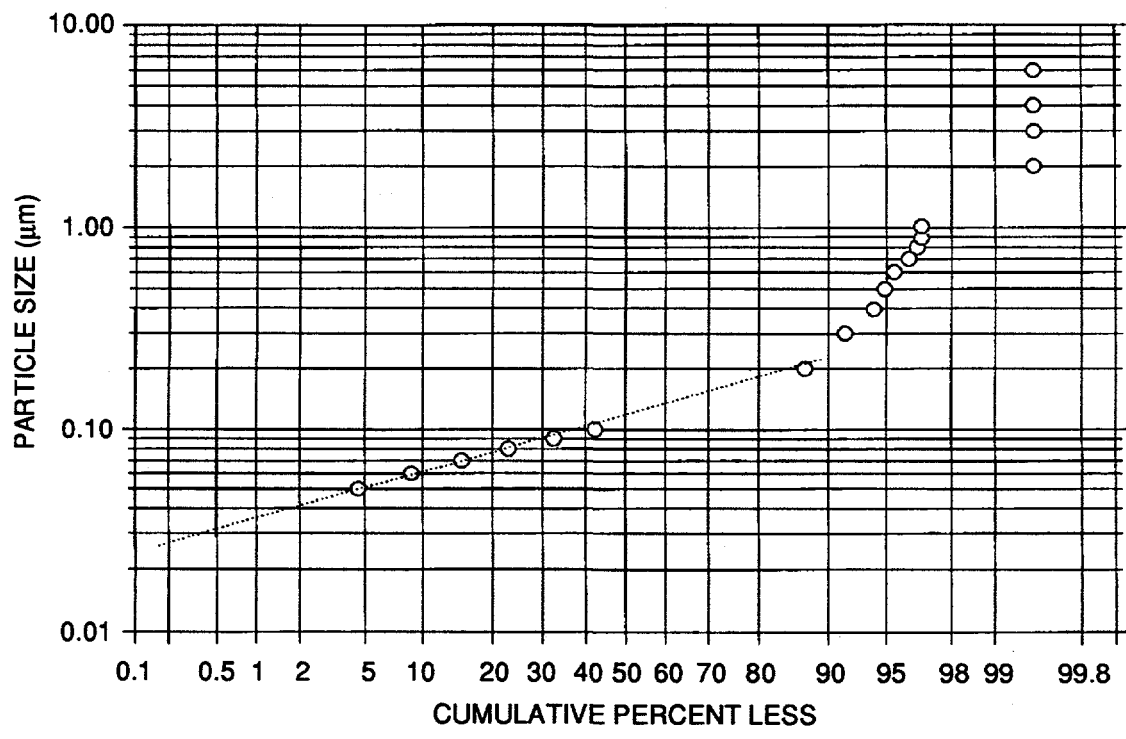
Desired Particle Conc. In Gas Stream (mg/m ³)	Particle Flow (mg/min)	Particle Conc. In Liquid (mg/gm of Water)	Calculations Based on Droplet Size		
			# Particle Flow Req. (#/min)	# Particle Per Water Droplet	Size of Particle Cluster (μ m)
300	3.6	12	3.436×10^{11}	16.20	0.570
200	2.4	8	2.291×10^{11}	10.80	0.498
100	1.2	4	1.145×10^{11}	5.40	0.395
50	0.6	2	5.727×10^{10}	2.70	0.314
25	0.3	1	2.864×10^{10}	1.35	0.249

Relative humidity of dry air (%)	12
Abs. humidity of dry (kg/kg dry)	0.002
Times supersaturated	1.054
Density of air (25°C) (kg/L)	0.001
Abs. humidity after nebu (kg/kg dry)	0.021



CAM-3501-66

Figure 7-2. Size distribution of dispersed silica particles.



CM-3501-67

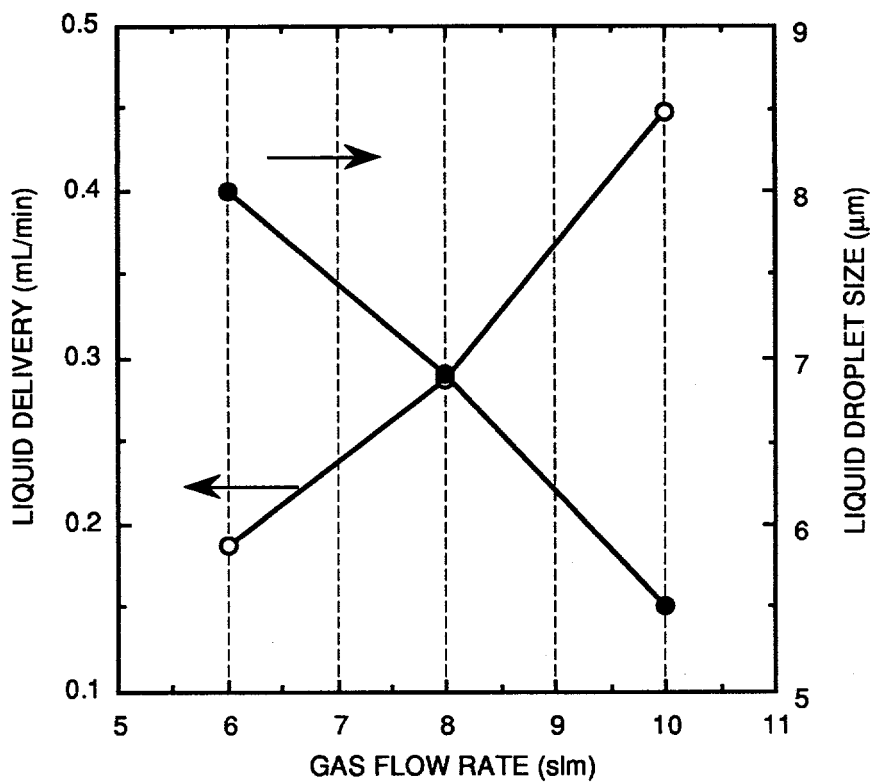
Figure 7-3. Log-normal distribution of dispersed silica particles.

We tested several nebulizers for their applicability to the present process. From Table 7-1, it can be inferred that to obtain the desired dry particle size (0.1-0.4 μm), the droplet size generated by a nebulizer must be as small as possible ($\sim 0.3 \mu\text{m}$). For all the nebulizers, based on their design, the liquid delivery rate is fixed for a certain gas flow rate. Typical performance characteristics of an Inspiron (Ominicare, Inc.) (400 cm^3) nebulizer are shown in Figure 7-4, which shows that an increase in the gas flow rate results in smaller droplet size, but also increases the liquid delivery rate. The droplet size distribution from the nebulizer was measured by Malvern Optical Instruments (laser aerosol spectrophotometer). While it is appropriate to get small droplets, it is undesirable to introduce high amounts of liquid into the gas stream because it creates difficulties in the particle analysis and alters the mechanism of particle deposition rates.

From our preliminary tests with several nebulizers, we successfully optimized the parameters with an Acorn II nebulizer (Marquest Medical Products, Inc., Englewood, CO) for generating particles with a suitable size range. The inlet gas flow rate to the system was 11.7 L/min and the corresponding liquid delivery rate was 0.29 mL/min. These operating parameters also generated a liquid droplet size of 3.4 μm . The properties of the gas stream at the exit of the nebulizer were 100% relative humidity and 15°C dew point. A section of the gas tubing was heated by electrical heating tape to bring down the humidity levels of the gas stream. This heating became necessary to vaporize the liquid droplets and to condition further the solid particles.

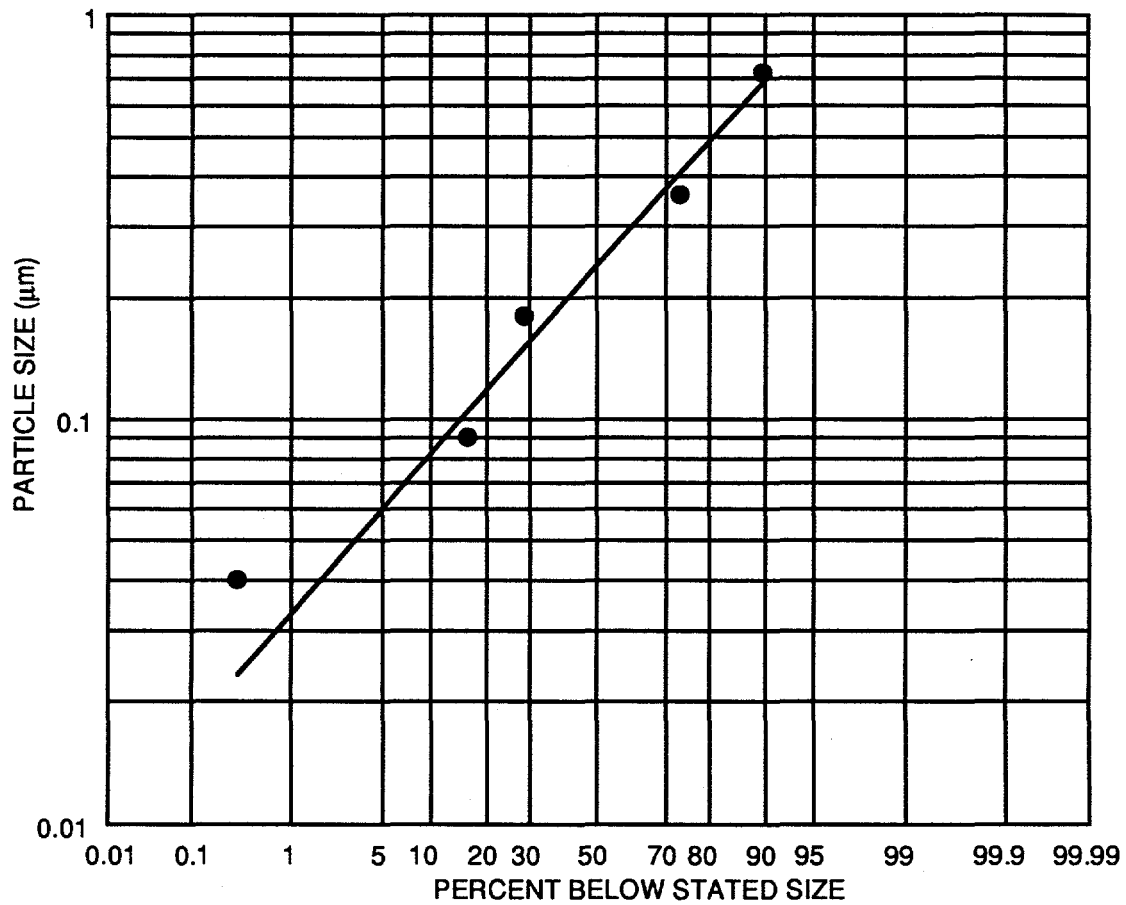
In an experiment, a known sample solution of silica dispersion was taken into the reservoir of the Acorn II nebulizer and was aerosolized with 11.7 L/min of gas flow rate. The wet particle-laden gas stream was heated and analyzed for particle size distribution. Silica dispersion sampling and characterization of aerosol was done using a Quartz Microscopic crystal cascade impactor. This instrument measures the size of the particles based on well established particle impaction theory. The instrument essentially contains a 10-stage cascade impactor equipped with quartz crystals. Depending on the entrance nozzle diameter and the distance between the crystal surface and nozzle outlet, only a certain size particles will be retained on the crystal surface. This retained particle mass is measured with electronic sensing meters. The sample to the meter was taken after the heated tube section. The gas properties at the sampling position are 72% relative humidity, 23°C dew point, and 28°C dry bulb temperature.

The sampling time to the instrument was varied from 1 to 20 seconds to verify the reproducibility of the results. Figures 7-5 and 7-6 show the size distribution curves from the same sample designed to produce a particle concentration of 30 mg/m^3 . The ordinate in the figure gives the particle size (μm) on a logarithmic scale, and the abscissa gives the cumulative percent below the stated size on a probability scale. The mass median aerodynamic diameter (MMAD) that



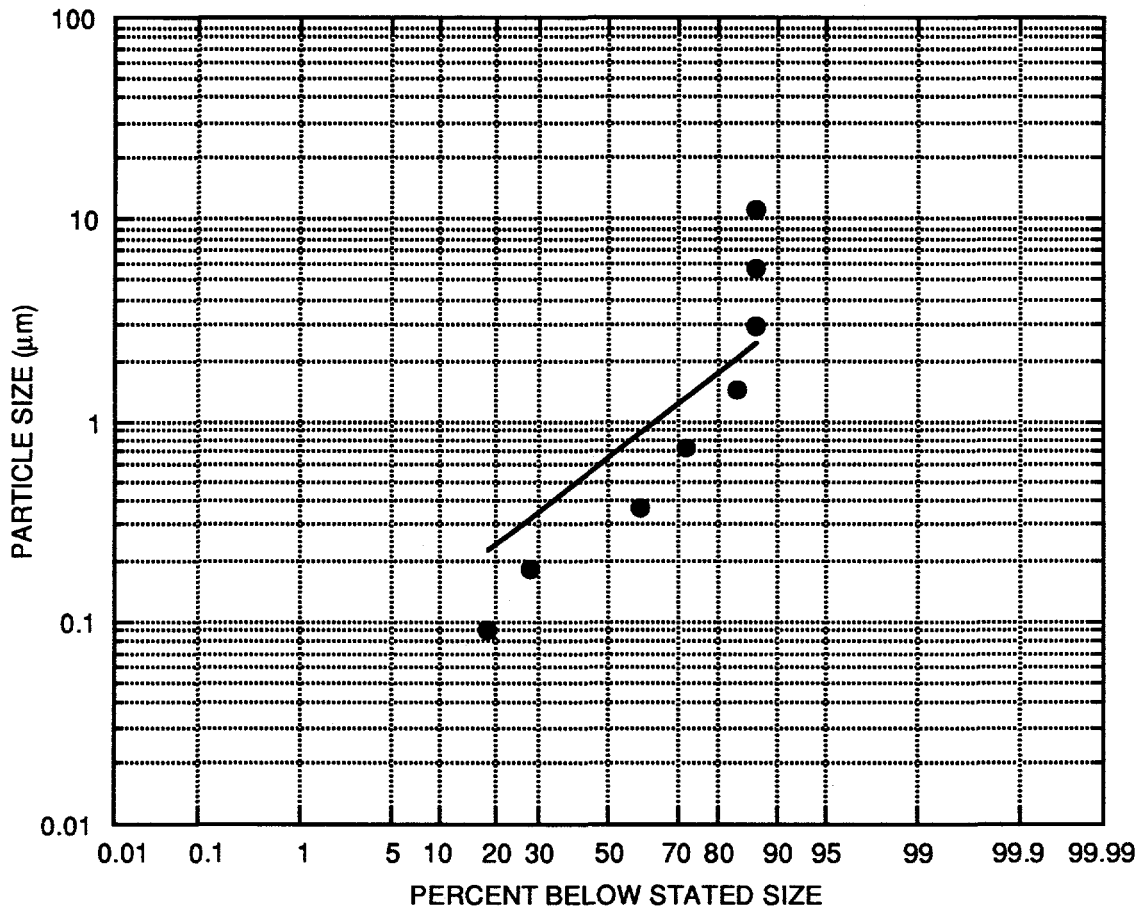
CM-3501-73

Figure 7-4. Inspiron (400 cm³) nebulizer performance characteristics.



CAM-3501-83

Figure 7-5. Particle size distribution for the sampling time of 1 s.



CAM-3501-84

Figure 7-6. Particle size distribution for the sampling time of 40 s.

corresponds to 50% on the abscissa according to Figure 7-5 is 0.25 μm . In Figure 7-6, the size distribution is somewhat distorted with a few larger particles close to 10 μm . Considering the practical difficulties involved with accurate sampling and method (e.g., mass based or number based) of analysis, one can neglect these few isolated particles. Then the MMAD for the Figure 7-6 is about 0.4 μm . This kind of correction is not unusual in particle size analysis experiments.

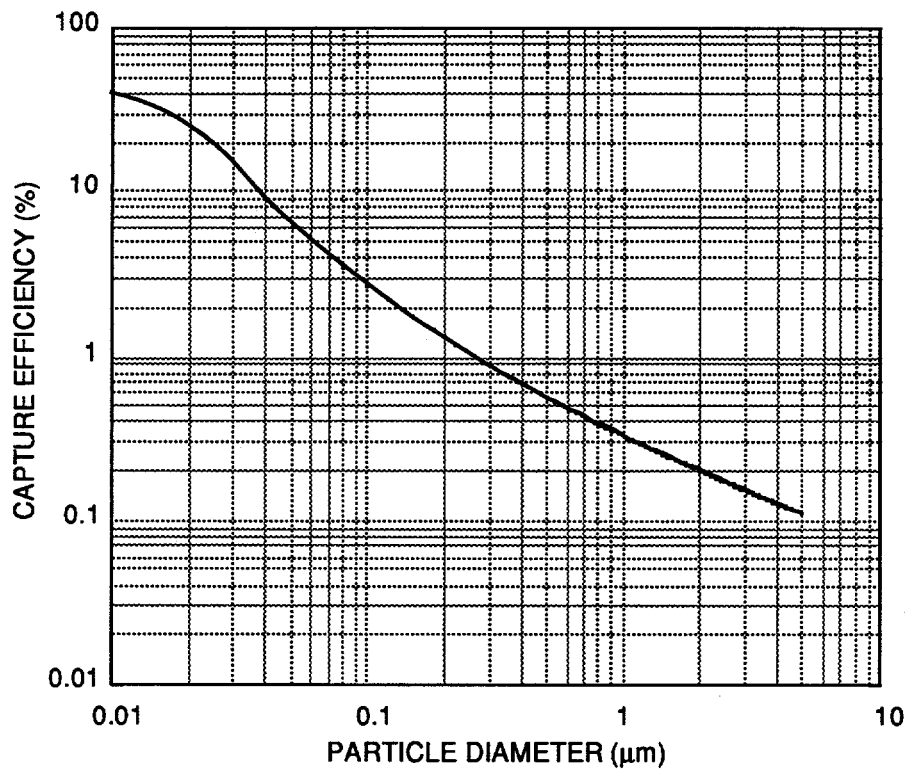
The average particle size measured here is about 3 to 4 times larger than the silica dispersion size measurements conducted in the liquid form, indicating that the silica particles agglomerate in the gaseous media. Still, the particle sizes in the gaseous media fall in a range similar to that found downstream of a bagfilter in a power plant. As a result, we estimated particle deposition rates before conducting the time-on stream tests with this particle generation technology.

Deposition of particles on the inner walls of hollow fibers can be estimated by using established theories. The gas flow inside the fibers is assumed to be laminar and the mechanism of particle deposition is varied according to the particle size. Figure 7-7 shows the deposition efficiency. Using the equations given in (Fuchs, 1964), the capture efficiency for 0.2- μm particles is about 1%, indicating that the time needed for a monolayer coverage is 290 hours.

Our next step was to deposit the generated particles onto the inner walls of the hollow fibers and to further estimate the effect of this deposition on SO_2 mass transfer. To examine the change in mass transfer, it was necessary to characterize the module immediately before the start of particle deposition. Then at suitable time intervals, we measured the mass transfer characteristics of the HFC repeatedly. This procedure allowed us to correlate the amount of particles deposited to the mass transfer efficiency of the module. In addition, we measured the mass of the particles in the exiting gas stream.

SO_2 absorption experiments were conducted in a 1000-fiber HFC. Water was shown (e.g., Task 4) to be a good absorbing solvent for SO_2 and hence was used as the absorption medium. Feed gas stream to the HFC contained 4000 ppm of SO_2 and balance N_2 . The exit gas stream from the HFC was monitored by a gas chromatograph (HP 5890) equipped with a Porapak Q column (6 ft x 2 mm ID, Alltech Assoc., Deerfield, IL). Since the detectable limit for this system is approximately 500 ppm, the 4000 ppm of SO_2 inlet concentration was found to be appropriate for analyzing the HFC exit gas stream.

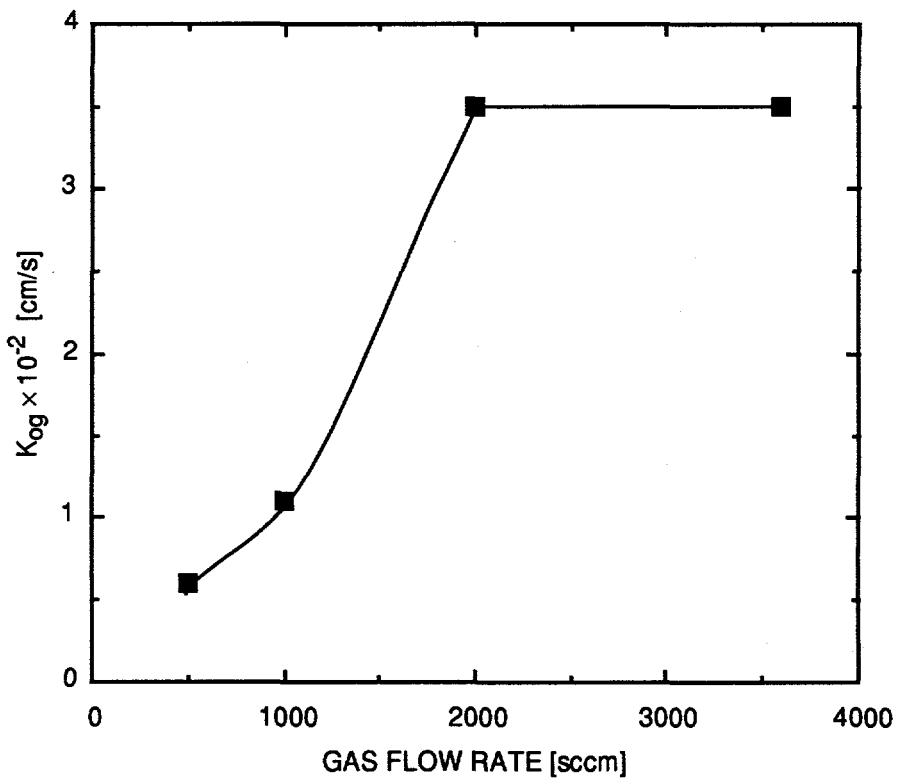
Experiments were conducted at various gas flow rates. The variation of the gas side overall mass transfer coefficient (K_{Og}) is shown in Figure 7-8. The liquid flow rate was maintained at 11.2 mL/min. K_{Og} increases rapidly (by a factor of 6) at the low gas flow rates and becomes almost flat at the high (>2 slm) gas flow rates. This behavior at the high gas flow rates is due to the attainment of equilibrium conditions for SO_2 in the liquid.



CM-340581-153

Figure 7-7. Particle capture efficiency in an HFC.

Fiber length 23 cm, no. of fibers 1155, ID 240 μm, gas flow 11.7 slm.



CAM-3501-77

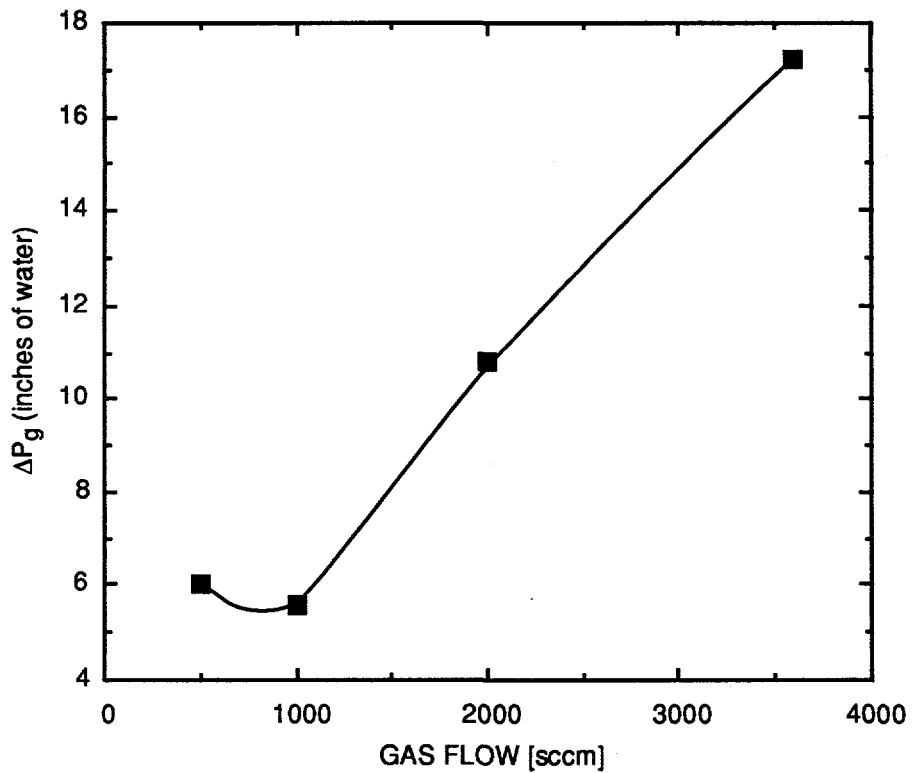
Figure 7-8. Variation of gas-side overall mass transfer coefficient with gas flow rate.

Another factor in this study was the gas pressure drop (ΔP_g) across the HFC. This is important because of its fourth power functional relationship with the diameter of the fiber (see Equation 14-4, Task 14). Since the fiber diameter will change after repeated exposure to the particle-laden gas stream, ΔP_g will be greatly affected. The differential pressure across the HFC was measured with a digital pressure meter (Air-Neutronics, Ltd., Oxford, England). The dependency of ΔP_g on the gas flow rate is given in Figure 7-9. The overall trend is linear with laminar flow conditions except for one 1000-sccm point, which could be due to a wrong zero set point in the pressure meter or a leak during the measurements. Again, these stated results will serve as baseline measurements for all the future work with the particle deposition system.

It was also critical to determine the mass of the particles in the outlet gas stream in order to quantify the amount of particles deposited on the walls of the hollow fibers. As noted above, accurate particle size measurements are very difficult with the smaller particles ($< 1 \mu\text{m}$). In an attempt to observe the particle collection efficiency using filters, we purchased an in-line stainless-steel filter holder and 0.2- μm pore size filter membranes from Millipore (Bedford, MA). These filter membranes were claimed to show 99.99% particle collection efficiency by the manufacturer.

The particle-laden stream was generated using an Acorn-II nebulizer system. Liquid containing known amount of colloidal silica particles was pumped into the nebulizer reservoir using a peristaltic pump. The level of the liquid in the reservoir was maintained at about 4 mL to provide a constant liquid delivery rate. This ensured a uniform particle generation and particle size range. The gas stream was heated to reduce the humidity level, and the particles were filtered using two 0.2- μm filters for 2 hours. During the run, the amount of liquid being nebulized was also recorded. It was calculated that only 90% of the particles that were generated were actually collected by the two filters. This 10% discrepancy even for a simple generate-and-capture test gives the error we may expect to have while generating and then depositing particles on an HFC. Our earlier calculations showed that 1% of the generated particles should be deposited on an HFC, which is well within our experimental 10% measurement error. As a result, we abandoned efforts to quantify the amount of particles deposited and focused only on its effects on mass transfer. Before presenting the test results, it is appropriate to compare the operating parameters of the present system with those of the actual power plant.

Gas flow rate through the fibers determines the residence time of a gas molecule and, therefore, affects the deposition of particulate matter. The flow rate for all the experiments was fixed at 11.7 slm. This flow rate was chosen only to generate an appropriate particle size distribution and not to simulate actual plant conditions. However, this flow gives a residence time of 0.053 s in



CAM-3501-78

Figure 7-9. Effect of gas flow on the pressure drop across the HFC.

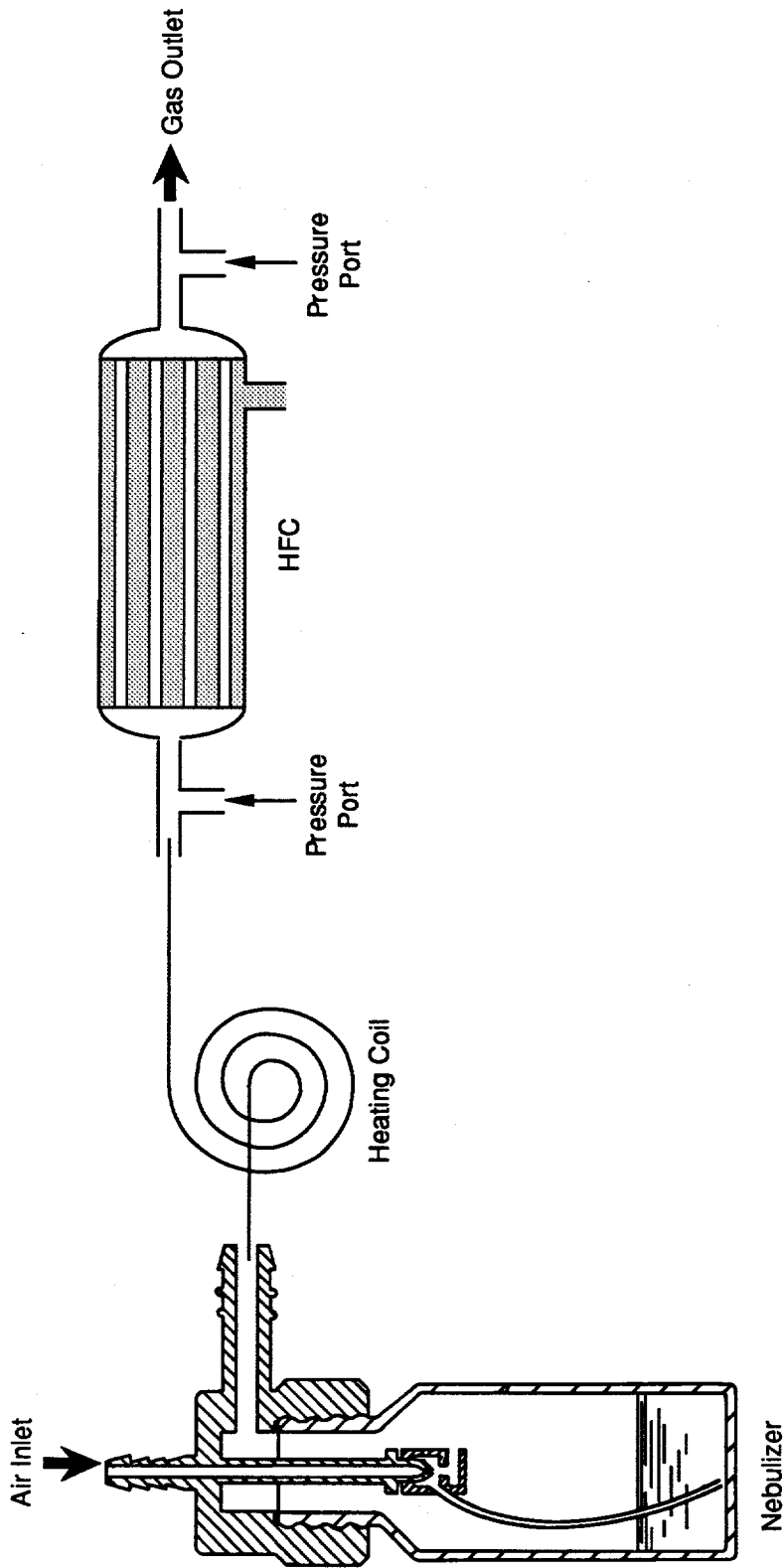
contrast to a value of 0.073 s (based on 14-cm long, 240- μm -ID fibers, see Task 14) that corresponds to a more practical situation. Since these two values are within a difference of $\sim 25\%$, the flow rate under consideration fairly represents actual plant conditions.

The temperature of gas stream affects the diffusion rates of particles. In our experiments the gas stream entering the module was at about 40°C as opposed to an approximate power plant flue gas temperature of 50°C . Humidity levels were indeed difficult to maintain as the temperature of the stream dropped down along the module. At the inlet to the module the relative humidity of the stream was about 70% and the exiting stream was at room temperature and completely saturated. Even water droplets were noticed occasionally at the outlet of the device, indicating the condensation of water. If the condensation occurs well into the module, it is very likely that this process alters the particle deposition phenomenon because of the high tendency of the particles to agglomerate. Having these factors in mind, we conducted time-on-stream studies and the results are presented below.

The experimental arrangement for generating particles is shown in Figure 7-10. The liquid level in the Acorn II nebulizer reservoir was maintained at about 4 mL. The liquid sample was prepared by diluting the original colloidal silica dispersion so as to produce a particle concentration of 30 mg/m^3 . During the initial stages of particle deposition process, we measured the mass transfer frequently. We also monitored the pressure drop across the module (ΔP_g) periodically during particle deposition.

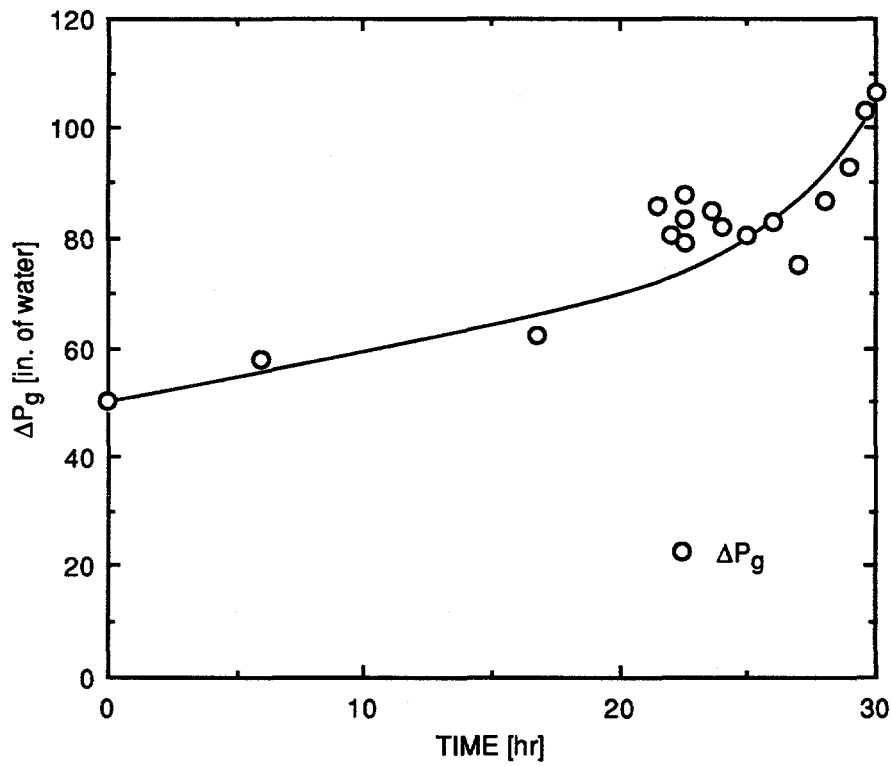
During the first 30 hours, as can be seen from Figure 7-11, ΔP_g increased monotonically and reached about 115 inches of water. At this time, the particle deposition process was stopped and the module was dismantled to observe the fibers. We noticed a particle cake at the gas inlet end of the fiber bundle, which was an unexpected result. Photographs of the cake and fiber ends are given in Figures 7-12 and 7-13.

As shown earlier, the particle size generated could vary anywhere from 0.1 to $5 \mu\text{m}$, with a mean around $0.2 \mu\text{m}$. It is likely that the large particles did not follow the gas stream lines. In this case, these particles clung onto the inner surface of the fibers, closer to the fiber inlets. As the experiment progressed, this obstructing particle started growing due to interception of other particles and further agglomeration. This process eventually led to blocking the fiber and the cake buildup. We believe that this blockage might run a few inches into the module from the gas inlet. We intend to present our compiled mass transfer results in the future, including our efforts to reverse this blocking.



CM-3501-60B

Figure 7-10. Experimental SETUP for particle generation.



CM-3501-75A

Figure 7-11. Variation of ΔP_g across HFC.

Figure 7-12. Pictures of HFC end caps and gas inlet and outlet ends of fibers. Particle cake is formed at gas inlet end. A lump of particles is seen on the gas inlet end cap.

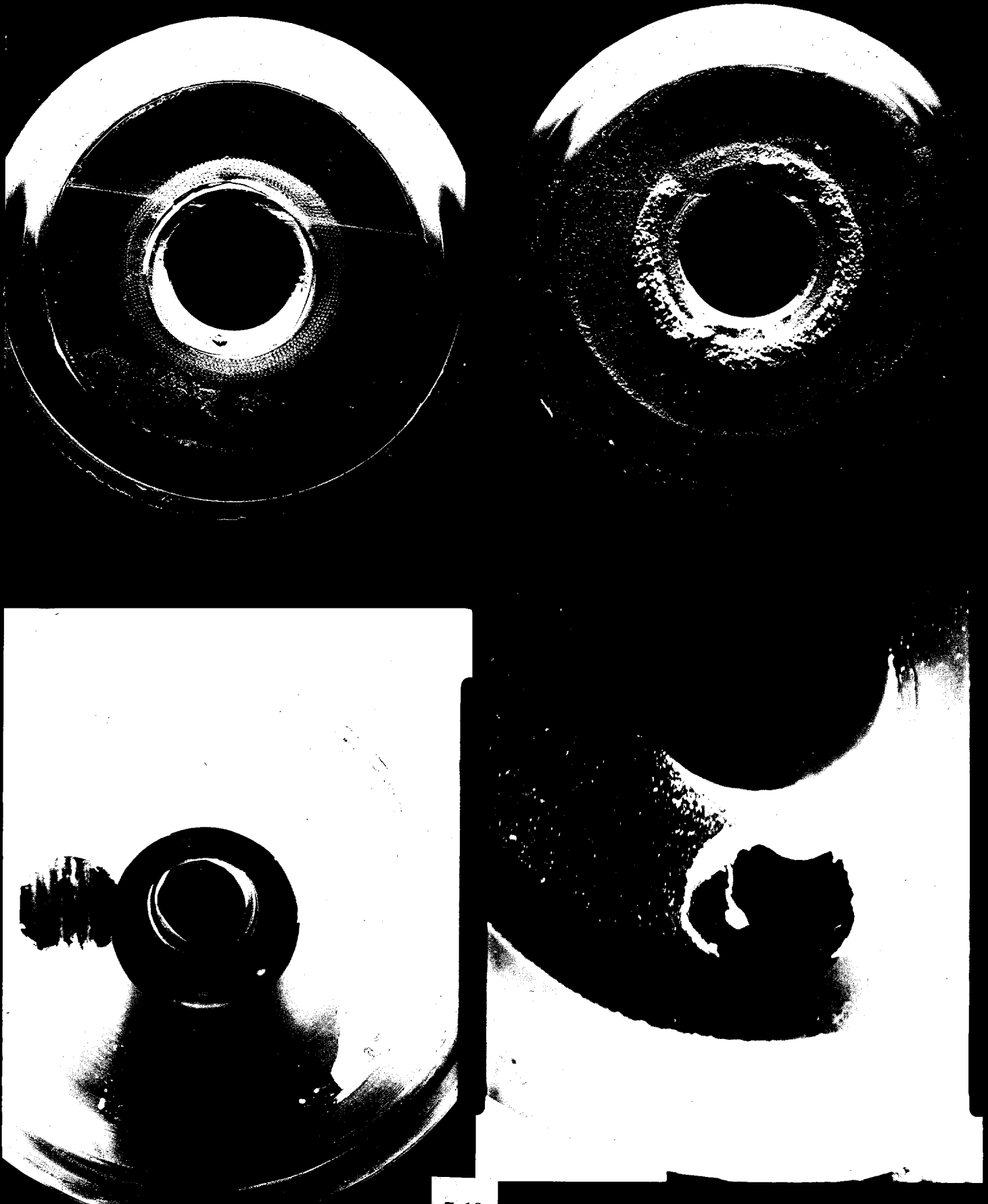




Figure 7-13. Enlarged view of a portion of particle cake formed at gas inlet end of HFC.

TASK 14: ECONOMIC EVALUATION

The objective of this task is to perform increasingly detailed economic analyses of the overall process to guide the research to most critical problems and to assist management decision points.

As per the present understanding of the option A (liquid-liquid extraction of SO₂) of the process, we estimated the size and cost major battery limit equipment and the results, as presented below. Option B of the process is in progress (Tasks 4 and 6) and its economic calculations will be reported later.

Figure 14-1 shows the process flow sheet with all the major equipment labeled. The design bases for our 500-MW(e) plant are given in Table 14-1. Given these design specifications, we can proceed to sizing and costing of various equipment. The calculations involved with absorbers (SO_x and NO_x) and liquid-liquid extractor are presented in a more detailed manner.

SO₂ ABSORBER

Based on the mass transfer data from Task 4, the following are the important parameters and thermodynamic conditions:

SO ₂ absorbing liquid:	0.2 M Na ₂ SO ₃
Approach to equilibrium:	50% (assumed)
Liquid flow rate:	2.88 x 10 ⁴ L/min (98% removal basis)
Assumption:	p* <<< p (liquid has significant absorption capacity)
Mass transfer correlation:	

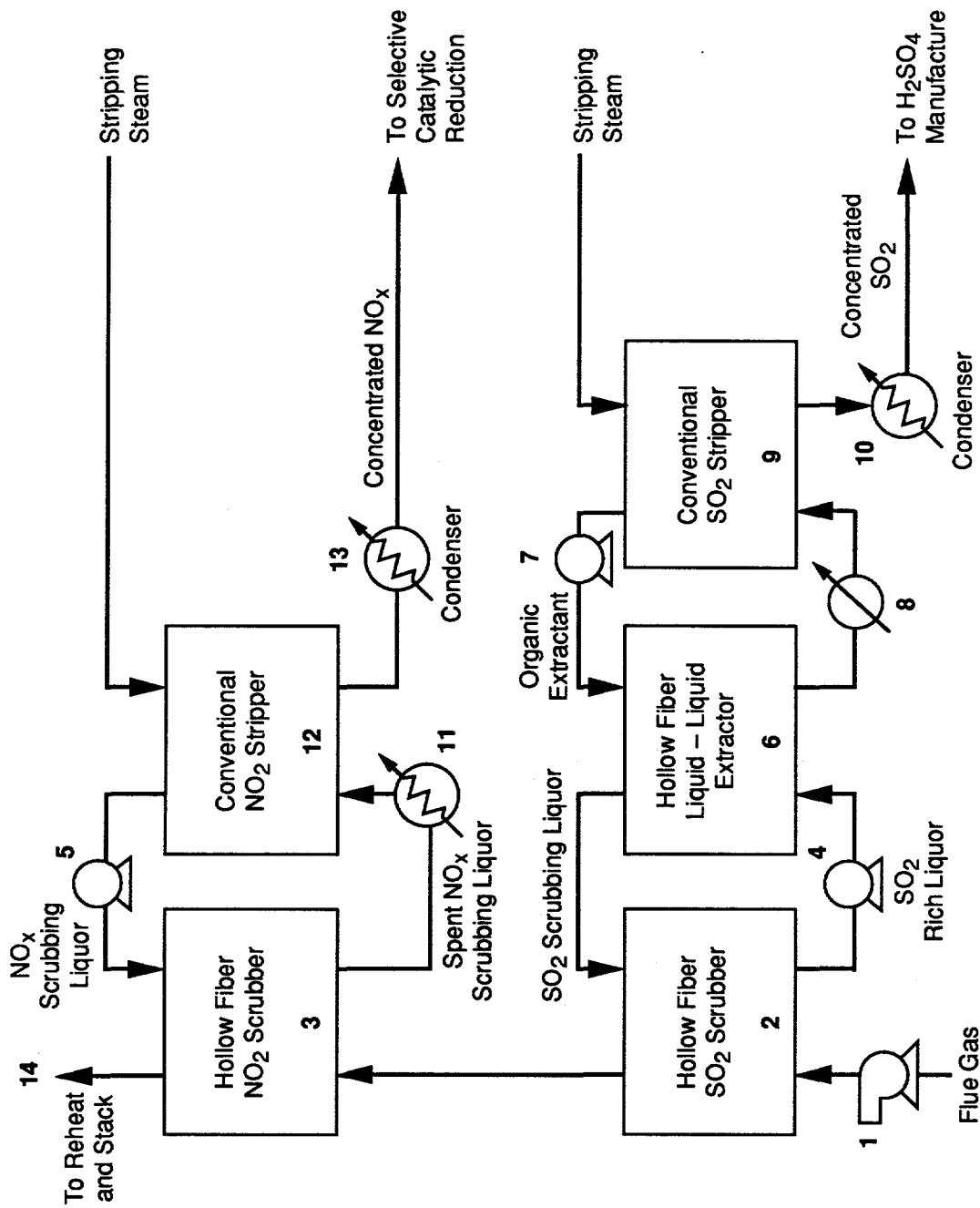
$$K_{og} = 0.079257 Re^{0.33211} \quad (14-1)$$

where Re is the gas-side Reynolds number and is given as

$$Re = \frac{4 \rho_g Q_g}{\pi \mu_g d_i N} \quad (14-2)$$

Here

ρ_g	=	gas density (g/cm ³)
Q_g	=	volumetric gas flow rate (cm ³ /s)
μ_g	=	viscosity of flue gas (g/cm s)
d_i	=	ID of the fiber (cm)
N	=	number of fibers



CM-360583-49D

Figure 14-1. Proposed SO_x/NO_x wet scrubbing with hollow fiber contacting devices.
Option A for SO₂ liquor regeneration.

Table 14-1
BASIS FOR EXAMPLE DESIGN OF 500-MW(e) SO_x/NO_x PLANT

Flue gas flow rate	1 million actual ft ³ /min (2.25 x 10 ¹⁰ sccm)
Flue gas temperature	160°F
Flue gas pressure	760 mmHg
Flue gas composition	
SO _x	3000 ppm(v)
NO _x	450 ppm
CO ₂	14%
H ₂ O	8%
O ₂	3.3%
N ₂	74.4%
Fraction of SO _x /NO _x removed in absorbers	
SO _x	98%
NO _x	85%
Pressure drop	
SO _x scrubber (flange to flange)	10 inches H ₂ O
NO _x scrubber (flange to flange)	10 inches H ₂ O

Equation (14-1) is obtained from the experimental results of Task 4. Our equilibrium calculations for Na₂SO₃/SO₂ systems indicate that the partial pressure of SO₂ (p*) in equilibrium with the liquid is much lower than the actual partial pressure (p) and for these conditions, the mass balance yields

$$\ln \frac{p_0}{p_L} = K_{og} \pi d_o L N / Q_g \quad (14-3)$$

Here, p₀ and p_L indicate the partial pressures of SO₂ in the entering and exiting gas streams, respectively.

The pressure drop in the module should not exceed 10 inches of water, and this constraint is imposed using Hagen-Poiseulle equation (Bird et al., 1960).

$$Q_g = \frac{\pi d_i^4 \Delta P N}{128 \mu_g L} \quad (14-4)$$

where

$$\begin{aligned}\Delta P &= \text{pressure drop [dynes/cm}^2\text{]} \\ L &= \text{length of the fiber [cm]}\end{aligned}$$

Using the above four equations, we can explicitly find the number of fibers and then the length of the fiber, given the ID of the fiber. Commercially available 400- μm -ID is chosen to report cost information. The cost of the membrane is taken as \$0.20/ft² as per the arguments presented in our proposal (PYU 90-167).

NO_x ABSORBER

The key assumptions and conditions are

Absorbing liquid:	0.1 M Co(II)phthalocyanine
Approach to equilibrium:	10% (assumed based on the lab data)
Liquid flow rate:	48115 L/min (85% removal basis)

The mass transfer correlation (from Task 5) is

$$K_{og} = 0.0011907 \text{ Re}^{1.0307} \quad (14-5)$$

The mass balance equation for NO at any point in the absorber is given as

$$Q_g \int_{p_L}^{p_0} \frac{dp}{p - p^*} = K_{og} \pi d_o L N \quad (14-6)$$

The integral value in Equation (14-6) is calculated by a numerical scheme and is a fixed number for a constant NO removal desired (85%). Similar to SO₂ absorber calculations, Equations (14-5) and (14-6) are to be used in association with Equations (14-3) and (14-4) to estimate the membrane area requirements.

LIQUID-LIQUID EXTRACTOR

The spent aqueous SO₂ liquor flow rate and SO₂ concentration in the solution are known from SO₂ absorber calculations. The partition coefficient from Task 6 is obtained as 0.5 (C_{org}/C_{aq}). Again, organic phase (DMA) is assumed to approach 50% equilibrium corresponding to aqueous liquor inlet SO₂ concentration. Therefore,

$$\text{DMA flow rate:} \quad 1.146 \times 10^5 \text{ L/min (99\% removal basis)}$$

From the laboratory data, the relation between organic side overall mass transfer coefficient ($K_{ov,org}$) and the shell-side Re is given as

$$K_{ov,org} = 0.044754 Re^{1.3829} \quad (14-7)$$

However, using the proposed rectangular type modules with length of 50 cm, the Re numbers turn out to be in the range of a few hundreds, leading to unacceptably high mass transfer coefficients. In a situation where organic side and aqueous side resistances are negligibly small, we have the stagnant membrane phase (pore) resistance. This membrane resistance can be fairly well calculated using the following relation:

$$K_{ov,org} = \frac{D_{SO_2}}{t} \quad (14-8)$$

Here,

t = membrane wall thickness [cm]

D_{SO_2} = diffusion coefficient of SO_2 [cm^2/s]

Now, using the above $K_{ov,org}$ value and the log-mean concentration (ΔC_{ln}) driving force, the membrane area requirements can be calculated as

$$J_{SO_2} = K_{ov,org} \pi d_o L N \Delta C_{ln} \quad (14-9)$$

where J_{SO_2} = rate of SO_2 transfer [mole/s]

Knowing the gas and liquid flow rates at each point in the process, we can estimate the sizing of pumps and their costs using the simulation program, ASPEN. Likewise, the flue gas blower, stack gas reheating system, heat exchangers, and conventional strippers are designed and the corresponding utility costs are estimated. These details are given in Table 14-2. We intend to compare the overall plant costs with those for the traditional processes in our next report.

Table 14-2
COST OF MAJOR EQUIPMENT AND UTILITY ITEMS IN OPTION A
FOR A 500-MW(e) POWER PLANT
(Liquid-Liquid Extraction of SO₂ Liquor)

<u>Item No.</u>	<u>Item Name</u>	<u>Capital Cost (dollars)</u>	<u>Utility Cost (dollars/hr)</u>
1	Flue gas fan	\$750,000	\$170
2	SO ₂ scrubber	916,000	—
3	NO _x scrubber	2,060,000	—
4	SO ₂ liquor pump	27,000	7
5	NO _x liquor pump	34,000	4
6	SO ₂ extractor	500,000	—
7	Extractant pump	87,000	18
8	Extractant heat exchanger	424,000	1,560
9	Extractant steam stripper	400,000	100
10	Condenser after SO ₂ stripper	50,000	9
11	NO _x heat exchanger	473,000	1,880
12	NO _x steam stripper	188,000	484
13	Condenser after NO _x stripper	219,000	156
14	Stack gas reheating system	<u>1,729,000</u>	<u>231</u>
	Total	\$7,857,000	\$4,619

REFERENCES

- Bird, R. B., W. E. Stewart, and E. N. Lightfoot (1960) [need complete ref.]
- Cussler, E. L. (1984) *Diffusion* (Cambridge Press).
- Dean, J. A., Ed. (1979), *Lange's Handbook of Chemistry*, 12th ed. (McGraw-Hill, New York), p. 10-5. [where cited?]
- Demyanovich, R. J., and S. Lynn (1987), *Ind. Eng. Chem. Res.* **26**, 548-555.
- EPRI (Electric Power Research Institute) (19??), "Title??" Report CS-2894 (Electric Power Research Institute, Palo Alto, CA). [see ref page 7-2]
- Fuchs, N. A. (1964), *Mechanics of Aerosols* (Pergamon Press, London), pp. 205-206.
- Geankoplis, C. J. (1972), *Mass Transport Phenomena* (Ohio State University Bookstores, Columbus, Ohio).
- Karoor, S. (1992), "Gas Absorption Studies Using Microporous Hollow Fiber Membranes," Ph.D. Thesis, Stevens Institute of Technology, Hoboken, NJ.
- Kreik, F., and W. Z. Black (1980), *Basic Heat Transfer* (Harper and Row, Cambridge).
- Majumdar, S., et al. (1988) "Title?," *AIChE J* **34**, 1135.
- Sada, E., H. Kumazawa, and Y. Takada (1984), "TITLE?," *Ind. Eng. Chem. Fund.* **23**, 60-64.
- Wickremasinghe, S. R., M. J. Semmens, and E. L. Cussler (1992), "Hollow Fiber Modules Made with Hollow Fiber," (publisher or journal?, city?).
- Yang, M. C., and E. L. Cussler (1986), "Designing Hollow-Fiber Contactors," *AIChE Journal* **32**, 1910-1916.

Appendix A
INITIAL PRESSURE

INITIAL PRESSURE

In the test absorption apparatus, the sample cell is initially evacuated to a low pressure $P_{sc}(0)$, higher than the test adsorbent's vapor pressure. At this point, the sample cell contains N_2 and the adsorbent's vapor. The sample cell is then isolated and the headspace evacuated to a lower pressure $P_{HS}(0-)$, containing pure N_2 . The headspace is then pressurized to $P_{HS}(0)$ with a SO_2/N_2 gas mixture containing y^0 mole fraction SO_2 . At this point, the total moles of each gas is

$$\text{moles } N_2(0) = [P_{sc}(0) - P_v] \left[\frac{V_{sc} - V_L}{RT} \right] + P_{HS}(0) \frac{V_{HS}}{RT} + (1-y^0) [P_{HS}(0) - P_{HS}(0-)] \frac{V_{HS}}{RT} \quad (A-1)$$

$$= [P_{sc}(0) - P_v] \left[\frac{V_{sc} - V_L}{RT} \right] + (P_{HS}(0) - y^0 [P_{HS}(0) - P_{HS}(0-)]) \frac{V_{HS}}{RT} \quad (A-2)$$

$$\text{moles } SO_2(0) = y^0 [P_{HS}(0) - P_{HS}(0-)] \frac{V_{HS}}{RT} \quad (A-3)$$

where P is the pressure, V is the volume, P_v is the adsorbent's vapor pressure, R is the gas constant, and T is the absolute temperature. The subscripts HS, SC, and L refer to the headspace, sample cell, and liquid adsorbent, respectively.

At time 0, the headspace and the sample cell are connected by opening a valve. Here, we shall make two assumptions: (1) the gases in the headspace and sample cell instantly mix, and (2) the liquid adsorbent instantly exerts a vapor pressure in the headspace and sample cell. Thus, the partial pressure of each gas is given by

$$P_{N_2}(0) = \frac{[\text{moles } N_2(0)] RT}{V_{HS} + V_{sc} - V_L} \quad \text{and} \quad P_{SO_2}(0) = \frac{[\text{moles } SO_2(0)] RT}{V_{HS} + V_{sc} - V_L} \quad (A-4)$$

and the total pressure is given by

$$P(0) = P_{N_2}(0) + P_{SO_2}(0) + P_v \quad (A-5)$$

Substituting Eqs. (A-2) and (A-3) into Eq. (A-4) and then into (A-5) yields

$$P(0) = \frac{[P_{sc}(0) - P_v] [V_{sc} - V_L] + P_{HS}(0) V_{HS}}{V_{HS} + V_{sc} - V_L} + P_v \quad (A-6)$$

Note the absence of $P_{HS}(0-)$ from Equation (A-6). The initial mole fraction of SO_2 , $y_{SO_2}(0)$ is given by

$$y_{SO_2}(0) = \frac{P_{SO_2}(0)}{P(0)} = \frac{y^0 [P_{HS}(0) - P_{HS}(0-)] V_{HS}}{[P_{sc}(0) - P_v] [V_{sc} - V_L] + P_{HS}(0) V_{HS} + P_v (V_{HS} + V_{sc} - V_L)} \quad (A-7)$$

Appendix B
CALCULATION OF H AND H*

CALCULATION OF H AND H*

The partition coefficient, H, is defined as

$$H = \frac{P_{\text{SO}_2(f)}}{x_{\text{SO}_2(l)}} = P_{\text{SO}_2(f)} \left[1 + \frac{\text{moles adsorbent}}{\text{moles SO}_2 \text{ in liquid}} \right] \quad (\text{B-1})$$

where $P_{\text{SO}_2(f)}$ is the equilibrium partial pressure of SO_2 and $x_{\text{SO}_2(l)}$ is the mole fraction of SO_2 in the liquid adsorbent at equilibrium. At equilibrium we can also write a SO_2 mass balance:

$$\frac{P_{\text{SO}_2(f)}}{RT} [V_{\text{HS}} + V_{\text{SC}} - V_{\text{L}}] + \frac{P_{\text{SO}_2(f)} C_{\text{L}} V_{\text{L}}}{H - P_{\text{SO}_2(f)}} = y^{\circ} [P_{\text{HS}(0)} - P_{\text{HS}(0-)}] \frac{V_{\text{HS}}}{RT} \quad (\text{B-2})$$

where C_{L} is the concentration of liquid adsorbent (moles/L) and the remaining symbols were defined in Appendix A. The first term on the left side in Eq. (B-2) is the number of moles of SO_2 in the gas phase at equilibrium; the second term is the number of moles of SO_2 in the liquid adsorbent at equilibrium [rearrange Eq. (B-1)]; and the right-hand side of Eq. (B-2) is the number of moles of SO_2 initially [see Eq. (A-3)].

Eq. (B-2) may be rearranged to yield

$$H = \frac{[V_{\text{HS}} + V_{\text{SC}} - V_{\text{L}}] P_{\text{SO}_2(f)}^2 - [C_{\text{L}} V_{\text{L}} RT - y^{\circ} (P_{\text{HS}(0)} - P_{\text{HS}(0-)})] P_{\text{SO}_2(f)}}{[V_{\text{HS}} + V_{\text{SC}} - V_{\text{L}}] P_{\text{SO}_2} - y^{\circ} [P_{\text{HS}(0)} - P_{\text{HS}(0-)}] V_{\text{HS}}} \quad (\text{B-3})$$

Each term on the right side of this equation is known during an experiment.

Because H is defined in terms of mole fraction liquid, comparing absorption into different liquids can be difficult. Hence, we define H^* :

$$H^* = \frac{\text{volume (STP) of SO}_2 \text{ absorbed}}{\text{volume of liquid adsorbent}} \quad (\text{B-4})$$

$$= \frac{(\text{moles SO}_2 \text{ in liquid}) 22410}{V_{\text{L}}} \quad (\text{B-5})$$

where V_{L} is the liquid volume in cm^3 . We may substitute the second term of Eq. (B-2) into Eq. (B-5) and rearrange:

$$H^* = \frac{22410 C_{\text{L}} P_{\text{SO}_2(f)}}{H - P_{\text{SO}_2(f)}} \quad (\text{B-6})$$

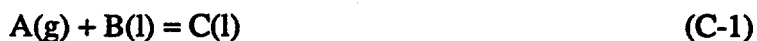
Hence, knowing H, we can calculate H^* .

Appendix C

EQUILIBRIUM CONSTANT FROM BREAKTHROUGH CURVES

EQUILIBRIUM CONSTANT FROM BREAKTHROUGH CURVES

Consider the reaction



where A is in the gas phase and B is a compound in the liquid phase that complexes with A to form C, also in the liquid phase. When A at concentration C_0 is fed to a bubbler containing B, the concentration of A leaving the bubbler will be reduced initially. As B becomes saturated with A, this exit concentration of A will increase with time. This concentration change of A over time is called the breakthrough curve. A typical curve was shown in Figure 2-16 for NO being absorbed by aqueous Fe(II)-EDTA. From such data, we can readily calculate the solubility of A in the liquid as well as the equilibrium constant K for the reaction listed in Eq. (C-1).

To obtain the solubility, we first write a mass balance:

$$\begin{aligned} \text{amount of solute} &= \text{amount of solute in} - \text{amount of solute out} \\ \text{accumulated in liquid} & \\ &= QC_0t_s - Q \int_0^{t_s} C \, dt \end{aligned} \quad (C-2)$$

where Q is the total gas flowrate, C_0 is the inlet concentration of A, and t_s is the time at which the outlet and inlet concentration of A are the same. Dividing by the liquid volume V yields:

$$C_s = \frac{QC_0}{V} t_s - \frac{Q}{V} \int_0^{t_s} C \, dt \quad (C-3)$$

where C_s is the total solubility of A in the liquid. Thus the area between the breakthrough curve and a horizontal line at C_0 , i.e., the area above the breakthrough curve, is proportional to the solubility as implied by Eq. (C-3).

From these data, we can also compute the equilibrium constant. First, however, we write the reaction in the form



where A(l) is assumed to be in equilibrium with A(g). This equilibrium is often written as a Henry's law partition coefficient:

$$A(l) = H A(g) \quad (C-5)$$

Thus, we may write the equilibrium constant for the reaction listed in Eq. (C-4) as:

$$K = \frac{[C]}{[A(l)][B]} = \frac{[C]}{H[A(g)][B]} \quad (C-6)$$

By stoichiometry, we have

$$[C] = [B]_0 - [B] = C_s - [A(l)] \quad (C-7)$$

where $[B]_0$ is the concentration of B initially and C_s is given by Eq. (C-3). Thus we obtain

$$K = \frac{C_s - H[A(g)]}{H[A(g)]\{[B]_0 - C_s + H[A(g)]\}} \quad (C-8)$$

All quantities on the right side of this expression are now known, and we may readily calculate K.

Appendix D

**EQUATIONS USED FOR OVERALL MASS TRANSFER
COEFFICIENT CALCULATIONS**

EQUATIONS USED FOR OVERALL MASS TRANSFER COEFFICIENT CALCULATIONS

In the Task 4 experiments with hollow fiber contactors, the mass transfer coefficient was defined as

$$K_{OLM} = (V_L C_L^{OUT}) / (A \Delta C_{LM})$$

where

K_{OLM} = Overall mass transfer coefficient, cm/s

V_L = Liquid flow rate, cm³/s

A = Area of transfer based on outside diameter of fiber, cm²

C_L^{OUT} = Concentration of CO₂ in the liquid outlet, moles/cm³

ΔC_{LM} = Logarithmic mean concentration difference, mole/cm³
= $[(C_G^{IN} - C_L^{OUT}) - C_G^{OUT}] / \ln [(C_G^{IN} - C_L^{OUT}) / C_G^{OUT}]$

C_G^{IN}, C_G^{OUT} = Liquid phase concentration of CO₂ in equilibrium with feed gas at inlet and outlet, respectively, mole/cm³

The values of C_G^{IN} and C_G^{OUT} are calculated by the equations

$$C_G^{IN} = P_G^{IN} * H$$

$$C_G^{OUT} = P_G^{OUT} * H$$

where C_G^{IN}, C_G^{OUT} = Liquid phase concentration of CO₂ in equilibrium with feed gas at inlet and outlet, respectively, moles/cm³

P_G^{IN}, P_G^{OUT} = Gas inlet and outlet pressures, respectively, atm

H = Henry's law constant, mole/cm³ atm

PROCEDURE TO DETERMINE THE VALUE OF H

Carbon dioxide solubility in water at different temperatures (in the units of atm/mole fraction in liquid) are available in Geankoplis (1972). The following correlation is developed from those data:

$$h = [0.07245 + 0.00295 t + 0.00003 t^2] \times 10^4$$

where h = Henry's law constant, atm/mole fraction in liquid
 t = temperature, °C

For a given temperature, h is calculated from the above equation and converted to the units of mole/cm³ atm using the following expression

$$H = 1 / (MW_{H_2O} / \rho_{H_2O} * h)$$

where H = Henry's law constant, mole/cm³ atm.
 MW_{H_2O} = molecular weight of water, g/mole
 ρ_{H_2O} = density of water, g/cm³

Appendix E

CALCULATION OF MINIMUM LIQUID FLOW RATE

CALCULATION OF MINIMUM LIQUID FLOW RATE

$\text{Fe}^{\text{II}}(\text{edta})$ is known to complex with NO according to the liquid-phase reaction:



whose equilibrium constant, K, is given by

$$K = \frac{[\text{Fe}^{\text{II}}(\text{edta})(\text{NO})^{2-}(\text{l})]}{[\text{NO}(\text{l})][\text{Fe}^{\text{II}}(\text{edta})^{2-}(\text{l})]} \quad (\text{E-2})$$

All species in the two equations above are assumed to be dissolved in an aqueous solution. From these relations, we can obtain the maximum gas phase NO concentration that can be absorbed by a scrubbing solution. To do so, we first assume that a linear isotherm exists between NO dissolved in the liquid phase and NO in the gas phase:

$$[\text{NO}(\text{l})] = \alpha[\text{NO}(\text{g})] \quad (\text{E-3})$$

Next we note that the total NO in the liquid phase is that complexed plus that uncomplexed:

$$[\text{NO}(\text{l})]_{\text{total}} = [\text{Fe}^{\text{II}}(\text{edta})(\text{NO})^{2-}(\text{l})] + [\text{NO}(\text{l})] \quad (\text{E-4})$$

and the amount of $\text{Fe}^{\text{II}}(\text{edta})$ initially in the liquid phase is that complexed plus that uncomplexed:

$$[\text{Fe}^{\text{II}}(\text{edta})^{2-}(\text{l})]_{\text{initial}} = [\text{Fe}^{\text{II}}(\text{edta})(\text{NO})^{2-}(\text{l})] + [\text{Fe}^{\text{II}}(\text{edta})^{2-}(\text{l})] \quad (\text{E-5})$$

Substituting Eqs. (E-3), (E-4), and (E-5) into Eq. (E-2) and rearranging yields:

$$[\text{NO}(\text{l})]_{\text{total}} = \frac{\alpha[\text{NO}(\text{g})] \{ 1 + K\alpha[\text{NO}(\text{g})] + K[\text{Fe}^{\text{II}}(\text{edta})^{2-}(\text{l})]_{\text{initial}} \}}{1 + K\alpha[\text{NO}(\text{g})][\text{Fe}^{\text{II}}(\text{edta})^{2-}(\text{l})]_{\text{initial}}} \quad (\text{E-6})$$

Thus, knowing the initial concentration of $\text{Fe}^{\text{II}}(\text{edta})$ in the liquid phase and the concentration of NO in the gas phase, we can compute the total NO concentration absorbed by the liquid phase at equilibrium. This is essentially the liquid's sorption capacity.

Now imagine we treat a flue gas having a concentration of [NO(g)] with a scrubbing liquid having a sorption capacity of [NO(l)]_{total}, then a quick calculation shows that

$$\frac{\text{Liquid Flow rate}}{\text{Gas Flow rate}} = \frac{10^{-6}}{22.4} \frac{[\text{NO(g)}]}{[\text{NO(l)}]_{\text{total}}} \quad (\text{E-7})$$

where the liquid flow rate is in L/min, the gas flow rate is in L(STP)/min, [NO(g)] is in ppm, and [NO(l)]_{total} is in mol/L. This ratio represents the minimum liquid flow rate necessary to treat a given gas flow rate; it may be combined with Eq. (E-6) to yield

$$\frac{\text{Liquid Flow Rate; L/min}}{\text{Gas Flow Rate; L(STP)/min}} = \frac{10^{-6}}{22.4} \frac{1 + K\alpha[\text{NO(g)}][\text{Fe}^{\text{II}}(\text{edta})^{2-}(\text{l})]_{\text{initial}}}{\alpha\{1 + K\alpha[\text{NO(g)}] + K[\text{Fe}^{\text{II}}(\text{edta})^{2-}(\text{l})]_{\text{initial}}\}} \quad (\text{E-8})$$